Université PARIS DESCARTES PARIS 5

THESE

Pour obtenir le grade de

DOCTEUR DE L'UNIVERSITE PARIS DESCARTES

Ecole doctorale Frontières du Vivant

Biologie interdisciplinaire

Design and optimization of small animal non-invasive imaging approaches for evaluating the effects of innovative treatments of Primary Central Nervous System Lymphomas

Présentée par :

Jérémie COSETTE

Soutenue publiquement le 11 Juillet 2014

JURY

Dr. Lori BRIDAL, rapporteur

Pr. Andràs PALDI, rapporteur

Dr. George AZAR, examinateur

Dr. Peter KIESEL, examinateur

Pr. Patrice FLAUD, co-directeur de thèse

Pr. Sylvain FISSON, co-directeur de thèse

ACKNOWLEDGMENTS

Cette partie est la seule qui est rédigée en français.

Je tiens à remercier sincèrement le Professeur Hervé Fridman de m'avoir accueilli au sein du Centre de Recherche des Cordeliers.

Je remercie le Professeur Catherine Sautès-Fridman de m'avoir acceuilli au sein de l'équipe 13, et d'avoir fait le pari soutenir ce projet interdisciplinaire.

Je remercie le Professeur Sylvain Fisson de m'avoir proposé ce projet, d'avoir cru en moi pour réaliser ce travail de thèse. Pour nos discussions de début de thèse et conversations téléphoniques de plusieurs heures. Merci pour tes conseils et ton aide.

Je remercie le Professeur Patrice Flaud d'avoir accepté de nous accompagner, Sylvain et moi, dans cette aventure partie d'une simple discussion. Merci pour vos enseignements, pour vos conseils avisés et pour votre disponibilité.

Je remercie chaleureusement le Professeur Andràs Pàldi d'avoir accepté de présider le jury et d'être rapporteur de ce travail.

Je remercie le Docteur Lori Bridal d'avoir accepté d'être rapporteur de ce travail.

Je remercie le Docteur Georges Azar d'avoir accepté d'être examinateur de la soutenance.

Je remercie le Docteur Peter Kiesel d'avoir accepté d'être examinateur de la soutenance et de s'être déplacé depuis la Californie. I would like to sincerly thank Dr. Peter Kiesel for his acceptance to be a part of my PhD thesis jury committee as examinator, and for his travel from California to do so.

Etant données les difficultés que j'ai rencontrées au début de ma thèse pour trouver un financement, je tiens à remercier très chaleureusement toute l'équipe de l'école doctorale FdV et du centre de recherche interdisciplinaire. Vous avez cru en mon projet, et malgré mon profil atypique, vous avez fait le nécessaire pour que j'obtienne une bourse. Merci également de votre disponibilité, de votre aide pour parfaire notre approche scientifique et notre rayonnement à l'international.

Cette bourse m'a été attribuée par l'INCA, l'Institut National du CAncer. Je tiens également à les remercier car sans leur aide, cette thèse n'aurait pas été possible.

Je remercie également Jean-Claude Jeanny pour son aide au commencement de ce projet, ainsi que Francine Béhart-Cohen.

Pour son accueil en son sein au début de cette aventure, je remercie le centre d'imagerie cellulaire et de cytométrie du centre de recherche des cordeliers, et tout particulièrement Christophe Klein.

Je tiens également à remercier ceux que j'aime à appeler « les opticiens ». Attention, rien à voir avec Alain Afflelou et Johnny buvant un coup dans un Atoll ! Ce sont des spécialistes de l'optique. Ils sont à l'ESPCI et m'ont beaucoup aidé dans réalisation des montages expérimentaux. Merci à vous, Alexandra, Vincent, Thomas et bien sûr Sophie, qui ressemble toujours beaucoup à ma petite sœur !

Nous avons collaboré de près avec la troupe des « Opticiens » et il se trouve que nous déposâmes conjointement il y a quelques années un dossier pour un appel à projet de l'Université Pierre et Marie Curie. Le projet fut accepté et nous fûmes gratifiés de 30 k€ pour du matériel. Autant dire une manne providentielle à un moment où on manquait cruellement de matériel. Cette subvention nous a permis d'acheter les lasers, les détecteurs, les logiciels d'analyse ; cela nous a été indispensable en somme. Merci donc à tous les acteurs du projet Convergence de l'UPMC, aux créateurs de l'appel à projet et aux décideurs qui ont bien voulu miser sur notre projet.

Je remercie également tout le personnel du centre d'exploration fonctionnelle du centre de recherche des cordeliers.

Je souhaite remercier Claude Boccara pour son aide à me lancer dans ce projet.

Evidemment je voudrais remercier toutes les personnes que j'ai rencontrées au laboratoire.

En premier lieu, je voudrais remercier Jean-Luc Teillaud qui m'a accepté comme stagiaire de M1 alors que je n'avais encore jamais fait de biologie (à part en cours, mais tout le monde sait que les cours ne comptent pas !). Le plus drôle dans cette histoire c'est que lorsque je cherchais mon stage de M1, il y a de ça 6 ans, j'ai commencé par appeler Sylvain qui m'a aiguillé vers Jean-Luc. Après mon stage de M1, c'est avec Sylvain qu'on s'est embarqué dans cette aventure. Cocasse.

Merci à Julien de m'avoir accueilli lors de mon premier jour de stage pour me faire un cours sur la luciférase… Ca a porté ses fruits !

Merci à Riad. Un grand merci à Riad même. Tu m'as tout appris sur la culture cellulaire sur la façon de faire de la recherche. Tu as toujours été à mon écoute et as toujours répondu à toutes mes questions naïves. Tu as grandement participé à élargir mes connaissances en biologie et plus précisément en immunologie. De plus, c'est grâce à toi que j'ai rencontré la femme avec qui je partage ma vie. Et pour cela, je ne te remercierai jamais assez.

L'équipe PIOL. Ah ! L'équipe PIOL… Exclusivement féminine (moi inclus), dans laquelle j'ai commencé mon M2 puis ma thèse. Merci à toutes pour vos conseils, votre bonne humeur et vos sourires. Claire G (dite la bonne sœur), qui avait d'ailleurs une tendance à m'accuser de tous les maux du monde, mais tout allait beaucoup mieux sitôt qu'elle souriait ; Cécile, précédée par une réputation de diablesse… Mais de diablesse elle n'avait que la coque de téléphone portable ! Lucile, ou l'exemple même que le monde est minuscule. Nous étions ensemble au collège et au lycée. Puis, perdus de vue, nous nous retrouvons par hasard, ensemble, dans la même équipe de recherche, travaillant sur le même sujet ! J'ai toujours eu une affection toute particulière pour toi, et je suis content de te savoir épanouie en Angleterre ! Je me demande juste si tu as trouvé un skatepark à Londres… Hanane, ou l'illustration de la définition du secret pour une fille : ''une phrase qu'on ne dit qu'à une seule personne… à la fois !'' Ajoutez à cela le côté nord-africain, et vous avez le téléphone secret arabe ! Ultra sécurisé… Hanane, toujours de bonne humeur, toujours prête à rigoler de mes blagues (dont tout le monde dit qu'elles sont nulles…), toujours au courant (en plus ce n'est même pas vrai, parfois je fais des blagues super drôles) de tout ce qui se passe dans labo ! Ma compagne de café, avec qui je venais quasiment tout le temps boire mon coffee Hanane ! (AH ! Qu'est ce que je disais, elle n'est pas géniale celle-là ?). Sabrina, dite madame Krav' Maga'. A vrai dire elle fait un sport de combat, mais je ne sais pas lequel c'est, et comme je trouve que Krav' Maga' c'est un mot rigolo… D'ailleurs Krav Maga, ca ferait un super nom pour des barres chocolatés ! Sabrina était mon épaule

dans les moments difficiles, une compagne pour rigoler et une collègue pour travailler ! On est resté en contact malgré ses allers-retours entre le labo et Angers et nous nous retrouvons aujourd'hui au sein de la même structure ! On dirait qu'on se suit ! Sabrina eut à un moment donné une stagiaire qui s'appelait Abigail Messenger. Bon déjà, elle avait le même nom de famille qu'MSN, passe encore. Mais je tiens à lui adresser un grand merci, car elle m'a apporté une preuve que j'attendais depuis longtemps. Abi est une femme qui est encore plus tête en l'air que moi. Et ça, Abi, tu n'as pas idée du plaisir que c'est… pour moi ! Finalement, Rym, collègue de bureau, et de gourdin dirais-je (rapport à sa tentative de m'assommer avec un stylo qui clignote). Malgré mes conseils de 'mettre du l'huile dulive' dans ses tubes, elle n'a jamais voulu… Elle aurait pu faire de grandes choses ! Merci à vous toutes. Merci de m'avoir accueilli dans l'équipe, merci pour vos sourires, vos rires et votre bonne humeur. Merci de m'avoir tellement intégré à l'équipe que j'étais devenu une PIOL girl… et merci d'y croire tellement que vous vouliez me travestir en femme… enfin je ne suis pas certain du merci là tout bien réfléchi !

Merci à Mélanie pour son accueil lors de mon arrivé, merci de m'avoir initié à la biologie moléculaire, et aux secrets de l'ADN ! Merci pour tous les bons moments passés ensemble, et pour nos petits déjeuners au restaurant japonais.

Jeremy, mi-homme mi-cytomètre et re mi-homme derrière ! A l'instar du père de Will Turner dans Pirates des Caraïbes, mi-homme mi-palourde, Jeremy pourrait se voir pousser des excroissances cytometriques. Pour tes blagues aussi bonnes que les miennes (et c'est un compliment !) et pour toutes les fois où on a refait les épisodes de kaamelott ! Merci.

Romain, ou le rugbyman des boulangeries ; un homme qui, curieusement, préfère tirer dans les brioches (le fameux 'drop de la brioche') plutôt que de les manger. Pour ton humour et ta bonne humeur, merci. Caroline quant à elle, aurait pu être élue meilleure salariée de l'année au Starbuck car elle sait faire du bon café, mais elle sait surtout le renverser ! Nous avions une relation explosive, et même si je t'ai pardonné de m'avoir jamais dit bonjour pendant mon stage de m2, nous avons appris à nous connaître et je suis ravi que tu sois aujourd'hui épanouie outre-Atlantique.

Sophia, merci pour tes conseils avisés, pour nos petites pauses, et pour tous les moments qu'on a passé ensemble. Sophia m'a appris une chose importante dont je me souviendrai : ''Cok Dilaao''. C'est du russe. Ca veut dire ''ça va ?''. Ca peut toujours servir. Merci Sophia, j'te revaudrai ça !

Je tiens également à remercier toutes les personnes de l'équipe 13 que j'ai rencontrées, avec qui j'ai discuté et partagé. Merci à tous.

Merci à Charlotte pour ses cours de danse et ses playlists. Tu as élu domicile chez les squelettes désormais. Je ne suis pas sûr qu'ils soient aussi bons danseurs que moi…

Tessa, ma copine de check ou la randonneuse de la mort ! Vous aimez partir en vacances au soleil et vous reposer à la plage, sous cette agréable brise ? C'est normal. Moi aussi. Tessa par contre, elle préfère faire 2000 kilomètres à pieds au Groenland avec un sac à dos de 28 kg et manger des Saumons crus ! Tessa est professeur de Tennis. Nous sommes allés jouer un peu une fois. Ca s'est très bien passé. Non. J'ai failli y rester. Merci Tessa, pour m'avoir rappelé que j'étais aussi bon qu'un minime !

Claire ! Collègue de bureau et amie, nous avons partagé tellement de choses ces dernières années. Il y aurait tellement à dire ! Nous nous sommes très bien entendus dès notre rencontre et nous nous sommes vite trouvés des atomes crochus. Merci pour ta bonne humeur, pour avoir toujours été à mon écoute, pour tes mimiques improbables, tes onomatopées inattendues, tes cris de petite souris et tes éternuements de hamster russe. Tu pourrais te reconvertir dans les cosmétiques et faire fortune avec ton soin du visage révolutionnaire à base de … crêpes. Merci à toi pour tous ces bons moments partagés. J'espère sincèrement que tu atteindras tous tes objectifs à l'avenir. Merci bien sûr à Aurélien, dont les pâtisseries artistiques régalaient aussi bien nos yeux que nos papilles !

Merci à tous les membres présents et passés de l'équipe 14, Sophie, Quentin, Jonathan et tous les autres.

Helen, mon anglaise préférée, j'ai été très content d'avoir fait ta connaissance. Malgré nos cultures différentes, et ton incapacité à parler le français et à le comprendre (admettons-le), nous avons appris à nous connaître. Je dois t'avouer que tu as fait de gros progrès en Français, et j'imagine que tu as bien retenu que 'j'ai chaud' et 'je suis chaude' ont en français une signification bien différente ! (même si en anglais…). Merci de m'avoir aidé à perfectionner mon anglais et merci pour tous nos beaux moments passés ensemble

Merci à tous les membres de l'équipe 15 que j'ai rencontré, Nicolas, Etienne, Laetitia, Mihaela, Lucie et tous les autres.

Merci à Johanna, Eliane et Nathalie pour leurs attentions et pour leurs sourires !

Merci à toutes les personnes que j'ai rencontré durant mon séjour au centre de recherche des cordeliers.

Merci à tous les Turn Over, Fx, Yannis, Pascal et Mathilde de m'avoir supporté pendant la rédaction de mon manuscrit. Tout simplement merci d'être mes amis.

Je tiens à remercier sincèrement Vanessa pour son aide inestimable.

Depuis environ 15 ans, je pars tous les ans pêcher en Haute-Savoie. Au bord d'un petit lac, magnifique à la fin du printemps, survolé parfois par un héron cendré. Un cadre idéal pour profiter du spectacle quotidien de la nature. Depuis 15 ans donc, je suis accueilli par une famille au cœur sur la main. Ils m'ont vu grandir, passer les étapes importantes de ma vie et m'ont toujours soutenu pendant ma thèse. D'ailleurs pour la petite histoire, le premier coup de téléphone que j'ai passé à Sylvain pour mon stage de M1 l'a été depuis là-bas. Merci à vous tous, Marie-Hélène, Yves, Anatole, Léopold, Arthur, Mi-joe, Paupaul, Martine, Jean-Christophe, Corentin et Morgane.

Bien entendu je remercie mes sœurs, Eva et Déborah, qui m'ont toujours épaulé et soutenu tout au long de ma thèse mais aussi tout au long de ma vie. Déborah, ma grande sœur ; plus jeune, tu as voulu faire de la recherche en biologie. Tu as choisi un domaine médical plus appliqué : comme ça t'as réussi ! Aujourd'hui je fais de la recherche en biologie, c'est cocasse ; la boucle est bouclée ! Enfin pas tout à fait, petit je voulais être pilote de rafale. P'tite sœur, tu sais ce qu'il te reste à faire ! Eva tu es un peu jeune encore pour les choix de carrière, mais j'espère que tu feras ce qui te plaira et tu trouveras la voie qui fera de toi une femme épanouie. Merci à toutes les deux.

Merci à mes parents pour tout ce qu'ils ont toujours fait pour moi. Merci de vous être investi pour que je puisse faire des études et si je suis là aujourd'hui, c'est grâce à vous et je ne l'oublierai jamais. Merci d'avoir insisté pour que je travaille mon saxo et mes cours. Aujourd'hui je comprends. Merci de m'avoir donné goût à la musique, à la science et tout simplement à la vie. Merci infiniment.

Et ma mémé qui voulait que je ''fais l'inginieur'' ! Je suis sûr qu'elle sait.

Merci enfin à Elodie. J'aurais tellement de choses à te dire. Une rencontre aux cordeliers ; j'étais en stage, tu étais en thèse. Merci pour ton soutien quotidien, pour ton aide précieuse et pour ta bonne humeur permanente. Notre histoire a commencé quasiment en même temps que ma thèse. Nous partageons aujourd'hui nos vies et je te remercie d'être à mes côtés tous les jours. Du fond du cœur, merci.

Merci à toutes et à tous. Tout le monde a joué un rôle dans mon aventure, et je suis content que les circonstances m'aient amené jusqu'ici. Merci.

ABSTRACT

Primary central nervous system lymphomas (PCNSL) are very aggressive malignancies with poor survival rate even with treatments (survival median is 44 months). This disease affects immune cells (lymphocytes) and forms diffuse and non-surgically removable tumor in the central nervous system. High-dose chemotherapy and radiotherapy are the common treatments with severe side effects. New therapeutic approaches are required for increasing treatment efficiency. We focused on primary intraocular lymphomas (PIOL) and primary cerebral lymphomas (PCL), which are subtypes of PCNSL. PIOL and PCL cells have a high propensity to migrate and form metastases in the brain and in the controlateral eye in the case of PIOL, and in the eye in the PCL case. However, metastatic dissemation mechanisms remain unclear.

The objective of the present work was to study the effects of innovative treatments of B-cell lymphoma on primary tumor, on metastases, and on circulating tumor cells in PIOL and PCL immunocompetent syngeneic murine models of lymphomas using non-invasive *in vivo* imaging methods. We studied the effects of Ublituximab, a glycoengineered anti-CD20 monoclonal antibody (mAb), and CpG-ODN, a TLR-9 agonist, in mouse models. We showed that Ublituximab exhibits significant anti-tumor effect in PIOL and PCL, while CpG showed significant anti-tumor effect in PCL. We monitored the tumor burden and metastases using innovating non-invasive optical imaging or cell detection methods: bioluminescence imaging (BLI) and in vivo flow cytometer (IVFC). BLI was used to locate metastasis and to quantify tumor burden. We indeed developed a bioluminescence-based tumor burden quantification method that reduces user-dependence, allows comparisons between experiments, reveals statistical relevance, and which is easy to use. An IVFC device was set up to investigate the role of circulating tumor cells (CTCs) in PIOL and PCL. This fluorescence-based technique allows detection of CTCs by analyzing the cells flowing in blood vessels. However we had to overcome the problem of autofluorescence and tissue absorption. Two approaches were studied in parallel: a elaborating new cell line expressing far red fluorescent proteins, modulating the excitation light of an IVFC device to give the cell a unique signature therefore enhancing sensitivity, increasing signal to noise ratio. The modulated excitation IVFC allowed us to calculate the velocity of cells, and infer their position in blood vessel phantoms. The analysis of treatment effects on tumor burden, metastases and CTCs in PIOL and PCL could help understanding lymphoma metastatic dissemination and contribute to treatment follow-up, thus allowing design of new therapeutic approaches with increased efficacy.

Table of contents

SYMBOLS AND ABBREVIATIONS

Ab	Antibody
ADCC	Antibody Dependant Cell Cytotoxicity
AIDS	Acquired ImmunoDeficiency Syndrome
AL	Achromatic Lense
AP	Anamorphic Prism
APC	Antigen Presenting Cell
ATP	Adenosine TriPhosphate
BCL	Biconvex Lens
BCR	B-Cell Receptor
BFP	Blue Fluorescent Protein
BLI	Bioluminescence Imaging
BP	Bandpass Filter
BQV	Bioluminescence Quantification Value
CD	Cluster of Differenciation
CDC	Complement Dependant Cytotoxicity
CFP	Cyan Fluorescent Protein
CL	Cylindrical Lens
CNS	Central Nervous System
CP	Calcite Prism
CSF	Cerebrospinal Fluid
CTC	Circulating Tumor Cell
DLBCL	Diffuse Large B Cell Lymphoma
DM	Dichroïc Mirror
DNA	DesoxyriboNucleic Acid
DPSS	Diode-Pumped Solid-State Laser
EBV	Epstein - Barr Virus
EGFP	Enhanced Green Fluorescent Protein
EMT	Epithelial to Mesenchymal Transition
EpCAM	Epithelial Cell Adhesion Molecule
ESOCA	Ear Skin Optical Clearing Agent
Fab	Fragment, antigen binding
Fc	Fragment, crystallizable

FCS	Fetal Calf Serum
FcγR	Fcγ Receptor
FISH	Fluorescence In Situ Hybridization
FSC	Forward SCatter
GFP	Green Fluorescent Protein
HL	Hodgkin Lymphoma
Ig	Immunoglobulin
ISL	Intra-Splenic Lymphoma
IVFC	*In Vivo* Flow Cytometry
IVIS	*In Vivo* Imaging System
kDa	*Kilo Dalton*
LCA	Leukocyte Common Antigen
LFB	*Laboratoire* français du Fractionnement et des Biotechnologies
M	Mirror
Mab	Monoclonal antibody
MAC	Membrane Attack Complex
MAC	Membrane Attack Complex
MHC	Major Histocompatibility Complex
NHL	Non-Hodgkin Lymphoma
NK	Natural Killer
ODN – CpG	OligoDeoxyNucleotide Cytosine – Phosphodiester Bond – Guanine Can be found as CpG – ODN or CpG – DNA
P	Polaroid
PAFC	PhotoAcoustic Flow Cytometry
PAI	PhotoAcoustic Imaging
PAMPs	Pathogen-Associated Molecular Patterns
PCL	Primary Cerebral Lymphoma
PCL	Primary Cerebral Lymphoma
PCNSL	Primary Central Nervous System Lymphoma
PCR	Polymerase Chain Reaction
PDMS	*PolyDiMethylSiloxane*
ph	photon
PIOL	Primary Intra-Ocular Lymphoma
PMT	Photomultiplier Tubes
qPCR	quantitative Polymerase Chain Reaction
R-CHOP	Rituxan - Cytoxan HydroxydaunorubicinOncovin Prednisone
RFP	Red Fluorescent Protein

Rh	Rhesus
RLU	Relative Luminescence Units
RNA	RiboNucleic Acid
ROI	Region Of Interest
RPMI	Roswell Park Memoral Institute
SCL	Sub-Cutaneous Lymphoma
SNR	Signal To Noise Ratio
SPM	Signal Processing Method
sr	steradian
SSC	Side SCatter
TEM	Transverse Electromagnetic Mode
TLR	Toll-Like Receptor
TPA	Two-Photon Absorption
YFP	Yellow Fluorescent Protein

FIGURES AND TABLES

INTRODUCTION

PREFACE

This thesis research has been performed in the Team 13 “immune microenvironment and tumor” of the INSERM UMRS 872 in Paris at the Cordeliers Research Center, and in the team “biofluidics” of the MSC laboratory (Matter and Complex Systems) of the UMR 7057 in Paris.

This work has been interdisciplinary in the context of the Frontiers in Life Science doctoral school. The scope of this school is indeed the study of biological questions with an interdisciplinary approach.

We studied the effects of different treatments on different types of mouse models of lymphomas. We also developed methods and set up devices to detect tumor cells circulating in the blood.

Therefore, the first part of the introduction will treat the biological side of the question and the second part will treat the physical side of the question. Each part will be divided into two subparts: the first one will be constituted with background knowledge, while the second part will introduce my work deeper in the details.

I will then present my result through published articles or non-published data, discuss the results and conclude.

1. PART I: LYMPHOMAS

1.1. Cancer background

Cancer cells grow and divide in an unregulated pace. Gene mutations are almost always the cause of this unregulated growth. Eventually, a considerable amount of mutated cells can form a primary tumor and some of them can invade other organs then constituting metastases.

This often happens, and sometimes, a cancel cell can appear, but it is destroyed very quickly by the immune system (especially Natural Killer cells), which are specialized in destruction of damaged cells, thus creating an equilibrium. If the equilibrium is broken, the tumor cells can grow enough to form a tumor.

Another interesting point is that cancer cells are immortals. They can have a mutation in gene that regulates apoptosis, or lack the activity of telomerase, resulting in a loss of telomeric DNA that could play a role in immortalization (and ageing) (Counter *et al.*, 1992). This is the reason why cancer cell lines can be cultured; provided they have enough nutrients, the cells will proliferate.

1.1.1. Metastasis

A metastasis is the consequence of the migration of tumor cells from the primary tumor. When those cells achieve to form a secondary tumor, the secondary tumor is called a metastasis. Metastases usually happen in late disease, but it is not always the case. Metastases can invade vital organs, thus reducing dramatically the survival of patients. Metastases often occur in brain, lungs, liver and spleen.

Metastatic cells that disseminate in the blood are called circulating tumor cells (CTCs). CTCs are tumor epithelial cells that have undergone the Epithelial to Mesenchymal Transition (EMT). This transition is characterized by the loss of certain adherence molecules, which give the ability for the cell to 'escape' from the primary tumor. Even though they have undergone EMT, they still express some epithelial proteins that are expressed by no other cells in the blood under physiological conditions.

1.1.2. Circulating Tumor Cells (CTCs)

Circulating Tumor Cells (CTCs) are identified as tumor cells that are circulating in the blood. They are very rare, and their role in metastases dissemination has been investigated for years. No correlation has been found between the number of CTCS and the number of metastases. It appears, however,

that the CTCs count is a relevant prognosis biomarker. Many studies have been done to study those CTCs but also to try to detect them, *in vitro* and *in vivo*. The detection of CTCs in human patients is a challenge because CTCs are very rare (1 CTC / 1 000 000 000 Circulating cells). A lot of experimental devices have been developed to detect and quantify circulating tumor cells. Moreover, conventional techniques such as flow cytometry (in case of high number of CTCs), filtering (tumor cells are bigger than normal cells) or PCR or qPCR on targeted oncogenes have also been used in this field (cf table 1). The detection of CTCs is based on either phenotypic analysis or DNA analysis assuming that CTCs have the same expression profiles. However in spite of all these techniques, only one device has been approved and is widely used for clinical use. This device is the CellSearch® from Veridex.

As CTC have kept epithelial proteins and it is well established that CTCs can be characterized by 3 different phenotypic assessments:

EpCAM^{+}: Epithelial Cell Adhesion Molecule is a transmembrane glycoprotein mediating calcium independent cell-cell adhesion in epithelia. CTCs are EpCAM positive.

Cytokeratins^{+}: Cytokeratins are proteins found in the intracytoplasmic cytoskeleton of epithelial tissue. There are about 20 different cytokeratins split up in two categories. The type I acid cytokeratins; and the type II, basic or neutral cytokeratins. Different types of cytokeratins are used for characterizing CTCs according to the origin of cancer cells.

CD 45^{-}: CD45 is a transmembrane receptor widely expressed in white blood cells. Initially, CD45 was called leukocyte common antigen (LCA). Of course, CTCs are nucleated unlike red blood cells, giving a first way to differentiate tumor cells from blood cells. Sort CD45 negative cells ensure that there is no more leukocytes in the cells of interest.

By combining these 3 parameters, most of methods, especially CellSearch® are able to isolate and quantify CTCs.

In most cases, a blood sample is required (7.5 mL for CellSearch®) and a positive patient for CTCs can have from one up to hundreds of CTCs. Currently, Veridex claims that only one positive cell is sufficient to consider the patient positive for CTCs.

Author / *Journal* / Year	Country	Technique	Cell lines	Type	Mouse	Marker	Fluorophore	Wavelength	Detector
• **M.Thorsteinsson et al.** • *Anticancer Res.* • 01/2011	Denmark	CellSearch		Human colon adenocarcinoma		EpCAM, CK8-18-19, CD45			
• **I.Desitter et al.** • *Anticancer Res.* • 01/2011	USA France	ScreenCelll (filtering), qRT-PCR, Immunocytochemistry, FISH	• NCI-H2030, NCI-H1975 ○ HT29	• Non-Small Cell Lung Cancer (NSCLC) ○ Colorectal adenocarcinoma		EGFR			CCD camera
• **A.Gadrilone et al.** • *Jour. Cellular and Molecular Med.* • 02/2011	Italia	CELLection (Dynabeads) PCR		Metastatic Breast Cancer		EpCAM, CK8-18-19, CD45, BerEP4, Fibronectin, Vimentin			
• **Qing Li et al.** • *Internat. Jour. of nanomedecine* • 06/2011	China	Immunomagnetic nanoparticle assay RT-PCR		NSCLC		CK7-8, CK19, LUNX			
• **L.A. Devriese et al.** • *Lung Cancer* • 07/2011	The Netherlands	QPCR		NSCLC		CK7, CK19, EpCAM, FN1			
• **A. Lecharpentier et al.** • *British Jour. Of Cancer* • 10/2011	France	ISET – RareCells, Confocal microscopyt		NSCLC		Vimentin, CK7	AF488, AF647, SYTOX Orange		CCD camera
• **T.M.Scholtens et al.** • *Cytometry Part A* • 11/2011	The Netherlands	CellTracks (Veridex) Analyzer II TDI analyzer		• Breast & Colorectal Cancer ○ Metastatic Carcinoma		CK8-18-19, CD45	DAPI, PE, APC	375nm 532nm 639nm	CCD camera
Author / *Journal* / Year	Country	Technique	Cell lines	Type	Mouse	Marker	Fluorophore	Wavelength	Detector
• **H.Nakanishi et al.** • *Jour. of Cancer Res. & Clin. Oncol.* • 06/1999	Japan	PCR	HY-1	Human Medullary Carcinoma from Liver Metastatic Lesion	Nude				
• **M.Katoh et al.** • *Anticancer Research* • 04/2004	Germany	PCR	• HT29 ○ K562	• Human Colon Cancer ○ Human Lymphoma	SCID/SCID	Carcino Embryonic Antigen			
• **I.Georgakoudi et al.** • *Cancer Research* • 08/2004	USA	IVFC	• LNCap ○ MLL	• Human prostate cancer ○ Rate prostate Cancer	Rat SCID		GFP DiD	488nm 635nm	PMT CCD camera
• **O.Scatton et al.** • *Oncogene* • 02/2006	France	Flow Cytometry, Histology, Real-time mtDNA quantification	Mahlavu	Human Hepatocellular Carcinoma (HHC)	NOD/SCID	HLA, Cyt B mitochondrial gene			
• **L.M.Backhus et al.** • *jour of Thoracic & Cardiovasc. Surgery* • 08/2006	USA Canada	Immunohistochemistry, Western Blot, Cell Adhesion Assay	A549	Human lung adenocarcinoma	SCID/bg	COX2, CD44			
• **Yazan Alsayed et al.** • *Blood* • 04/2007	USA	Confocal Microscopy, FACS, ELISA, Immunoblotting, IVFC, 2-v microscopy, Bioluminescence imaging	MM.1S, KAS 6/1, U266, OPM2	HMM	NOD/SCID	CXCR4, CXCL12	PE, APC, PerCP, YFP, DiD, luciferase	635nm	PMT CCD Camera
• **Xunbin Wei et al.** • *Mol. Imaging* • 01/2010	USA	IVFC	MatLyLu	Rat Prostate Adenocarcinoma		Annexin-V	AF467	635nm	PMT
• **Zhigang Fan et al.** • *Nature Med.* • 06/2010	USA	IVFC Endomicroscopy FACS			C57BL/6 Rag$^{-/-}$		GFP DsRed	488nm 635nm	PMT
• **J.M. Runnels et al.** • *Jour. Biomedical Optics* • 01/2011	USA	In Vivo Flow Cytometry, Bioluminescence imaging, Multiphoton microscopy	MM.1S	Human Multiple Myelloma (HMM)	SCID/bg BALB/c Col2.3GFP		GFP, luciferase, DiD, DiO, Angiosense 750, Qtracker Qdots 800, Osteosense 750	473nm 633nm	PMT
• **K.Kolostova et al.** • *Anticancer Research* • 04/2011	Czech Republic USA	Immunomagnetic beads FLuorVivo Imaging System	PC-3	Human Prostate Cancer	Nude	EpCAM, GFP, PSMA	GFP		
• **D.A.Nedosekin et al.** • *Cytometry Part A* • 06/2011	USA	In Vivo Photoacoustic Flow Cytometry	B16F10, HTB-65, SK-3, SK-MEL-1	Human melanoma	Nude			1064nm 820nm	CCD camera Acc. Transducer
• **Yan Li et al.** • *Cytometry Part A* • 08/2011	China Germany	IVFC	• PC-3 ○ HepG2, HCCLM3	• Human prostate Cancer ○ HHC	Nude		DiD	488nm 635nm	PMT CCD Camera
• **M.Sarimollaoglu et al.** • *Optics Letters* • 10/2011	USA	In vivo PAFC	• B16F10 ○ MDA-MB-231	• Mouse melanoma ○ Human Breast cancer	Nude			671nm 820nm 1064nm	Acc.Transducer
• **Chao Fan et al.** • *Cancer Research* • 03/2012	China	In vivo Flow Cytometry	HCCLM3-GFP	HHC	BALB/c nude		GFP	488nm	PMT

Table 1: *Brief review of different types of techniques for Circulating Tumor Cells detection. The blue part (top) corresponds to human, whereas the red part (bottom) corresponds to mouse models. As can be seen on the table, only one team – J.M. Runnels et al. – is working on Balb/c immunocompetent mice.*

1.2. Lymphomas

Lymphoma is a type of blood cancer that occurs when lymphoid cells of the immune system divide faster than normal cells or live longer than they should. Lymphoma can develop (as first site) in the lymph nodes, spleen, bone marrow or other tissues (Parham *et. al*). As a matter of fact, in normal conditions, immune cells have the property to migrate in all organs to destroy pathogens. That would explain all these first tumor site localization.

Lymphoma presents as a solid tumor of lymphoid cells. However, lymphoid cells can circulate in the blood. In the case where the cancer cells are circulating cells, the diseases are referred to as lymphoid leukemias. Lymphomas and lymphoid leukemias are indeed closely related.

In most of cases of lymphomas, malignant cells originate in lymph nodes, resulting in an enlargement of the node. It can also, as previously mentioned, affect other organs; in that case, it is called extranodal lymphoma. Extranodal sites include the tonsils, skin, bowels, brain, eyes, spleen, bones, etc. There are many types of lymphomas, and they are a part of the broad group of diseases called hematological neoplasms.

Lymphoma is the most common form of hematological malignancy (blood cancer) in the developed world. Lymphomas represent 5.3% of all cancer in the United States of America and 55.6% of all blood cancer. In France, 11 000 new cases of lymphomas are diagnosed every year and lymphoma is ranked 6th of the most frequent cancers.

Lymphomas are diagnosed through a lymph node biopsy. The histology analysis may reveal histopathological features and may indicate a lymphoma. Further analysis such as immunophenotyping of flow cytometry or FISH (Fluorescence In Situ Hybridization – a technique that permits the detection of specific DNA sequences inside chromosomes) will complete and confirm the diagnosis.

Circulating Tumor Cells and Lymphomas

As for CTCs, things are a little bit different in the case lymphomas. Lymphoma cells are indeed initiated from hematopoietic cells, which are by definition, not epithelial cells. Therefore, they don't express EpCAM; moreover, as they are hematopoietic-like cells, they may express CD45, making the CellSearch® approach not suitable for studying circulating lymphoma cells.

Another point must be taken into consideration. It is a controversial point whether CTC can be used for lymphoma cells. The term 'CTC' is not used for lymphoblastic leukemia cells nor in any kind of leukemia cells as it is well known that those cancer cells are circulating. In the case of lymphoma, it is slightly different because lymphoma cells mostly form solid tumor, still they have the ability to migrate, throughout lymphatic or vascular system and form metastases. However, lymphoma metastasis does exist and often are, due to the lymphoma cells' propensity to migrate, the cause of the death.

N.B.: In this manuscript, lymphoma circulating cells will be referred as to circulating tumor cells, because fundamentally this is what they are: tumor cells that are circulating. Nonetheless, this controversy must be kept in mind.

1.3. Lymphoma Subtypes

Hodgkin lymphoma and non-Hodgkin Lymphomas are the two main subtypes of lymphomas. However, according to the World Health Organization, non-Hodgkin lymphomas are divided in 3 subtypes.

1.3.1. Hodgkin Lymphomas (HL)

Hodgkin lymphomas, also known as Hodgkin's disease is a type of lymphoma characterized by the presence of abnormal sized and multinucleated cells called Reed-Sternberg cells (RS cells).

Incidence: In France, the Hodgkin's disease affects almost equally male and females and affects young adult or the elderly (+75 years old). It is ranked 20th of male cancers and 21st of female cancers. The 5-years survival rate is in France 85% for males and 92% for females

Treatment: Hodgkin lymphoma can be treated by radiotherapy, chemotherapy or hematopoietic stem cells (HSC) transplantation. The choice of the treatment depends on the age and the sex of the patient, but also on the stage and the histopathological subtype of the disease. Hodgkin's disease can be treated quite efficiently.

Source: France Lymphome Espoir website

1.3.2. Non-Hodgkin Lymphomas (NHL)

There are many lymphomas subtypes in this category. It turns out that the subtype may vary according to the localization and to the cell type.

Incidence: In France, NHL is ranked 6th of most frequent cancers and ranked 9th of cancers in terms of mortality – 5000 deaths a year.

N.B.: During my PhD thesis, I worked on an animal model of lymphoma that was very close to "diffuse large B cell lymphoma", belonging to the non-Hodgkin lymphoma group. That is why, among the great number of non-Hodgkin lymphomas, I will present only the diffuse large B cell lymphoma in this paragraph.

The diffuse large B cell lymphoma (DLBCL) is a cancer of B-cells. It is the most common type of NHL among adults (30% to 40%). The DLBCL is an aggressive cancer that can arise not only in lymph nodes but in extranodal localizations such as digestive system, testicles, skin, breast, thyroid, central nervous system or bone marrow.

3000 to 4000 new cases of DLBCL are diagnosed in France every year.

Treatments: The DLBCL is usually treated with the combination of chemotherapies and Immunotherapies: R-CHOP. R-CHOP stands for Rituximab (**R**ituxan) – Cyclophosphamide (**C**ytoxan), Doxorubicin (**H**ydroxydaunorubicin), Vincristine (**O**ncovin) and **P**rednisone.

We worked on a particular location of DLBCL: Central Nervous System Lymphomas, which are presented in the next part.

1.4. Primary Central Nervous System lymphomas (PCNSL)

The Central Nervous System – CNS (brain, meninges, spinal cord, and eyes) – localization for a lymphoma is very rare. When a lymphoma is diagnosed and there is no other location than the CNS, the lymphoma is referred as to **Primary** CNS lymphoma (PCNSL).

This disease is only 2% of NHL, and 5% of primary cerebral tumors. It represents 300 new cases per year in France.

The origin of this lymphoma remains unclear. Immunodeficiency is a clearly identified risk factor, though most of diagnosed patients are immunocompetent.

CNS (including the eye) is an immune sanctuary; it means that there are few immune cells in the CNS in physiological conditions. The blood brain barrier (or blood retinal barrier) is supposed to prevent cells and molecules from entering those pressure-sensitive organs. Both brain and eye are in a confined structure, and the increase of the inside pressure can lead to permanent damage. High pressure in the eye induces damages of the optic nerve leading to blindness (glaucoma). Intracranial hypertension can lead to ischemia and then to cellular anoxia (Irthum B & Lemaire JJ, 1999). To avoid pressure increases, the microenvironment in these organs is constitutively immunosuppressive. The presence of immune cells that lose control of division is surprising in such a controlled environment. Some researchers showed that primary intra cerebral lymphomas were highly associated with viruses, especially EBV – Epstein - Barr Virus, well known as the cause of infectious mononucleosis (Fine *et al.*, 1993).

We studied in our lab two sorts of PCNSL, the primary intra-ocular lymphoma, which first occurs in the eye, and the primary cerebral lymphoma, which occurs in the brain.

1.4.1. Primary Intra-Ocular Lymphomas (PIOL)

Primary intra-ocular lymphomas first occur in the eye. PIOL is a subset of PCNSL and belongs in most cases to diffuse large B-cell lymphoma subtype.

Diagnosis, incidence and survival: PIOL are often misdiagnosed because the cells have a high propensity to migrate from the eye to the brain. In 85% of the cases, PIOL patients will get or already have a subsequent brain tumor, and 80% will develop a tumor in the controlateral eye (Bardenstein *et al.*, 1998 ; Chan *et al.*, 2004 ; Cassoux *et al.*, 2000). Once tumor cells have migrated from the eye to the brain, the location of the primary tumor is no more identifiable. On top of that, the differential diagnosis for PIOL is uveitis (an inflammation of the uvea), which is very common thus leading PIOL misdiagnosis. This might explain the only 50 cases diagnosed per year in France.

The need for a new tool for PIOL diagnosis is then obvious. Our team developed a kit to distinguish uveitis from intraocular lymphoma (Fisson *et al.*, 2013). The technique relies on the titration of cytokines in the vitreous of patients. The combination of IL-10/IL-6 and IL-10/IFNγ ratio was highly informative for discriminating PIOL patients from uveitis patients.

The five-year survival rate for this disease is around 5% with treatment.

N.B.: Treatments are very similar from PIOL to PCL. Therefore, PIOL treatments will be combined with PCL treatments in the next paragraph.

1.4.2. Primary Cerebral Lymphomas (PCL)

PCL is a rare intracranial tumor that starts in the lymph tissues of the brain or spinal cord. PCL is known to be a form of extranodal, high-grade non-Hodgkin B-cell neoplasm, usually large cell or immunoblastic type. 90% are DLBCLs; the remaining 10% are Burkitt lymphomas, T-cell lymphomas and other poorly characterized lymphomas.

Incidence and survival: The median survival for immunocompetent patients with treatment is 44 months. Immunodeficient patients (AIDS) have only a 4-month median survival with treatment; untreated their survival barely reach 2.5 months.

Treatments: The goal of the treatment is eradication of tumor cells in the brain, spine, leptomeninges, and vitreous. Successful therapy in immunocompetent patients leads to a median survival of 44 months.

The standard treatment for DLBCL is systemic combination of chemotherapeutic drugs such as CHOP. However, the optimal treatment for PCNSL has not been established yet. Although used, CHOP treatment is not really satisfactory on PCNSL. This certainly reflects the difficulty for the chemotherapeutic drugs to penetrate the brain thought the blood brain barrier.

Methotrexate is actually the single effective chemotherapeutic agent for PCNSL. Methotrexate is a folate analogue that interferes with DNA synthesis and repair. For PCNSL, patients receive high-dose systemic methotrexate. (Hoang-Xuan *et al.*, 2003; Hoang-Xuan *et al.*, 2003; Cassoux *et al.*, 2000)

Other drugs have nevertheless shown benefic effects such as cytarabine (systemic) (Ferreri *et al.*, 2014; Brito *et al.*, 2014) or thiotepa (intrathecal – inside the cerebrospinal fluid (CSF)). Intrathecal injections are however very heavy treatment for patients.

DLBCL often form solid tumors, however, in the case of cerebral lymphoma, the cell are diffused in the whole brain. They may form apparent solid tumors that are detectable with MRI (Magnetic Resonance Imaging). Still, a high number of diffused cells form infra-clinical tumor lesions that are not detectable; those lesions are the reason why surgery provides no help in PCNSL. Finally, as cerebral lymphoma is very diffuse, the chemotherapy may be accompanied with whole brain radiotherapy.

Even though, corticosteroids are not recommended in the early treatment, they might be used to improve patient's quality of life by minimizing symptoms.

In a study including more than 200 patients with brain and ocular lymphoma, Grimm and his team (Grimm *et al.*) found that dedicated ocular therapy improved disease control but do not affect overall survival. In the case of PIOL, bilateral disease is frequent and often requires ocular external beam radiotherapy. Systemic methotrexate still remains the more used treatment, but in the case of non-responding patients, methotrexate is administered locally via intra-vitreous route.

Long-term sequelae of radiation therapy and chemotherapy in PCNSL are significant. Early senility and cognitive dysfunctions have been observed (Taillia *et al.*). Serious leukoencephalopathy (Kamio *et al.*; Bhojwani *et al.*) can also occur in patients receiving methotrexate. New therapies have to be designed to minimize toxicity to cerebral white matter, and to maximize the efficacy.

1.5. New therapeutic approach: Immunotherapy

There are different therapeutic approaches for PCNSL. New therapies are being designed, and often, they combine different already known approaches. For about 20 years, monoclonal antibodies and more generally immunotherapies have shown very promising results. Now, immunotherapies are a new weapon oncologists have in their arsenal. Of course there, are a lot of innovative therapeutic approaches in cancer, however, only immunotherapy is suitable for PCNSL.

There are different sorts of immunotherapies: cell immunotherapy, which consists in administering immune cells to a patient; administration of cytokines or immune system activators; and antibody immunotherapy, which consists in administering antibodies to a patient (Wang *et al.*, 2014).

For a long time, immunology was not considered linked to cancer. Now, the interaction between the immune system and the cancer cells at different scales is widely admitted. The immune system plays a role in the carcinogenesis (genesis of the cancer), in the equilibrium (the tumor does not grow and is controlled by immune system), and even in the escape of the tumor (the tumor escapes the immune control and spreads).

The principle of cancer antibody-based immunotherapy is not to destroy tumor cells themselves – which is the case for chemotherapies or radiotherapies, but to help the immune cells to do so. The final aim is to educate the immune system and create an immune memory and avoid relapses.

1.5.1. Antibody-based immunotherapy

The real challenge in antibody immunotherapies is to find a target molecule (very often surface proteins) that is specific for the tumor cell. Such a molecule is called a tumor antigen. If the tumor antigen is also expressed on healthy cells, these healthy cells can be destroyed during the immunotherapy treatment. Sometimes, the risk worth it, but it has to be taken wisely. Indeed, autoimmune diseases could affect patients as a side effect of immunotherapies in which the target protein would also be expressed on non-tumor cells.

1.5.1.1 Antibodies

An antibody (Ab) is a protein produced by a B-cell. Also know as immunoglobulin (Ig), this Y-shaped protein is specific for one antigen. It is made up of a heavy chain and a light chain, kept together with disulfide bridges (Figure 1). Each tip of the "Y" is a region that contains the antigen-binding site. The few peptides that are specific for the antigen are called the paratope. Similarly, the antigen pattern which is recognized by the paratope is called the epitope. The two-branched sides of

the “Y” are called Fab regions for ‘fragment, antigen binding’, and the paratopes are indeed included in the Fab region.

The base of the “Y” is called Fc region for ‘fragment, crystallizable’. It is indeed the first fragment of the antibody that has been crystallized, allowing then the study of the protein using X-ray diffractometry. This Fc fragment is as important as the antigen binding fragment. The Fc region is the part of the antibody which is recognized by effector cells. Almost all hematopoietic cells express at their membrane surface proteins that belong to Fc receptors family.

Isotypes:

There are five types of heavy chains is mammals, denoted as following: chain α, δ, ε, γ, μ. These chains define the class or isotype of the antibody.

- Chain α : IgA
- Chain δ : IgD
- Chain ε : IgE
- Chain γ : IgG
- Chain μ: IgM

Those isotypes differ by their shape (IgG, igE and igD are monomers, IgA is a dimer, and IgM is a pentamer) or by their affinity and avidity for the antigen. One can also find different isotypes in the blood after primo-infection at different time points. For instance, in the early immune response, IgM can be found in the blood in high quantities whereas IgG are more present in the late response.

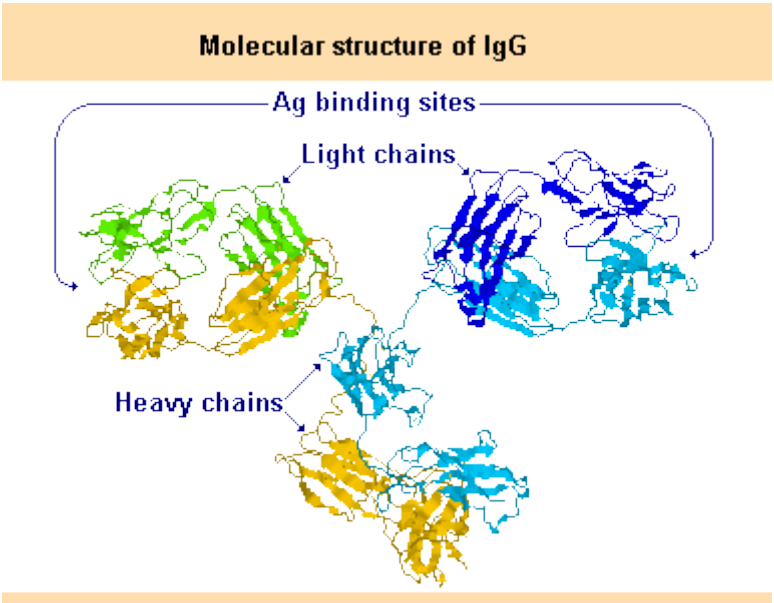

Figure 1: Molecular structure of an IgG. The IgG is ‘Y’ shaped and has two chains, the heavy (blue and golden) and the light (green and dark blue) chains.
From http://myplace.frontier.com/~dffix/medmicro/igs.htm

Monoclonal and polyclonal antibodies:

The epitope is rarely the whole polypeptidic sequence of the target protein. This induces that two antibodies can have the same target protein but different epitopes. This only happens if different clones of B cells secrete antibodies that have the same target protein. In the case where antibodies come from different clones of B cells, those antibodies are said to be polyclonal. On the other hand, if the antibodies come from the same clone of B cell, they are said to be monoclonal: they have the same epitope. Affinity to the target protein is higher for monoclonal antibodies than for polyclonal antibodies. In cancer antibody-based immunotherapies, most of the antibodies used are monoclonal IgG. That is why I will focus my study on IgG isotypes.

Almost all immune cells express the Fcγ receptor (FcγR), which is the receptor for the γ chain of the Fc region of the IgG. FcγR belong to the immunoglobulin super family. There are several members in this family :

- FcγRI or CD64
- FcγRIIA or CD32A
- FcγRIIB or CD32B
- FcγRIIIA or CD16A
- FcγRIIIB or CD16B

All FcγR – exept FcγRIIB – trigger an activation of the effector cells when engaged and an effect on the target cell (Teillaud JL, 2012). This effect can be done by different pathway, however the result is the same. The effector cells, whose FcγR is engaged, interact with the target cell – phagocytosis, exocytosis of perforin and Granzyme B – until its death.

1.5.1.2 Monoclonal Antibodies and anti-tumor effects

The use of antibodies in anti-cancer treatments is quite recent (about 20 years). It is quite efficient in certain cases. The basic principle is to turn an 'invisible' target for the immune system into a 'visible' target. The antibody acts like a flag by labeling the tumor cell and either destroy the cell by itself, or allow the recruitment of immune effector cells that recognize the antibody and destroy the tumor cell.

a. ADCC: Antibody Dependent Cell Cytotoxicity

ADCC is a mechanism that involves an antibody, a target (cell) and an effector cell. The antibody binds to a surface protein of the target cell. The antibody acts like a flag in this case, making easier the recognition of the target cell by the immune effector cells. In particular, Natural Killer cells (NK cells) express on their surface Fcγ receptors, that recognize the γ chain of IgG (Figure 2). When engaged, the Fcγ receptor activates activate the effector cells through intracellular signalization; the effector cell then destroy the target cell by secreting perforin and granzyme B. Those aforementioned proteins can indeed perforate the target cell and Granzyme B is released inside the target cells to trigger apoptosis.

Not only NK cells can perform ADCC, several Antigen Presenting Cells (APC) can also perform ADCC; for instance macrophages, dendritic cells and rarely B-cells.

b. CDC: Complement Dependent Cytotoxicity

The complement is a molecular system of defense against pathogens. The complement system belongs to the innate immunity, and is adept at recognizing molecular patterns (PAMPs: pathogen-associated molecular patterns) and destroying the recognized pathogen. It consists in various small proteins found in the blood, generally synthesized in the liver, and circulating as inactive precursors in physiologic conditions.

When stimulated by one of its several activation stimuli, proteases cleave specific proteins, and initiate a biochemical cascade of other cleavages that come along with a release of cytokines, resulting in an amplification of the immune response.

Finally, several complement proteins cleaved and associated together can form the membrane attack complex (MAC) – typically found at the surface of bacteria – which is a molecular complex that disrupts the phospholipid bilayer of target cells, resulting in cell lysis an death.

It turns out that the Fc part of an antibody is a trigger for the complement system. There are then two main possibilities:

- the C1q (protein of the complement) binds to the Fc part of the antibody, and form, after a cleavage cascade, the MAC.

- the C3b binds to the Fc part, triggers the secretion of cytokines, and enhances the recruitment of immune effector cells. Moreover, a large number of effector cells (Natural Killer, Macrophages, etc.)

express receptors for C3b; they then recognize the C3b bound to the antibody, which enhances the anti-tumor response.

c. Cell death

Some studies (Weiner *et al.* 2010) showed that *in vitro*, the engagement of the receptor at the surface of a tumor cell by an antibody can by itself induce cell death.

Here is recapitulative scheme:

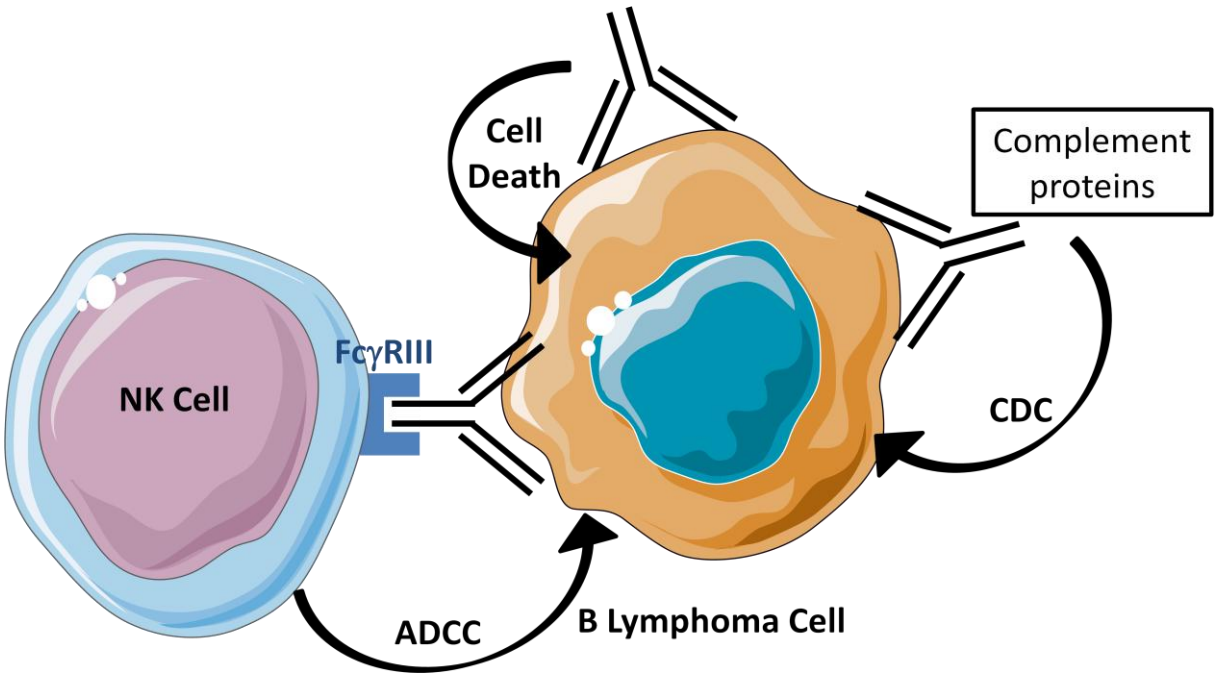

Figure 2: Recapitulative scheme of the different mechanisms of apoptosis induction after binding of the antibody on its target. The three mechanisms of Antibody dependent cell death are represented here. Antibody dependent Cell Cytotoxicity (ADCC), mediated through engagement of FcγRIII receptor of effector cells (*e.g.* NK cells); Complement Dependent Cytotoxicity (CDC) mediated through complement proteins; and direct cell death induced by engagement of the therapeutic antibody.

1.5.1.3. Anti CD20 monoclonal antibodies and lymphomas

a. B-cells

B cells are part of the adaptive immunity. They belong to a group of white blood cells called lymphocytes. They can be identified and distinguished from other lymphocytes by the presence in their outer surface of a protein called B cell receptor (BCR).

The principal functions of B cells are:

- produce antibodies against antigens

- perform antigen presentation

- turn into memory B cells specific for an antigen

- secrete immunosuppressive cytokines – IL-10. (Mori *et al.* 2012)

In humans and mice, B cells are produced in bone marrow. They are immature at this stage. They then migrate to the secondary lymphoid tissues (spleen, lymph nodes, etc.) and differentiate into mature B lymphocytes.

Some cells such as dendritic cells (sentinels) or marcrophages or even B cells themselves are called antigen presenting cells (APC). If those cells are in contact with a pathogen, they internalize the pathogen by phagocytosis, digest its proteins and present polypeptides on the MHC class II molecules (Major Histocompatibility Complex) at their membrane surface. Then the APCs migrate to the lymph node to present those antigens to naïve B cells (and T cells).

The presented antigen is internalized by the naïve cell, which becomes activated. Then the naive B cells have the ability to differentiate again in either a memory B cell or a plasma cell. Memory B cells are specific for an antigen. Those cells have a long lifetime and can respond very quickly in the case of a second infection with the same pathogen. As for them, plasma cells have the ability to secrete large amount of antibodies. In the case of the primo infection, the B-cells have to create antibodies specific for the antigen by recombining the genes coding for the antibody protein. After that only, they can replicate and secrete high amount of antibodies. If the antigen has been encountered before, this whole process is by-passed thanks to memory B cells that are specific for this very antigen. This is the principle of vaccination. As previously seen, antibodies are proteins excreted in the vascular system and in the lymphatic system by plasma cells which recognize a precise pattern in a pathogen organism (for instance a membrane protein).

b. Anti-CD20 monoclonal antibodies

In our case, we are working on B-cells lymphomas. B-cells express at their surface the CD20 protein which is membrane spanning protein with 4 membrane crossing domains. This protein is only expressed on B-cells, making it an identification marker of B-cells, and is coded by the *MS4A1* gene. Moreover, CD20 is also present at the surface of tumor B-cells. Interestingly, this marker is expressed on all stages of B cell development except the first and the last. It is thus not present on either early pro-B cells or plasma cells.

Anti-CD20 monoclonal antibodies (Mab) were used in Immunotherapies since the 2000's with very good results in B-cell lymphomas. The most anti-CD20 Mab used until now is the Rituximab

c. Rituximab

Rituximab is an anti-CD20 chimeric monoclonal antibody. Monoclonal antibody means that they are all from the same B-cell clone. Therefore, all the antibodies from a same batch have the same epitope, affinity and avidity.

It is actually very difficult to have human antibodies recognizing human proteins. Indeed, in physiological state, there shouldn't have antibodies against human CD20.

The first step of mAb therapies would have been to use mouse antibodies against human CD20. It is quite feasible: a mouse can be immunized against human CD20 peptides, and the mouse's B-cells specific for CD20 peptides can be harvested in the spleen of the mouse. This way, monoclonal antibodies against human CD20 can be produced. However, a problem still remains; the antibodies are mouse proteins, and will be detected as potential threat by the human immune system. The immune system will react against the antibody and can trigger allergies or other types of responses, even the production of antibodies against the mouse anti-CD20 mAb.

The solution to this problem was the use of chimeric antibodies. As chimera is a mythic monster mixing a goat body, a lion head and snake instead of the tail, a chimeric antibody is a protein that contains polypeptide sequences from different species, almost always human and mouse. The chimeric antibody is an IgG that has a human constant chain, heavy and light (that contains the gamma chain, recognized by the Fcγ Receptor) and a mouse variable chain (that contains the paratopes). It has the great advantage to be more accepted by the host immune system, to have the correct paratope (recognizing human CD20 in this case) and to have the human Fc, which will activate more efficiently the immune system and the effector cells than the mouse Fc.

Rituximab is a chimeric anti-human CD20 monoclonal antibody and has all these advantages.

Nevertheless, there is another category of engineered antibodies which are the humanized antibodies (Figure 3). Unlike chimeric Ab, they only have mouse hyper variable chains, heavy and light (that still contain the paratope). The humanized Ab is almost all human and is even more tolerated by the host than the chimeric antibody. Its efficiency can also be improved due to its longer half-life in the host body (Schneider CK, 2008).

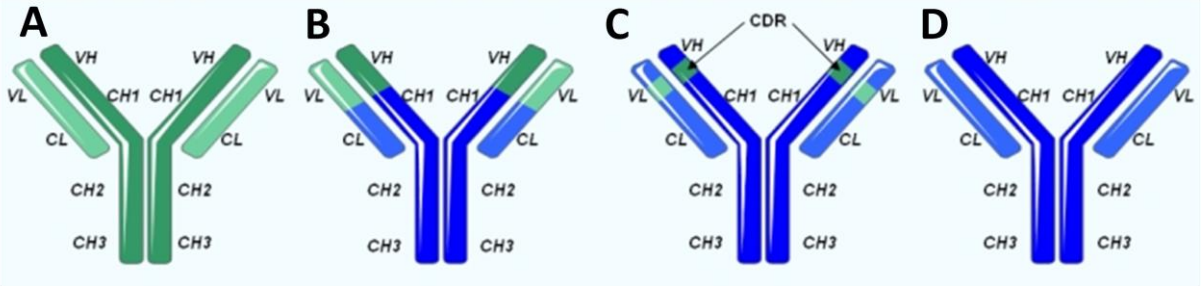

Figure 3: The different classes of therapeutic antibody. A: Mouse antibody. B: Chimeric antibody, the variable chains are mouse chains, but the Fc part is human. C: Humanized antibody, the antibody is almost totally human, only the hypervariable parts are from mouse. D: Human antibody.

As we saw previously, rituximab antibody can induce cell death, can activate complement proteins and can recruit effector cells, antigen presenting cells and activate adaptive immunity.

A lot of clinical trials have been done using rituximab, not only in the case of B-cell lymphomas, but also in lupus (Cobo-Ibañez *et al.* 2014) or rheumatoid polyarthritis (Baji *et al.* 2014), which are autoimmune disease involving B-cells. It has also been tested for multiple sclerosis or chronic lymphoid leukemia (Hauser *et al.* 2008; Hallek *et al.* 2010)

d. Ublituximab

Ublituximab (TGTX-1101) is a chimeric antibody, produced by the LFB (Laboratoire de Fractionnement des Biotechnologies) and owned by TG Therapeutics (New York – USA). It is targeting a unique epitope on the human CD20 antigen, and has been glyco-engineered (low fucose) to enhance affinity for all variants of FcγRIIIA receptors. This antibody is thus developed to enhance ADCC (Le Garff-Tavernier *et al.* 2014).

The laboratory worked very closely to the LFB and we performed pre-clinical studies (on mouse) for this antibody in the treatment of PIOL and PCL. To do so we used mouse models of lymphomas.

1.5.2 TLR-9 agonist CPG-ODN

1.5.2.1. Toll like receptors and cancer

Toll like receptors (TLRs) are membrane-spanning proteins expressed in sentinel cells of the innate immune system like macrophages or dendritic cells.

Those proteins are pattern recognition receptors, and recognize molecular pattern that are shared by a lot of pathogens, quite different from the host molecules. Those molecular patterns are commonly called Pathogen-Associated Molecular Patterns (PAMPs). They can be Lipopolysaccharides (found in the outer membrane of Gram-negative bacteria) or pathogenic RNA/DNA (from virus or bacteria), etc (Kreig AM, 2002).

Some TLRs are located at the membrane of the cell, others are located at the membrane of endosomes; this means that the cell have to capture the pathogen by endocytosis for the receptors to be engaged.

When engaged, those receptors trigger an intracellular biochemical pathway that leads to the expression of inflammatory cytokines (signaling factor), which are necessary for the recruitment of immune effector cells.

TLRs are counted as key molecules for alerting the immune system (effector cells) in case of microbial infection.

There are thirteen different TLRs in humans named from TLR1 to TLR13. Each TLR have a specific ligand and trigger a specific biochemical pathway; however, the intracellular signalization might have common points.

For a long time, the strategy for therapies was to aim and target only tumor cells. Now, we do know that activating the immune system and polarizing the effector cells towards the cancer cell is a strategy that has been shown to be efficient. There are a lot of different ways to activate the immune system in the case of lymphomas therapies; one of them is to engage a toll like receptor to activate the immune system and recruit effector cells (Murad YM *et al.* 2007).

It happens that sometimes cancel cells do express TLRs, especially in the case of a lymphoma. It has been shown that the biochemical pathway induced by the TLR engagement can lead to cancer cell apoptosis (Rym BenAbdelwahed *et al.* 2013).

Today, some treatments for melanomas – Immiquimod (Fields *et al.* 2014), skin cancer or cutaneous T-cell lymphomas use this strategy of both recruiting effector cells and triggering apoptosis in cancer cells, with very good results (Huen *et al.* 2014) .

1.5.2.2. TLR-9 and its ligands

TLR9 belongs to the toll like receptors family. It is a protein also designated as the cluster of differentiation 289 (CD289) encoded by the *TLR9* gene.
TLR9 recognizes unmethylated CpG sequences in DNA (both in human and mouse). As a matter of fact, CpG sites are rare (1%) in the human or mouse genome, in comparison to bacterial genomes or virus DNA, thus making CpG a PAMP.

1.5.2.3. ODN-CPG

CpG is a ligand for TLR-9, a receptor present in the endosomes of different immune cell populations. This receptor recognizes single-strand DNA patterns from pathogenic microorganisms.

Oligodeoxynucleotides CpG (ODN-CPG) are short single-stranded DNA molecules. Those synthetic molecules contain a cytosine triphosphate deoxynucleotide ('C') followed by a guanine triphosphate deoxynucleotide ('G') linked together with a phosphodiester ('p'). Unmethylated, those CpG motives are immunostimulants.

Different types of CpG-ODN sequences exist (*e.g.* CpG 7909), but only nuclease-stable phosphorotioate-modified CpG 1826 (CpG) will be introduced.

CpG sequence: 5_-TCCATGA**CG**TTCCTGACGTT

(the bold and underlined nucleotides represent the immunostimulatory CpG sequence)

The control for CpG 1826 is the ODN-ctrl, which also is a single-stranded DNA molecule, identical to CpG 1826 except for the immunostimulatory CG sequence which is inverted, making thus ODN-ctrl a molecule that does not bind TLR-9.

ODN-ctrl sequence: 5_-TCCATGA**GC**TTCCTGAGCTT

N.B.: In this manuscript, CpG-ODN will refer to CpG 1826

1.6. Murine models of lymphomas by cell engraftment.

Murine models are a powerful tool for understanding biological complex mechanisms. It is even an indispensable tool for searchers.

Cancer is a very complex disease; there are a lot of interactions between immune system, tumor cells, metabolism enhancers etc. To study those mechanisms, there are different types of models by engraftment: syngeneic models, allogeneic models and xenogeneic models.

Those models are actually related to the gene background of both grafted cells and animals. In small animal experimentation, to limit variability, the animals belong to a line of mice – these lines are called "strain" not to be confused with strain in the following biofluidics part. This means that they all have the same genome. BALB/c is for instance an albino mouse quite used, whereas C57BL/6 is one of the most used mouse strain.

Syngeneic model: Cells and animals have the same gene background. For example, let's consider the BALB/c strain: injecting tumor cells that initially came from a BALB/c mouse is a syngeneic model. Cells and mouse have the same Major Histocompatibility Complex (MHC), and the tumor cells will not be rejected from the host mouse.

Allogeneic model: Cells and animals have different gene background but they belong to the same species. For instance, let's still consider a BALB/c strain: injecting tumor cells coming from a C57BL/6 mouse in a BALB/c is called an allograft. As the MHC molecules are different, the mouse may reject tumor cells.

Xenogeneic model: Cells and animals do not belong to the same species. For instance, injecting human cells in mouse whatever would be its gene background is called a xenograft. In normal conditions, the mouse would reject tumor cells.

In the case of allogeneic and xenogeneic models, an immunocompetent host will reject the tumor whereas in the case of syngeneic, no reject occurs. This is the reason why almost all allogeneic and xenogeneic models are developed with immunodeficient mice. Those models are widely used to characterize human tumor cells lines harvested on patient. The most famous is HeLa (Scherer *et al.* 1953). However, these models have disadvantages; they don't allow the study of interactions between immune system and tumor cells.

N.B.: In this manuscript, when "syngeneic models" will be presented or discussed, it will actually refer to the fact that the non-syngeneic models are associated to immunodeficient mice.

The table 2 hereafter (Donnou *et al.* 2012), gives a very complete overview of the different types of lymphomas mouse models by engraftment. The injection site, name of cells, lymphoma model, strain, and immune status are precised here.

The models used in the laboratory are highlighted in the table with the red boxes. The strain used is BALB/c and the cells used are A20.IIA-GFP (Touitou *et al.* 2008). A20.IIA-GFP cells originate from A20 cells, a reticulum cell sarcoma of an old BALB/c mouse. The reticulum cell sarcoma is also known as histiocytic lymphoma, which is a rare subtype of NHL characterized by the presence of large tumor cells resembling histiocytes* morphologically but considered to be of lymphoid origin. A20.IIA is an FcγR negative clone from A20. The cells have been transduced to express GFP, humanCD20 or both of them. In the table, only three of our models are described, however a forth model of subcutaneous lymphoma was set up in between (Ben abdelwahed *et al.* 2013).

*a histiocyte is a macrophage of conjonctive tissue

Induced models of B-cell lymphoma. (m): murine origin; (h): human origin; (i): syngeneic models; (ii): syngeneic models with murine tumor cells engineered to express human antigens; (iii): xenogenic models; (iv): humanized models; CLL: chronic lymphocytic leukemia; DLBCL: diffuse large B-cell lymphoma; MALT: mucosa associated lymphatic tissue; n.d.: not determined; PCL: primary cerebral lymphoma; PCNSL: primary central nervous system lymphoma; PIOL: primary intraocular lymphoma; SCID: severe combined immune deficiency.

Injection site	Name	Lymphoma model	Recipient mice			Major reference
			Strain (haplotype)	MHC compatibility	Immune status	
Intravenous	B6 spontaneous model (m)	High-grade B lymphoma	C57Bl/6 (H-2^b)	Syngeneic (i)	Immunocompetent	[51]
	Pi-BCL1 (m)	DLBCL	BALB/c (H-2^d)	Syngeneic (i)	Immunocompetent	[52]
	38C13 (m)	Non-Hodgkin lymphoma	C3H/HeN (H-2^k)	Syngeneic (i)	Immunocompetent	[53]
	FL5.12 transfected by Bcl2 (m)	Non-Hodgkin lymphoma	BALB/c (H-2^d)	Syngeneic (i)	Immunocompetent	[42]
	A20 (m)	DLBCL	BALB/c (H-2^d)	Syngeneic (i)	Immunocompetent	[54]
	4TOO (m)	n.d.	BALB/c (H-2^d)	Syngeneic (i)	Immunocompetent	[55]
	BCL1 (m)	CLL	BALB/c (H-2^d)	Syngeneic (i)	Immunocompetent	[56]
	38C13 Her2/neu (m)	Non-Hodgkin lymphoma	C3H/HeN (H-2^k)	Syngeneic (ii)	Immunocompetent	[40]
	Z138 (h)	Human mantle cell lymphoma	SCID mice (H-2^d)	Xenogenic (iii)	Immunodeficient	[57]
	BJAB (h)	Burkitt lymphoma	SCID mice (H-2^d)	Xenogenic (iii)	Immunodeficient	[58]
	SU-DHL-4 (h)	DLBCL	SCID mice (H-2^d)	Xenogenic (iii)	Immunodeficient	[59]
Intrasplenic	A20 (m)	DLBCL	BALB/c (H-2^d)	Syngeneic (i)	Immunocompetent	[60]
	A20.IIA-GFP (m)	DLBCL	BALB/c (H-2^d)	Syngeneic (i)	Immunocompetent	[50]
Subcutaneous	LY-ar or LY-as (m)	n.d.	C3Hf/kam (H-2^k)	Syngeneic (i)	Immunocompetent	[37]
	S11 (m)	Burkitt lymphoma	BALB/c nude (H-2^d)	Syngeneic (i)	T-cell deficiency	[62]
	LMycSN-p53null (m)	Non-Hodgkin lymphoma	C57Bl/6 (H-2^b)	Syngeneic (i)	Immunocompetent	[18]
	A20 (m)	DLBCL	BALB/c (H-2^d)	Syngeneic (i)	Immunocompetent	[63]
	38C13 Her2/neu (m)	Non-Hodgkin lymphoma	C3H/HeN (H-2^k)	Syngeneic (ii)	Immunocompetent	[40]
	Myc5-M5 (m)	n.d.	SCID mice (H-2^d)	Allogenic	Immunodeficient	[17]
	Splenic Hodgkin lymphoma cells (h)	Hodgkin disease	Nude mice (H-2^b)	Xenogenic (iii)	T-cell deficiency	[64]
	Human hodgkin cell line (h)	Hodgkin disease	SCID mice (H-2^d)	Xenogenic (iii)	Immunodeficient	[47]
	Ramos (h)	Burkitt lymphoma	SCID mice (H-2^d)	Xenogenic (iii)	Immunodeficient	[58]
	BJAB (h)	Burkitt lymphoma	SCID mice (H-2^d)	Xenogenic (iii)	Immunodeficient	[58]
	SC-1 (h)	Follicular lymphoma	SCID mice (H-2^d)	Xenogenic (iii)	Immunodeficient	[58]
	DoHH-2 (h)	Follicular lymphoma	SCID mice (H-2^d)	Xenogenic (iii)	Immunodeficient	[58]
	SuDHL-4 (h)	DLBCL	C.B-17 SCID mice (H-2^d)	Xenogenic (iii)	Immunodeficient	[65]
	Granta 519 (h)	Mantle cell lymphoma	C.B-17 SCID mice (H-2^d)	Xenogenic (iii)	Immunodeficient	[65]
	HKBML (h)	Brain DLBCL	C.B-17 SCID mice (H-2^d)	Xenogenic (iii)	Immunodeficient	[46]
	Daudi (h)	Burkitt lymphoma	SCID/beige mice (H-2^d)	Xenogenic (iv)	Partially rebuilt	[66]
	Jijoye (h)	Burkitt lymphoma	SCID/beige mice (H-2^d)	Xenogenic (iv)	Partially rebuilt	[66]
Intracerebral	A20.IIA-GFP (m)	PCL (PCNSL)	BALB/c (H-2^d)	Syngeneic (i)	Immunocompetent	[50]
	38C13 CD20$^+$ (m)	PCL (PCNSL)	C3H/HeN (H-2^b)	Syngeneic (ii)	Immunocompetent	[68]
	Raji (h)	PCL (PCNSL)	Nude mice (H-2^b)	Xenogenic (iii)	T-cell deficiency	[69]
	Patient's cells (h)	PCL (PCNSL)	Nude mice (H-2^b)	Xenogenic (iii)	T-cell deficiency	[70]
	MC116 (h)	PCL (PCNSL)	Nude rats (RT1^u)	Xenogenic (iii)	Immunodeficient	[71]
Cisterna magna	L1210 (m)	Leptomeningeal metastases	DBA/2 (H-2^d)	Syngeneic (i)	Immunocompetent	[72]
Intraocular	A20.IIA-GFP (m)	PIOL	BALB/c (H-2^d)	Syngeneic (i)	Immunocompetent	[45]
	38C13 CD20$^+$ (m)	PIOL	C3H/HeN (H-2^b)	Syngeneic (ii)	Immunocompetent	[68]
	CA46 (h)	PIOL	SCID mice (H-2^d)	Xenogenic (iii)	Immunodeficient	[73]

Table 2: From Donnou et al. Different murine of lymphomas according to the cell type and to the tumor location

2. PART II: NON-INVASIVE OPTICAL METHODS FOR *IN VIVO* OF DETECTION OF CNS LYMPHOMA CELLS AND MONITORING TREATMENT EFFECTS IN SMALL ANIMAL

There are several techniques for detection of PCNSL cells. We wanted non-invasive techniques so we could study the effect of treatments over time and not only at a given time point. We wanted to combine two methods to address two questions: the localization of the primary tumor and the metastases, and the way cells metastasize from the primary tumor to the metastases.

The real problem with CNS lymphoma is the fact that unlike nodal lymphomas, it is not really a solid tumor. It usually is disseminated all over the organ. For instance, the cells are not only lying on the retina in the case of PIOL, but they are in the whole eye (Touitou et al, 2008) from the vitreous to the anterior chamber. This is also the case for PCL where the cells are indeed disseminated in all the brain, making that lymphoma very hard to treat. And as we saw, the only way to be sure the radiotherapy treatment is efficient is to perform whole brain irradiation, because the tumor cannot be clearly located.

Before getting into the substance of imaging and detection techniques, I will present some reminders about several optical phenomena and biofluidics.

2.1. Optical phenomena backgroud

2.1.1. Bioluminescence

Bioluminescence is a light-based phenomenon. It involves a chemical reaction between a substrate and an enzyme – that is why it has the 'bio' prefix. The enzyme is produced by different animals in nature and is called luciferase. The most known animal that produces bioluminescence is the firefly (Gould *et al.* 1988). Yet, other animals like sea pansy – Renilla – can produce their own luciferase and thus bioluminescence (Shimomura O, 1985). Some fishes for instance, belonging to the lophiiforms family, uses bioluminescence to catch their prey. They have a little appendix on their head, which is full of bioluminescent bacteria and the light produced by this appendix attracts the prey. Those fishes do not produce luciferase but live in symbiosis with bacteria which produce luciferase and its substrate: luciferin (Baldwin *et al.* 1995).

Bioluminescence systems require a luciferase and a luciferin (substrate) and molecular oxygen to produce light (Figure 4).

Luciferin + O_2 -> Oxyluciferin*

Oxyluciferin* -> Oxyluciferin + light

Thus, luciferase can be considered as an oxygenase that oxidizes luciferin with molecular oxygen. (Inouye *et al.* 1997; Day *et al.* 2004)

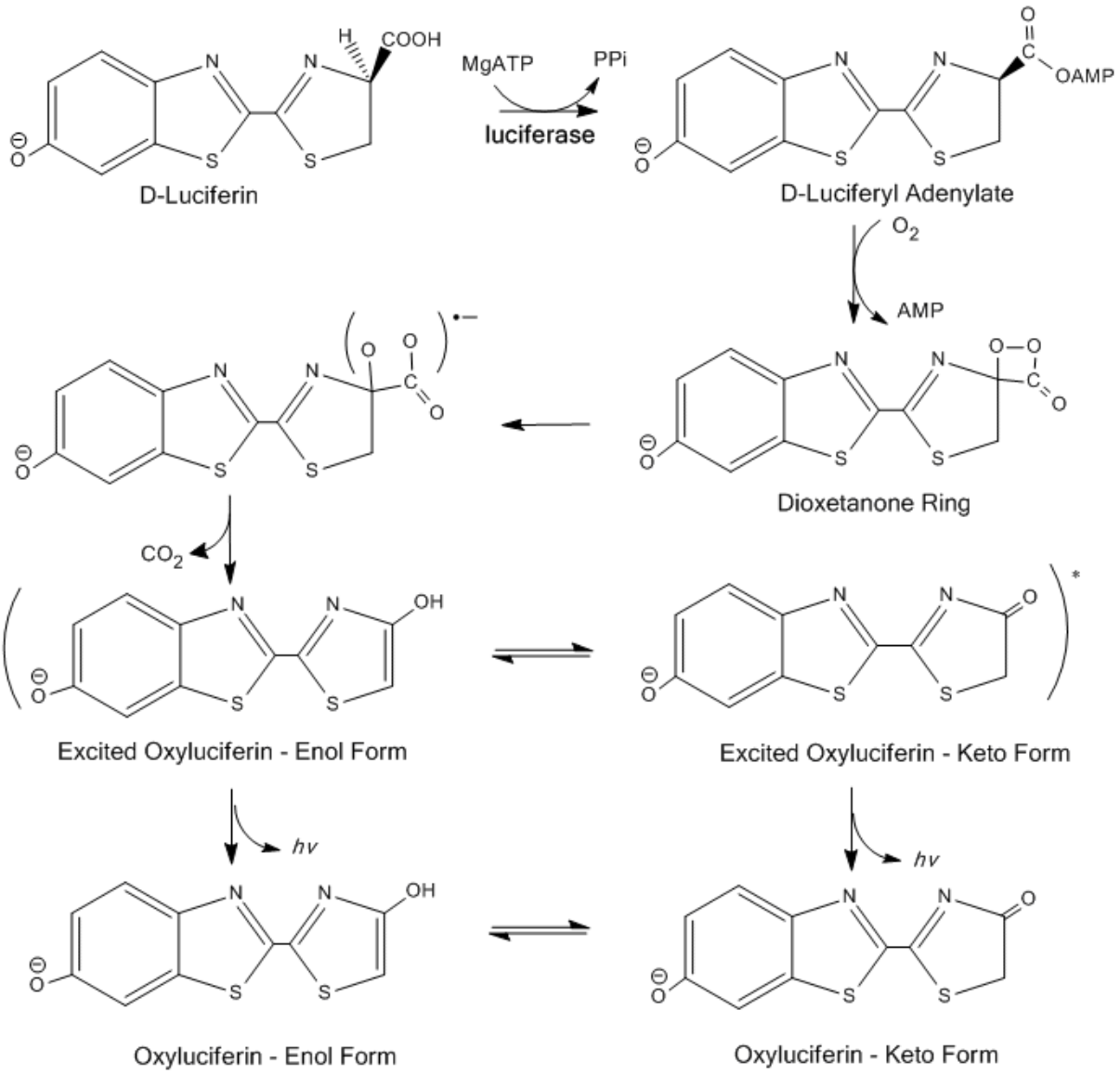

Figure 4: Here is the complete chemical mechanism of luciferase-luciferin reaction. This reaction requires ATP, Mg^{2+} cofactor and a molecule of Oxygen, O_2. One could see that this mechanism is dual due to a mesomer form of a reaction intermediate.

Actually, the chemical reaction of oxygenation of the luciferin gives to the product (oxyluciferin) a high amount of energy. Oxyluciferin gets rid of this energy by emitting a luminescence photon and

thus comes back to its fundamental energy state. As this luminescence chemical reaction involves a protein, it is called bioluminescence.

The substrate depends on the used luciferase. For instance the substrate for firefly luciferase is luciferin, whereas the substrate for Renilla luciferase is the coelenterazine (which is also the substrate for other photoproteins such as aequorin). The emission wavelength also depends on the substrate and on the oxygenase. For instance, luciferin and firefly luciferase gives the color of shining fireflies, which is mostly green. However, Renilla luciferase (Renilla is also known as see pansy) and other proteins from marine animals, whose substrate is coelenterazin emits mostly blue photons, which are indeed the photons that are less absorbed by water (Inouye *et al.* 1997).

In order to perform imaging of living tissue, the emitted photons must not be absorbed by the nearby tissues. It turns out that red is less absorbed that green, which is himself less absorbed than blue – by the nearby tissue. We thus chose to use firefly luciferase for bioluminescence imaging as red luciferase has not yet been discovered nor developed.

2.1.2. Fluorescence

Fluorescence is an optical phenomenon that involves electronic energy transfer within a molecule (which can be a protein). Every molecule has a lowest energy level, and whatever can be done to this molecule, it will always tend to return to its lowest energy level, called the fundamental state.

There are a lot of ways to get a molecule out of its fundamental state, but they all require energy. In the case of fluorescence, the energy is carried by photons (elementary particle of light).

In other words, a photon can be absorbed by a fluorescent molecule – the photon is then called “excitation photon”. The energy carried by the excitation photon is transferred to the fluorescent molecule and allow some electrons to leave the fundamental state, and to access higher discrete energy levels. Those electrons cannot stay in this high energy level. Very quickly (about 10ns), they go back to their fundamental state, and return the received energy by emitting a new photon, which is called “emission photon” or “fluorescence photon”.

This photon has several properties: it cannot have more energy than the excitation photon (energy cannot be created). When excitation energy is transferred to the molecule, several phenomena actually happen at the same time. The molecule dissipates energy in rotation and vibration, resulting in a lower amount of energy available for the fluorescence photon. The fluorescence photon is thus always lower in energy than the excitation photon in the case of one-photon fluorescence (Figure 5).

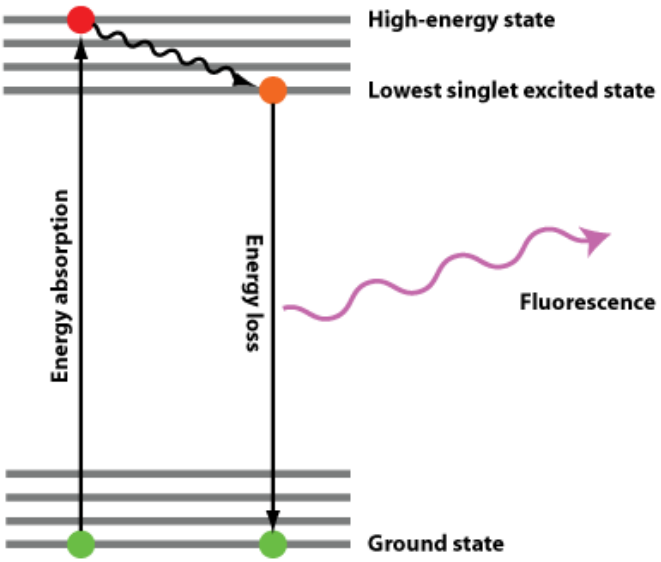

Figure 5: Energy diagram of a fluorescent molecule excited. Energy is absorbed and allows electrons to access a higher level of energy. A part of this energy is lost in vibration transitions and finally the electrons go back to the fundamental state, emitting a fluorescence photon.

As E= h*C/λ where E is energy and C is speed of light and h is plank constant, and λ is the wavelength; the fluorescence photon have a higher wavelength, corresponding with lower energy.

$\lambda_{excitation} < \lambda_{emission}$

The excitation light source is often a laser in the case of fluorescence applied to biology. The laser has the advantage to be monochromatic, which means that all the photons have the same wavelength. However, a molecule – even more a protein – has a lot of atoms and electrons. Thus there is a lot of degenerated energy level available. That would explain why fluorescent molecules (including proteins) have a continuous spectrum and not a line spectrum.

The fluorescence phenomenon is always present and even molecules that are not told to be fluorescent can be fluorescent. A fluorescent molecule is actually a molecule in which the fluorescence phenomenon is preponderant. It can be quantified by comparing the "quantum yield".

The quantum yield is the number of times a specific event occurs (a fluorescence photon is emitted) per photon absorbed by the system. In other words, if the quantum yield is equal to 1, it means that all the photon absorbed result in an emitted fluorescence photon.

For GFP* (green fluorescent protein), the quantum yield is 0.74 (Shaner *et al.* 2005), which means that if the one GFP absorbs 100 excitation photons, it will returns 74 fluorescence photons.

The quantum yield must not be confused with the cross section. Cross section is actually the probability that the fluorescent molecule absorbs excitation photons. The cross section is often expressed in cm^{-2} and does depend on the size of the molecule.

Prior to using a fluorescent dye, a study must be done about the quantum yield, the spectra (excitation and emission spectrum), the cross section and the nature of the dye – organic small molecule (ie: fluorescein, rhodamin, etc.) or protein (GFP, YFP, CFP, mCherry, etc.).

Fluorescence can be easily found in nature. A lot of fluorescent proteins come from animals. For instance, the GFP was first isolated from the jellyfish *Aequoria Victoria (Shimomura et al. 1962)*.

The cuticle of scorpions (Figure 6) contains fluorescent molecules such as beta-carboline that are fluorescent under certain wavelenght of UV light.

Figure 6: Scorpios are naturally fluorescent under UV-light. It is a good mean to find them!

Photobleaching

Photobleaching is the photochemical destruction of a fluorescent molecule; this becoming optically inactive. Some molecules are more sensitive to photobleaching than others.

The signal from fluorescence varies proportionnaly with excitation light (fluorescence is a linear phenomenon). The more excitation light, the more fluorescence signal. However, the more excitation light, the more photobleaching.

Photobleaching must always be taken into account for designing fluorescence-based assays. The ways to control photobleaching is to reduce excitation intensity, or to increase the number or dyes. To a reasonable approximation, a given molecule will be optically inactive after a constant exposure because each absoption emission cycle has an equal probability of causing photobleaching.

GFP – Green Fluorescent Protein

GFP is the most known fluorescent protein. It is composed of 238 amino acid (26.9 kDa) and exhibits bright green fluorescence when exposed to light from blue to UV wavelengths (Prendergast *et al.* 1978; Tsien 1998). GFP refers to the first fluorescent protein isolated from the jellyfish *Aequoria*

victoria. The GFP from *A.victoria* has a major excitation peak at 395 nm and a minor one at 475nm; the emission peak is at 509nm.

The GFP gene can be introduced into organisms and maintained in their genome. This gene thus became a new reporter of expression. It has been introduced in almost all cells or animals used for biologic models (bacteria, yeast, fly, plant etc.).

Many different mutants of GFP have been engineered. The first major improvement was a mutation (S65T) reported in 1995 by Roger Tsien team (Heim *et al.* 1995). This mutation improved dramatically the optical characteristics of GFP, increasing fluorescence, photostability and shifting the major excitation peak at 488nm, making GFP suitable for FITC (a wide used fluorescent marker) filters sets. A second mutation (F64L) to this enhanced GFP (EGFP) was discovered in 1995 (U.S. patent 6172188 ; Cormack *et al.* 1996) allowing the use of GFP in mammalian cells.

Many other mutations have been made, especially color mutants in particular blue fluorescent protein (BFP), cyan fluorescent protein (CFP) and yellow fluorescent protein (YFP). Those proteins have shifted spectrum making the simultaneous expression of fluorescent proteins detectable (Table 3). The maximum emission peak of EGFP, at 509nm wavelength, corresponds to absorption maximum of hemoglobin, making GFP difficult to detect for *in vivo* imaging. The use of recent red-shifted protein as mKate could resolve this problem.

mKate and mKate2

Mkate (also known as TagFP635 for Tag Fluorescent Protein 635) is a monomeric far-red fluorescent protein from the wild-type red fluorescent protein (RFP) from sea anemone *Entacmaea quadricolor* (Shcherbo *et al.*, 2007; Shcherbo *et al.* 2009). It possesses far-red fluorescence (Figure 7) with an excitation peak at 588nm (yellow-orange) and an emission peak at 635 nm (red). Like EGFP, the mKate gene can easily be cloned, and included within a plasmid or within a virus to stably transform mammalian cells.

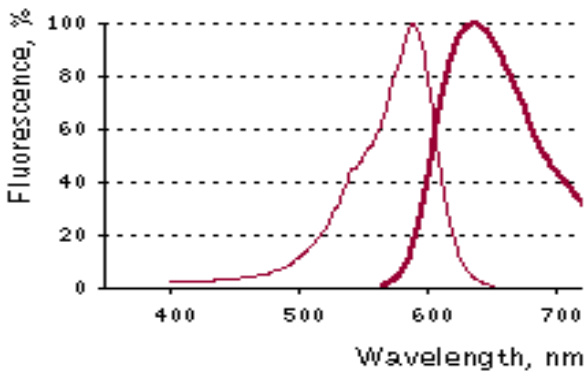

Figure 7: Absorption and emission spectra of TagFP635 (aka mKate). Normalized excitation (thin line) and emission (thick line) correspond to wavelength suitable with in vivo imaging.

The mKate2 protein belongs to the next generation of TagFP635 (mKate). It possesses an excitation peak at 588 nm and emission peak at 633nm. It has better photostability and brightness than mKate.

Table 1 | Properties of the best FP variants[a,b]

Class	Protein	Source laboratory (references)	Excitation[c] (nm)	Emission[d] (nm)	Brightness[e]	Photostability[f]	pKa	Oligomerization
Far-red	mPlum[g]	Tsien (5)	590	649	4.1	53	<4.5	Monomer
Red	mCherry[g]	Tsien (4)	587	610	16	96	<4.5	Monomer
	tdTomato[g]	Tsien (4)	554	581	95	98	4.7	Tandem dimer
	mStrawberry[g]	Tsien (4)	574	596	26	15	<4.5	Monomer
	J-Red[h]	Evrogen	584	610	8.8*	13	5.0	Dimer
	DsRed-monomer[h]	Clontech	556	586	3.5	16	4.5	Monomer
Orange	mOrange[g]	Tsien (4)	548	562	49	9.0	6.5	Monomer
	mKO	MBL Intl. (10)	548	559	31*	122	5.0	Monomer
Yellow-green	mCitrine[i]	Tsien (16,23)	516	529	59	49	5.7	Monomer
	Venus	Miyawaki (1)	515	528	53*	15	6.0	Weak dimer[j]
	YPet[g]	Daugherty (2)	517	530	80*	49	5.6	Weak dimer[j]
	EYFP	Invitrogen (18)	514	527	51	60	6.9	Weak dimer[j]
Green	Emerald[g]	Invitrogen (18)	487	509	39	0.69[k]	6.0	Weak dimer[j]
	EGFP	Clontech[i]	488	507	34	174	6.0	Weak dimer[j]
Cyan	CyPet	Daugherty (2)	435	477	18*	59	5.0	Weak dimer[j]
	mCFPm[m]	Tsien (23)	433	475	13	64	4.7	Monomer
	Cerulean[g]	Piston (3)	433	475	27*	36	4.7	Weak dimer[j]
UV-excitable green	T-Sapphire[g]	Griesbeck (6)	399	511	26*	25	4.9	Weak dimer[j]

Table 3: Properties of best fluorescent protein variants. Excitation and emission wavelengths, brightness and photostability must be chosen very carefully for in vivo experiments. From Shaner et al.

2.1.3. 2-photon absorption

Unlike single photon fluorescence, two-photon absorption (TPA) belongs to the group of non-linear optical processes. This phenomenon was predicted in 1931 by Maria Goeppert-Mayer (Goeppert-Mayer M, 1931– Nobel Laureate).

TPA is actually the simultaneous absorption of two photons of identical or different wavelength to excite a single molecule from its ground state to a higher energy electronic state. The energy between those two states must be equal to the sum of the energy of the two incident photons. Usually, TPA is per performed with two identical photons (same wavelength).

In that case, the energy of the gap is equal to twice the energy of the photons (Figure 8).

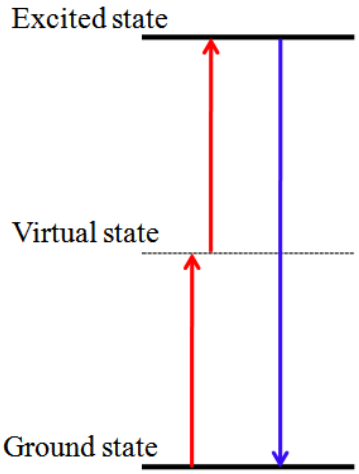

<u>Figure 8:</u> Energy diagram of 2-photons absorption. 2 photons have to be at the same time at the same place, and be exactly half the required energy to trigger 2-photons absorption. This phenomenon is rare, and that is why high frequency (femtosecond) pulsed laser are used for 2-photons microscopy.

For TPA, the Beer's law (1) becomes a relation (2) that expresses the output intensity as a function of cross section x (probability that TPA occurs at the molecule level), of concentration c, and of β, the TPA coefficient. The TPA coefficient may vary according different parameters such as input light frequency, the density of molecules or the incident photon energy.

$$I(x) = I_0 e^{-\alpha c x} \quad (1)$$

$$I(x) = \frac{I_0}{1+\beta c x I_0} \quad (2)$$

However, the probability that TPA occurs remains quite low. A high spatial and temporal coherence is required for the input light source to obtain TPA. In other words, a lot of photons have to be at the same place at the same moment. Only very high instant power pulsed laser fit those conditions. Usually each pulse last for less than 10 ps and can reach an instant power of several Watts whereas in conventional flow cytometry or confocal microscopy, lasers are continuous with an average power of several milliwatts.

Most of living tissues are not transparent to visible wavelengths. For common fluorophores (GFP, rhodamine, alexa fluor, etc.) TPA is possible. As the incident energy have to be twice as less as the one photon absorption energy would be, the corresponding wavelengths are in the infrared domain of radiation, in which living tissues show good transparency (Tseng *et al.*). For instance, for GFP

excitation, at 488nm (GFP maximum excitation wavelength - blue) the radiation penetrates several micrometers; but, at 976nm (infrared) the radiation penetrates several **hundreds** of micrometers (Padmanabhan *et al.* 2010).

Due to its good penetration in living tissues, the infrared domain offers very interesting possibilities. That is why two photons fluorescence is widely used for intra-vital microscopy.

2.1.4. Photoacoustic imaging

Photoacoustic imaging (PAI) is a hybrid biomedical imaging modality. It relies on the photoacoustic effect first described in 1979 (Ducharme *et al.*, 1979) to perform spectroscopy on condensed matter.

A laser is focused on living tissues and softly warms them. The increase of the temperature is very low (a fraction of degree) but sufficient to induce a brief thermoelastic expansion of cells and thus a wideband ultrasonic emission.

This technique is widely used for tumor imaging and is currently a very promising technique that can be made portable and compatible with existing imaging techniques. Moreover, it uses nonionizing radiation, and does not necessarily rely on exogenous imaging agents. PAI has been described for tumor imaging of breast, lymph nodes, skin, thyroid, eye, prostate, ovaries, bladder, and for circulating tumor cells detection (Zackrisson *et al.*, 2014).

Photoacoustic flow cytometry was described by V. Zharov's team in 2007 (Zharov *et al.*, 2006; Galanzha *et al.*, 2007; Zharov *et al.*, 2007) and is very promising for efficiently detecting circulating tumor cells. The ultrasonic transducer detects the acoustic waves created by the laser-illuminated flowing cells (Figure 9). CTCs can thus be detected and may be identified according to their signature.

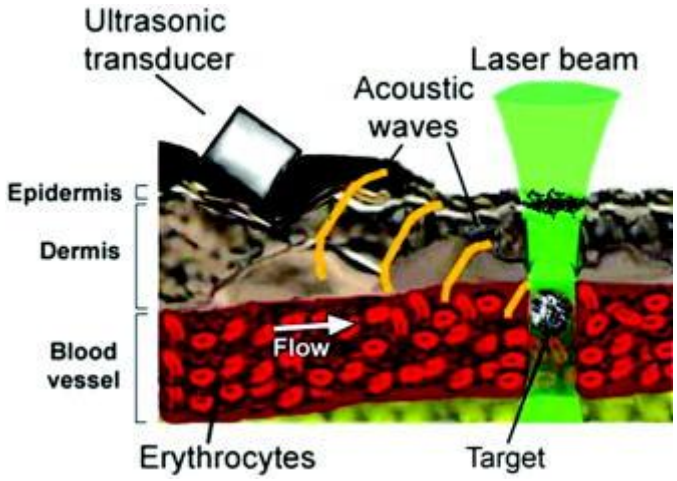

Figure 9: In vivo Photo Acoustic Cytometry principle. The laser beam warm the flowing cell. The subsequent dilatation of cells produces an acoustic wave that can be detected. From Zharov et al.

2.2. Biofluidics and fluid mechanics background

2.2.1. Rheology and Poiseuille flow

Rheology is the study of the flow of matter, mostly in the liquid state. However, it applies to 'soft solids' or substances that have a complex microstructure and respond with plastic flow to an applied force. The study of biological fluids such as blood or lymph is also a part of rheology.
Fluids are mainly characterized by their viscosity, and rheology precisely studies how viscosity can be modified by the environment of the fluid.
Viscosity of Newtonian fluids depends only on the temperature but does not depend on the relative velocity of the flow. This is the case of water viscosity for instance, thus making water a Newtonian fluid. Only a small group of fluids have this property.
On the other hand, non-Newtonian fluids are fluids whose viscosity depends on the strain rate or on the stress – force per surface unit – applied on the fluid. This is the case for instance of ketchup; its viscosity can be reduced by shaking.

Suspensions of particles whatever would be the suspending medium, have viscosity depending on the concentration. This is the case for blood.
We are interested in biologic fluids; they are submitted to a very large panel of conditions in the body. Blood can flow in either very large arteries (more than 1 cm diameter) or very small capillaries (less than 10µm diameter). It will have very different behavior according to its environment. Moreover, blood is a fluid that has a complex microstructure because it is carrying particles. The concentration of particles carried by blood is a key parameter for its viscosity (Einstein A, 1906; Quemada D, 1981;Brouwers HJ, 2010).

Blood is non-Newtonian fluid and its viscosity is an inherent property. However, the diameter of the vessels in which it circulates has an influence on the flow characteristics. The diameter of the vessel will change the shear stress and thus the velocity profiles.

2.2.2. Viscosity and cell concentration

The relation between viscosity and concentration of spherical rigid monosized particles (an approximation that can be done in our work) is expressed by calculating the relative viscosity μ_r. It is

the ratio between fluid viscosity with particles and pure fluid viscosity. μ_r is a function of the particle volume concentration, Φ, and the particle shape.

$$\mu_r = \frac{\mu_{susp}}{\mu_{pure}}$$

Where μ_{susp} is the viscosity of the particle suspension and μ_{pure} is the viscosity of pure fluid.

Einstein showed in 1906 that the relative viscosity can be expressed as follow:

$$\mu_r = 1 + k.\phi$$
$$k = 2.5 \; for \; spherical \; particles$$

Where Φ is the particle volume concentration and k is a coefficient that depends on the particle shape.

Calculation of a cell suspension relative viscosity μ_r:

B Lymphoma cell-lines (both murine and human) can be fairly considered as spherical and their diameter is between 7 to 15µm.

We would take 7.5µm for the radius, which corresponds to the upper threshold of the size range.

Our experiments were done at concentrations that never exceeded 1.10^6 per mL so we chose this concentration for validating the hypothesis.

Let's calculate Φ:

The volume of those cells is: $1.10^6 \times \frac{4}{3}\pi(7,5.10^{-6})^3 = 1.8.10^{-9}\,cm^3$

Φ = Volume of cells / Volume of fluid

$= 1.8.10^{-9} / 1$

$$\mu_r = 1 + 2.5 \times 1.8\,10^{-9} \approx 1$$

The cell suspension viscosity at this cell concentration is almost not different that the pure fluid viscosity.

A cell suspension at 1.10^6 cells per mL in PBS can be considered as a non Newtonian fluid whose viscosity is equal to PBS viscosity.

As long as we considerate a channel whose diameter does not imposes the cell to change shape, the aforementioned approximation remains true.

Other models have been proposed to calculate the viscosity of fluid containing particles, especially Quemada's model (Quemada D, 1981; Quemada D, 1986). This model gives very similar results for

low concentrations. It is based on the decomposition of the "k" factor. That way, it covers more situations, and is particularly adapted for blood flow conditions.

2.2.3. Velocity profiles in Poiseuille flow

The fact that the cell suspension can be considered as a Newtonian fluid also means that the flowing cells (at this concentration) can then be considered as fluid particles (related to the *continuum hypothesis** in fluid mechanics). Therefore the cells suspension will obey the Navier-Stokes equations (rule fluid flow), which are in a way the mirror image of the fundamental principle of dynamics describing the Newton's point mechanics.

$$\rho \frac{Dv}{Dt} = -\overrightarrow{grad}\, P + \rho f_{visc} + \rho f_{gr}$$

ρ is the fluid density, Dv/Dt is the substantive derivative (also called the material derivative), v is the velocity vector, f_{visc} is the volumic density of viscosity forces, f_{gr} is the volumic density of gravity forces and P is a pressure. Dv/Dt = 0 in non-time dependant flow in a rectiline tube.

The geometry of the tube provides cylindrical symmetry, thus the velocity only depends on the radial position. Navier-Stokes equation is integrated (constant flow rate condition) in a tube knowing that the velocity only depends on r, and that the velocity of the edges is zero (the inner surfaces stay immobile): the velocity of the fluid is described by a parabolic profile (Poiseuille flow – Figure 10).

The velocity follows this law:

$$v(r) = v_0 \left(1 - \frac{r^2}{R^2}\right)$$

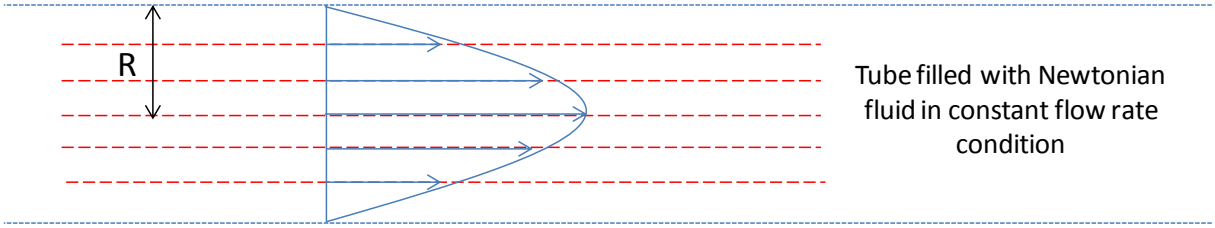

Figure 10: Velocity profile of Poiseuille flow

Where v_0 is the velocity at the middle of the tube (r=0). It happens that v_0 is the maximum speed of the fluid. R is the radius of the tube, and r is the radial position of the considered fluid particle or

monosized particle in the conditions where it can be considered as a fluid particle (Happel *et al.*, 1983; Richardson, 1989).

To consider the flow as a Poiseuille flow, in which we can apply those equations, we have to ensure several conditions:

- The flow must be permanent and laminar (non-turbulent)
- The suspending medium must be Newtonian
- The particle concentration should not be too high to prevent non-Newtonian behavior of the fluid

2.2.4. Shear forces

The shear forces are the forces that the different layers of a flowing fluid apply to each other.

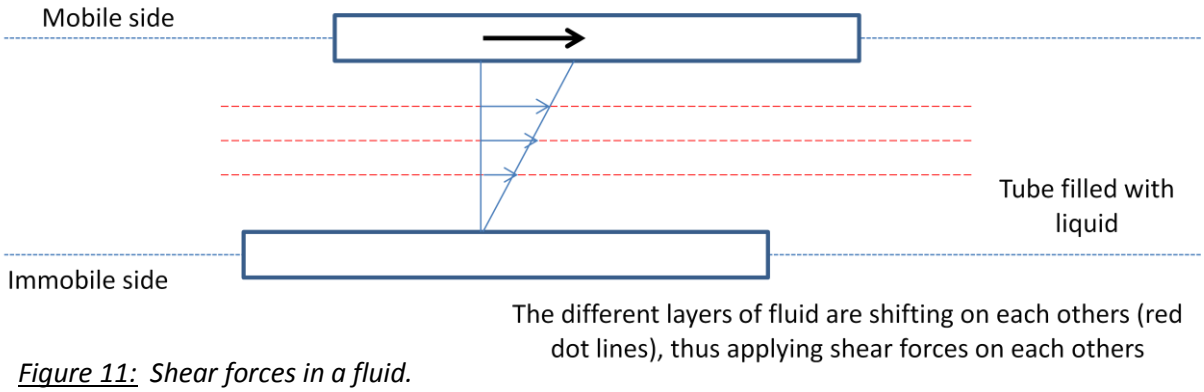

Figure 11: Shear forces in a fluid.

The shear forces per surface unit (called shear stress) depend on the difference of velocity between the "fluid layers" (Figure 11). In the case of cylindrical symmetry, in a blood a vessel, it depends on the difference of velocity along the radius of the vessel.

Shear forces are given by: $$\tau = \mu \frac{dv}{dr}$$

In the case of Poiseuille flow, $$\tau = \mu \left| \frac{d\left(v_0 \left(1-\frac{r^2}{R^2}\right)\right)}{dr} \right|$$

$$\tau = \mu \frac{2v_0 r}{R^2}$$

The shear stress is maximum when r is high, in other words, when r =R, at the inner surface of the tube. The shear forces increase with velocity and viscosity, and for cells, they must not be too high otherwise the cell could explode. Of course this case never happens in blood, but could happen in an ex-vivo flowing device, and this is why controlling flow output and cell concentration is crucial.

2.3. Optical detection techniques for tumor cells detection

We have reviewed the principal optical phenomena that are used in biology, and some rheology considerations about blood flow. Non-invasive optical detection techniques are presented here.

2.3.1. Bioluminescence imaging

The main principle of bioluminescence imaging is to somehow include bioluminescent trackers or reporters into a living animal and to follow over time the position and the brightness of the trackers (Hooper *et al.* 1990).

For tumor imaging, the most used technique is the establishment (or the purchase) of stable luciferase-expressing tumor cell lines. The luciferase encoding gene is *luc2*. (Stanley PE, 1997)

These cell lines are inoculated to mice, and an injection of luciferin is performed prior to imaging. The image is recorded 10 minutes after the luciferin injection as previously described (Inoue *et al.*, 2010).

After injection the signal grows exponentially (characteristic time $\tau_{plateau}$) to reach a plateau, which will last as long as there is available luciferin in excess. Then, the signal slowly decreases. It is crucial to record the image when the plateau is reached to avoid underestimation of the signal. However, the $\tau_{plateau}$ depends on the size of the tumor. If the tumor has just been injected, it has not yet blood vessels around to bring the luciferin directly in the tumor. In this case diffusion is the only mechanism that brings the luciferin to the tumor cells. And the plateau is reached after a long time. On the other hand, if the tumor is big and well irrigated, the luciferin reaches the tumor site very quickly and the plateau is also reached very quickly. Nevertheless some tumor can be necrotic, and the bioluminescence chemical reaction requires molecular oxygen; a necrotic tumor will not easily be detectable by bioluminescence imaging. When a murine model is developed for bioluminescence imaging, one must verify that the tumor does not get necrotic during the experiment time frame to

avoid bias in the tumor burden estimation. According to Inoue *et al.*, the optimal time point that allows to record data is 10 minutes after luciferin injection. They showed that at this time point, the plateau is reached whatever would be the tumor size.

This technique is non-invasive and requires only the animal to be anaesthetized. This also allows longitudinal analysis of tumor burden on the same animal and is really an advantage when attempting to quantify the effects of a treatments for instance.

2.3.2. *In vivo* flow cytometry

2.3.2.1. Device and capacities

2.3.2.1.1. Fluorescence-based detection, imaging and multi-color analysis:

In vivo flow cytometry was first described in 2004 by John Novak as a new technique 'for real-time detection and quantification of circulating cells' (Novak *et al.*, 2004). This technique relies on fluorescence. The principle is very close to conventional flow cytometry, except for its being performed on living animal.

In conventional flow cytometry, a cell suspension is guided thought a microfluidic flow to a place called "flow cell" in the cytometer. At this place, a laser is focused and the light is scattered in forward direction (detector called "forward scatter or FSC") giving information on the size of the cell; the light is also scattered in the perpendicular direction (detector called "side scatter or SSC") giving information on the granularity of the cell. Moreover, a fluorescently labeled cell would emit fluorescence light which is gathered by an optic bench. According the generation of cytometer, the number of detectors (Photomultiplier tubes PMT) changes: there were four PMTs in 1980's cytometers; today last cytometers integrates up to 18 detectors allowing 16-colors analyses. Indeed, optic filters precede each detector in order to select a bandwidth that corresponds to a given fluorophore. On top of that a brand new generation of spectral cytometer was recently launched by Sony. It integrates more than 30 PMTs that gather the whole light emitted by the cell and performs spectral unfolding to recover spectrum of the different labeling dyes.

In vivo flow cytometry directly analyses fluorescently labeled cells circulating in the blood of a living small animal. The fluorescence light emitted by the cells is collected, filtered, detected, and the final signal is computed.

Performing fluorescent-based detection techniques on living tissues is actually quite a challenge because of different reasons:

1. Tissue absorption

Living tissues have very high absorption coefficients in visible wavelengths that are widely used in most of applications of fluorescence in biology. However, it turns out that absorption of living tissues (especially hemoglobin (Hb) and oxidized hemoglobin (HbO)) dramatically decrease when the wavelength is between 600 to 1000nm (red and blue lines on the Figure 12, Zackrisson et al., 2014), which correspond to red / near infra-red wavelengths. That is why in the first *in vivo* flow cytometry system described, the cells were labeled with a far-red dye ($\lambda_{em} \approx 700$nm) excited by a 633nm red laser.

There are two pathways for light in *in vivo* fluorescence modalities. The excitation light must penetrate deep in the tissues to excite the fluorescent molecules. As fluorescence is an optical linear phenomenon, the more excitation light is absorbed, the less fluorescence you gather. On top of that, blue to green wavelength do not penetrate very deep in living tissues, up to 200nm. However, red, far red, and infra red light penetrate better, up to 500µm (Figure 12). This means that for IVFC, the analyzed blood vessel should be very close to the skin, and easily accessible.

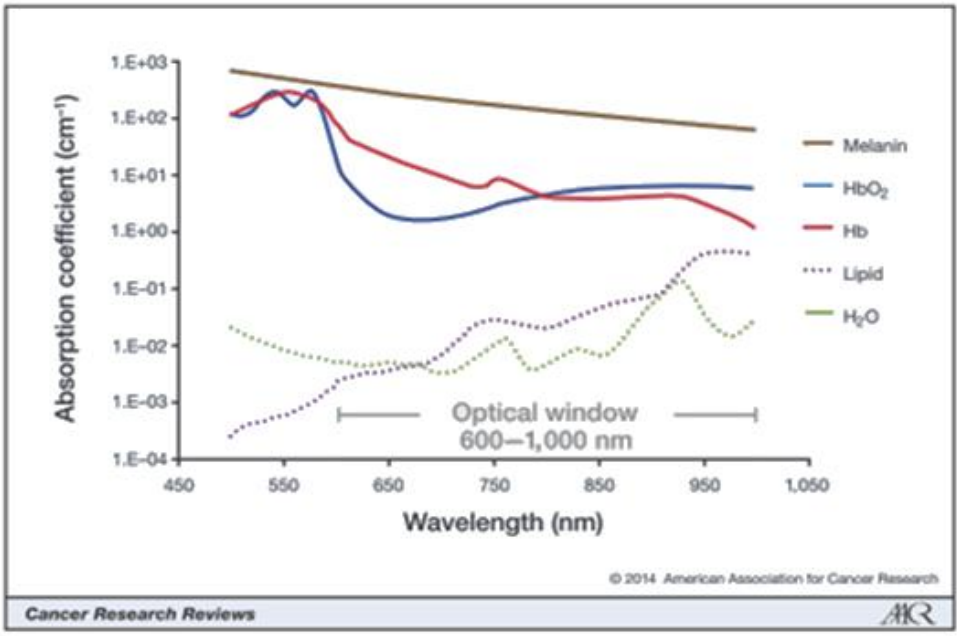

Figure 12: Absorption coefficient of major component of living tissues. The optical window between 600 and 1000 nm is optimum for in vivo imaging

2. Tissue autofluorescence

Living tissues contain plenty of fluorescent molecules. For the analysis, this non-wanted fluorescence light will induce a background noise. This intrinsic living tissue fluorescence is often referred as to “autofluorescence” or “native fluorescence”.

3. The problem of space

As previously mentioned, the analyzed blood vessel should be very close to the skin, implying that no forward detection can be performed. This is why epifluorescence is the set up always chosen for IVFC devices.

The location of the blood vessel must be chosen very carefully. It must be accessible, close to the skin, and this technique should be non-invasive. In Georgakoudi's paper (Goergakoudi *et al.*, 2004), they chose the ear. The ear of a mouse is very thin, about 200µm. The blood vessels are very close to the skin, and they can even been seen with bare eyes.

Here is the experimental device they used.

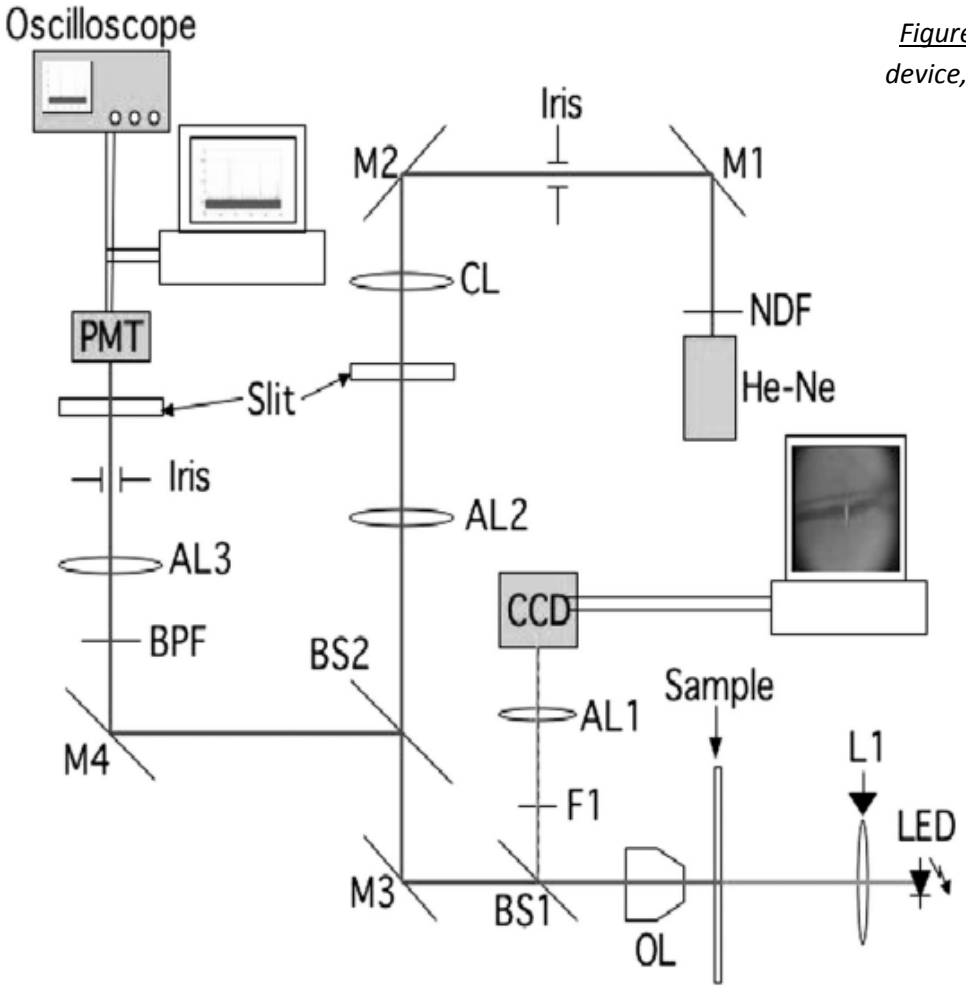

Figure 13 : Experimental IVFC device, from Geogakoudi et al.

Schematic of the *in vivo* flow cytometer experimental setup: L1, condenser lens; OL, microscope objective lens (40×, 0.6 numerical aperture, infinity corrected); BS1, BS2, dichroic beam splitters; AL1–AL3, achromats; CL, cylindrical lens; M1–M4, mirrors; NDF, neutral-density filter; BPF, bandpass filter; PMT, photo-multiplier tube.

The excitation light is a 633nm Laser, the beam is shaped by different cylindrical and spherical lenses and focused through a microscope objective. The light is gathered and detected by a PMT. A CCD camera monitor to location of the laser beam (Figure 13).

The system is able to detect fluorescent cells labeled ex vivo with a far-red dye, but also cells *in vivo* labeled with an injected antibody conjugated with a dye.

During the years following this paper, other papers describing IVFC were published by different teams that had different approaches. First of all, the initial team of C.P. Lin and I.Georgakoudi continued on the exploration of its device and its possibilities. After the proof of principle in 2004, they published in 2005 the first application of their device for detection of apoptotic circulating cells (Wei X *et al.*, 2005). Then, they published in 2006 the imaging version of the cytometer (Ho Lee *et al.*, 2006). Basically, the PMT is linked to a pulse generator. When a fluorescent event is detected, a pulse is sent to a high sensitivity camera, which takes a confocal picture of the cell in the blood vessel (Figure 14).

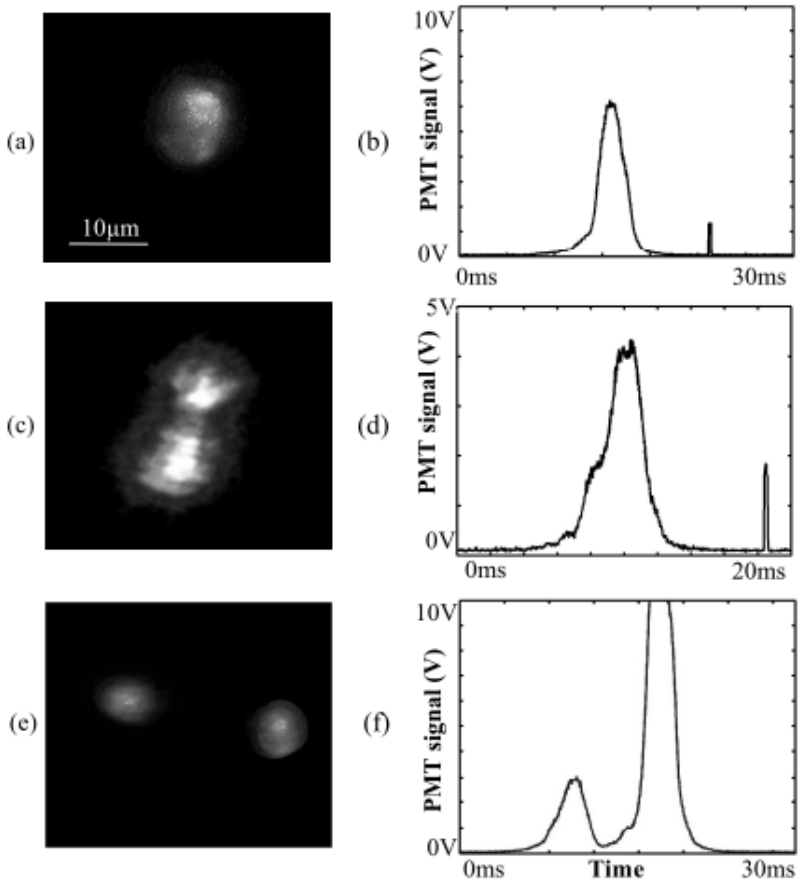

Fig. 4. *In vivo* images and corresponding PMT traces of a single T cell ((a), (b)), a cluster of two T cells ((c), (d)), and two cells traveling in close proximity to each other ((e), (f)).

Figure 14: Experimental image cytometer from Lee et al. The IVFC device is linked to a trigger which take a confocal picture of the mouse's ear.

Later, they published the two-color version of their IVFC device (Noval *et al.*, 2007), and finaly made this flow cytometer portable so that it can be easily moved from a room to another (S.Boutrus *et al.*, 2007).

2.3.2.1.2. Sensitivity optimization and explored volume

Sensitivity of IVFC is a key point. Circulating tumor cells are indeed very rare events, and the detection of cells inside a blood vessel is limited by the "explored volume". In humans, there are typically between 0.2 and 10 CTC per mL of blood. The question is: what volume has to be explored to be statistically sure that a CTC will be detected, if there is at least one CTC in the blood?

In other words, let's take the example of 1 CTC per mL: What is the probability to find at least one cell in an explored volume of $\mathcal{X}$ mL? This probability tends to 1 when the explored volume $\mathcal{X}$ tends to the total blood volume $\mathcal{V}tot$; but is never 1 while $\mathcal{X} < \mathcal{V}tot$.

By presenting the problem in these terms, we assess the strong hypothesis that the blood flow is perfectly homogeneous and that cell concentration does not depend on the place where it is considered.

This problem is in fact a Bernouilli test. The test is: "We randomly choose one cell in the explored volume, is it a CTC?" Let's admit (for the example) that we have 1 CTC among 10^6 healthy cells in this explored volume. The probability to succeed *i.e.* to detect the CTC is 10^{-6}.

$$P(X = 1) = 10^{-6} = p \; and \; P(X = 0) = \frac{10^6 - 1}{10^6} = 1 - p$$

The Bernouilli test is repeated n = 10^6 times, which would mean in this example that 10^6 cells are picked up. To know the probability to have at least one tumor cell, I use an analogy with random draw.

V: volume of a tumor cell ϕ: volume fraction of tumor cells.

If we draw the volume N.v in a very large volume, what is the probability to have **at least** one tumor cell in this volume?

To answer this question, we do an analogy with black and white balls in a box: there are N_b black balls and N_w white balls, each ball whether it is black or white has a volume v. The volume fraction of white balls is: $\phi = \frac{N_w}{N_b + N_w}$. We take a sample of N balls (volume N.v), What is the probability (p_w) to have at least one white ball? It is the complementary of the probability to have N black balls at each draw (p_b). The hypothesis of the total volume of balls is very high in front of the drawn volume,

implies that the concentration ϕ does not change. The probability to have a black ball is similar than in the case of white balls and is:

$$p_b = \frac{N_b}{N_w + N_b}$$

After N independent draws:

$$p_b = \left(\frac{N_b}{N_w + N_b}\right)^N = (1 - \phi)^N$$

$$\ln p_b = N \ln (1 - \phi)$$

In the case N >> 1 and ϕ << 1

$$\ln p_b \sim -N.\phi \Rightarrow p_b = e^{-N.\phi}$$

The probability of have at least one white ball is then:

$$p_w = 1 - e^{-N.\phi}$$

To conclude, if in a volume V_0, there are n white balls and we sample this volume q times, then, $n.q = N.\phi$.

So if there are 1 CTC / cm3, $p = 1 - e^1 = 0.632$

So if there are 2 CTC / cm3, $p = 1 - e^2 = 0.865$

So if there are 3 CTC / cm3, $p = 1 - e^3 = 0.950$

It is a bit counterintuitive, that by picking 10^6 cells in a volume where there is 1 CTC for 10^6 cells, the probability to find the CTC is 0.63; still, it is the case.

To increase this probability the explored volume must be increased either by increasing the observation time or by choosing another vessel (Figure 15).

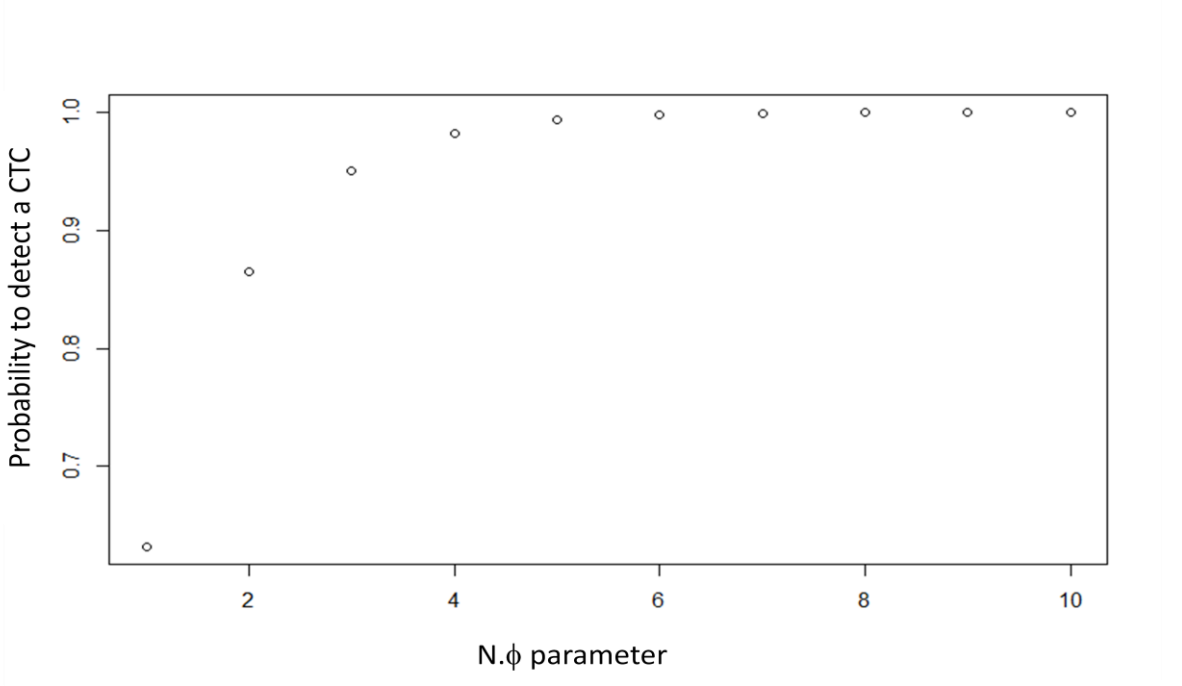

Figure 15: Probability to detect a CTC against the N.ϕ parameter. Actually, in our example, N.ϕ =1 because we picked exactly 10^6 cells. What happens if 2.10^6 or 3.10^6 or 4.10^6 cells are picked? These cases correspond respectively to N.ϕ = 2,3,4, etc. We see on the chart, that by taking twice as much cells as 1/p, P(X≥1) = 0.865, and if three times as much cells as 1/p are analyzed, P(X≥1) = 0.95. Increasing the number of cell analyzed in our case, is equivalent to increase acquisition time.

Alt et al. study exhibits a way to increase the explored volume by selecting more vessels at the same time. In this device, the analysis is performed on the eye of the mouse (Figure16). A circular scan on the retina is created thanks to two mirrors. The excitation laser, coupled with a confocal microscope aiming device, illuminate a circular pattern around the optic nerve.

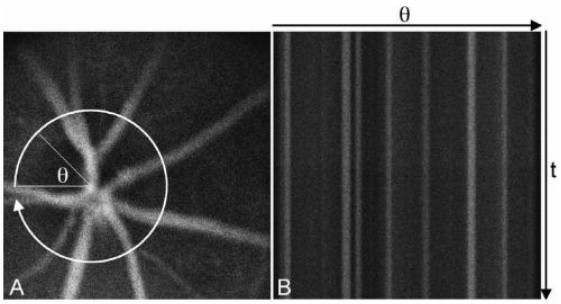

Fig. 2. Confocal fluorescence image of mouse retinal vessels visualized with the fluorescent dye Evans Blue, A, with a cartoon of the circular retinal flow cytometer scan. Evans Blue has similar excitation and emission characteristics as DiD. Consecutive circular scans are mapped to straight horizontal lines in the retinal flow cytometer file, B. Thus retinal vessels appear as vertical, fluorescent structures.

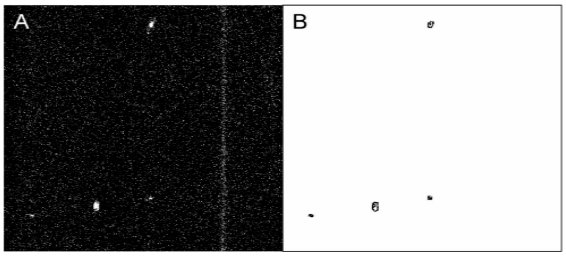

Fig. 3. Typical frame of retinal flow cytometer raw file from DiD-labeled lymphocytes, A, and the same frame analyzed by ImageJ, B. The four cells in the raw file mark the position of three blood vessels (oriented vertically; compare Fig. 2). The long streak is a single cell that is moving very slowly in a capillary. This location was rejected from the analysis throughout the data set since it is not a major retinal vessel. The other four cells are correctly counted and outlined.

Figure 16: Retinal flow cytometer analyzing pattern. The laser spins around the optic nerve and intercepts 8 blood vessels. This technique is very relevant to increase the explored volume provided that each vessel has sufficient diameter. A signal processing software allows detecting fluorescent spots assumed to be fluorescent cells. From Alt et al.

This method allows to simultaneously scan up to 8 blood vessels and thus increases 8 fold the explored volume for a given time. Each line of figure 16 corresponds to a circle on the retina of the mouse.

Finally, an image processing home-made software reveals the presence of spots, each one of them corresponding to a fluorescent event.

2.3.2.1.3. Noise elimination by action on tissues

To overcome the problem of noise, Ding et al (Ding *et al.*, 2013) recently) described a technique to enhance detection and imaging depth by injecting ESOCA (Ear Skin Optical Clearing Agent), an agent that can make the ear skin more transparent. They compare it to glycerol used traditionally to provide adherence of the ear to the slide and to facilitate light transmission (Figure 17).

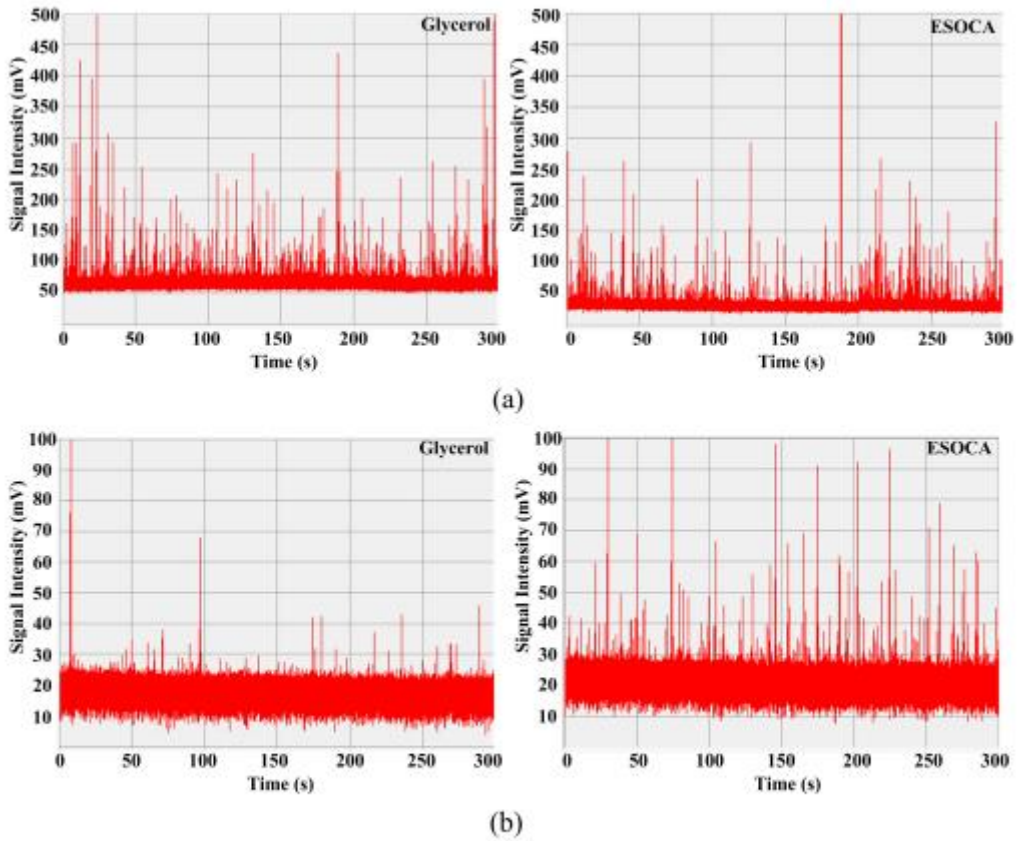

Fig. 3. IVFC signals of DiD-labeled red blood cells (left: treated by glycerol; right: treated by ESOCA). The signals were recorded at the depth of 80 μm (a), and 180 μm (b) for 6 minutes. Each peak represented a DiD-labeled cell traversing the excitation slit.

Figure 17: Here is the typical signal obtained with an IVFC device. From Ding et al. They used an agent that reduces the tissue absorption. As can be seen on the ESOCA graphs, the continuous component of the signal is lower, and the peaks are higher suggesting a great increase in signal over noise ratio.

Another pioneer team in this field is the team of Vladimir P Zharov. They have worked on *in vivo* flow cytometry for almost 8 years. They first described a fluorescence-base device very close to I.Georgeakoudi device (cf page 55, Fig. 13).

They chose another location for the blood vessels. They worked on the mesentery. Mesentery is a highly vascularized tissue that surrounds the intestine. By performing surgery, the mesentery can be taken out of the body of the mouse, yet kept linked to the vascular system. Moreover, the mesentery contains not only blood vessels but lymph vessels, completing the approach of IVFC.

Their device is fluorescence-based, and is linked to 6 detectors (E.I.Galanzha *et al.* 2007 – Figure 18)

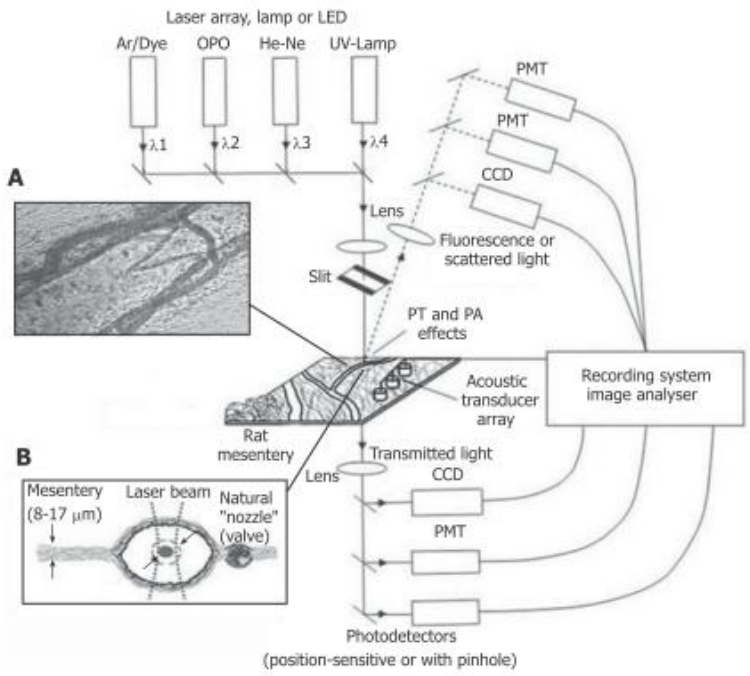

Figure 4 Integrated, multispectral FC *in vivo*. **A**: Typical transmission image of rat mesentery segment with lymph and blood microvessels; **B**: Schematic of the mesentery cross-section.

<u>Figure 18:</u> One of the first devices of IVFC from a pionner team (Zharov) in the field. They were performing IVFC on mesentery blood and lymph vessel.

Then, they focused on another technology: photoacoustic flow cytometry (PAFC). This technique has been previously explained in the Photoacoustic Imaging paragraph.

Many studies have investigated the role of circulating tumor cells in different types of cancer and in different organs using *in vivo* photoaccoustic flow cytometry. From detecting circulating tumor cells or bacteria in the cerebrospinal fluid (Nedosekin *et al.*, 2013), to monitoring blood rheology parameters (Galanzha *et al.*, 2011) through the proof of concept of *in vivo* plant cytometry (tomato plants – Nedosekin *et al.*, 2011). This non-invasive technique might increase detection thresholds in disease where early diagnosis is crucial for treatment efficacy.

Moreover photothermal flow cytometry (PTFC) have been described (Lapotko *et al.*, 2002; Lapotko *et al.* 2002; Zharov et al, 2006) to be very efficient for both detecting (Zharov *et al.*, 2007) and destroying circulating tumor stem cells identified as CD44 positive cells. (Galanzha *et al.*, 2009; Galanzha *et al.*, 2009; Galanzha *et al.*, 2009; Galanzha *et al.*, 2013). The team of V. Zharov has definitely kept innovating on PAFC.

LABELED ENTITY	METHOD	CELLS STUDIED	REFERENCES
Endogenous chromophores			
(melanin)	PAFC/PTFC	mMel	Galanzha, EI et al., 2009 (23)
(hemoglobin)	PAFC/PTFC	RBCs	Zharov V, et al., 2006 (21)
In vivo fluorescent cell labeling			
(ICG)	PAFC	Blood flow, Ret	Zharov V, et al., 2006 [21]
Fluorescent antibodies			
(CD45)	IVFC	WBCs	Novak J, et al., 2004 [1]
(c-kit, sca-1)	IVFC	WBCs , HSCs	Boutrus S, et al., 2007 [7]
Fluorescent proteins			
(Annexin V)	IVFC	Ann V^+ Pr CA cells	Wei X, et al., 2005 [4]
Fluorescent vitamins			
(Folate)	IVFC	huNP, OvCa, mLymph	He, W, et al., 2007 [15]
Ex Vivo membrane labeled tumor or blood cells			
(DID)	IVFC	CD4+ T CELLS	Lee H, et al., 2006 [5]
	IVFC	huALL	Sipkins DA, et al. 2005 [3]
	IVFC	MM	Alsayed Y, et al., 2007 [8]
	IVFC	WM	Leleu X, et al., 2007 [9]
	IVFC	RBCs	Novak J, et al., 2004 [1]
	IVFC	RBCs	Tkaczyk ER, et al., 2008 [17]
	RFC	Leukocytes	Alt C, et al., 2007 [6]
Ex vivo cytoplasmic labeling of tumor cells			
(calcein)	IVFC	MM	Azab A, et al., 2009 [10]
	IVFC	WM	Roccaro AM, et al., 2010 [12]
(Q dots)	IVFC	Br CA cells	Tkaczyk ER, et al., 2008 [17]
Transgenic fluorescent proteins in tumors or leukocytes			
(GFP,DsRed)	IVFC	MM	Runnels JM, et al., 2011 [14]
	IVFC	T cell populations in rejection	Fan Z, et al., 2010 [13]
	IVFC	huBr CA cells	Boutrus S, et al., 2007 [7]
	IVFC	mLuCa	Le TT, Huff TB, Chen, J-X, 2009 [16]
Nanoparticles			
(gold nanorods)	PAFC	free NP, bacteria	Zharov V, et al., 2007 [20]
	PAFC/PTFC	free NP, huSqCa	Zharov VP, et al., 2006 [21]
(magnetic nanoparticles)	PAFC	Br CA	Galanzha EI, et al., 2009 [22]
(carbon nanotubes)	RaFC	HeLa cells	Biris, et al., 2009 [18]
	PAFC	free NP, bacteria	Zharov V, et al., 2007 [20]
(folate conj-gold plated C nanotubes)	PAFC	Br CA	Galanzha EI, et al., 2009 [22]

<u>Table 4:</u> Labelling strategies in IVFC. Except for Hela MM (myeloid myeloma) mMel (melanoma) cells, this table shows that few approaches are done with tumor cells, and none was done with hematopoietic cancer cells such as lymphomas.From Pitsillides et al. RFC/RaFC: Raman Flow Cytometry

In PAFC, as can be seen on table 4, nanoparticles can be used as labeling agents because their heat conducing properties increase the thermoelastic expansion of cells, thus increasing the acoustic signal (Pitsillides *et al.*, 2011). The presence of chemical agents (contrast or clearing agents) or nanoparticles inside the vascular system of the mouse may interfere with the dissemination of tumor cells or with the primary disease itself.

To get rid of this bias, in spite of the power of PAFC technique, Peter Kiesel's team studied the way to enhance detection of circulating cells in a microfluidic device without the need of chemical agents, based on multi-illumination systems (Kiesel *et al.*, 2012; Kiesel *et al.*, 2011).

2.3.2.2. Multi-illumination systems

2.3.2.2.1. Multi-illumination systems for time of flight measurements

Photoacoustic imaging is initially designed to have one excitation beam and one detector. However, V. Zharov team described (Sarimollaoglu *et al.*, 2011) a multi-illumination system where the excitation light is not only one beam but three successive slit of light (Figure 19).

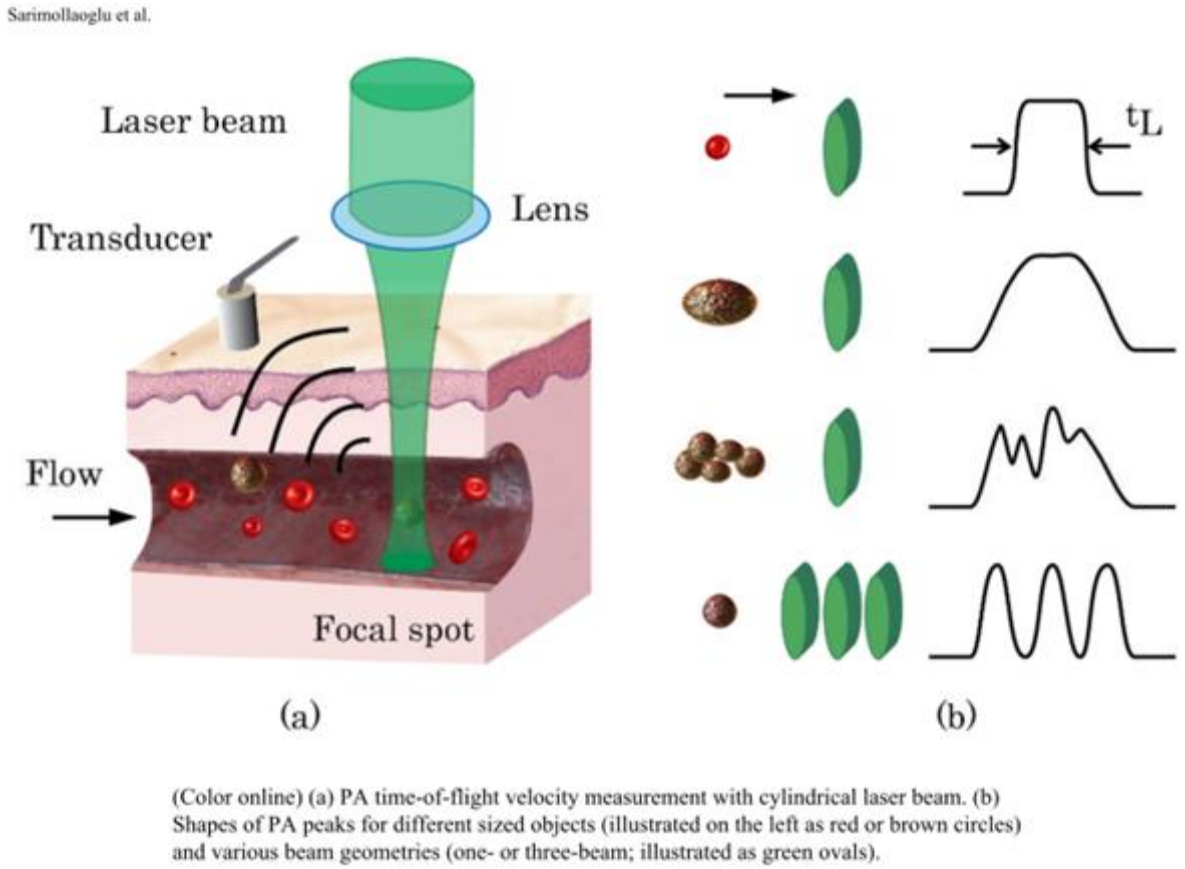

Figure 19: Multi illumination PAFC on blood cell for in vivo measurement of cell time of flight

The advantage is that the time of flight of each detected event can be measured and then the velocity can be calculated. They detect 3 types of events and are able to distinguish: individual cells, aggregate of cells and rolling cells.

However, they did not use the multi signal to enhance detection and to eliminate noise.

2.3.2.2.2. Multi-illumination systems for enhanced detection of fluorescence

One way to extract a signal from noise is to know exactly what shape the signal to extract has. In the case of cells flowing in a vessel under a laser beam (which is in almost all cases Gaussian-shaped), the signal from a cell will be a Gaussian peak of fluorescence, which might be very difficult to extract from the noise, as it is a quite "common" shape. The idea is therefore to give the cell a unique signature, which will be easy to extract from background noise.

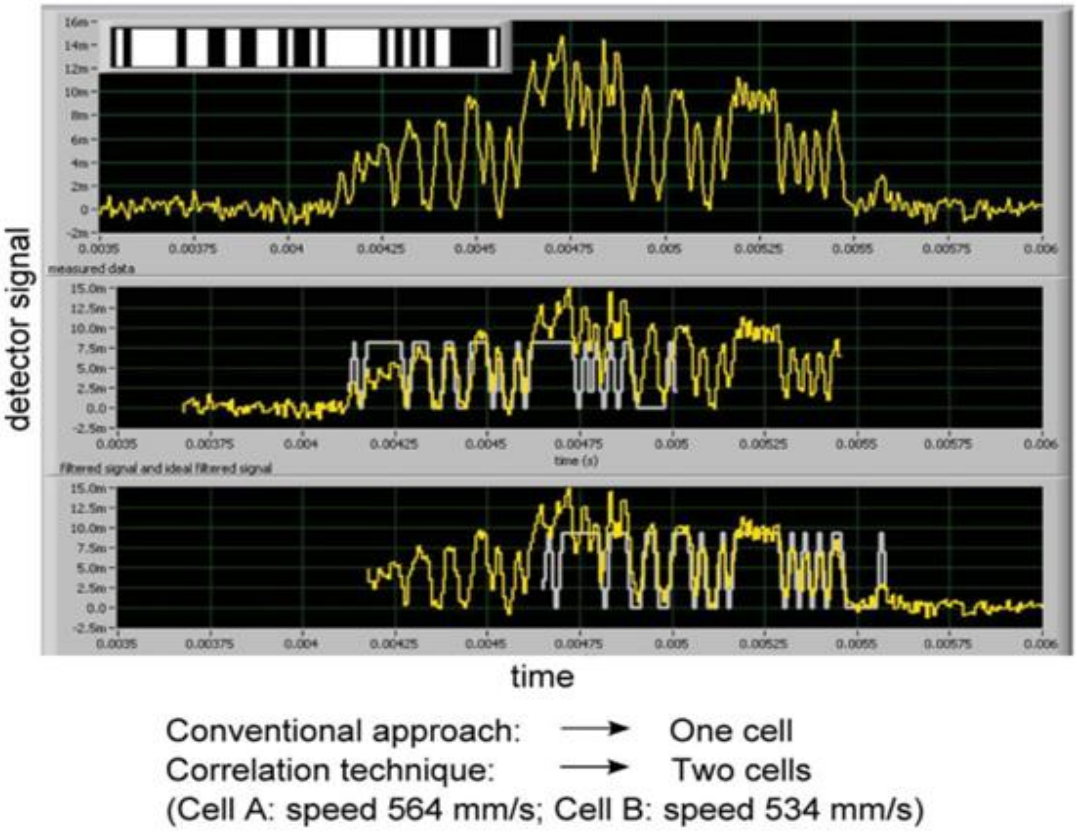

Figure 20: Pattern recognition in signal from CD4$^+$ T-cells in a microfluidic device. The signal is modulated by a patterned mask. The signal processing using pattern recognition is very efficient for distinguishing close cells. The expected pattern, in white, is identified twice in this signal. From

Kiesel *et al.* described a system where the excitation light is modulated by a spatial mask (Kiesel *et al.*, 2011). The excitation light is focused on a microfluidic chip where cells are flowing. The cells are excited by a unique pattern of light that will give the cell a unique pattern (the same) of fluorescence. This pattern being known, the cell signal can be very efficiently extracted from noise. Precision optics is no longer required as the signal detection is enhanced. The device has high performance, is robust, compact and easy to use for a low cost.

Correlation between the expected waveform (the mask) and the actual detected signal allows extracting very efficiently the signal from the background noise. Moreover, the correlation technique is very powerful to separate two coincident cells, thus significantly increasing spatial resolution (Figure 20).

The device has been adapted for two color detection by filtering fluorescence emission of different particles through two "color masks" interlocked with each other's (Kiesel *et al.*, 2012). With the described device, the velocity of particles can also be measured.

OBJECTIVES

Designing innovative treatments that combine high efficacy and low side effects is a real necessity for Primary Central Nervous System Lymphomas (PCNSL). Metastasis dissemination mechanisms are still unclear in PCNSL, yet, in the case of PIOL, most of patients develop lethal brain metastases. In regard of the survival rates, the understanding of these mechanisms is crucial to adapt therapeutic approaches.

When I arrived in the laboratory, four syngeneic models had been developed in the laboratory: Primary Intra-Ocular Lymphoma (PIOL), Primary Cerebral Lymphoma (PCL), Intra-Splenic Lymphoma (ISL), Sub-Cutaneous Lymphoma (SCL). The cells used are murine A20.IIA B-cell lymphomas originating from a BALB/c mouse, grafted in immunocompetent BALB/c mice. There are 3 types of cell lines: A20.IIA Non Transfected, A20.IIA- GFP^+ and double positive A20.IIA-human$CD20^+$-GFP^+.

Commonly, cytometry or histology are performed to characterize cancer progression and treatment response, however, those techniques require the euthanasia of the mouse. Our objective was to longitudinally study the lymphoma disease in mice without euthanasia.

My PhD work has been articulated around a central biological question. This question actually polarized the objectives of the PhD and investigating this question is the main objective of the thesis.

<u>The main objective</u> of my work was to study the effects of innovative treatments of B-cell lymphoma (CpG-DNA and ublituximab-based immunotherapy) on primary tumor, on metastases, and on circulating tumor cells in mouse lymphoma models using non-invasive *in vivo* imaging methods.

This general task was divided in several subtasks:

1. Monitoring primary tumor growth of previously described mouse lymphoma models, metastases spread and **CpG-DNA** effects using **non-invasive bioluminescence imaging**.
2. Monitoring primary tumor growth on previously described mouse lymphoma models, metastases spread and **ublituximab** effects using **non-invasive bioluminescence imaging**.
3. Development of a **standardized quantification method** for **tumor burden estimation** from bioluminescence imaging data.
4. Setting up an ***in vivo*** **flow cytometry** device to monitor **circulating tumor cells** in the mouse model of primary central nervous system lymphomas with or without treatment.

All those tasks aimed to be non invasive to perform longitudinal studies. The evaluation of mice for a long period is indeed crucial to understand adaptive immunity mechanisms of mAbs-therapies induced long-lasting responses.

In the context of the monitoring of new therapeutic approaches, with the treatments presented here, I closely cooperated with a concomitantly arrived PhD Student (Rym Ben Abdelwahed), and completed the data previously obtained.

RESULTS

In this part, I will present the results I have obtained during my PhD thesis. This work led to four articles: two of them are published, and the other two are going to be submitted.

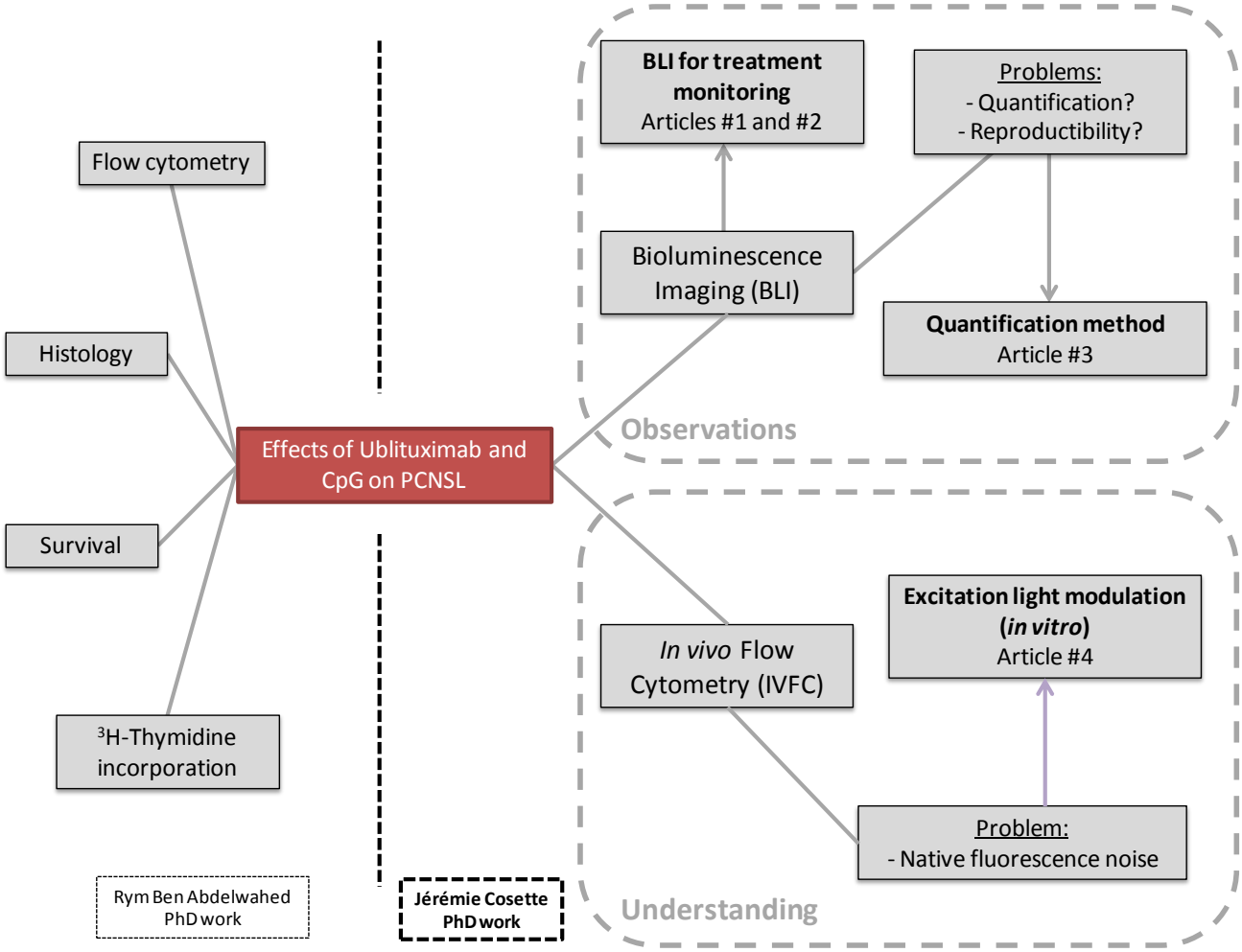

This scheme summarizes the PhD thesis work. The work is articulated around a biological question which is the effects of both treatments in PCNSL. Rym Ben Abdelwahed had a biological approach on her PhD work, and I used new pluridisciplinary approaches during my work (BLI and IVFC) to complete and have multiple points of view on our topic. My approach was separated into two different pathways. Bioluminescence imaging was used in both articles #1 and #2 to complete Rym's approach; yet, issues were discovered in the analysis of bioluminescence data, and this led to article #3. In parallel, we addressed the question of circulating tumor cells by IVFC, and this led to article #4.

We first investigated the treatment effects on lymphoma cells bearing mice in the case of Ublituximab treatments and CpG treatments. This led to two published articles (#1 and #2), in which I participated. My contribution to these works was essentially performing the imaging part.

We then realized that the images could have been quantified, while the two first articles' images were qualitatively used for localization. We screened many papers using bioluminescence imaging for tumor models. Over 300 papers were analyzed from 2006, and more than 80% of the users own the same device, yet there is no consensus on the unit to be used. The problem of reproducibility was addressed as very few papers possess a material and method part describing the BLI protocol, even when quantification charts are presented. The investigation of quantification of bioluminescence data sets led to article #3.

I am first author of article #3 and the main message is the proposal of a method that allows a bioluminescence score to be associated to an animal. This score reflects the tumor burden and can be compared from an animal to another. The study has been done in the case of CpG treatments in subcutaneous lymphomas.

Article #3 and #4 were the core of my work. However they address different questions that belong to different concepts. The BLI scoring method corresponds to describing the model, describing the effects of treatments and trying to quantify tumor burden in a way that reduces uncertainties. It is a matter of **observation**.

On the other hand, we wanted to **understand** the metastatic dissemination mechanism at the cellular level; while only the effects (at the tumor cell population level) are accessible with BLI. This work led to article #4, in which we addressed the question of circulating tumor cells. We indeed saw metastases in both cases of PIOL and PCL. However, we wanted to find the link between metastases and primary tumor, and investigate the role of CTCs in the metastasizing process of PCSNL lymphomas models. To do so we designed an In Vivo Flow Cytometry device inspired by Novak et al. Nevertheless, we had native fluorescence issues and we designed a device that improves fluorescence detection and enables velocity measurements in an *in vitro* model.

ARTICLE # 1

Preclinical study of Ublituximab, a glycoengineered anti-human CD20 antibody, in murine models of primary cerebral and intraocular B-cell lymphoma

Rym Ben Abdelwahed, Sabrina Donnou, Hanane Ouakrim, Lucile Crozet, **Jeremie Cosette**, Alexandra Jacquet, Isabel Tourais, Benedicte Fournes, Melanie Gillard Bocquet, Amine Miloudi, Valerie Touitou, Cecile Daussy, Marie-Christine Naud, Wolf Herman Fridman, Catherine Sautès-Fridman, Remi Urbain and Sylvain Fisson

1. Anti-CD20 monoclonal antibodies for treatment of PCNSL

PIOL and PCL are disease that have very low survival rates, and whose treatments are very invasive and can have heavy side effects. The development of new therapeutic approaches is crucial.

In the following article, which is the first one presented on this manuscript, we described the preclinical study of Ublituximab, an anti-hCD20 monoclonal antibody in mouse models of PIOL and PCL.

The analysis of the effects of Ublituximab was done in comparison with Rituximab, another anti-hCD20 monoclonal antibody, used in clinical practice for DLBCL, but also in most B-cell lymphomas. The positive effects of rituximab on auto-immune diseases such as lupus were also described. However, Ublituximab has been engineered to enhance ADCC. The final aim is of course to cure the disease, but also to create a long-lasting response, in other words, an immune memory.

Mice were injected with tumor cells in the eye or in the brain according the studied model and the treatment was administered in situ. The investigations on the effects of Ublituximab were done with different techniques such as cytometry, histology and bioluminescence imaging.

My contribution to this works was essentially performing the imaging part. Nevertheless, I also contributed to tumor cell injection, cell culture, and tumor cell engineering. As a matter of fact, only A20.IIA and A20.IIA-GFP (expressing GFP) were available. Those cell lines are not suitable with bioluminescence imaging (that requires luciferase expression). I thus developed new cell lines: A20.IIA-*luc2* (expressing luciferase) and A20.IIA-*luc2*-CD20 that served as a new tool for investigations. This cell line was used for all bioluminescence imaging experiments.

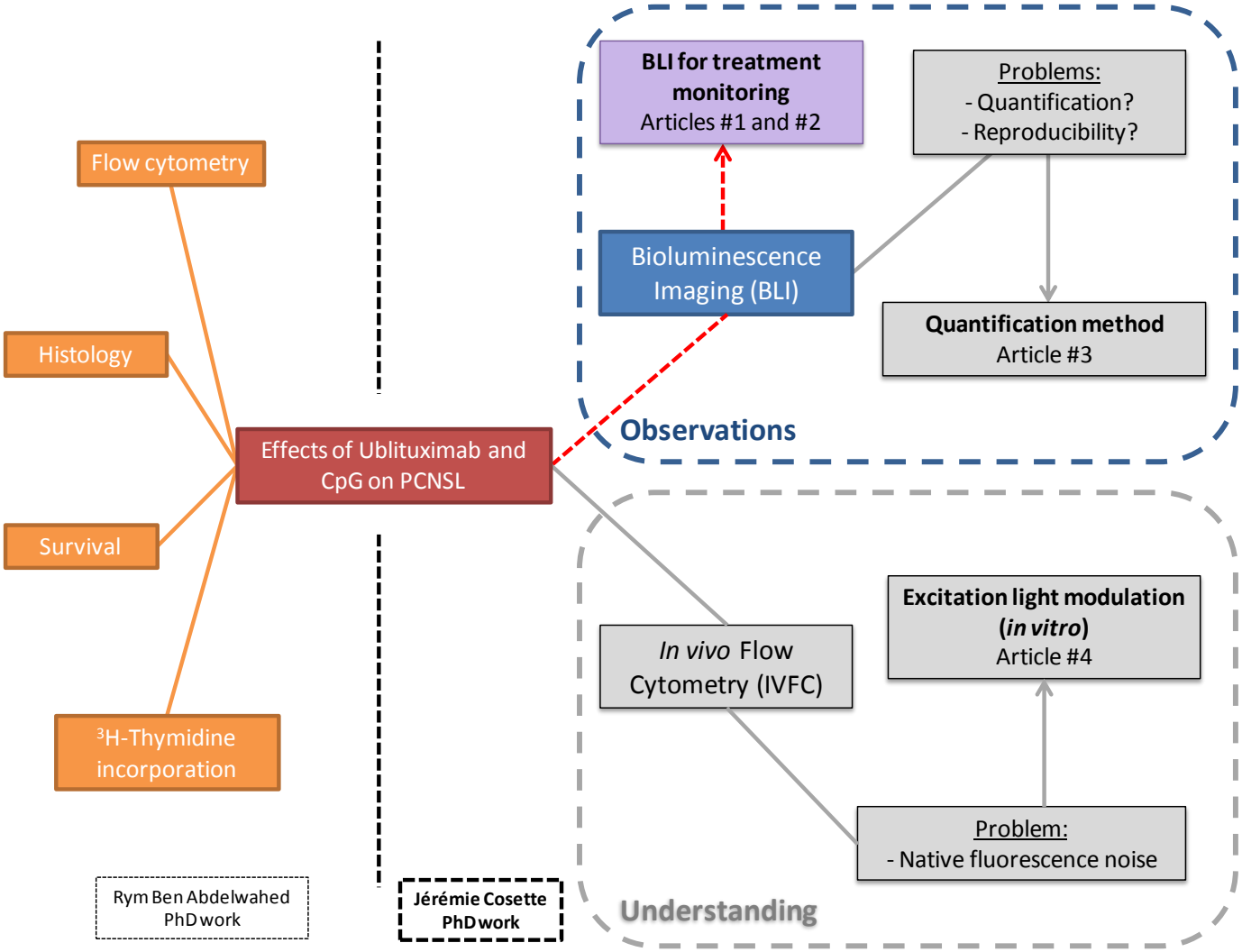

For articles #1 and #2, bioluminescence imaging was performed for treatment monitoring (highlighted in the scheme). Actually, conventional methods such as histology or cytometry etc. were used to assess the effects (comparative) of Ublituximab and CpG treatments. Those conventional methods were completed with the bioluminescence approach that gives pertinent information on early identification of responding animals, thanks to longitudinal and non-invasive studies.

Preclinical Study of Ublituximab, a Glycoengineered Anti-Human CD20 Antibody, in Murine Models of Primary Cerebral and Intraocular B-Cell Lymphomas

Rym Ben Abdelwahed,[1–4] Sabrina Donnou,[1–3] Hanane Ouakrim,[1–3] Lucile Crozet,[1–3] Jérémie Cosette,[1–3] Alexandra Jacquet,[5] Isabel Tourais,[5] Bénédicte Fournès,[5] Mélanie Gillard Bocquet,[1–3] Amine Miloudi,[1–3] Valérie Touitou,[1–3,6] Cécile Daussy,[1–3] Marie-Christine Naud,[1–3] Wolf Herman Fridman,[1–3] Catherine Sautès-Fridman,[1–3] Rémi Urbain,[5] and Sylvain Fisson[1–3,7–9]

[1]Institut National de la Santé et de la Recherche Médicale (INSERM), UMRS872, Centre de Recherche des Cordeliers, Paris, France
[2]Université Pierre et Marie Curie-Paris 6, UMRS 872, Paris, France
[3]Université Paris Descartes, UMRS 872, Paris, France
[4]Université de Monastir, Monastir, Tunisie
[5]Laboratoire français du Fractionnement et des Biotechnologies (LFB), Les Ulis, France
[6]Département d'Ophtalmologie, Hôpital de la Pitié-Salpêtrière, Paris, France
[7]Généthon, Evry, France
[8]INSERM, U951, Evry, France
[9]Université d'Evry Val d'Essonne, UMRS 951, Evry, France

Correspondence: Sylvain Fisson, Généthon, INSERM UMRS 951, 1 bis rue de l'Internationale, Evry F-91002, France; sylvain.fisson@univ-evry.fr.

RBA and SD contributed equally to the work presented here and should therefore be regarded as equivalent authors.

Submitted: June 1, 2012
Accepted: April 16, 2013

Citation: Abdelwahed RB, Donnou S, Ouakrim H, et al. Preclinical study of ublituximab, a glycoengineered anti-human CD20 antibody, in murine models of primary cerebral and intraocular B-cell lymphomas. *Invest Ophthalmol Vis Sci.* 2013;54:3657–3665. DOI:10.1167/iovs.12-10316

Purpose. Primary cerebral lymphoma (PCL) and primary intraocular lymphoma (PIOL) belong to the systemic diffuse large B-cell lymphoma family and are characterized by the presence of $CD20^+$ lymphoma B cells in the brain or the eye. These highly aggressive malignancies have a poor prognosis and no specific therapy. The presence of effector immune cells in the damaged brain and vitreous suggests that treatment with anti-human CD20 (hCD20) monoclonal antibodies might be effective. We developed murine models of PCL and PIOL to assess the intracerebral and intraocular antitumor effect of ublituximab, a promising glycoengineered anti-hCD20 mAb with a high affinity for FcγRIIIa (CD16) receptors.

Methods. The murine lymphoma B-cell line A20.IIA-GFP-hCD20 (H-2^d) was injected into the right cerebral striatum or the vitreous of immunocompetent adult BALB/c mice (H-2^d). Four to 7 days later, ublituximab was injected intracerebrally or intravitreously into the tumor site. Rituximab was the reference compound. Survival was monitored for injected mice; histopathological and flow cytometric analyses were performed to study tumor growth and T-cell infiltration.

Results. Single doses of ublituximab, injected intracerebrally or intravitreously, had a marked antitumor effect, more pronounced than that obtained with the same dose of rituximab in these conditions. The reduction in tumor cells was correlated with an increased proportion of $CD8^+$ T cells. This efficacy was observed only against lymphoma B cells expressing hCD20.

Conclusions. These in vivo results confirm the potential of the glycoengineered anti-hCD20 mAb ublituximab as an innovative therapeutic approach to treat primary central nervous system lymphoma and other B-cell lymphomas.

Keywords: glycoengineered monoclonal antibody, human CD20, primary intracerebral B cell lymphoma (PCL), primary intraocular B cell lymphoma (PIOL), primary vitreoretinal lymphoma (PVRL), ublituximab

Primary central nervous system lymphoma (PCNSL) is a form of extranodal high-grade non-Hodgkin B-cell neoplasms[1] that can originate in the brain, leptomeninges, spinal cord, or eyes,[2,3] typically remains confined to the CNS, and rarely spreads outside the nervous system. PCNSL accounts for 1% to 4% of primary brain tumors.[4]

Primary cerebral lymphoma (PCL) and primary intraocular lymphoma (PIOL, also called primary vitreoretinal lymphoma, PVRL) are closely related subsets of PCNSL that reach these two immunoprivileged sites.[5] PCL is a tumor of the brain parenchyma. Tumor cells are usually found around blood vessels and PCL can develop as a uni- or multifocal tumor. PIOL is an aggressive malignancy in which lymphoma cells spread in the retina, vitreous, or optic nerve. It may be limited to the eye, but may also include CNS involvement. Approximately 95% of PCLs and 98% of PIOLs express CD19 and CD20.[4] The

prognosis of immunocompetent patients diagnosed with PCNSL has improved over the past decade with methotrexate administration and cranial radiotherapy.[6] This first-line therapy fails in 35% to 60% of cases, however, and the prognosis for patients with PCL or PIOL or both remains poor, with a median overall survival of only 33 to 40 months.[7] Because these tumor cells express CD20, a well-characterized antigen, immunotherapy has become a new area of active research.

mAbs have already been used successfully to treat tumors: trastuzumab for Her/Neu-positive breast cancer,[8] and rituximab, a mouse-human chimeric mAb that targets human CD20 (hCD20), for CD20-positive non-Hodgkin lymphomas.[9] Studies have shown it is active against central nervous system (CNS) lymphoma after both intravenous[10] and intraventricular[6] injection and have thus demonstrated the interest of such a strategy for brain tumors. Clinical response was nonetheless limited, which might be explained by rituximab's inadequate engagement of antibody-dependent cell-mediated cytotoxicity (ADCC) or the limited availability of the complement system in the central nervous system.[11] Ublituximab is a promising glycoengineered chimeric anti-hCD20 mAb that has a high affinity for FcγRIIIa (CD16) receptors and therefore greater ADCC activity than rituximab.[12,13]

In this study, we sought to evaluate the efficacy of ublituximab in murine models of PCNSL. B-lymphoma cells were stably transfected with the human CD20 antigen. After implantation in the brain (PCL model) or the eye (PIOL model), we evaluated the therapeutic potential of ublituximab administered directly into the tumor. In these conditions, these injections into the brain and vitreous body resulted in more effective regression of the induced tumor than with rituximab.

Materials and Methods

Mice

Female BALB/c mice (H-2^d) were obtained from Charles River Laboratories (L'Arbresle, France) and used between 6 and 8 weeks of age. They were provided with sterile food and water ad libitum and kept on a 12-hour light-dark cycle. All mice were manipulated according to the ARVO Statement for the Use of Animals in Ophthalmic and Vision Research, the European Union guidelines, and with the approval of the local research ethics committee (Charles Darwin Ethics Committee in Animal Experiment, Paris, France; Permit Number: p3/2009/004).

Cells

A20.IIA (also called IIA1.6) is an FcγR-negative clone originating from the A20-2J B-cell lymphoma line.[14] A20.IIA cells were transfected by an electroporation system with the green fluorescent protein (GFP) gene or with a gene containing a fusion protein of GFP and the human CD20 (hCD20, cloned from the Raji cell line). These cells, hereafter referred to as A20.IIA-GFP or A20.IIA-GFP-hCD20 cells (Supplementary Fig. S1A), were maintained at 37°C, 5% CO_2 in complete Roswell Park Memorial Institute (RPMI) 1640 Medium GlutaMAX Plus (RPMI; Gibco-Invitrogen, Saint Aubin, France) supplemented with 10% fetal calf serum (FCS; PAA laboratories, Cölbe, Germany); 100 U/mL penicillin and 100 μg/mL streptomycin (both from Eurobio, Courtaboeuf, France); 10 mM sodium pyruvate (Gibco-Invitrogen); 50 μM 2-mercaptoethanol (Gibco-Invitrogen); and 0.5 mg/mL neomycin (G418; Gibco-Invitrogen). To obtain the A20.IIA- GFP-hCD20- luc2 cell line, A20.IIA-GFP-hCD20 cells were transfected with pGL4.50[luc2/CMV/hygro] (Promega, Madison, WI), in a commercial device (Amaxa Nucleofector II; Lonza, Basel, Switzerland) and were cultured in 1 mg/mL neomycin and 0.75 mg/mL hygromycinB (Gibco-Invitrogen) medium.

Tumor Implantation

Mice were first anesthetized by intraperitoneal injection of a mixture containing 120 mg/kg of ketamine (Virbac, Carros, France) and 6 mg/kg of xylazine (Rompun 2%; Bayer Healthcare, Loos, France). Anesthetized mice were immobilized on a stereotaxic frame (David Kopf Instruments, Tujunga, CA) for the intracerebral tumor implantation. Tumor cells (5×10^4 in a final volume of 2 μL) were injected into the specific cerebral location (right striatum), located 2 mm to the right of the medial suture and 0.4 mm in front of the bregma, through a Hamilton syringe attached to a penetrating depth controller. The penetrating depth of the syringe was 2.5 mm from the surface of the brain. Each injection delivered the solution slowly, and the syringe was held in place for an additional minute to reduce backfilling of tumor cells. The same procedure was used for control mice injected with 1× phosphate-buffered saline (pH7.4; PBS). For the intravitreal tumor implantation, we used a 32-gauge needle attached to a syringe to inject 10^4 cells in a final volume of 2 μL into the vitreous under a dissecting microscope. Eye drops (Lacrinorm 2%; Bausch + Lomb, Montpellier, France) were instilled after intravitreal injection.

Description of Ublituximab

Ublituximab is a chimeric mAb produced by LFB Biotechnologies (Les Ulis, France) and has previously been described as EMAB-6.[12] Briefly, this chimeric mAb was generated from a mouse IgG2a kappa type I light chain, anti-human CD20 mAb named CAT-13.6E12 (DSMZ, Braunschweig, Germany). IGKV and IGHV were cloned into expression vectors containing a human kappa light chain constant region (IGKC) or a human heavy chain constant gamma 1 region (IGHG1), respectively. Compared with rituximab, this antibody has a lower fucose content in its Fc region. Apoptosis and complement-dependent cytotoxicity (CDC) were almost comparable with that induced by rituximab, whereas FcγRIIIA binding and FcγRIIIA-dependent effector functions were highly improved.

Anti-hCD20 Injections and Clinical Follow-Up

The brain tumors were treated by a single therapeutic injection made intracranially 7 days after the tumor inoculation. Each mouse was treated by PBS (control groups), or by 1, 5, or 20 μg of ublituximab, or by 20 μg of rituximab. Survival was monitored daily.

In the PIOL model, the therapeutic mAbs were injected directly into the eye 4 or 7 days after tumor inoculation. Ublituximab was used at doses of 1, 4, or 20 μg, and rituximab at 20 μg. Control groups received 2 μL of PBS. All doses of ublituximab and rituximab were administered intracranially or intravitreously in a final volume of 2 μL.

In Vivo Tumor Growth Assay

A20.IIA stable cell line (1×10^4) cells expressing luciferase (luc2 gene) were injected via the intravitreal route into immunocompetent 7-week-old BALB/c mice. Tumor formation and metastases were analyzed every week for 8 weeks. Mice were injected with 150 mg/kg of D-luciferin potassium salt (Interchim, San Pedro, CA) via the intraperitoneal route and underwent imaging within 15 minutes afterwards by a commercial imaging system (IVIS LUMINA2; Caliper LS, Hopkinton, MA). The exposure time was set to optimize the

Investigative Ophthalmology & Visual Science

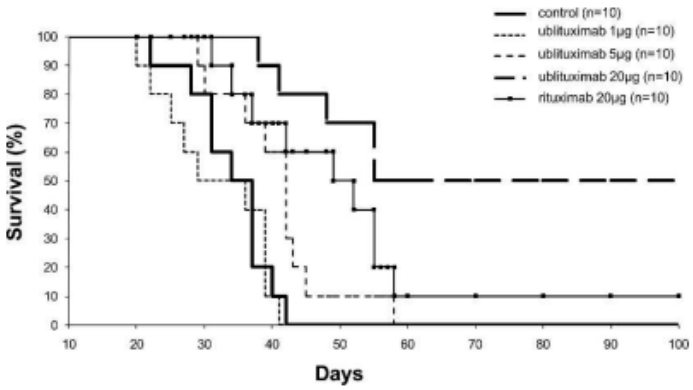

FIGURE 1. Analysis of the dose-response antitumor effect of anti-hCD20 mAb on the murine PCL model and comparison with rituximab. Kaplan-Meier survival analysis after brain inoculation with A20.IIA-GFP-hCD20 cells. On day 7 after this inoculation, the mice were treated intracerebrally with 1 µg/2 µL or 5 µg/2 µL or 20 µg/2 µL anti-hCD20 ublituximab, and compared with a control group treated with PBS 1× and another group treated with 20 µg/2 µL rituximab. Survival was followed daily, and results obtained from two independent experiments were pooled. Statistical test: Log-rank between the PBS 1× control group and group treated with: 5 µg/2 µL ublituximab ($P = 0.024$); 20 µg/µL ublituximab ($P < 0.001$); 20 µg/µL rituximab ($P = 0.028$).

signal and obtain the best signal over noise ratio. The unit of the bioluminescence signal is photons per second. Images were taken of the front and of the back of each mouse. A region of interest (RoI) was drawn around the mice to insure inclusion of potential metastases. The total influx of photons used to quantify the tumor growth is the sum of the influx of photons gathered from the front and back of the mouse.

Brain and Ocular Cell Isolation

The tumor-injected brain or eye of each mouse was harvested and minced with surgical scissors; incubated for 30 minutes in RPMI containing 0.1 mg/mL DNAse I (Roche Diagnostics, Meylan, France) and 1.67 Wûnch U/mL Liberase (Roche); and filtered through a 70-µm membrane (BD Falcon; BD Biosciences, San Jose, CA). A Percoll gradient was used to separate live mononuclear cells from myelin.

Flow Cytometric Analyses

After 20 minutes of Fc receptor saturation with 10 µg/mL anti-CD16/CD32 mAb (clone 2.4.G2), cells were incubated for 20 minutes with the following mAbs: rat IgG2a anti-CD19/APC, or rat IgG2a anti-CD8/AF700, or the corresponding isotypic mAb controls (all from BD Biosciences). The living cells were defined with side scatter and forward scatter, after exclusion of autofluorescent cells. Cell phenotypes were analyzed with the LSRII cytometer and commercial analytical software (BD FACSDiva; BD Biosciences).

Histopathological Analyses

After sacrifice at day 21, eyes and brain were collected, postfixed in 4% paraformaldehyde (PFA) for 4 hours (eyes) or overnight (brain), PFA containing 5% sucrose for 2 hours, and PFA containing 15% sucrose overnight. After alcohol and toluene baths, serial sections (8 µm) were performed by a microtome (Leica RM 2145; Leica Microsystems GmBH, Wetzlar, Germany) from paraffin-embedded preparations and stained with hematoxylin-eosin-safran for eye sections or with hematoxylin-phloxine-safran for brain sections. Images were collected with commercial equipment and software (Nikon Eclipse E600W, Nikon Instruments, Champigny sur Marne, France; Cartograph; Microvision Instruments, Evry, France).

Statistical Analysis

Comparisons used Mann-Whitney test and Kaplan-Meier curves, performed with commercial graphing software (GraphPad Prism; GraphPad Software, La Jolla, CA). Statistical significance was defined by P values less than 0.05.

RESULTS

Anti-hcd20 Ublituximab Has a More Sustained and Better Antitumor Effect Than Rituximab on Primary Cerebral Lymphoma In Vivo

To evaluate the efficacy of the anti-human CD20 ublituximab mAb in our PCL murine model, A20.IIA lymphoma B cells transfected with GFP and hCD20 (A20.IIA-GFP-hCD20) were injected stereotactically into the right striatum of adult syngeneic BALB/c mice. Seven days later, these mice received 1 µg, 5 µg, or 20 µg of anti-hCD20 ublituximab, or 20 µg of rituximab, or PBS (the control group). The PBS 1× control group differed significantly from all ublituximab-treated groups, except the group receiving the smallest dose (1 µg anti-hCD20 ublituximab; Fig. 1), which indicates a dose-effect relation. Specifically, it differed from ublituximab at 20 µg ($P < 0.001$) and at 5 µg ($P = 0.024$). Interestingly, half of the mice treated with 20 µg of this new mAb rejected their tumors. An irrelevant glycoengineered mAb of the same isotype as ublituximab was used as a positive control, and this control group did not differ significantly from the PBS negative control group (Supplementary Fig. S1B).

Because results from clinical use of rituximab have been encouraging, it was chosen in this study as the reference for ublituximab. Clinical manifestations in our PCL model appeared the week before death and were characterized by weight loss, postural prostration, and/or spiky hairs. Surviving mice did not develop any clinical signs. Results in Figure 1 show that when injected at the same dose of 20 µg, ublituximab had a stronger effect on lymphoma cells than rituximab ($P = 0.0028$). Moreover, the overall survival of these two treatment groups was clearly different: 50% survival (5/10) with ublituximab versus 10% survival (1/10) with rituximab. These results were confirmed by flow cytometry analyses showing the percentage of GFP^+ $CD19^+$ tumor cells among live

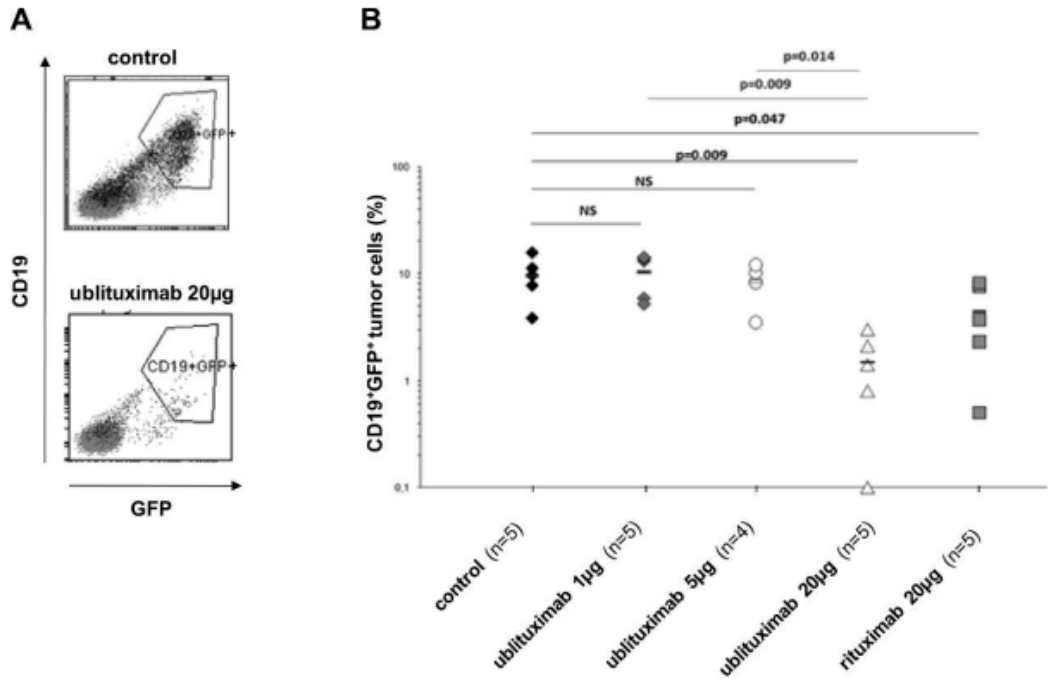

FIGURE 2. Analysis of the effect of anti-hCD20 ublituximab on tumor growth. (**A**) Flow cytometric analysis at day 21 of GFP$^+$ CD19$^+$ tumor cells in the brain treated with 2 µL PBS (control; *top panel*) or 20 µg anti-hCD20 ublituximab (*lower panel*). (**B**) Percentage of CD19$^+$ GFP$^+$ tumor cells among live mononuclear cells, as determined by flow cytometry, in the brain of mice treated with 1 µg/2 µL, 5 µg/2 µL, or 20 µg/2 µL anti-hCD20 ublituximab, compared with the PBS control group and the group treated with 20 µg/2 µL rituximab ($n = 5$). Statistical test: Mann-Whitney; NS, not significant.

mononuclear cells 14 days after treatment (Fig. 2). As expected, the antitumor effect of ublituximab at 20 µg was very significant ($P = 0.009$) at the cellular level, compared with the PBS 1× control group. The difference between the lower doses tested (1 µg and 5 µg) and the control did not reach statistical significance at this time point. Flow cytometric analyses of the percentage of CD19$^+$ GFP$^+$ tumor cells in the brain also confirmed the therapeutic efficacy of rituximab at 20 µg, but showed that it was weaker ($P = 0.047$) than that of ublituximab. Moreover, the decrease of the percentage of tumor cells was correlated with an increase in the number (Fig. 3) and percentage (Supplementary Fig. S2A) of CD8$^+$ T cells in the brains of treated mice.

The bioluminescence imaging system allowed us to assess total photon influx, which is representative of the tumor burden of the whole mouse, and to compare it between ublituximab-treated mice and PBS-injected (control) mice. On day 10 (i.e. 3 days after treatment), the intracerebral tumor was no longer detectable in the treatment group (Fig. 4A). This was confirmed by histological analysis showing that no tumor mass could be detectable at day 21 in ublituximab-treated mice in contrast with control mice (Fig. 4B). At day 29, some control mice had cervical lymph node metastasis, with 1.6×10^6 ph/s/cm^2/sr luminescence signal (Fig. 4A, RoI 1 in the upper panel), which is a 100 times higher than the signal from an area expected to be negative (Fig. 4A, RoI 2 in the upper panel). The ublituximab-treated representative mouse had 4.4×10^3 ph/s/cm^2/sr in the right cervical lymph node, a photon influx one-thousandth less intense than in the control mouse.

To rule out the possibility of a nonspecific effect of ublituximab, animals were implanted with tumors that did (A20.IIA-GFP-hCD20) or did not (A20.IIA-GFP) express the human CD20 antigen and were treated with 20 µg of the therapeutic mAb. As expected, mice without treatment all died after 37 days regardless of the tumor (Fig. 5). Ublituximab was

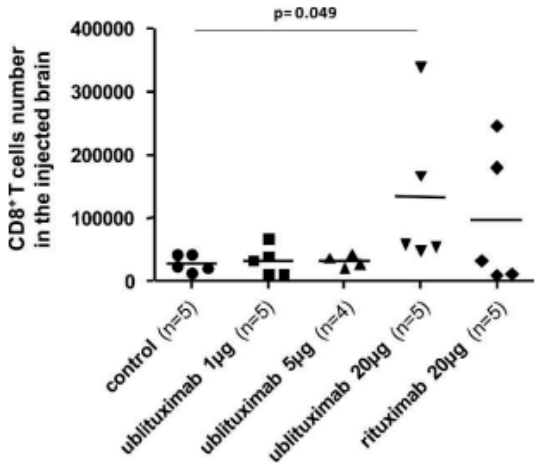

FIGURE 3. Effect of an intracerebral injection of anti-hCD20 mAb on the absolute number of CD8$^+$ cells in the brain. Absolute number of CD8$^+$ T-cells was analyzed by flow cytometry in the brain of mice treated with 1 µg/2 µL, 5 µg/2 µL, or 20 µg/2 µL anti-hCD20 ublituximab, in comparison with the PBS control group and the group treated with 20 µg/2 µL rituximab. Statistical test: Mann-Whitney.

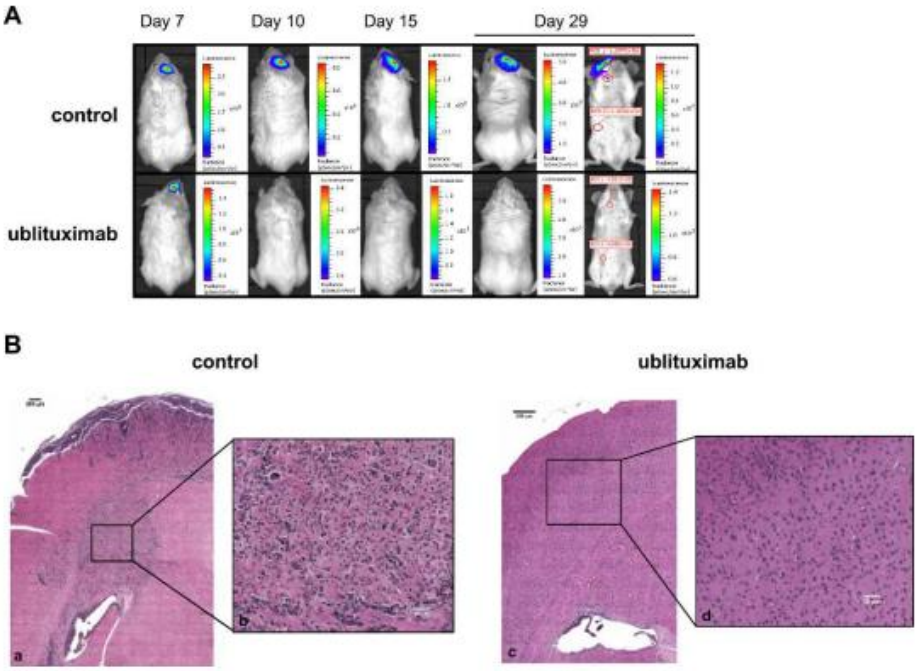

FIGURE 4. Representative bioluminescence images and histopathological analysis comparing ublituximab treatment with PBS injection in PCL murine model. (**A**) Representative bioluminescence images of PBS control PCL mice (*upper panel*) and ublituximab-treated PCL mice (*lower panel*). The mice were injected with 5.10^4 A20.IIA-GFP-hCD20-luc2 cells on day 0 via the intracranial route. The ublituximab treatments were administered in situ on day 7. The figure shows a view of the front of mouse on day 29, with a metastasis detected in the right cervical lymph node. (**B**) Representative histological aspect of PBS control PCL mice (*left panels*) and ublituximab-treated PCL mice (*right panels*). The mice were injected with 5.10^4 A20.IIA-GFP-hCD20-luc2 cells on day 0 via the intrastriatal route. The ublituximab treatments were administered in situ at day 7 and sacrificed at day 21. (**a**, **c**) Magnification ×20 and *bars* represent 200 μm. (**b**, **d**) Magnification ×40 and *bars* represent 50 μm.

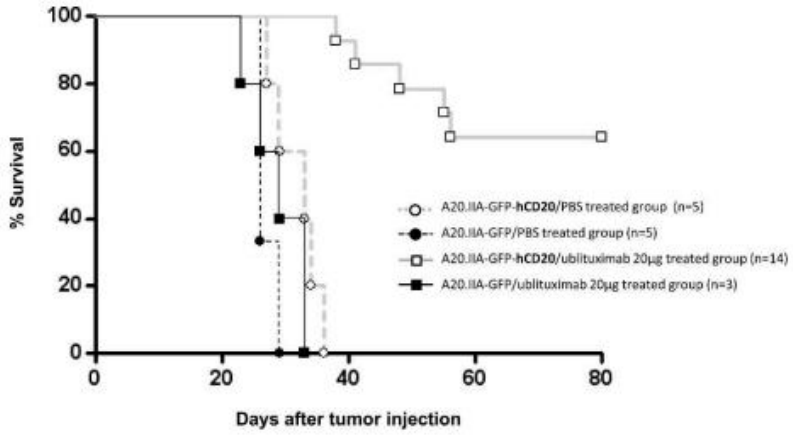

FIGURE 5. Analysis of the anti-hCD20 specificity of ublituximab in the murine PCL model. Kaplan-Meier survival analysis after brain inoculation with A20.IIA-GFP-hCD20 or A20.IIA-GFP tumor cells. On day 7 after this inoculation, the mice received an intracerebral injection of 20 μg/2 μL anti-hCD20 ublituximab, and were compared with the control group receiving an injection of PBS. Survival was followed daily. Statistical test: Log rank between the group injected with A20.IIA-GFP-hCD20 tumor cells and treated with ublituximab 20 μg and the group injected with A20.IIA-GFP tumor cells and treated with ublituximab 20 μg ($P < 0.0001$) and between the group injected with A20.IIA-GFP-hCD20 tumor cells and treated with PBS 1× (control group) and the group injected with A20.IIA-GFP tumor cells and treated with ublituximab 20 μg ($P < 0.0001$). Moreover a significant difference ($P < 0.0001$) was found between the group injected with A20.IIA-GFP-hCD20 tumor cells and treated with PBS 1× (control group) and the group injected with A20.IIA-GFP-hCD20 tumor cells and treated intracerebrally with ublituximab 20 μg.

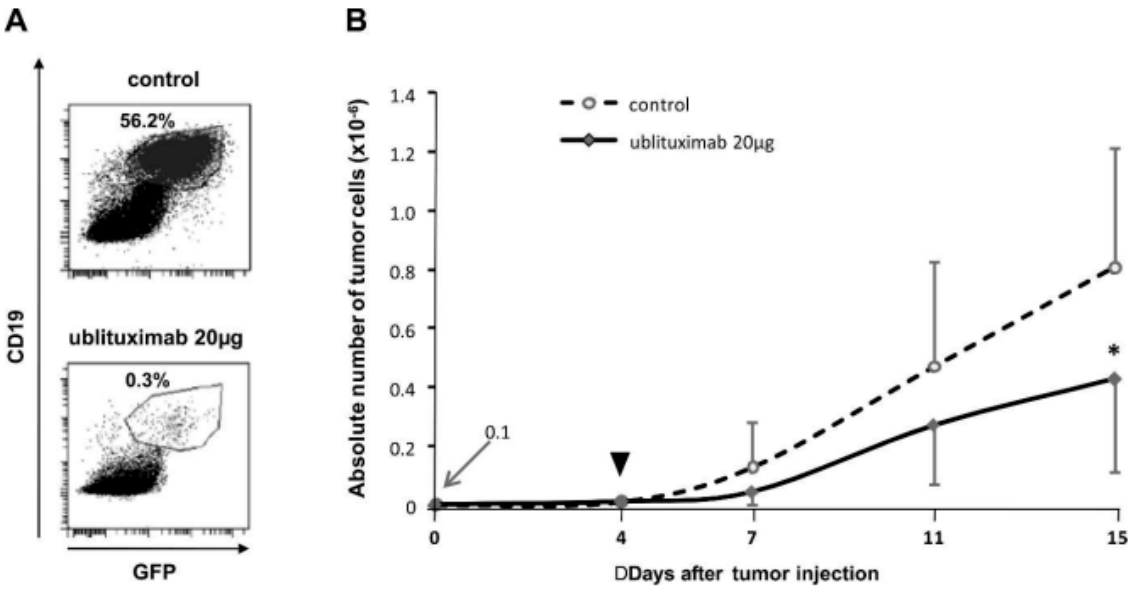

FIGURE 6. Analysis of the in vivo antitumor effect of anti-hCD20 ublituximab on PIOL. (**A**) Flow cytometric analysis on day 8 of PIOL eyes injected intravitreously in the tumor with 2 µL formulation buffer (control; *top panel*) or 2 µL containing 20 µg anti-hCD20 ublituximab (*lower panel*). (**B**) Kinetic analysis of the tumor burden by flow cytometry of PIOL eyes injected at day 4 in the tumor with 2 µL of formulation buffer (as control) or with 2 µL of anti-hCD20 ublituximab (20 µg).

unable to rescue mice implanted with the hCD20-negative tumor, but the survival time of mice with an hCD20-expressing tumor was greatly enhanced ($P < 0.0001$). Moreover, as previously observed, this treatment allowed 65% of the mice to reject their tumor. These results highlight the specificity against hCD20 of the antitumor response obtained after ublituximab therapy.

Anti-hCD20 Ublituximab Has a More Sustained and Better Antitumor Effect Than Rituximab on Primary Intraocular Lymphoma In Vivo

To determine if the anti-hCD20 ublituximab mAb had an antitumor effect on PIOL, immunocompetent BALB/c mice received an intravitreal injection of A20.IIA-GFP-hCD20 syngeneic lymphoma B cells 7 days before treatment. Mice were euthanized at different times following tumor implantation for ethical considerations related to the eye swelling. Clinically, as previously described,[15] vitreous and retinal invasion appeared at day 7 and increased progressively in control animals. However, vitreous haze or in some cases cataract after the second intraocular injection prevented clinical evaluation; the eyes were harvested for flow cytometric analyses (Fig. 6). Figure 6A illustrates the typical appearance of the tumor with and without anti-hCD20 therapy. The kinetics of tumor growth was also examined in mice that were or were not treated with 20 µg of ublituximab (Fig. 6B); tumor burden slowed after therapy, becoming significantly lower at day 15. Irrelevant glycoengineered mAbs of the same isotype as ublituximab were used as controls, and these groups (anti-D and anti-P24 mAbs) did not differ significantly from the PBS negative control group (Fig. 7).

A dose-response analysis was done with several concentrations of ublituximab (1, 4, and 20 µg/2 µL; Fig. 7). When ublituximab was injected at 4 µg/2 µL, the absolute number of tumor cells decreased significantly in comparison to the PBS 1X group ($P = 0.04$). In contrast, ublituximab injected at 1 µg/2 µL did not display significant efficacy.

Simultaneously, we sought to determine if the antitumor effect of ublituximab was superior to that of rituximab in the PIOL model, as it was in the PCL model, when these mAbs were administered at the same dose (20 µg/2 µL). Comparison of the absolute number of tumor cells 8 days after treatment showed it had decreased significantly in the ublituximab-

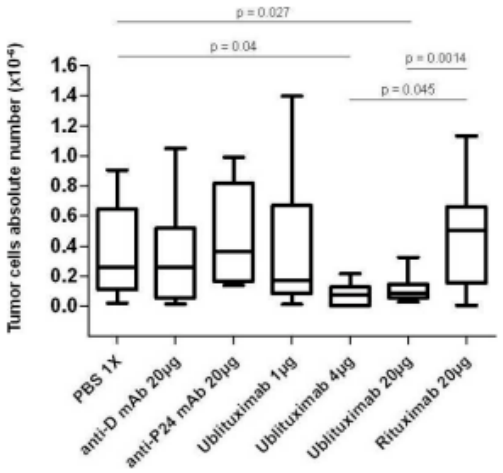

FIGURE 7. Analysis of the dose-response antitumor effect of anti-hCD20 ublituximab on PIOL. Tumor burden analysis by flow cytometry on day 8 of PIOL eyes injected at day 4 in the tumor with 2 µL of PBS (control group); anti-D mAb (20 µg); anti-P24 mAb (20 µg); rituximab (20 µg); or anti-hCD20 ublituximab (1, 4, or 20 µg). Statistical test: Mann-Whitney.

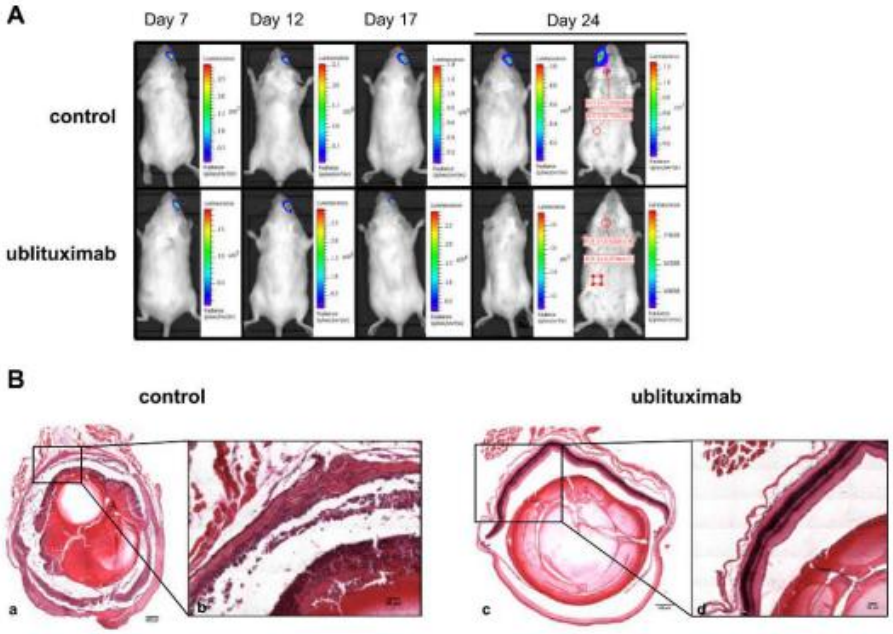

FIGURE 8. Representative bioluminescence images and histopathological analysis comparing ublituximab treatment with PBS injection in PIOL murine model. (**A**) Representative bioluminescence images of PBS control PIOL mice (*upper panel*) and ublituximab-treated PIOL mice (*lower panel*). The mice were injected with 10^4 A20.IIA-GFP-hCD20-luc2 cells on day 0 via the intravitreous route. The ublituximab treatments were administered in situ at day 7. (**B**) Representative histological aspect of PBS control PIOL mice (*left panels*) and ublituximab-treated PIOL mice (*right panels*). The mice were injected with 10^4 A20.IIA-GFP-hCD20-luc2 cells on day 0 via the intravitreal route. The ublituximab treatments were administered in situ at day 7 and sacrificed at day 21. (**a**, **c**) Magnification ×10 and *bars* represent 250 μm. (**b**, **d**) Magnification ×20 and *bars* represent 50 μm.

treated mice ($P = 0.027$) but not in those treated with rituximab (Fig. 7). The difference between the ublituximab and the rituximab-treated groups was highly significant ($P = 0.0014$) and confirmed the superiority of ublituximab in these conditions.

In bioluminescence assays, unlike in the PCL murine model, the effect of ublituximab in the PIOL model appeared later: a decrease of the tumor burden was visible at day 17 (i.e. 10 days after treatment; Fig. 8A). After 24 days, the representative PBS control mouse had a bioluminescence signal more than 200 times stronger than the ublituximab-treated mouse. In some cases (20%), histological analysis has revealed that no tumor mass could be detectable at day 21 in ublituximab-treated mice in contrast with control mice (Fig. 8B). Interestingly, some control mice had cervical lymph node metastasis, with 1×10^6 ph/s/cm^2/sr luminescence signal (Fig. 8A, RoI 1 in the upper panel), whereas the ublituximab-treated representative mouse had 2.6×10^4 ph/s/cm^2/sr in the right cervical lymph node (Fig. 8A, RoI 1 in the lower panel). Interestingly, anti-lymphoma antibodies were not detected in the control mice at day 19 (Supplementary Fig. 2B).

DISCUSSION

Most PCNSLs belong to the diffuse large B-cell lymphoma family. Although their incidence is low, it has nevertheless tripled over the past 10 years, for unknown reasons.[16] The main treatment against these tumors has been radiation coupled with chemotherapy.[17] As B-cell lymphomas express a well-characterized antigen, monoclonal antibodies are a promising therapy. Rituximab is a chimeric mAb directed against the human CD20 antigen shared by all B-cells, including B tumor cells. This antibody has shown its efficacy against systemic B-cell lymphomas,[18,19] and it has now been used for PCNSL.[20] In this study, we analyzed the efficacy of a glycoengineered anti-human CD20 monoclonal antibody developed by LFB for PIOL and PCL models and compared it with the efficacy of rituximab.

Until now, most preclinical evaluations of new therapies have used immunodeficient animals implanted with human tumors. These models are useful for assessing the direct efficacy of the treatment but cannot evaluate the immune system's influence on the therapeutic response. Syngeneic models can be useful for this purpose, but for an antigen-specific therapy, they must express the target antigen.[21] For this reason, we chose to work with two models based on the implantation of tumor cells transfected with the human CD20 gene, in the eye for the PIOL model[15,22] and in the brain for the PCL model[23] of adult syngeneic mice.

A significant increase in survival time without clinical signs was observed after a single injection of the new antibody into the brain of PCL-bearing mice, and half of the mice receiving the highest dose rejected their tumor. An interesting next step might be to multiply the number of therapeutic injections. However, repetitive injections into the brain are unlikely to be practical except if a delivery pump is implanted in the patient. Another possibility is to administer the therapeutic antibody intrathecally, which would allow its distribution throughout the entire CNS. This method has already been used clinically with rituximab with promising results,[24,25] and is currently under evaluation for ublituximab.

In our study and our conditions, rituximab was clearly less effective than ublituximab at the same therapeutic dose; only 10% of the rituximab-treated mice survived. The efficacy of rituximab against B-cell lymphoma in the brain has already been tested with the same general strategy we are using, and the authors reported a tumor rejection rate exceeding 50% after a single therapeutic injection of 25 μg.[4] However, they used a different mouse model and, more importantly, they applied the treatment very early (day 1) after tumor injection. This difference might explain the discrepancy with the results presented here.

Because we used immunocompetent mice, it was possible to determine the consequences of this therapy on the recruitment of effector immune cells. Our results clearly showed that after ublituximab therapy, $CD8^+$ T cells were recruited in the brain of PCL-bearing mice. These results are in line with recent studies showing that mAb therapy can create a memory response to a peripheral $CD20^+$ tumor[26] or to a subcutaneously implanted Neu^+ tumor.[27] This could be assessed in our model by rechallenging surviving mice with tumor cells.

It is interesting to note that results obtained on the PIOL model were less impressive. Tumor growth was delayed but not inhibited by the therapy with the optimized antibody. Eyes are often considered an extension of the CNS and they are thus thought to involve the same kind of immunoprivileged environment. Our results here suggest that eyes cannot respond as well as the brain to a B-cell lymphoma. One specific feature of the eye is its ability to suppress immune reactions even in inflammatory conditions.[28] More specifically, potential ocular antigen-presenting cells are maintained under a tolerogenic form, due to the high concentration of immunosuppressive factors in this site.[29] Ublituximab was developed to increase capacity to activate the ADCC pathway, compared with rituximab. It also induces the CDC pathway effectively. It is thus conceivable that the ocular environment decreases the capacity of the therapeutic antibodies to activate the ADCC effectively, whereas the brain environment is more permissive. Rituximab's lesser efficacy in inducing ADCC, compared with ublituximab, might also explain the difference in the results obtained with the two antibodies.

In this study, we demonstrated the efficacy of ublituximab in eliminating a B-cell lymphoma growing in two specific CNS locations, after a single therapeutic injection. Although the therapy did not cure all the animals, the results obtained in our study conditions were very encouraging and superior to those for rituximab, the reference mAb currently used. The new ublituximab mAb is thus a candidate for phase I/II studies of PIOL and PCL.

Acknowledgments

The authors thank the animal facility core (CEF, Centre de Recherche des Cordeliers, Paris, France) for mice housekeeping. Flow cytometry and acquisitions were done at the cellular imaging and cytometry platform (CICC, Centre de Recherche des Cordeliers, Paris, France). The authors thank Bernard Gjata, Thibaut Wiart, and Daniel Stockholm for their respective contribution to histological preparation and image acquisitions (histology and imaging cytometry platforms, Généthon, Evry, France). We thank Peter Sportelli for allowing the use of ublituximab, and Jo Ann Cahn for her careful reading of the manuscript.

Supported by the Institut National du Cancer (Grants RC013-C06N631-2005 and C06N748-2006); the Association pour la Recherche contre le Cancer; the Institut National de la Santé et de la Recherche Médicale; the University Pierre and Marie Curie; the University Paris-Descartes; the pole de compétitivité Ile de France (ImmuCan project); the Tunisian Direction Générale de la Recherche Scientifique; the Franco-Tunisian CMCU project; grants from the DGRS-INSERM and the CMCU (RBA); a grant from the Institut National du Cancer (SD, CD); and study grants from the Fédération des Aveugles de France and the Fondation de France (Fouassier; VT). The authors alone are responsible for the content and writing of the paper.

Disclosure: **R. Ben Abdelwahed**, LFB (F); **S. Donnou**, LFB (F); **H. Ouakrim**, LFB (F); **L. Crozet**, LFB (F); **J. Cosette**, LFB (F); **A. Jacquet**, LFB (F, E); **I. Tourais**, LFB (F, E); **B. Fournès**, LFB (F, E); **M. Gillard Bocquet**, LFB (F); **A. Miloudi**, LFB (F); **V. Touitou**, LFB (F); **C. Daussy**, LFB (F); **M-C. Naud**, LFB (F); **W.H. Fridman**, LFB (F); **C. Sautès-Fridman**, LFB (F), P; **R. Urbain**, LFB (F, E), P; **S. Fisson**, LFB (F), P

References

1. Miller DC, Hochberg FH, Harris NL, Gruber ML, Louis DN, Cohen H. Pathology with clinical correlations of primary central nervous system non-Hodgkin's lymphoma. The Massachusetts General Hospital experience 1958–1989. *Cancer*. 1994;74:1383–1397.
2. Algazi AP, Kadoch C, Rubenstein JL. Biology and treatment of primary central nervous system lymphoma. *Neurotherapeutics*. 2009;6:587–597.
3. Soussain C, Hoang-Xuan K. Primary central nervous system lymphoma: an update. *Curr Opin Oncol*. 2009;21:550–558.
4. Mineo JF, Scheffer A, Karkoutly C, et al. Using human CD20-transfected murine lymphomatous B cells to evaluate the efficacy of intravitreal and intracerebral rituximab injections in mice. *Invest Ophthalmol Vis Sci*. 2008;49:4738–4745.
5. Rosenzweig HL, Planck SR, Rosenbaum JT. NLRs in immune privileged sites. *Curr Opin Pharmacol*. 2011;11:423–428.
6. Hong SJ, Kim JS, Chang JH, et al. A successful treatment of relapsed primary CNS lymphoma patient with intraventricular rituximab followed by high-dose chemotherapy with autologous stem cell rescue. *Yonsei Med J*. 2009;50:280–283.
7. Motomura K, Natsume A, Fujii M, Ito M, Momota H, Wakabayashi T. Long-term survival in patients with newly diagnosed primary central nervous system lymphoma treated with dexamethasone, etoposide, ifosfamide and carboplatin chemotherapy and whole-brain radiation therapy. *Leuk Lymphoma*. 2011;52:2069–2075.
8. Amadori D, Milandri C, Comella G, et al. A phase I/II trial of non-pegylated liposomal doxorubicin, docetaxel and trastuzumab as first-line treatment in HER-2-positive locally advanced or metastatic breast cancer. *Eur J Cancer*. 2011;47:2091–2098.
9. van Oers MH, Van Glabbeke M, Giurgea L, et al. Rituximab maintenance treatment of relapsed/resistant follicular non-Hodgkin's lymphoma: long-term outcome of the EORTC 20981 phase III randomized intergroup study. *J Clin Oncol*. 2010;28:2853–2858.
10. Jahnke K, Thiel E. Treatment options for central nervous system lymphomas in immunocompetent patients. *Expert Rev Neurother*. 2009;9:1497–1509.
11. van Beek J, Elward K, Gasque P. Activation of complement in the central nervous system: roles in neurodegeneration and neuroprotection. *Ann N Y Acad Sci*. 2003;992:56–71.
12. de Romeuf C, Dutertre CA, Le Garff-Tavernier M, et al. Chronic lymphocytic leukaemia cells are efficiently killed by an anti-CD20 monoclonal antibody selected for improved engagement of FcgammaRIIIA/CD16. *Br J Haematol*. 2008;140:635–643.
13. Le Garff-Tavernier M, Decocq J, de Romeuf C, et al. Analysis of CD16+CD56dim NK cells from CLL patients: evidence supporting a therapeutic strategy with optimized anti-CD20 monoclonal antibodies. *Leukemia*. 2011;25:101–109.

14. Jones B, Tite JP, Janeway CA Jr. Different phenotypic variants of the mouse B cell tumor A20/2J are selected by antigen- and mitogen-triggered cytotoxicity of L3T4-positive, I-A-restricted T cell clones. *J Immunol*. 1986;136:348–356.
15. Touitou V, Daussy C, Bodaghi B, et al. Impaired th1/tc1 cytokine production of tumor-infiltrating lymphocytes in a model of primary intraocular B-cell lymphoma. *Invest Ophthalmol Vis Sci*. 2007;48:3223–3229.
16. Gerstner ER, Batchelor TT. Imaging and response criteria in gliomas. *Curr Opin Oncol*. 2010;22:598–603.
17. Ferreri AJ. How I treat primary CNS lymphoma. *Blood*. 2011; 118:510–522.
18. Molina A. A decade of rituximab: improving survival outcomes in non-Hodgkin's lymphoma. *Annu Rev Med*. 2008;59:237–250.
19. Niitsu N. Current treatment strategy of diffuse large B-cell lymphomas. *Int J Hematol*. 2010;92:231–237.
20. Tai WM, Chung J, Tang PL, et al. Central nervous system (CNS) relapse in diffuse large B cell lymphoma (DLBCL): pre- and post-rituximab. *Ann Hematol*. 2011;90:809–818.
21. Donnou S, Galand C, Touitou V, Sautes-Fridman C, Fabry Z, Fisson S. Murine models of B-cell lymphomas: promising tools for designing cancer therapies. *Adv Hematol*. 2012;2012: 701704.
22. Touitou V, Bodaghi B, de Kozak Y, Lehoang P, Sautes-Fridman C, Fisson S. Animal models of intraocular lymphomas. *Ophthalmic Res*. 2008;40:208–211.
23. Donnou S, Galand C, Daussy C, et al. Immune adaptive microenvironment profiles in intracerebral and intrasplenic lymphomas share common characteristics. *Clin Exp Immunol*. 2011;165:329–337.
24. Maximiano Alonso C, Sanchez Ruiz AC, Cantos Sanchez de Ibarguen B, Mendez Garcia M, Ronco IS, Provencio Pulla M. Ocular relapse of primary brain lymphoma in immunocompetent patient, treated with intrathecal rituximab. *Clin Transl Oncol*. 2010;12:701–703.
25. Rubenstein JL, Fridlyand J, Abrey L, et al. Phase I study of intraventricular administration of rituximab in patients with recurrent CNS and intraocular lymphoma. *J Clin Oncol*. 2007; 25:1350–1356.
26. Abes R, Gelize E, Fridman WH, Teillaud JL. Long-lasting antitumor protection by anti-CD20 antibody through cellular immune response. *Blood*. 2010;116:926–934.
27. Park S, Jiang Z, Mortenson ED, et al. The therapeutic effect of anti-HER2/neu antibody depends on both innate and adaptive immunity. *Cancer Cell*. 2010;18:160–170.
28. Mo JS, Wang W, Kaplan HJ. Impact of inflammation on ocular immune privilege. *Chem Immunol Allergy*. 2007;92:155–165.
29. Wilbanks GA, Streilein JW. Fluids from immune privileged sites endow macrophages with the capacity to induce antigen-specific immune deviation via a mechanism involving transforming growth factor-beta. *Eur J Immunol*. 1992;22:1031–1036.

Investigative Ophthalmology & Visual Science

Conclusion on Article #1

In this work, not only the effects of Ublituximab on PCNSL mouse models were investigated. The study is indeed a comparative study between a gold standard (Rituximab) and Ublituximab. Rituximab and Ublituximab are targeted therapy, belonging to immunotherapy. These mAbs are targeting only tumor cells; and as preliminary results showed that Rituximab was not that efficient for treating PCNSL, we studied the effects of a glycoengineered mAb, which was designed to have improved effects on tumor cells.

We showed in this article that Ublituximab has a more pronounced anti-tumor effect at the same dose than Rituximab. The reduction in cell number was accompanied with a substantial increase of effector cytotoxic $CD8^+$ T-cells. Interestingly, Ublituximab also prevents metastases apparition.

Ublituximab is supposed to target only tumor cells. However, an other strategy involving a compound that activates immune system and induces cell death could lead to improved effects on the tumors. It turns out that Ron Levy's team has shown that CpG, an immunostimulatory molecule have these very effects on A20 cells subcutaneously engrafted. We then wanted to know if those effects are still significant in PCNSL.

ARTICLE # 2

Lymphoma B-Cell responsiveness to CpG-DNA depends on the tumor microenvironment

Rym Ben Abdelwahed, **Jeremie Cosette**, Sabrina Donnou, Lucile Crozet, Hanane Ouakrim, Wolf Herman Fridman, Catherine Sautès-Fridman, Aouni Mahjoub and Sylvain Fisson

2. CPG-ODN treatments of PIOL PCL and SCL

As previously explained, PIOL and PCL are very aggressive diseases with a poor survival rate even with treatment. We explored new therapeutic approaches; first with the anti-hCD20 antibody, and here, we used a TLR-9 agonist, CPG-ODN. This 20-bases-long single strand DNA molecule is an activator of immune cells through TLR-9.

TLR agonists are currently being used in tumor treatments, and show very satisfactory results.

We investigated the effects of CpG on PIOL, PCL and SCL on mouse models. Mice were injected with tumor cells in the brain, in the eye, or subcutaneously, and as for Ublituximab, the treatment was administered in situ.

As for previous article, in this work I participated in the elaboration of new cell lines, and in performing bioluminescence imaging. The available cell line at the laboratory were not suitable with CpG-CFSE internalization assay, I thus developed A20.IIA-mKate (expressing mKate, a red fluorescent protein). In this work BLI was used as a tool to localize and to produce representative images of responding or non-responding animals.

Journal of Experimental & Clinical Cancer Research

RESEARCH Open Access

Lymphoma B-cell responsiveness to CpG-DNA depends on the tumor microenvironment

Rym Ben Abdelwahed[1,2,3,8,9], Jérémie Cosette[1,2,3,4], Sabrina Donnou[1,2,3,5,6,7], Lucile Crozet[1,2,3], Hanane Ouakrim[1,2,3], Wolf Herman Fridman[1,2,3], Catherine Sautès-Fridman[1,2,3], Aouni Mahjoub[8,9] and Sylvain Fisson[1,2,3,5,6,7*]

Abstract

Background: Toll-like receptor (TLR) agonists have important properties that can be exploited for immunotherapy against tumors. Locally injected immunostimulatory oligodeoxynucleotides containing CpG motifs (CpG-ODNs), which are TLR9 agonists, have shown promise in cancer models. Several studies have demonstrated that these motifs have immunologic effects similar to those of bacterial DNA and can stimulate monocytes, macrophages, dendritic, and B cells, which then produce several proinflammatory cytokines. However, these CpG-ODNs appear to produce opposite effects on tumor B cells.

Methods: In this study, we investigated the direct effects of a murine class B CpG (1826) ODNs on lymphoma B cells *in vitro* and *in vivo*, using mouse models of non-Hodgkin B lymphomas developing in immunoprivileged sites, specifically the brain and the eye, and in subcutaneous sites.

Results: *In vitro*, CpG-ODNs produced antiproliferative and proapoptotic effects on lymphoma B cells. *In vivo*, it had an antitumor effect when injected into tumors in murine models of subcutaneous lymphoma (SCL) and primary cerebral lymphoma (PCL). However, its intravitreal administration into a primary intraocular lymphoma (PIOL) mouse model did not produce an antitumor effect. *In vitro* experiments using supernatant from mouse PIOL samples demonstrated that the PIOL molecular microenvironment inhibits the antiproliferative effect of CpG-ODNs on lymphoma B-cells.

Conclusions: Responsiveness to CpG stimulation differs in subcutaneous, cerebral, and ocular tumors, according to the tumoral and molecular microenvironment, and this should be considered for further therapeutic approaches.

Keywords: TLR, CpG-DNA, Non-Hodgkin B-cell lymphoma, Subcutaneous lymphoma, Primary cerebral lymphoma, Primary intraocular lymphoma, Tumor microenvironment

Background

Toll-like receptors (TLRs) are pattern recognition receptors that trigger innate and adaptive immune responses. Triggering TLRs activates a set of common proinflammatory genes and leads to the expression of antimicrobial effector cells and to production of inflammatory cytokines [1]. Agonists for TLRs have been identified and are being developed as new drugs and vaccine adjuvants to treat cancer, allergies, and infectious diseases [2]. In particular, oligodeoxynucleotides containing CpG motifs (CpG-ODN), which are TLR9 agonists, have shown promise against several types of tumors, including renal cell carcinoma, glioblastoma, melanoma, cutaneous T-cell lymphoma, and non-Hodgkin lymphoma [3]. Unmethylated CpG-DNA motifs have immunologic effects similar to those of bacterial DNA and can stimulate monocytes, macrophages, and dendritic and B cells; these then produce several Th1-type cytokines [4].

At least 3 structurally distinct classes of synthetic CpG-ODNs have been described, all capable of stimulating cells that express TLR9 [5,6]. CpG-B (also known as class-B CpG or K-type CpG) ODNs encode multiple CpG motifs on a phosphorothioate backbone and trigger the differentiation of antigen-presenting cells and the proliferation

* Correspondence: sylvain.fisson@univ-evry.fr
[1]Institut National de la Santé et de la Recherche Médicale (INSERM), UMRS872, Centre de Recherche des Cordeliers, Paris F-75006, France
[2]Université Pierre et Marie Curie-Paris 6, UMRS 872, Paris F-75006, France
Full list of author information is available at the end of the article

and activation of B cells [3]. Although the CpG-B motif is an established immunostimulatory agent, its direct effect on normal and tumor B cells seems to differ: CpG-ODNs stimulate proliferation of healthy B cells, activate their production of polyreactive immunoglobulins, and protect them from apoptosis [6-8]. On the other hand, these ODNs predominantly activate malignant B cells and then increase the rate of cell death, thus reducing survival of malignant B cells over time [9-11].

Different types of non-Hodgkin B-cell lymphomas differ in their responsiveness to CpG-DNA, and only limited information is available [9] about the sensitivity of malignant B cells to this DNA motif according to their *in vivo* microenvironment, particularly in immune sanctuaries such as the brain and eyes. Unlike systemic lymphoma, primary cerebral lymphoma (PCL) and primary intraocular lymphoma (PIOL) are subsets of primary central nervous system lymphoma (PCNSL), and they affect immunologically privileged organs. Both usually appear as a diffuse large B-cell non-Hodgkin lymphoma in which malignant lymphoid cell types not normally present in the brain or eye are detected [12]. The internal tissues of the brain and eye are usually protected from the inflammatory processes mediated by the immune system.

In this study, we compare the effect of CpG-ODNs on cerebral and ocular diffuse large B-cell lymphoma and on subcutaneous lymphomas (SCL). We show that A20.IIA murine B-cell lymphoma expressed high levels of endogenous TLR9 protein that produced an antiproliferative effect when stimulated *in vitro* by CpG-ODNs. A proapoptotic effect accompanied this reduced proliferation. *In vivo* local administration had a similar antitumor effect on subcutaneous and cerebral lymphomas. However, local administration of CpG-ODNs in a PIOL mouse model did not produce an antitumor effect. *In vitro* experiments with supernatant from ocular lymphoma samples demonstrated that the molecular microenvironment of PIOL counteracts the direct antiproliferative effect of CpG-ODNs on lymphoma B-cells. These findings show that cerebral and ocular tumor cells differ in their responsiveness to CpG stimulation according to the tumor environment. The microenvironment of the eye must be further characterized to identify the negative regulators.

Methods

Reagents

Nuclease-stable phosphorothioate-modified CpG 1826 (CpG) with 5_-TCCATGA**CG**TTCCTGA**CG**TT (the nucleotides in bold represent the immunostimulatory CpG sequences), fluorescein isothiocyanate (FITC)-conjugated CpG 1826 ODNs, and control 1826 ODN with 5_-TCC ATGAGCTTCCTGAGCTT were purchased from InvivoGen (Cayla, France).

Cells

A20.IIA is an FcγR-negative clone originating from the A20-2 J B-cell lymphoma line [13]. For *in vivo* experiments, A20.IIA cells were transfected by an electroporation system with the green fluorescent protein (GFP) gene. These cells, hereafter referred to as A20.IIA or A20.IIA-GFP cells as appropriate, were maintained at 37°C, 5% CO_2 in complete Roswell Park Memorial Institute (RPMI) 1640 Medium Glutamax plus (RPMI; Gibco-Invitrogen, France) supplemented with 10% fetal calf serum (FCS; PAA Laboratories, Germany), 100 μg/mL penicillin and 100 μg/mL streptomycin (both from Eurobio, France), 10 mM sodium pyruvate (Gibco-Invitrogen), and 50 μM 2-mercaptoethanol (Gibco-Invitrogen). The A20.IIA-GFP cell culture was also supplemented with 0.5 mg/mL neomycin (G418; Gibco-Invitrogen). To obtain the A20.IIA-*luc*2 cell line, A20.IIA cells were transfected with pGL4.50[luc2/CMV/hygro] (Promega), in the AMAXA Nucleofector II device (Lonza, Switzerland) and were cultured in 0.75 mg/mL hygromycin B (Gibco-Invitrogen) medium.

Proliferation assay

A20.IIA cells at a concentration of 10^5cells/mL were incubated with serial dilutions of CpG 1826 or control 1826 ODNs at concentrations ranging from 0.0003 to 60 μg/mL or with complete RPMI medium alone. After 3 days, [^{3}H] thymidine (GE Healthcare) was added for the last 4 h. Cells were harvested onto fiber filters and [^{3}H] thymidine incorporation was measured in a scintillation counter (Microbeta, Perkin Elmer).

Apoptosis assay

A20.IIA cells (10^4) were cultured in complete RPMI medium in 96-well plates in the presence or absence of 3 μg/mL or 30 μg/mL of CpG or control ODNs. Staining with Annexin V/allophycocyanin (APC) and propidium iodide (PI) (BD Biosciences, France) was performed 72 h later and then analyzed by flow cytometry. Apoptotic cells were defined as those positive for Annexin V and PI.

Mice

Female BALB/c mice (H-2^d) were obtained from Charles River Laboratories (L'Arbresle, France) and used between 6 and 8 weeks of age. They were provided with sterile food and water *ad libitum* and kept on a 12-hour light–dark cycle. All procedures involving mice conformed with European Union guidelines, French regulations for animal experimentation (Ministry of Agriculture Act No. 2001–464, May 2001), and the guidelines of the Institut National de la Santé et de la Recherche Médicale Committee on Animal Research, and were approved by the relevant local committees (Charles Darwin Ethics Committee

for Animal Experiments, Paris, France; Permit Number: p3/2009/004).

Tumor implantation

Mice were first anesthetized by intraperitoneal injection of a mixture containing 120 mg/kg of ketamine (Virbac, France) and 6 mg/kg of xylazine (Rompun 2%; Bayer Healthcare). To obtain a subcutaneous lymphoma (SCL) murine model, BALB/c mice were inoculated subcutaneously with 5×10^6 A20.IIA-GFP tumor cells in a final volume of 50 μL of RPMI, at 2 different sites: the right and left abdomen. For the intracerebral tumor implantation, anesthetized mice were immobilized on a stereotaxic frame (David Kopf Instruments, Tujunga, CA, USA). Tumor cells (5×10^4 in a final volume of 2 μL RPMI) were injected into the specific cerebral location (right striatum), located 2 mm to the right of the medial suture and 0.4 mm in front of the bregma, through a Hamilton syringe attached to a penetrating depth controller. The penetrating depth of the syringe was 2.5 mm from the surface of the brain. Each injection delivered the solution slowly, and the syringe was held in place for an additional minute to reduce backfilling of tumor cells. For the intravitreal tumor implantation, we used a 32-gauge needle attached to a syringe to inject 10^4 cells in a final volume of 2 μL of RPMI into the vitreous under a dissecting microscope. Lacrinorm 2% (Bauch&Lomb) drops were instilled after intravitreal injection. For each tumor model, control mice received either 1× phosphate-buffered saline (pH7.4; PBS) or control 1826 ODNs instead of CpG 1826 ODNs.

Treatment injections

Tumor growth in the SCL model was monitored by caliper measurements 3 times a week. Treatment began when the longest tumor diameter reached 0.5 to 0.7 cm. The mice then received daily intratumor injections of CpG-ODNs for 5 days (100 μg per injection in a final volume of 50 μL RPMI) in the right tumor only; the left tumor served as an untreated control tumor. Mice were killed one week after the last treatment injection. Lymphomas established in the brain and eye were treated 7 days after tumor inoculation, by a single local injection of 60 μg (brain) or 20 μg (eye) CpG-ODNs in 2 μL of RPMI (treatment groups) or 2 μL of PBS (control groups). Tumor burden was analyzed in the sacrificed mice one week after treatment administration.

Isolation of brain, ocular and subcutaneous lymphomas

The tumor-injected brains and eyes and the subcutaneous tumors were harvested one week after treatment injection, minced with surgical scissors, incubated for 30 minutes in RPMI containing 0.1 mg/mL DNAse I (Roche Diagnostics, Meylan, France) and 1.67 Wünch U/mL Liberase (Roche), and filtered through a 70-μm membrane (BD Falcon). Mononuclear cells were separated from myelin with a Percoll cell density gradient.

In vivo tumor growth assay

The A20.IIA (1×10^4) cells expressing luciferase (luc2 gene) were injected via subcutaneous, intracerebral or intravitreal routes into immunocompetent 7-week-old BALB/c mice. CpG or control ODNs were administered in *situ* for each lymphoma model according to the same experimental design and at the time points and doses described above. The tumor burden was thereafter monitored by bioluminescence imaging. Mice were injected intraperitoneally with 150 mg/kg of D-luciferin potassium salt (Interchim) and underwent imaging within the next 10 minutes with the IVIS LUMINA II (Caliper LS) imaging system. The exposure time was set to optimize the signal and obtain the best signal-to-noise ratio. The bioluminescence signal is expressed in photons per second.

Supernatant harvesting

Mice were implanted with tumor cells in the brain (PCL), eye (PIOL) or flank (SCL) or injected with PBS in the eye (PIE). Either 14 days later (brain and eye) or when tumor diameter reached 0.5 to 0.7 cm (SCL), the relevant cells were isolated and cultured for 36 h in complete RPMI medium in 96-well (10^4 cells per well) plates. Supernatant was then harvested from each well.

Flow cytometry

To analyze TLR9 expression on A20.IIA cells, these cells underwent intracellular staining with the Fixation/Permeabilization solution kit (BD Biosciences) and an anti-TLR9/PE mAb (BD Biosciences).

Tumor burden was analyzed according to the following protocol: Fc receptors were saturated for 20 min with 10 μg/mL of anti-CD16/CD32 mAb (clone 2.4.G2), and then the cells were incubated for 20 min with either rat IgG2a anti-CD19/APC mAb, or the corresponding isotypic mAb control (all from BD Biosciences). The living cells were defined with side scatter (SSC) and forward scatter (FSC) after autofluorescent cells were excluded. Cell phenotypes were analyzed with the LSRII cytometer and Diva software (BD Biosciences).

Statistical analysis

Comparisons used Student's t-test, performed with GraphPad Prism (GraphPad Software, La Jolla, CA, USA). Statistical significance was defined by p values less than 0.05.

Results

CpG-ODNs inhibit cell proliferation and induce apoptosis of malignant A20.IIA B cells *in vitro*

TLR9 is an intracellular receptor that recognizes CpG-DNA. Cell stimulation by CpG motifs requires that they bind to TLR9. We therefore began by confirming with flow cytometry that A20.IIA B lymphoma cells express TLR9 (Figure 1A).

We next evaluated the direct effect of CpG-ODNs on the proliferation of A20.IIA lymphoma *in vitro*. Based on our study of its proliferation kinetics (data not shown), tumor cells were incubated for 72 h with CpG 1826 ODNs at concentrations ranging from 0.0003 to 30 μg/mL. Cell proliferation was measured with the [^{3}H] thymidine incorporation assay. The CpG-ODNs inhibited A20.IIA [^{3}H] thymidine incorporation in a dose-dependent manner, whereas control ODNs had no effect on cell proliferation (Figure 1B). The maximum inhibitory effect was obtained from 0.3 to 30 μg/mL of CpG-ODNs.

Based on these results, we analyzed the induction of apoptosis of A20.IIA cells by CpG- ODNs and found that they induced apoptosis of about 30 to 35% of the cells (that is, 30-35% stained positive for Annexin V and PI), compared with 5% for RMPI Medium and 5-10% with the control ODNs (Figure 1C).

Lymphoma cell responsiveness to CpG sequences differs according to their tissue microenvironment

After showing that the CpG motif has a direct antiproliferative and proapoptotic effect on A20.IIA lymphoma cells, we sought to explore its effects *in vivo* when injected intratumorally, by comparing the 3 types of murine models of lymphoma: SCL, PCL and PIOL. A20.IIA-GFP cells were implanted on the left and right flank of the mice for the SCL model. Tumor size was measured by a caliper 3 times a week. When the tumors reached 5–7 mm in diameter, the left site was treated by local injections of CpG- ODNs, while the right one was used as an untreated control tumor. As described by Houot & Levy in 2009 [14] mice did or did not receive daily intratumoral injections of 100 μg/50μL CpG-ODNs for 5 days. Tumor size was then measured daily until sacrifice, one week after the last treatment injection. The tumor burden of mice treated with CpG and control ODNs was compared with a bioluminescence imaging system that assessed total photon influx. The CpG-ODNs inhibited tumor growth very soon after treatment in this SCL model. On day 7 after treatment, the untreated tumor was more than 100 times brighter than the CpG-treated one, and on day 20, 120 times brighter (Figure 2A). Flow cytometric analysis of CD19$^+$GFP$^+$

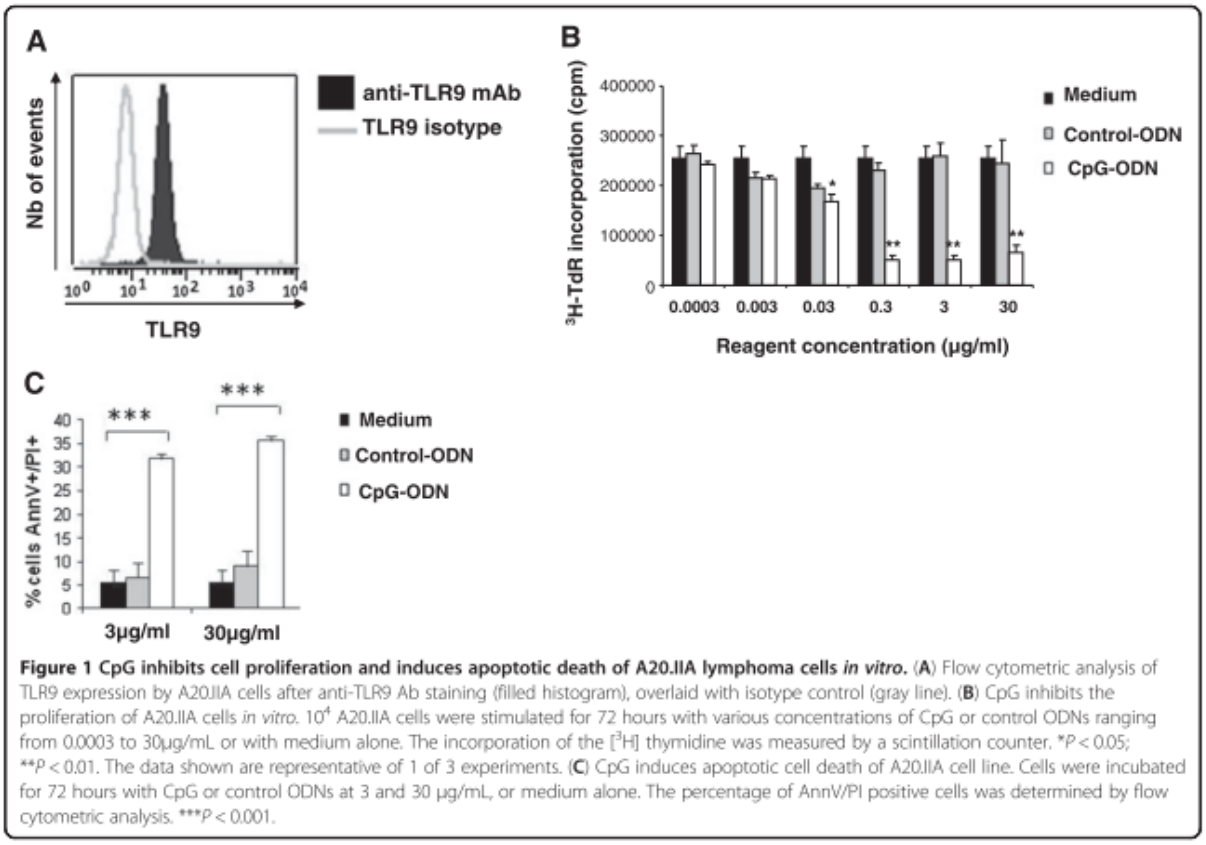

Figure 1 CpG inhibits cell proliferation and induces apoptotic death of A20.IIA lymphoma cells *in vitro*. (**A**) Flow cytometric analysis of TLR9 expression by A20.IIA cells after anti-TLR9 Ab staining (filled histogram), overlaid with isotype control (gray line). (**B**) CpG inhibits the proliferation of A20.IIA cells *in vitro*. 10^4 A20.IIA cells were stimulated for 72 hours with various concentrations of CpG or control ODNs ranging from 0.0003 to 30μg/mL or with medium alone. The incorporation of the [^{3}H] thymidine was measured by a scintillation counter. *$P < 0.05$; **$P < 0.01$. The data shown are representative of 1 of 3 experiments. (**C**) CpG induces apoptotic cell death of A20.IIA cell line. Cells were incubated for 72 hours with CpG or control ODNs at 3 and 30 μg/mL, or medium alone. The percentage of AnnV/PI positive cells was determined by flow cytometric analysis. ***$P < 0.001$.

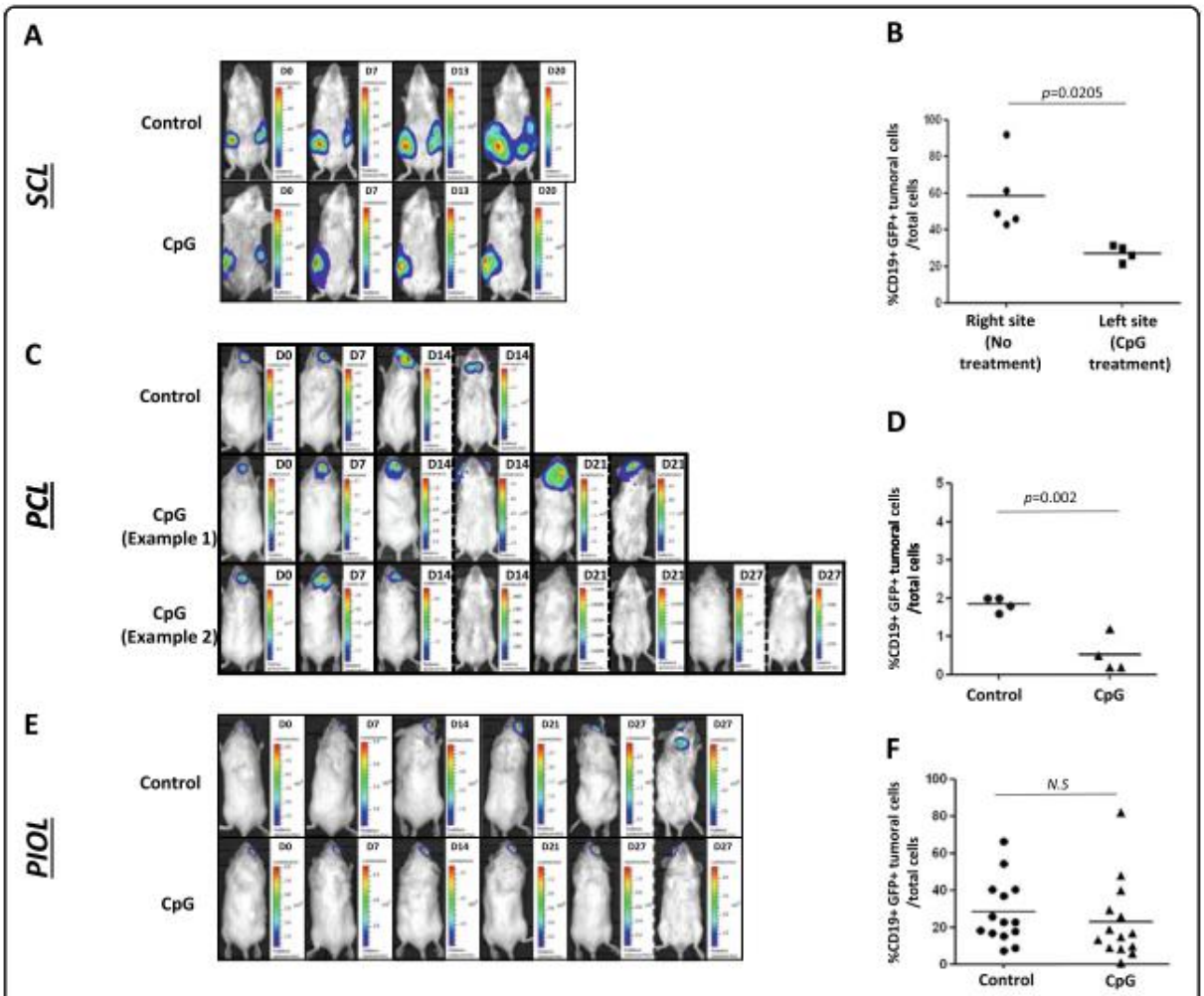

Figure 2 CpG-ODNs decrease the burden of subcutaneous and cerebral tumors but fail to induce PIOL regression. The 2-tumor-site SCL model: (**A**) Representative bioluminescence images of SCL treated with control ODNs (upper panel) and CpG-ODNs (lower panel). The mice were injected with $5x10^6$ A20.IIA-GFP-luc2 cells. Treatment was injected *in situ* when the tumor reached 0.5 to 0.7 cm in diameter. (**B**) Flow cytometric analysis of GFP^+ $CD19^+$ tumor cells, 7 days after the end of CpG-ODN administration in right tumors compared to left (untreated) tumors. PCL lymphoma model: (**C**) Representative bioluminescence images of PCL mice treated with control ODNs (upper panel) and CpG-ODNs (both lower panels), showing 2 different profiles of responsiveness to CpG motifs. The mice were injected with $5x10^4$ A20.IIA-GFP-luc2 cells and treated one week after tumor inoculation. (**D**) The percentage of $CD19^+$ GFP^+ tumor cells, as determined by flow cytometry, in the brain of mice treated with CpG at 60 μg/2μL, in comparison with PBS 1X (Control)-injected mice (n = 5 per group). PIOL lymphoma model: (**E**) Representative bioluminescence images of PIOL mice treated with control ODNs (upper panel) and CpG-ODNs (lower panel). The mice were injected with 10^4 A20.IIA-GFP-luc2 cells. CpG-ODN treatment was administered on day 0 intravitreously. (**F**) Flow cytometric analysis of the percentage of GFP^+CD19^+ tumor cells in PIOL-inoculated right eyes (n = 14 per group). A week after tumor injection, right eyes of mice were treated intravitreally by 20 μg/2 μL of mice injected with CpG-ODNs or PBS 1X (Control). Results obtained from 2 independent experiments were pooled. Statistical test: Mann–Whitney; NS: not significant.

cells confirmed that tumor cells decreased significantly more in the treated than the untreated tumors (Figure 2B).

We next addressed the question of whether CpG motifs have the same antitumor effect in cerebral lymphomas. Imaging analysis showed two different profiles. Some mice did not respond to *in situ* CpG-ODN treatment, and the lymphoma developed in the brain and even developed in lymph nodes at day 21; this timing was nonetheless later than in the control group (Figure 2C – Example 1). Some mice did respond to the treatment; the tumor grew from day 0 to day 7 after treatment, and then decreased until it was undetectable (Figure 2C – Example 2). We also examined the percentage of $CD19^+GFP^+$ cells in the group treated by CpG-ODNs, compared it with the control group and observed a significant decrease in the proportion of tumor cells (Figure 2D).

Next we investigated the antitumor effect of CpG-ODNs on PIOL mice that had a tumor implanted in the right eye only and were then treated with CpG-ODNs (20 μg/2μL) or control ODNs (20 μg/μL). As shown in Figure 2E, CpG-ODNs seem to have had no detectable effects on the primary eye tumor. Nevertheless, they appeared to prevent lymph node invasion at day 27 (Figure 2E). Flow cytometric analysis showed no significant difference in tumor growth between CpG ODN-treated and control (PBS 1X) treated eyes (Figure 2F).

These results suggest that the behavior of tumors in the eye is different from that of systemic lymphomas, but also from that of cerebral lymphoma, and thus, that tumor cells responsiveness to CpG-DNA depend on the tissue microenvironment.

Soluble molecules from the PIOL microenvironment counteract the antiproliferative effect of CpG-ODNs on malignant B-cells in a dose-dependent-manner

As described above, *in vivo* experiments showed that the responsiveness of lymphoma B cells to CpG-ODN administration was tissue-dependent. To confirm that the blockade of CpG-ODN antitumor effects was due to the PIOL molecular microenvironment, we tested whether supernatant from PIOL could counteract the inhibitory effect of CpG-ODNs on the proliferation of A20.IIA cells *in vitro*. A [^{3}H] thymidine incorporation assay was performed as described above, with the addition of supernatant obtained from PBS-injected eyes (PIE) (as control), or from the mouse model SCL, PCL, and PIOL. As shown in Figure 3, the addition of PIE (Figure 3A) and SCL (Figure 3B) supernatants did not modify the ability of CpG-ODN treatment to inhibit tumor growth. PCL supernatant (Figure 3C) increased proliferation, but CpG-ODNs were still active at doses of 30 and 60 μg/mL. In contrast, CpG-ODNs were unable to inhibit tumor cell proliferation after incubation with PIOL supernatant (Figure 3D) and to induce apoptosis (data not shown). Moreover, their antiproliferative effect was recovered upon dilution of the PIOL supernatant (Figure 4). These data confirm our *in vivo* results and show that a soluble factor, released in eye tumors but not in normal eyes, was able to counteract the antiproliferative effect of CpG motifs.

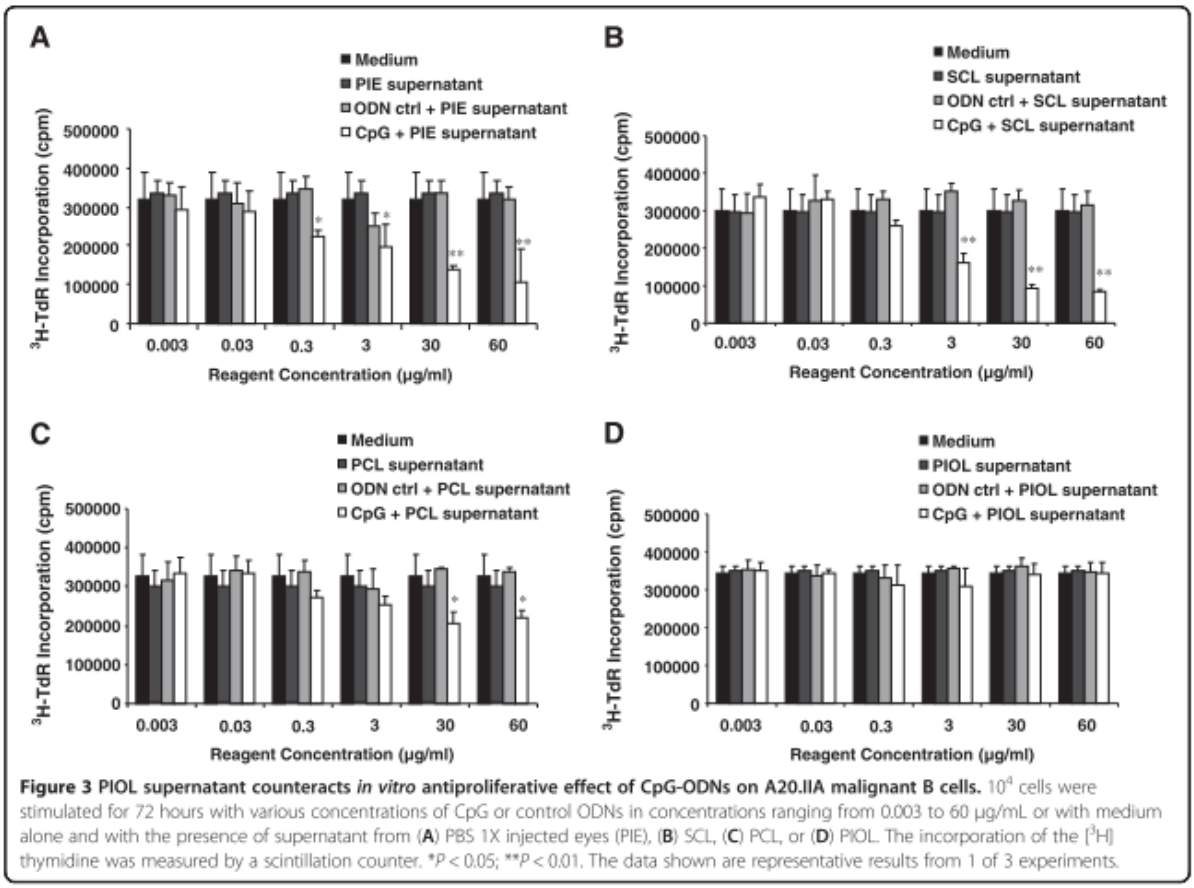

Figure 3 PIOL supernatant counteracts *in vitro* antiproliferative effect of CpG-ODNs on A20.IIA malignant B cells. 10^4 cells were stimulated for 72 hours with various concentrations of CpG or control ODNs in concentrations ranging from 0.003 to 60 μg/mL or with medium alone and with the presence of supernatant from (**A**) PBS 1X injected eyes (PIE), (**B**) SCL, (**C**) PCL, or (**D**) PIOL. The incorporation of the [^{3}H] thymidine was measured by a scintillation counter. *$P < 0.05$; **$P < 0.01$. The data shown are representative results from 1 of 3 experiments.

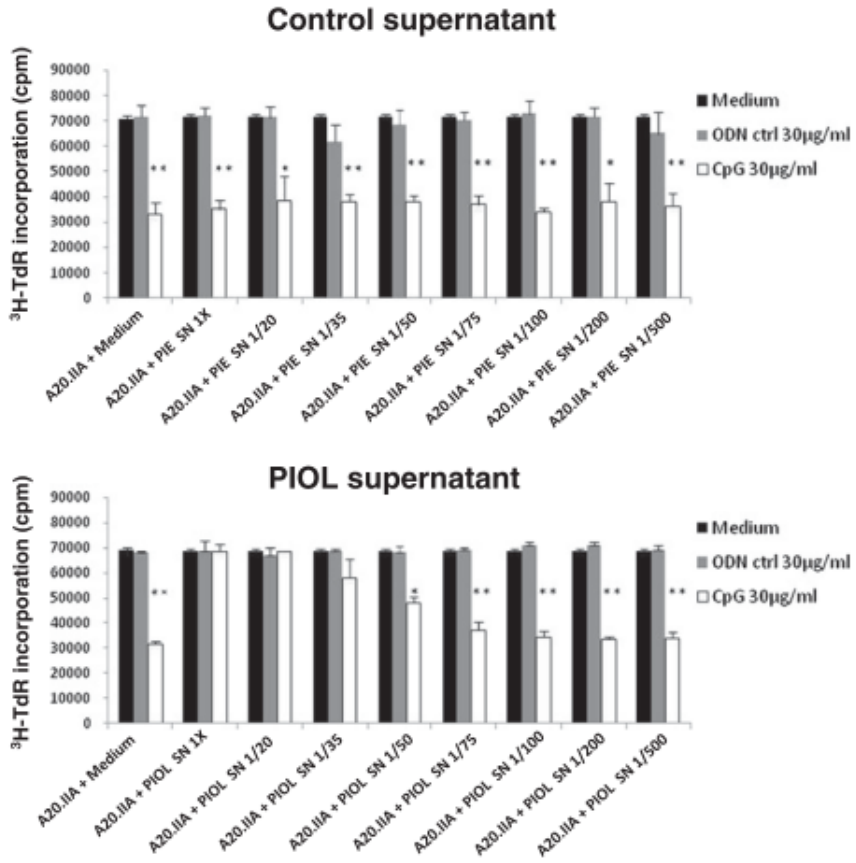

Figure 4 Soluble molecule present in PIOL but not in normal ocular microenvironment is able to abrogate *in vitro* effect of CpG-ODNs in a dose-dependent manner. 10^4 cells were stimulated for 72 hours with CpG or control ODNs at 30 µg/mL and in the presence of several diluted doses of control supernatant (PIE) or PIOL supernatant (1X, 1/20, 1/35, 1/50, 1/75, 1/100, 1/200, 1/500). The incorporation of the [^{3}H] thymidine was measured by a scintillation counter. *$P < 0.05$; **$P < 0.01$.

The PIOL microenvironment did not modify either TLR9 expression or the internalization of CpG-ODNs by tumor cells

To investigate the possibility that the loss of the CpG-ODNs antitumor action was associated with modulation of TLR9 expression, we used flow cytometry to compare TLR9 expression on A20.IIA cells after incubation with supernatant from medium alone, PIOL or PIE. No differences were found between these conditions (Figure 5A).

Next we examined whether the PIOL molecular microenvironment inhibited internalization of CpG ODNs by tumor cells. FITC-labelled CpG 1826 ODNs were added for 24 hours at a concentration of 3 µg/mL to A20.IIA lymphoma cells in the presence of PIOL or PIE supernatant. Flow cytometric analysis indicated that FITC expression by tumor cells with PIOL supernatant was similar to that incubated with PIE supernatant (Figure 5B).These findings show that the addition of PIOL supernatant does not modify CpG internalization by lymphoma B-cells, even *in vivo* in our three model (data not shown).

Discussion

The ultimate goal of cancer immunotherapy is to eradicate tumors through vaccine strategies. Recent studies have demonstrated that synthetic CpG-ODNs induce regression of highly immunogenic tumors by engaging both the innate and the adaptive immune systems. CpG-ODNs are currently being tested in clinical trials for the treatment of non-Hodgkin B-cell lymphoma, which expresses TLR9 [15]. However, only limited information is currently available about the sensitivity to CpG-ODNs of primary malignant B-cells of different non-Hodgkin lymphoma entities. Understanding their direct effect on malignant B-cells is important as we consider how this potent class of agents might be used in the immunotherapy of lymphoma.

Here, we found that A20.IIA malignant murine cells, related to diffuse large B cells, express TLR9 and

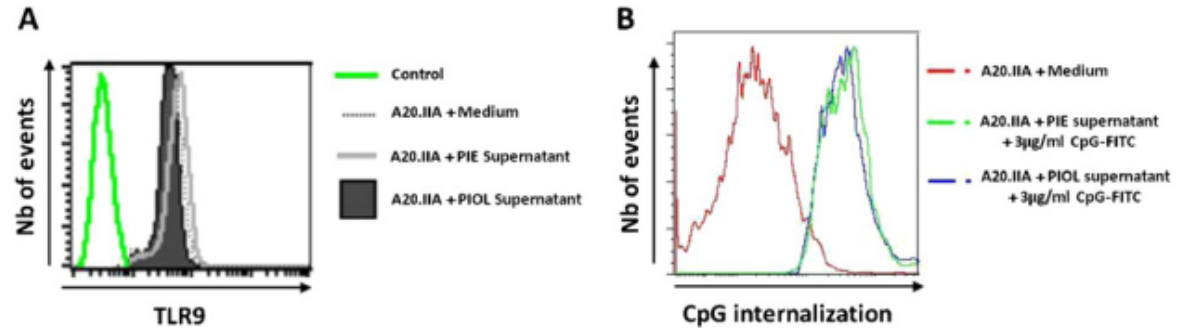

Figure 5 The PIOL microenvironment did not modify TLR9 expression or internalization of CpG-ODNs by tumor cells. (**A**) 10^4 A20.IIA cells were incubated with PIOL or PIE supernatant. 3 days later, cytometric analysis was performed of TLR9 expression by cells incubated with PIOL supernatant, overlaid with isotype control and compared to TLR9 expression by cells incubated with PIE supernatant or medium alone. (**B**) 10^4 A20.IIA cells were incubated for 24 hours with medium alone or with PIOL or PIE supernatant and in the presence or absence of FITC-labeled CpG-ODNs at 3 µg/mL. FITC expression by A20.IIA tumor cells was analyzed by flow cytometry.

are sensitive to CpG-B ODN stimulation *in vitro*. As reported previously, CpG-ODNs induce a dose-dependent antiproliferative effect [16] and increase apoptotic cell death [17]. This apoptosis has been described as caspase-dependent and is accompanied by up-regulation of CD95/Fas and its ligand [9]. Another group demonstrated that TLR9 signaling by CpG-B ODNs leads to NF-kB-dependent production of autocrine IL-10, which then activates JAK/STAT pathway-dependent tyrosine phosphorylation of STAT1 proteins and thereby engenders an apoptotic pathway in human chronic lymphocytic leukemia B-cells [10]. Comparing primary B-cell lymphomas from patient samples, other authors have showed that cell responsiveness to CpG-ODNs varies, with different degrees of activation and apoptosis induction [9]. Several studies have reported that CpG-ODNs induce activation of normal B-cells and block apoptosis [7]. Although the molecular mechanisms of these effects remain unclear, it has been suggested that reactive oxygen species (ROS) and NFkB activation may play a role [18].

An important question is whether the *in vitro* responses to CpG motifs that have been observed could produce an *in vivo* antitumor effect on DLBCL lymphoma mouse models. We used 3 mouse models to begin to answer this question: a primary systemic lymphoma model (subcutaneous lymphoma) and 2 primary central nervous system lymphoma subtypes (cerebral and ocular lymphoma mouse models). The brain and eyes, considered to be immune sanctuaries, are relatively isolated from the systemic immune system by anatomic and physiologic barriers that maintain a local immune tolerance to protect neuronal cells from inflammation [19]. The use of these different models allowed us to compare the responsiveness to CpG-ODNs of the same tumor cells located in different immune microenvironments.

Thus, we demonstrated that local administration of CpG-ODNs into subcutaneous lymphoma decreased the tumor burden. This effect is probably attributable to immune cell activation of NK cells and DCs, which activates innate and adaptive immunity. In addition, the CpG-ODNs inhibited proliferation and induced apoptosis of TLR9-positive tumor cell lines *in vitro*. Interestingly, intratumor administration of CpG-ODNs induced tumor regression of cerebral but not intraocular lymphoma. The similarity in origin and classification of PCL and PIOL, which are related subsets sharing the particularity of developing in different immune-privileged sites, makes these results especially striking.

In addition, PIOL supernatant selectively abrogated the inhibitory effects of CpG-ODNs *in vitro*, in contrast to supernatant from nonmalignant eyes (PBS-injected eye) or SCL. PCL supernatant, on the other hand, had an intermediate inhibitory effect on the *in vitro* antiproliferative action of CpG-ODNs. Together, these data suggest that soluble factors are produced in the PIOL microenvironment, to a lesser degree in the PCL microenvironment, and not at all in subcutaneous microenvironment. These factors can inhibit the effect of this TLR9 agonist on lymphoma B-cells. This inhibition was not due to downregulation of TLR9 expression or to a blockade of CpG internalization by tumor cells. Further investigation is needed to characterize TLR9-mediated signaling and molecular mechanisms that might differ in the PIOL microenvironment.

Conclusions

In conclusion, we showed here that, in addition to their immune-enhancing effects, CpG-ODNs inhibit lymphoma B cell proliferation and induce apoptotic cell death *in vitro*. They also reduced tumor growth in systemic

and cerebral lymphomas *in vivo*. These findings support the value of developing TLR9-targeted therapy with CpG-B ODNs as a therapeutic agent for primary non-Hodgkin B-cell lymphoma. Further investigation should seek to identify and characterize the soluble factors from the PIOL microenvironment that inhibit the effects of CpG-ODNs and enable us to understand the potential immunosuppressive effect on host immune response that the ocular lymphoma microenvironment appears to produce.

Abbreviations

APC: Allophycocyanin; CpG: Cytosine phosphodiester guanine; FITC: Fluorescein isothiocyanate; GFP: Green fluorescent protein; H-TdR: Tritiated thymidine; mAb: monoclonal antibody; ODN: Oligodeoxynucleotide; PBS: Phosphate buffered saline; PCL: Primary cerebral lymphoma; PCNSL: Primary central nervous system lymphoma; PE: Phycoerythrin; PI: Propidium iodide; PIE: PBS-injected eye; PIOL: Primary intraocular lymphoma; RPMI: Roswell Park Memorial Institute; SCL: Subcutaneous lymphoma; TLR: Toll-like receptor.

Competing interests

The authors declare they have no financial conflicts of interest.

Authors' contributions

Contribution: RBA, JC, and SD performed the experiments and wrote the paper. LC and HO provided technical assistance; WHF, CSF, MA, and SF contributed to the writing and to the critical reading of the paper; SF conceived and planned the study. All authors read and approved the final manuscript.

Acknowledgments

Flow cytometry acquisition took place at the cellular imaging and cytometry platform (CICC, Centre de Recherche des Cordeliers, Paris F-75006, France). We are grateful to Jo Ann Cahn for her careful reading of the manuscript.

Grant support

This work was supported by the Institut National du Cancer (Grants RC013-C06N631-2005 and C06N748-2006), the Association pour la Recherche contre le Cancer (ARC), the Institut National de la Santé et de la Recherche Médicale (INSERM), the University Pierre and Marie Curie (UPMC, Convergence project), the University Paris-Descartes, the pole de compétitivité Ile de France (ImmuCan project), the Tunisian Direction Générale de la Recherche Scientifique, and the French-Tunisian DGRS-INSERM and CMCU (Egide-PHC Utique) projects. RBA received grants from the DGRS-INSERM and the CMCU. S.D. received a grant from the Institut National du Cancer (INCa).

Author details

[1]Institut National de la Santé et de la Recherche Médicale (INSERM), UMRS872, Centre de Recherche des Cordeliers, Paris F-75006, France. [2]Université Pierre et Marie Curie-Paris 6, UMRS 872, Paris F-75006, France. [3]Université Paris Descartes, UMRS 872, Paris F-75006, France. [4]Laboratoire MSC, Université Paris 7/CNRS, Paris, France. [5]Genethon, Evry, France. [6]INSERM, U951, Evry, France. [7]University of Evry Val d'Essonne, UMRS 951, 1 bis rue de l'Internationale, Evry F-91002, France. [8]Faculté de Pharmacie de Monastir, LR99 ES27, Monastir 5000, Tunisie. [9]Université de Monastir, Monastir 5000, Tunisie.

Received: 22 December 2012 Accepted: 30 March 2013
Published: 5 April 2013

References

1. Chang ZL: **Important aspects of Toll-like receptors, ligands and their signaling pathways.** *Inflamm Res* 2010, **59**(10):791–808.
2. Dunne A, Marshall NA, Mills KH: **TLR based therapeutics.** *Curr Opin Pharmacol* 2011, **11**(4):404–411.
3. Krieg AM: **Toll-like receptor 9 (TLR9) agonists in the treatment of cancer.** *Oncogene* 2008, **27**(2):161–167.
4. Weiner GJ, Liu HM, Wooldridge JE, Dahle CE, Krieg AM: **Immunostimulatory oligodeoxynucleotides containing the CpG motif are effective as immune adjuvants in tumor antigen immunization.** *Proc Natl Acad Sci USA* 1997, **94**(20):10833–10837.
5. Verthelyi D, Ishii KJ, Gursel M, Takeshita F, Klinman DM: **Human peripheral blood cells differentially recognize and respond to two distinct CPG motifs.** *J Immunol* 2001, **166**(4):2372–2377.
6. Hartmann G, Krieg AM: **Mechanism and function of a newly identified CpG DNA motif in human primary B cells.** *J Immunol* 2000, **164**(2):944–953.
7. Krieg AM, Yi AK, Matson S, Waldschmidt TJ, Bishop GA, Teasdale R, Koretzky GA, Klinman DM: **CpG motifs in bacterial DNA trigger direct B-cell activation.** *Nature* 1995, **374**(6522):546–549.
8. Kuo CC, Liang CM, Lai CY, Liang SM: **Involvement of heat shock protein (Hsp) 90 beta but not Hsp90 alpha in antiapoptotic effect of CpG-B oligodeoxynucleotide.** *J Immunol* 2007, **178**(10):6100–6108.
9. Jahrsdorfer B, Muhlenhoff L, Blackwell SE, Wagner M, Poeck H, Hartmann E, Jox R, Giese T, Emmerich B, Endres S, *et al*: **B-cell lymphomas differ in their responsiveness to CpG oligodeoxynucleotides.** *Clin Cancer Res* 2005, **11**(4):1490–1499.
10. Liang X, Moseman EA, Farrar MA, Bachanova V, Weisdorf DJ, Blazar BR, Chen W: **Toll-like receptor 9 signaling by CpG-B oligodeoxynucleotides induces an apoptotic pathway in human chronic lymphocytic leukemia B cells.** *Blood* 2010, **115**(24):5041–5052.
11. Jahrsdorfer B, Jox R, Muhlenhoff L, Tschoep K, Krug A, Rothenfusser S, Meinhardt G, Emmerich B, Endres S, Hartmann G: **Modulation of malignant B cell activation and apoptosis by bcl-2 antisense ODN and immunostimulatory CpG ODN.** *J Leukoc Biol* 2002, **72**(1):83–92.
12. Rubenstein J, Ferreri AJ, Pittaluga S: **Primary lymphoma of the central nervous system: epidemiology, pathology and current approaches to diagnosis, prognosis and treatment.** *Leuk Lymphoma* 2008, **49**(Suppl 1):43–51.
13. Donnou S, Galand C, Touitou V, Sautes-Fridman C, Fabry Z, Fisson S: **Murine models of B-cell lymphomas: promising tools for designing cancer therapies.** *Adv Hematol* 2012, **2012**:701–704.
14. Houot R, Levy R: **T-cell modulation combined with intratumoral CpG cures lymphoma in a mouse model without the need for chemotherapy.** *Blood* 2009, **113**(15):3546–3552.
15. Weiner GJ: **The immunobiology and clinical potential of immunostimulatory CpG oligodeoxynucleotides.** *J Leukoc Biol* 2000, **68**(4):455–463.
16. Li J, Song W, Czerwinski DK, Varghese B, Uematsu S, Akira S, Krieg AM, Levy R: **Lymphoma immunotherapy with CpG oligodeoxynucleotides requires TLR9 either in the host or in the tumor itself.** *J Immunol* 2007, **179**(4):2493–2500.
17. Jahrsdorfer B, Weiner GJ: **CpG oligodeoxynucleotides as immunotherapy in cancer.** *Update Cancer Ther* 2008, **3**(1):27–32.
18. Weiner GJ: **CpG oligodeoxynucleotide-based therapy of lymphoid malignancies.** *Adv Drug Deliv Rev* 2009, **61**(3):263–267.
19. Galea I, Bechmann I, Perry VH: **What is immune privilege (not)?** *Trends Immunol* 2007, **28**(1):12–18.

doi:10.1186/1756-9966-32-18
Cite this article as: Ben Abdelwahed *et al.*: Lymphoma B-cell responsiveness to CpG-DNA depends on the tumor microenvironment. *Journal of Experimental & Clinical Cancer Research* 2013 **32**:18.

Conclusion on article #2

This work investigated the effects of CpG on PCNSL. The *in situ* administration of CpG had been previously shown to be very efficient in subcutaneous lymphomas.

We showed that CPG-ODN produced an anti-tumor effect, in the case of PCL and SCL but is no significant effects were observed on PIOL. *In vitro*, PIOL cells supernatant inhibited the anti-tumor effects of CpG.

Conclusion on Bioluminescence for treatments monitoring

In relation to my PhD work, these two articles show evidences that bioluminescence imaging is suitable for **non-invasive** and **longitudinal** studies of treatment responses. BLI allows locating primary tumors (eye and brain in our models) and also metastases (lymph nodes). On top of that, BLI can serve as **an injection control** (at day 0); survival curve, histology and cytometry analysis does not actually provide evidences that tumor cells were correctly injected. BLI provides these evidences as can be seen on the articles figures were d0 is shown. Finally, BLI allows to early **identify responding animal** and to clearly distinguish responding from non-responding animals. This might be very important for adapting protocols and gathering more information.

The location of metastases remains however qualitative and requires an autopsy. Here we stated about the location, but we have knowledge of our model and after many analyses, we know that tumor cell often invade lymph nodes.

It turns out that there are not so much protocols about bioluminescence quantification available. They often require complex algorithms to be computed or custom made devices. Bioluminescence images contain more information than only qualitative location of tumor sites (primary and metastases). Using one of the most used bioluminescence imaging device and software, we tried in the next part of my work to find a way to fully use bioluminescence images information.

ARTICLE # 3

Bioluminescence-based tumor quantification method for monitoring tumor progression and treatment effects in mouse lymphoma models.

Jeremie Cosette, Rym Ben Abdelwahed, Sabrina Donnou, Catherine Sautès-Fridman, Wolf Herman Fridman, Patrice Flaud and Sylvain Fisson

2. Tumor Burden Quantification by Bioluminescence Imaging

After studying the Ublituximab and CpG effects on PCNSL mouse models, one thing came to us. We performed bioluminescence imaging on these tumors, but we did not use the full potential of the technique as it was used only for localization, and identification of metastases. We realized that there was no consensus in the analysis of bioluminescence data. Moreover more that 80% of published papers using bioluminescence in tumors are done with the same device IVIS (*In vivo* Imaging System) from Caliper (which has been recently bought by Perkin Elmer). The units used are also different among teams that own the same device.

We tried to fulfill this lack of consensus by proposing a reproducible acquiring and processing method, which removes user-dependence, and allow comparisons between different experiments.

The method is based on three main features:

- The choice of the correct unit
- The choice of a correct region of interest
- The systematic acquisition of two images (front and back)

This method leads to the attribution of a "**luminoscore**" to a mouse, which is a value that can be compared from an animal to another or from an experiment to another.

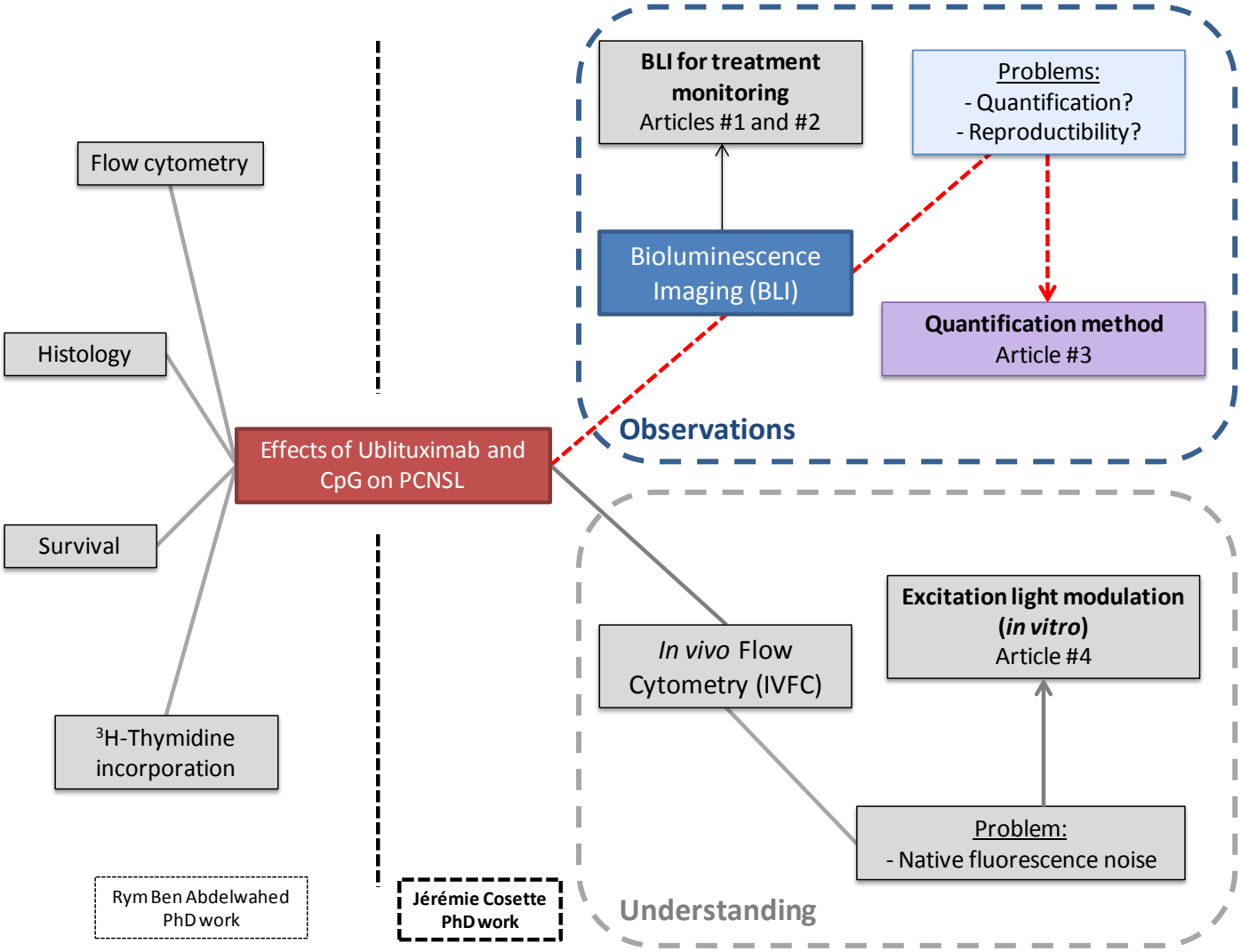

This article still corresponds to "observation" part of our approach. The problem of quantification of bioluminescence images was identified during the writing of both articles #1 and #2. We then proposed this article #3 to address the question of reproducibility and statistical significance of bioluminescence data sets.

BIOLUMINESCENCE-BASED TUMOR QUANTIFICATION METHOD FOR MONITORING TUMOR PROGRESSION AND TREATMENT EFFECTS IN MOUSE LYMPHOMA MODELS

Jérémie COSETTE[1,2,3,4,5,6] , Rym BEN ABDELWAHED[1,2,3], Sabrina DONNOU[1,2,3,6,7,8], Catherine SAUTÈS-FRIDMAN[1,2,3], Wolf Herman FRIDMAN[1,2,3], Patrice FLAUD[4,5,º] and Sylvain FISSON[1,2,3,6,7,8,*,º]

[1]Institut National de la Santé et de la Recherche Médicale (INSERM), UMRS872, Centre de Recherche des Cordeliers, Paris, F-75006, France; [2]Université Pierre et Marie Curie-Paris 6, UMRS 872, Paris F-75006, France; [3]Université Paris Descartes, UMRS 872, Paris F-75006, France; [4]Laboratoire Matière et Systèmes Complexes UMR 7057, Paris 75205 cedex 13, France; [5]Université Paris 7 Diderot 75205 Paris cedex 13, France; [6]Genethon, Evry, France ; [7]INSERM, U951, Evry, France; [8]University of Evry Val d'Essonne, UMRS 951, Evry, France.

º These authors should be considered as cosenior authors.

* Corresponding author: Sylvain Fisson. Généthon, INSERM UMRS951, 1 bis rue de l'Internationale, Evry F-91002, France.

Phone: +33 169 473 440

Fax: +33 160 778 698

e-mail: sylvain.fisson@univ-evry.fr

Abstract word count: 198

Text word count: 4974

Number of figures: 8

Number of table: 1

Number of references: 16

Keywords: Bioluminescence imaging, B-cell lymphoma, quantification, CpG-DNA, luminoscore.

ABSTRACT

Although bioluminescence imaging (BLI) shows promise for monitoring tumor burden in animal models of cancer, these analyses remain mostly qualitative. Here we describe a quantitative method for estimating tumor burden, mainly based on calculation of a "luminoscore", a value that can be compared between two animals from the same experiment or from different experiments. One of the most frequently used BLI instruments (IVIS lumina II – caliper) enables this luminoscore to be calculated, after optimizing three factors: the unit of measurement used, the acquisition of images from the animal's front and back, and the drawing of an appropriate region of interest (ROI). We validated this method by studying the effect of *in situ* cancer treatment (CpG-DNA) of a mouse model of subcutaneous lymphoma. We underline that an incorrect choice of the unit or the ROI increases the result's user-dependence, thus decreasing its reproducibility. Applied to a group of CpG-DNA-treated and untreated mice, this method enabled a statistical analysis in which the p-value declined from 0.0952 with the automatic quantification method to 0.0079 with the luminoscore method and was thus able to identify statistically significant results. We recommend this method for early estimates of treatment response in preclinical small-animal studies.

INTRODUCTION

Early tumor cell detection remains a challenge and is crucial to increasing treatment efficacy. Different techniques are now available for the early detection of tumor cells in small animals, but almost all of these techniques are qualitative.
In vivo bioluminescence imaging (BLI) is a very sensitive noninvasive optical technique, widely used for monitoring tumors in small animals; it often uses a pre-engineered cell line that expresses firefly luciferase [1,2]. This enzyme is an oxygenase that oxidizes its substrate, D-luciferin, with molecular oxygen [3]. Unlike renilla luciferase, the firefly enzyme requires two cofactors to do this: Mg2+ and adenosine triphosphate (ATP). On the other hand, its quantum yield is higher than for renilla luciferase [4], so that it is suitable for *in vivo* imaging, unlike renilla luciferase, which is more appropriate for *ex vivo* experiments.

The oxidized substrate – oxyluciferin – is in an excited state and spontaneously emits a photon to return to its fundamental state. Once it has done so, it becomes inactive. The light spectrum emitted has a maximum around 530 nm. A high-sensitivity camera can detect the luminescence photons from the inside of a small animal and provides images that make it possible to locate tumor cells.

The ability to quantify tumor burden accurately by photon counts could increase the reliability of experiments about tumor growth, treatment, and survival. It could also serve as a powerful and sensitive tool for quantifying treatment efficacy. This sensitivity could make it possible to determine the exact moment at which a treatment becomes effective, for its effects can be detected sooner.

Many study results are illustrated by images acquired on a single side of the mouse, at a given time point after a D-luciferin injection. As we show hereafter, however, single-side image acquisition may not reveal all the tumor sites. One way to quantify the tumor burden is to use the automated image acquisition and processing software tool to create a region of interest around the tumor location that is displayed. This technique may involve some uncertainty, because the software automatically

excludes some low signal points from the region of interest that might nonetheless be significant for analyzing results. Moreover, the user can change the display, which thus changes the reference for the automatic detection of tumor cells and results in a different value for the same tumor at the same time point.

Here we describe a method for quantifying tumor burden through a bioluminescence signal. This method relies on different aspects of the imaging procedure to optimize fidelity, reproducibility, non-user dependence and statistical significance. A bioluminescence quantification value (BQV) is attributed to the mouse; this value can be compared between animals and between experiments.

We applied different methods to quantify tumor burden in B-cell lymphoma models [5] and determined which method was most accurate. Images were acquired at a given time point, according to the recommendations of Inoue et al. [6]. To assess the effectiveness of the methods, we monitored the effects of CpG *in situ* therapy, previously been shown to be effective [7,8], on a subcutaneous B-cell lymphoma. CpG is an oligonucleotide sequence and a ligand of TLR-9, which in turn is an intracellular receptor, expressed by numerous cells of the immune system, including dendritic cells, B lymphocytes, monocytes, and natural killer cells. TLR-9 recognizes the CpG motif, widely present in bacterial DNA but very rare in the mammal genome. When TLR9 is engaged in the murine lymphoma we are studying, apoptosis is induced and the immune system is activated [9], thereby significantly reducing tumor burden [8,10].

The manual markup method, where a region of interest (ROI) is drawn closely around the mouse, eliminates user-dependence and can identify statistical significance in results that automatic quantification does not find to be significant.

MATERIALS AND METHODS

Cells

A20.IIA is an FcγR-negative clone derived from the A20-2J B-cell lymphoma line. A20.IIA cells were transfected with pGL4.50[luc2/CMV/hygro] (Promega) in the AMAXA Nucleofector II device (Lonza, Switzerland), as described previously [10]. These cells, referred to hereafter as A20.IIA-*luc2* cells, were maintained at 37°C, 5% CO_2 in complete Roswell Park Memorial Institute (RPMI) 1640 Medium Glutamax plus (RPMI; Gibco-Invitrogen, France) supplemented with 10% fetal calf serum (FCS; PAA Laboratories, Germany), 100 µg/mL penicillin, and 100 µg/mL streptomycin (both from Eurobio, France), 10 mM sodium pyruvate (Gibco-Invitrogen), 50 µM 2-mercaptoethanol (Gibco-Invitrogen), and 0.50 mg/mL hygromycinB (Gibco-Invitrogen).

Mice

Female BALB/c mice (H-2^d) were obtained from Charles River Laboratories (L'Arbresle, France) and used between 6 and 8 weeks of age. They were provided with sterile food and water *ad libitum* and kept on a 12-hour light-dark cycle. All procedures involving mice conformed with European Union guidelines, French regulations for animal experimentation (Ministry of Agriculture Act No. 2001-464, May 2001), and the guidelines of the Institut National de la Santé et de la Recherche Médicale (INSERM) Committee on Animal Research, and were approved by the relevant local committee (the Charles Darwin Ethics Committee for Animal Experiments, Paris, France; Permit Number: p3/2009/004).

Reagents

Nuclease-stable phosphorotioate-modified CpG 1826 (CpG) with 5_-TCCATGA**CG**TTCCTGACGTT (the bold and underlined nucleotides represent the immunostimulatory CpG sequences) and control ODN 1826 (ODN ctrl) with 5_-TCCATGAGCTTCCTGAGCTT were provided by InvivoGen (Cayla, France).

CpG is a ligand for TLR-9, a receptor present in the endosomes of different immune cell populations. This receptor recognizes single-strand DNA patterns from pathogenic microorganisms.

Tumor inoculation

Mice were first anesthetized by intraperitoneal injection of a mixture of 120 mg/kg of ketamine (Virbac, France) and 6 mg/kg of xylazine (Rompun 2%; Bayer Healthcare).

Systemic lymphoma model: To obtain a systemic (sys.) murine model, 5.10^5 A20.IIA-*luc2* cells in a final volume of 150 µL were inoculated intravenously in the tail vein. These mice were not treated, and the tumor growth was monitored by BLI.

Subcutaneous lymphoma model (SCL): To obtain a SCL murine model, BALB/c mice were inoculated subcutaneously with $5x10^6$ A20.IIA-*luc2* tumor cells in a final volume of 50 µL of PBS, at two different sites: right and left abdomen. For this model, control mice received either 1X phosphate-buffered saline (pH7.4; PBS) or the ODN 1826 control, rather than CpG 1826 (Fig.6A) [10].

Primary intracerebral lymphoma model (PCL): To obtain a PCL model, BALB/c mice were anesthetized and immobilized on a stereotaxic frame (David Kopf Instruments, Tujunga, CA, USA). Tumor cells (5.10^4 in a final volume of 2 µL RPMI) were injected into the specific cerebral location (right striatum), located 2 mm to the right of the medial suture and 0.4 mm in front of the bregma, through a Hamilton syringe attached to a penetrating depth controller [10].

Treatment injections

Tumor growth in the SCL model was monitored with calipers, and treatment started when the tumor reached 0.5 to 0.7 cm in its largest diameter. Mice then received daily injections of intratumoral CpG for 5 days (100 µg per injection in a final volume of 50 µL PBS) or ODN 1826 control in the right tumor; the left tumor served as a PBS control.

***In vivo* tumor growth assay**

Mice were anesthetized as for tumor inoculation and then were injected intraperitoneally with 150 mg/kg of D-luciferin potassium salt (Interchim). They underwent imaging 10 minutes afterwards with the IVIS LUMINA II (Caliper LS) imaging system for the acquisition of a bioluminescence image, which is actually the overlay of two images: one taken with a short exposure time and white light and displayed in grayscale, and the second with a longer exposure time and set to optimize the signal and use the CCD camera's entire dynamic range.

Software

The statistical analysis used Mann Whitney t-tests and linear regressions, performed with GraphPad Prism (GraphPad Software, La Jolla, CA, USA). Image processing, ROI drawing, and quantification were performed with Living Image software (Caliper LS).

Quantification method

The tumor quantification method relies on three main points: (i) the choice of the most appropriate unit of measurement for quantifying cell luminescence; (ii) the systematic acquisition of two images of each mouse (a front image is first acquired, and then a back image); (iii) the drawing of an appropriate region of interest (ROI).

These three factors combined make it possible to estimate a bioluminescence quantification value (BQV), a value associated with each mouse at a given time and corresponding to an accurate estimation of tumor burden.

RESULTS

Photon flux does not introduce bias in the *in vitro* BQV

For this study we analyzed more than 340 papers published from 2003 through 2013 that described BLI experiments to detect or quantify tumor burden. We focused on the units of measurement that these papers used to quantify tumor burden according to the luminescence information.

Most experiments are described by the photon flux (*i.e.*, photons per second) or average radiance (*i.e.*, photons per second per square centimeter per steradian) (Fig. 1A). Both those units can be obtained with Living Image software, a widely used program, especially for making comparisons between different experiments (Fig. 1B). Other analyses have used relative luminescence units (RLU) or bioluminescence intensity (BLI); relative units are not suitable for comparing experiments but they might be adaptable for use in certain cases. The utility of some other units might also depend on the instrument or software used.

These *in vitro* experiments allowed us to choose the best unit for quantifying tumor burden in relation to the number of cells inoculated or present at the time of image acquisition. To choose the most appropriate unit, we used a fixed number of bioluminescent cells and analyzed the photon flux and the radiance from those cells to calibrate the method.

The same number of tumor cells was put in wells of two different plates: a 96-well plate and 24-well plate differing by well volume and therefore by their surface. We analyzed the difference between the photon flux and the average radiance (Fig. 1C-1D) by drawing a round ROI that covered the entire surface of the studied well. Then we varied the number of cells from 10^4 to 10^6 in these two plates. Both photon flux (Fig. 1C) and average radiance (Fig. 1D) were proportional to the number of cells ($r^2 < 0.93$). However, the photon flux did not change according to the plate used (Fig. 1C), whereas the radiance value in the 96-well place was divided by 4 in the 24-well plate (Fig. 1D), as suggested by the definition of radiance: the photon flux divided by the surface of the ROI and by the solid angle with

which the CCD camera views the sample. The surface of the ROI quadruples from the 96-well to the 24-well plate. For different ROI surface and the same number of cells, radiance yields different values, whereas photon flux gives the same value. This means that if a ROI were drawn around two mice of different sizes, the BQV would differ according to average radiance, and the analysis would thus be biased. For this reason, we recommend using the photon flux for *in vivo* quantification.

Front and back *in vivo* acquisition are required for the detection of all metastases

Most tumor cells accumulate in the lungs in the systemic model (Fig. 2B), as also shown previously [12,13]. Tumors cells ($2.5x10^5$ A20.IIA-*luc2* initially inoculated) injected intravenously can be detected there after several days. Tumor cells invade the inguinal lymph node and even the popliteal lymph node 18 days after tumor inoculation (Fig. 2A and B). The inguinal lymph node tumor can be seen clearly only on the front view. The back view in this case provides little information about metastases; there is only a diffuse signal that corresponds to the other side of the inguinal lymph node tumor. Using only the back image to infer the tumor burden of the mouse is wrong. Moreover, the small popliteal lymph node tumor can only be seen on the front view.

Eighteen days after intra-striatal injection of lymphoma cells ($5.0x10^4$ A20.IIA-*luc2*), front and back images were acquired. The back image appears to be the best choice to evaluate the primary tumor burden (Fig. 2C). However, it turns out that in this model, tumor cells metastasize in the brain-draining deep cervical lymph nodes. The front view is required to detect those metastases. Moreover, the bioluminescence signal from the lymph nodes is not negligible compared to the signal from the primary tumor (Fig. 2D). In this case, more than in the previous one, performing quantitative analysis of the whole tumor burden (primary site and metastases) by analyzing only the back image produces misleading or inaccurate results, because a large part of the bioluminescent signal (from the lymph nodes) is not taken into account in the BQV.

Finally, it is the combination of the back and front view that makes it possible to determine the tumor's location more precisely and estimate its burden more accurately.

Rectangle and manual markup ROI systematically includes all metastases in the BQV

A region of interest can be drawn in different ways. First of all, there is an automatic drawing, by a tool available in the Living Image™ software. The software has also a free-draw feature for drawing a ROI in different shapes (round, square, or free ROI). Here we describe and compare different ways to draw the ROI (Fig. 3). This experiment was done with a mouse from the systemic lymphoma model on day 18.

The automatic drawing tool (Fig. 3A, B, and C) in the software automatically searches for the area where signals appear and draws a ROI around it, based on a user-settable threshold. We compared the automatic method for 3 thresholds: 5%, 15%, and 25%. For the 5% threshold, for instance, the ROI limit is set when the pixel value equals 5% of the maximum value in the ROI. In Fig. 3, the three first images are the automatic ROI drawing; according to the threshold, different ROI are automatically drawn, and the photon flux is plotted on the bar chart of the lower panel. The photon flux depends on the threshold: the lower the threshold, the higher the photon flux. The Automatic 5% ROI and the Automatic 15% ROI do not take the popliteal metastasis into account whereas the Automatic 25% ROI does.

Secondly, the rectangle drawing (Fig. 3D) is a user-made manual drawing of a rectangle around the mouse. The rectangle is then copied and pasted for each mouse at the different time points of the experiment to ensure the same ROI for the entire analysis. We highly recommend drawing the rectangle on the last day of the experiment; if drawn at the beginning, the tumor might grow and might become bigger than the rectangle.

Thirdly, the manual markup (Fig. 3E) involves the user free-drawing a ROI around the mouse, following the mouse's contour very closely. This free drawing must be done for each mouse, for each acquisition.

The rectangle and the manual markup ROI drawing give a photon flux which is higher than the automatic methods, but takes into account all the metastases that are in the mouse, even if they are not displayed by the software (Fig. 3F).

However, the photon flux in the rectangle ROI is slightly higher than the photon flux in the manual markup ROI. The rectangle ROI integrates the photon flux in areas that are not the mouse (around the mouse) and thus includes more background noise into the signal than the manual markup ROI. On this representative example (Fig. 3D, E and F), the difference between the two fluxes is 1.1x106 ph/s, which corresponds to 1.09% of the manual markup ROI photon flux. A comparison analysis was performed on 20 mice; the mean background noise was 1.19% of the manual markup ROI photon flux and ranged from 0.02% to 17%.

Processing time is very fast for the automatic ROI drawings and the rectangle ROI drawing: it is about 10 seconds per image. However, the manual markup ROI drawing requires more precision, and therefore more time to be processed — about 45 seconds per image.

Qualitative location of metastases and operator effects on the signal

The method should be robust and reproducible and should not depend on the user. The automatic ROI draw is based on the displayed image. If it does not show metastases, the signal from any metastases it misses will not be taken into account in the BQV (Fig. 4). Using only this method can therefore result in missing tumor sites and underestimating the tumor burden.

We study bioluminescence images, which are actually an overlay of a "bright field" image and a "raw bioluminescence" image. When the animal is put in the IVIS system, a black and white picture is taken under white light: it is called the bright field image. Then, the light is turned off and a picture

acquired: it is the raw bioluminescence image. All the pixels from the raw bioluminescence image are not displayed; if they were, the bright field image would no longer be visible, and co-localization would no longer be possible. The display settings are the lowest and the highest values set to display the raw bioluminescence image over the bright field image. The display settings are either automatic or user-tunable. Images from a systemic lymphoma mouse were studied; the display settings were modified from the auto (default setting after acquisition) to the manual setting and revealed a metastasis in the left inguinal lymph node of the mouse (Fig. 4A-4B). Similarly, images from a PCL-bearing mouse revealed a cervical lymph node metastasis when the display settings were modified from auto to manual (Fig. 4C-4D).

Thus, we recommend that a manual setting always be used to locate all metastases. The rectangle and the manual markup methods integrate the photon flux over the entire surface of the mouse. Thus, even metastases that are not displayed on screen are taken into account and included in the quantification.

Subcutaneous model

To further study and validate the different aspects of the BQV methods, we monitored a second group of tumor bearing mice. As described in the methods, each mouse was grafted with 5.10^6 A20.IIA-*luc2* cells subcutaneously on each side of the abdomen, so that there were two tumors per mice. One side was treated with either CpG-DNA or ODN-control, and the other side with PBS (Fig. 5A).

The BQV is calculated by summing the front photon flux and the back photon flux. For this experiment, which had two separate controls, we calculated two BQV per animal: one for the CpG-DNA/ODN-control treated side, and one for the PBS side (Fig. 5B). In such a case, we calculate a ratio defined by the BQV of the CpG-DNA/ODN-control treated side over the BQV of the PBS side. This ratio was set at 1 at day 0 (day of treatment), and the difference between day 0 and day 13 was

calculated for each animal; a decline in the ratio indicates a difference between the CpG-DNA/ODN-control treated side and the PBS side, and the larger the difference, the greater the decline.

A representative view of a mouse from each group shows that the CpG-DNA-treated tumor clearly tended to be resorbed (Fig. 6). Using the automatic method did not show that this resorption was statistically significant (Fig. 7) according to the 25% (default) threshold ($p = 0.0952$). For the 15% threshold, the result was significant ($p<0.01$). Surprisingly, when the threshold was lowered to 5%, the results appeared to be less significant, with $p < 0.05$ (Fig. 7). The rectangle method and the manual markup both yielded statistically significant results ($p = 0.0079$) whereas the automatic 25% threshold method, as mentioned above, did not. Moreover, the automatic methods seem to suggest the presence of two groups in the ODN control group (fig.7 – automatic 5% and 15%), which is not the case for the rectangle or manual markup methods. This might be due to the strong operator-dependence of the automatic method. This dependence might explain why this method does not to allow us, in some cases, to separate two different groups that are nonetheless statistically different.

With the appropriate method, non-user-dependent and reproducible, we can conclude that the intratumor injection of CPG strongly inhibited tumor progression.

Discussion

One limitation of imaging is that it is often hard to extract quantitative information from the images. Microscopy provides a great deal of information, but it remains mostly qualitative. Almost all the papers, among the 340 reviewed for Figure 1, described bioluminescence as a tool for localization, or for relative analysis concerning only one *in vivo* bioluminescence assay. Numerous parameters that have an influence on the bioluminescence signal must be taken into account, including but not limited to emission wavelength, tissue absorption, scattering, and skin pigmentation of the mouse [14].

Quantitative bioluminescence analyses are described and often require (for 2D BLI and 3D bioluminescence tomography) complex calculations to get close to absolute quantification [15,16]. These calculations, however, are difficult to include in routine protocols of bioluminescence analysis in a biology laboratory.

Here we describe a robust method to quantify tumor burden that is aimed at standardizing the acquisition protocol for comparing different assays done in different places at different times and that requires no calculations.

The back and front acquisition are required to collect all the photons that come from the tumor site. The photons from the back of the tumor might indeed not be detected by only the front acquisition. The two-sided acquisition provides qualitative depth localization as well. When the signal is stronger, on the front side than the back, as in Fig. 2A and B, we can conclude that the tumor site is more likely to be located on the front than on the back side (and vice versa): the inguinal lymph node produces a signal on the front and on the back view, but the signal is much stronger on the front view. Based on previous findings in this lymphoma model [5,10,11] – a high propensity to metastasize in the lymph nodes – and the two-sided acquisition, we can deduce that the bioluminescent signal comes from an

inguinal lymph node tumor, which is indeed located on the front side of the mouse. Because we used the same protocol on each mouse, the results can be compared.

We tested different ROI drawing methods: the three-threshold automatic, the manual markup, and the rectangle. The automatic method has the clear advantage of speed of execution, but lacks precision. The manual markup method is very precise but more time-consuming. The rectangle method could be a satisfactory compromise, with adequate speed and acceptable precision (Table 1). The rectangle ROI includes the background noise that comes from around the mouse into the BQV (Fig. 3). The manual markup ROI, close to the edges of the mouse, focusing on the effective surface, offers a better signal-to-noise ratio (SNR) and therefore increased precision.

The automatic 25% ROI drawing method does not take into account a large part of the signal and thus produces great variability, especially in the control group (Fig. 7), as well as overlap between the CPG-treated and the ODN-control group. The automatic 15% and 5% ROI drawing methods yield quite similar results: they are significant but seem to separate two subgroups of animals in the control group (empty circles, Fig. 7), which suggest that the ODN-control treated tumor is growing 10 to 100 times faster than the non-treated tumor. Surprisingly, those two subgroups disappear in the rectangle and the manual markup ROI drawing methods. The empty circles (which represent the ratio for ODN over PBS side) for those two methods are very close to each other and close to the value '1', which means, as expected and observed, that the growth of the ODN-control tumor is similar to that of the non-treated tumor (PBS-injected). The subgroups might be due to the operator-dependence of the automatic methods or to the fact that the automatic method does not take all metastases into account. For subcutaneous lymphomas, the signal from metastases must not be neglected in comparison to the primary tumor signal. These automatic ROI drawing could lead to over- or under-estimation of the tumor burden, and thus variability

The automatic 25% ROI drawing yields differences that are not statistically significant, whereas the automatic 15% is significant at $p<0.01$ and the automatic 5% is significant at $p<0.05$. One would expect that lowering the threshold would increase the statistical significance; unexpectedly, it does not do so here.

The rectangle and manual markup ROI drawing methods can statistically separate 2 groups of animals where the automatic method produces too much variability in terms of statistical significance.

For all these reasons, we recommend using the photon flux as the unit, acquiring both the front and back views, and applying the manual markup method to draw the ROI.

Based on these results, we laid out a reproducible protocol to calculate a bioluminescence quantification value, which can be compared between animals and experiments and which is not operator-dependent. We named this value the ***luminoscore***. The luminoscore is obtained as follows:

i) The mouse is anesthetized;

ii) 150 mg/kg D-luciferin is injected intraperitoneally, and a 10-minute interval passes;

iii) Back and front images are acquired;

iv) Manual markup ROI drawing are made;

v) The photon flux from the back and the front are added together.

The value thus obtained is this mouse's **luminoscore** in this experiment (Fig. 8).

Accuracy is essential in determining the treatment effect and may be crucial in reaching the correct conclusion about the experiment. The increase in the SNR of the manual markup makes it an excellent method when accuracy is crucial. However, to monitor tumor growth for the establishment of a murine cancer model, speed of execution might be needed for faster results. In that case, the rectangle method could lead to significant time savings. The rectangle method and the manual markup method yield quite similar results, so that the rectangle method is very satisfactory at a very good speed; A detailed analysis that requires the calculation of the **luminoscore** can be performed

retrospectively (it is the analysis and not the acquisition that is time-consuming). We also recommend changing the image settings for each mouse manually to locate potentially hidden metastases qualitatively (Fig. 8).

As described here with the subcutaneous lymphoma model, the **luminoscore** method can be adapted to fit the specific design of an experiment. By splitting the mouse and analyzing two *luminoscores* per mouse, we established a protocol that corresponds to this particular experiment. This method is reproducible and non-user-dependent; it enables comparisons between experiments and offers flexibility and adaptability to specific experimental needs.

Conclusion

We describe here the luminoscore method, a method for accurately estimating the tumor burden of a mouse with bioluminescence imaging. This method might not only increase the accuracy of the measurements, but it could also allow experiments to be compared and statistical significance assessed. The luminoscore method does not require new equipment or complex algorithms and calculations that might not be compatible with routine bioluminescence assays. The method is based on a reproducible and simple protocol that can be easily be set in an animal facility.

The standardization of this method, applied to several bioluminescence imaging experiments, enabled us to compare the luminoscores of animals from different experiments and thus provided us with a powerful tool for statistical compilations of bioluminescence data that can, for example, be used for retrospective analyses.

Acknowledgment

We thank the staff of the animal facility (CEF) of the Cordelier Research Center. This research was supported by the INSERM, the Paris Descartes University and the Pierre & Marie Curie University. J.C was supported by the Frontiers in Life Science doctoral school and by a fellowship from the INCA (Institut National du Cancer).

We thank Jean-Claude Jeanny for helpful discussions, and Jo Ann Cahn for her careful reading of the manuscript.

Conflict of interests

The author(s) declare(s) that there is no conflict of interests regarding the publication of this article.

REFERENCES

[1] Rehemtulla, Alnawaz, Lauren D. Stegman, Shaun J. Cardozo, et al.

2000 Rapid and Quantitative Assessment of Cancer Treatment Response Using In Vivo Bioluminescence Imaging. *Neoplasia* (New York, N.Y.) 2(6): 491.

[2] Edinger, M., Y.-a. Cao, Y.S. Hornig, et al.

2002 Advancing Animal Models of Neoplasia through in Vivo Bioluminescence Imaging. *European Journal of Cancer* 38(16): 2128–2136.

[3] Hastings, J. Woodland, and Quentin H. Gibson

1967 The Role of Oxygen in the Photoexcited Luminescence of Bacterial Luciferase. *Journal of Biological Chemistry* 242(4): 720–726.

[4] Inouye, Satoshi, and Osamu Shimomura

1997 The Use of Renilla Luciferase, Oplophorus Luciferase, and Apoaequorin as Bioluminescent Reporter Proteins in the Presence of Coelenterazine Analogues as Substrate. *Biochemical and Biophysical Research Communications* 233(2): 349–353.

[5] Donnou, Sabrina, Claire Galand, Valérie Touitou, et al.

2012 Murine Models of B-Cell Lymphomas: Promising Tools for Designing Cancer Therapies. *Advances in Hematology* 2012: 1–13.

[6] Inoue, Yusuke, Shigeru Kiryu, Makoto Watanabe, Arinobu Tojo, and Kuni Ohtomo

2010 Timing of Imaging after D-luciferin Injection Affects the Longitudinal Assessment of Tumor Growth Using in Vivo Bioluminescence Imaging. *International Journal of Biomedical Imaging* 2010: 471408.

[7] Qi, Xu-Feng, Li Zheng, Cheol-Su Kim, et al.

2013 CpG Oligodeoxynucleotide Induces Apoptosis and Cell Cycle Arrest in A20 Lymphoma Cells via TLR9-mediated Pathways. *Molecular Immunology* 54(3–4): 327–337.

[8] Houot R, Levy R.

2009 T-cell modulation combined with intratumoral CpG cures lymphoma in a mouse model without the need for chemotherapy. *Blood* 113(15):3546-52.

[9] Krieg, A. M.

2008 Toll-like Receptor 9 (TLR9) Agonists in the Treatment of Cancer. *Oncogene* 27(2): 161–167.

[10] Ben Abdelwahed, Rym, Jérémie Cosette, Sabrina Donnou, et al.

2013 Lymphoma B-cell Responsiveness to CpG-DNA Depends on the Tumor Microenvironment. *Journal of Experimental & Clinical Cancer Research*: CR 32: 18.

[11] Ben Abdelwahed, Rym, Sabrina Donnou, Hanane Ouakrim, et al.

2013 Preclinical Study of Ublituximab, a Glycoengineered Anti-human CD20 Antibody, in Murine Models of Primary Cerebral and Intraocular B-cell Lymphomas. *Investigative Ophthalmology & Visual Science* 54(5): 3657–3665.

[12] Miretti, Silvia, Ilaria Roato, Riccardo Taulli, et al.

2008 A Mouse Model of Pulmonary Metastasis from Spontaneous Osteosarcoma Monitored In Vivo by Luciferase Imaging. *PLoS ONE* 3(3): e1828.

[13] Mailloux, Adam W., Anna-Maria A. Clark, and M. Rita I. Young

2010 NK Depletion Results in Increased CCL22 Secretion and Treg Levels in Lewis Lung Carcinoma via the Accumulation of CCL22-secreting CD11b+CD11c+ Cells. *International Journal of Cancer*

127(11): 2598–2611.

[14] S. Lerondel and A. Lepape

2013 Bioluminescence Imaging in Rodents: When Light Illuminates Cancer Research. *Current Molecular Imaging*, 2, 18-29.

[15] S. Pesnel, A. Pillon, L. Créancier, N. Guilbaud, C. Bailly, A. Kruczynski, S. Lerondel and A. Lepape

2010 Quantification in Bioluminescence Imaging by Correction of Tissue Absorption for Experimental Oncology. *Molecular Imaging and Biology*. 13: 646-652

[16] C. Darne, Y. Lu and E. Sevick-Muraca.

2014 Small animal fluorescence and bioluminescence tomography: a review of approaches, algorithms and technology update. *Physics in Medicine and Biology*. 59: R1- R64

FIGURE LEGENDS

Figure 1: Compilation of currently used units and bioluminescence devices and *in vitro* study of the impact of the number of cells and the size of wells on photon flux and on average radiance

Over 340 papers from 2003 to 2013 describing experiments using BLI on tumor cells were analyzed. Photon flux (ph/s) and radiance (ph/s/cm²/sr) were the units used most frequently (A). The instrument used most often was the Caliper imaging system – IVIS (B).

In vitro luminescence test: different numbers of A20.IIA-*luc2* cells (in 300 µL PBS) were put in two plates (24 wells and 96 wells) that differed only by their surface. D-luciferin was added at the same concentration (7.1 g/L) in the wells of the two plates. Photon influx and radiance were proportional to the number of cells (C-D). Measurement of photon flux (C): regardless of the plate, the photon flux measured on the entire well surface remained the same for a given number of cells. Measurement of radiance (D): the well surface modified the value. The signal from the 96-well plate was four times higher as the signal on the 24-well plate. This experiment was repeated 4 times.

Figure 2: Interest of the systematic acquisition of back and front views of the animal

A – Back view and B – front view of a mouse, 18 days after i.v. tumor inoculation. The tumor was apparently in the lungs and reached the lymph nodes – inguinal and popliteal (B). The acquisition lasted for one minute and was performed 10 minutes after the D-luciferin intraperitoneal injection. The red circle shows a signal from the inguinal lymph node. The front view was required to locate this metastasis. The front view also revealed the presence of a metastasis in the popliteal lymph node, which was not detected with the back view (red arrows).

C – Back view and D – front view of a mouse, 27 days after intracerebral tumor inoculation. The acquisition settings were the same as above. The back view gave the best view of the primary tumor, which was in the right striatum (maximum signal). The lymph node metastases were still not detected by the back view. The front view revealed two significant metastases in the cervical lymph nodes (red arrows – D). Quantifying the tumor burden with only the back view yields incorrect results in such a case.

Figure 3: The different possible regions of interest

The BQV (Bioluminescence Quantification Value) of a mouse relies on the drawing of the region of interest (ROI).

There are 3 main ways to draw a ROI: (i) the automatic ROI, which is set by the software at different thresholds 25% - A, 15% - B, 5% - C; (ii) the rectangle ROI, which is a basic rectangle all around the mouse - D; (iii) the manual markup ROI, which is a free-drawn line that follows the contour of the mouse - E. This mouse is a representative mouse inoculated intravenously with 5.10^5 A20.IIA-*luc2* cells. The image was acquired on day 18 after tumor cell inoculation. The bar chart in the lower panel (F) is the photon flux of the same mouse in the same conditions, but integrated on different surfaces according to the different ROI drawing methods. For the automatic methods where different ROI were detected, the value on this chart was the sum of all detected areas.

Figure 4: Example of user dependence in the display of the luminescence signal and the detection of metastases

Front view of a systemic lymphoma-bearing mouse (A-B) and of a PCL-bearing mouse (C-D). A. Automatic display of the image after the acquisition. The lung tumor and the inguinal lymph node tumor can be clearly seen. The popliteal lymph node tumor can also be seen. B. The display settings

(minimum and maximum displayed values of the bioluminescent raw image) were modified manually (red arrows and rectangles). These modifications reveal more background noise and an unexpected contralateral inguinal lymph node tumor.

C. Automatic display of the image after acquisition. The brain tumor can be seen on the top of the mouse. By manually modifying the display settings, a cervical lymph node metastasis is revealed.

Figure 5: Experimental scheme of CpG-DNA treatment experiment and ROI drawing

A. Experimental scheme of subcutaneous model. Each mouse was grafted with 2 tumors. On the left side, the tumor was treated with PBS. On the right side, the tumor was treated with either CpG-DNA or ODN-control. B. The ROIs were drawn for each side of the animal, and 2 BQV were calculated, one for each side of the mouse. The ratio between the BQV from the right side and the left side was calculated and is representative of the relative resorption of the treated tumor.

Figure 6: Representative mice from the treated and untreated groups

Bioluminescence images of two representative mice from the ODN-control and the CPG-treated group. The ROIs were drawn on half the animal, using both the front and back views. The effect of CPG was clear on day 13. The CPG-treated group no longer had any detectable tumor on the treated side (red arrows) whereas the ODN-treated mouse still had two tumors.

Figure 7: Quantitative analysis of the effect of the treatment by calculating the photon flux ratio, depending on the ROI drawn

The ratio of the treated-to-untreated side was plotted and considered equal to 1 on the first day of CPG or ODN treatment. The ratio of the subsequent decreases was calculated in relation to that

value. On day 13, the ratios calculated for the different methods used for quantification were compared. Regardless of the method, there was a trend. The automatic method at a 25% threshold did not yield significant results. The automatic method at 5% yielded a significant result at $p < 0.05$. The automatic method at a 15% threshold, the rectangle method, and the manual markup method all yielded statistically significant results at $p < 0.01$ (ns: $p > 0.05$, *: $p < 0.05$, **: $p < 0.01$). The p value dropped from 0.0952 for the 25%-threshold automatic method to 0.0079 for the manual markup method.

Figure 8: A guide for luminoscore methods

Each step of the method is highlighted here. From the mouse anesthesia to the back and front acquisition, the protocol is exactly like a normal bioluminescence assay. At this point, two analyses are possible. The quantitative analysis can be performed by measuring the photon flux of the back and front acquisition with the manual markup ROI drawing. The values are then added to produce the animal's luminoscore. The qualitative analysis simply locates the metastases by modifying the display settings; the qualitative analysis also provides the coarse location of the depth of a tumor site by comparing the photon fluxes from the front and the back views.

Table 1: Advantages and disadvantages of the different ROI drawing

Method	**User dependance**	**Speed of execution**	**Precision**
Theoretically ideal	---	+++	+++
Automatic	+++	+++	--
Rectangle	---	++	+
Manual markup	---	-	+++

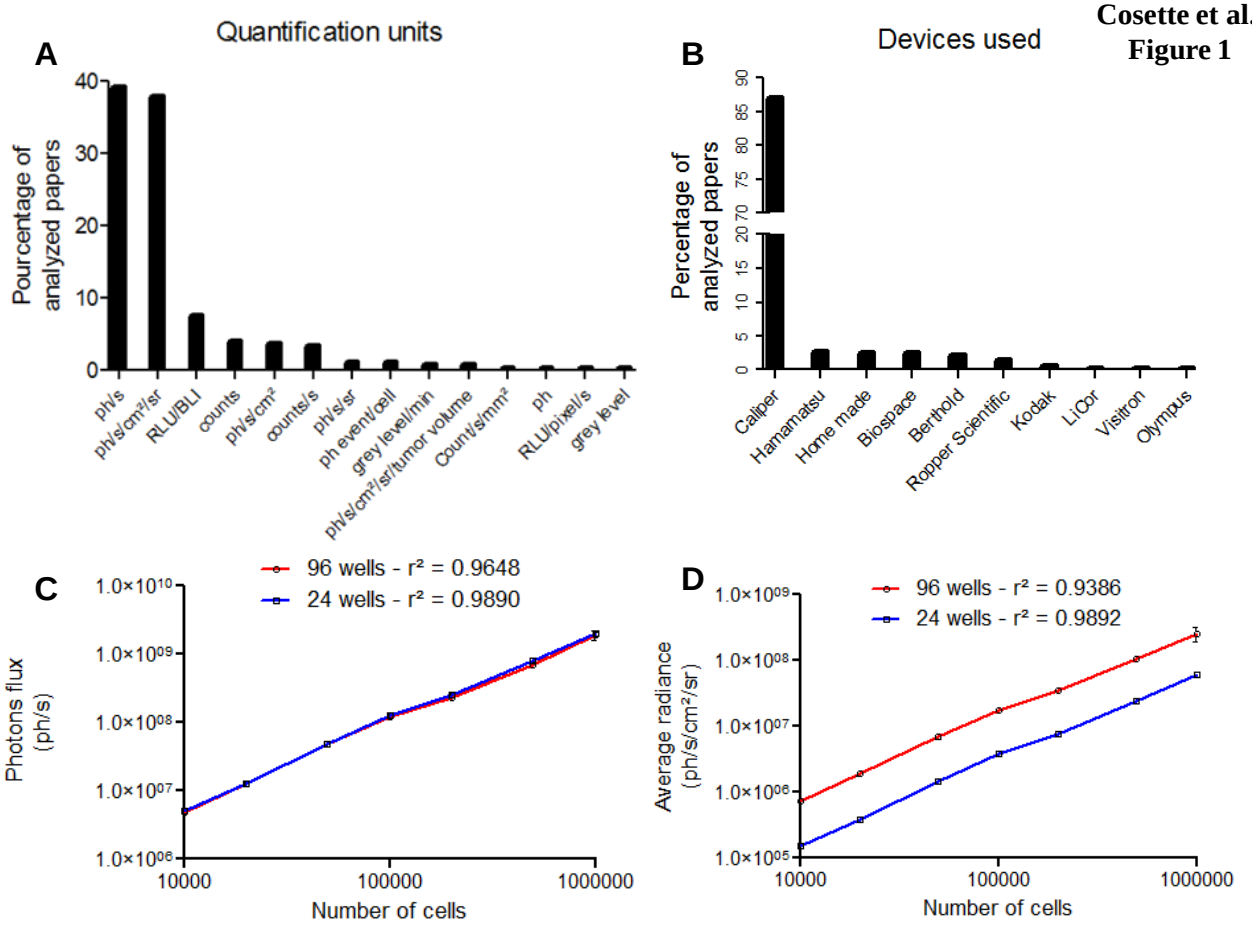
A
Quantification units
Pourcentage of analyzed papers
0
10
20
30
40
ph/s
ph/s/cm²/sr
RLU/BLI
counts
ph/s/cm²
counts/s
ph/s/sr
ph event/cell
grey level/min
ph/s/cm²/sr/tumor volume
Count/s/mm²
ph
RLU/pixel/s
grey level
B
Devices used
Percentage of analyzed papers
0
5
10
15
20
70
75
80
85
90
Caliper
Hamamatsu
Home made
Biospace
Berthold
Ropper Scientific
Kodak
LiCor
Visitron
Olympus
C
96 wells - r² = 0.9648
24 wells - r² = 0.9890
Photons flux (ph/s)
1.0×10⁶
1.0×10⁷
1.0×10⁸
1.0×10⁹
1.0×10¹⁰
10000
100000
1000000
Number of cells
D
96 wells - r² = 0.9386
24 wells - r² = 0.9892
Average radiance (ph/s/cm²/sr)
1.0×10⁵
1.0×10⁶
1.0×10⁷
1.0×10⁸
1.0×10⁹
10000
100000
1000000
Number of cells

Cosette et al.
Figure 2

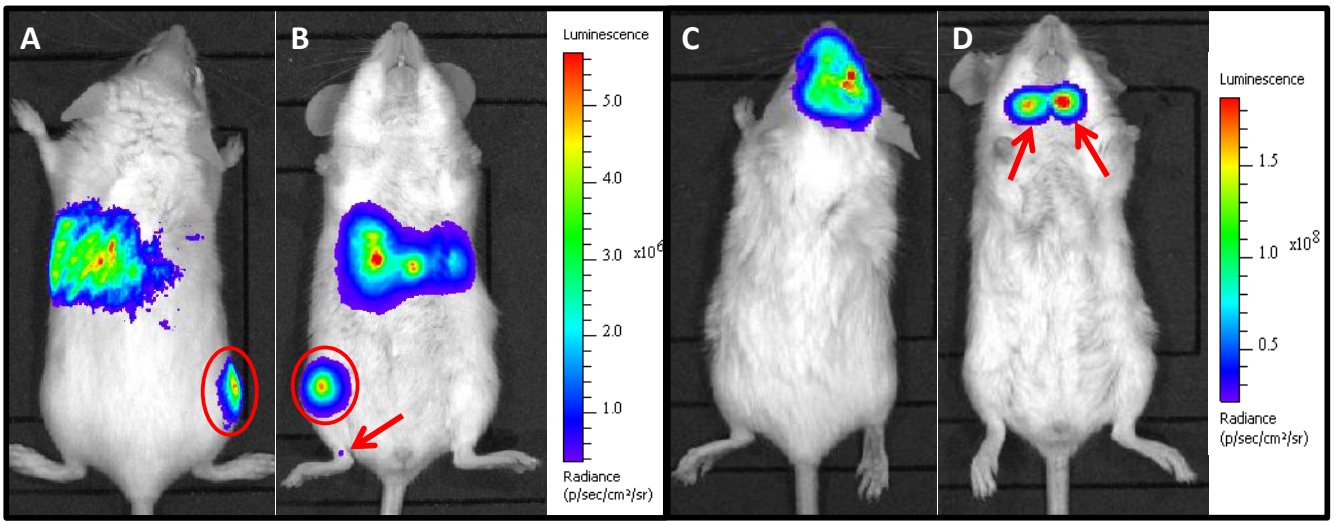

Cosette et al.
Figure 3

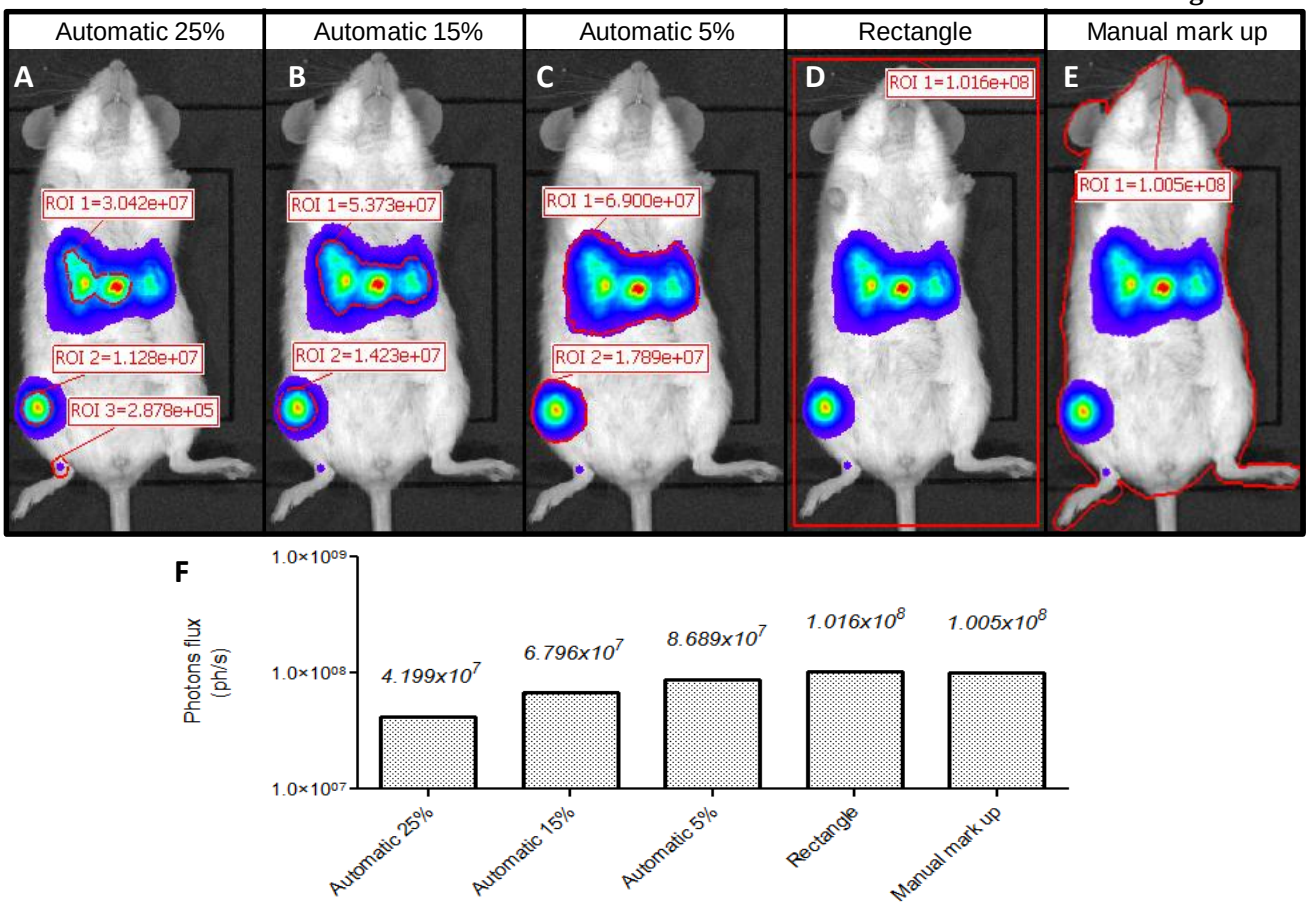

Cosette et al.
Figure 4

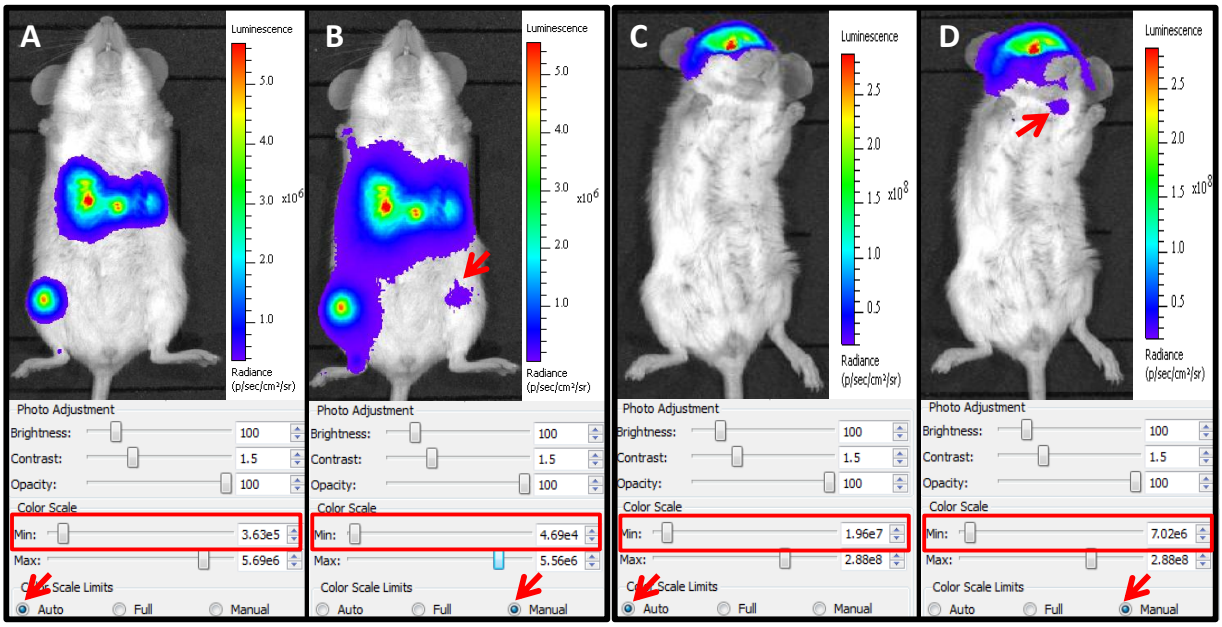

Cosette et al.
Figure 5

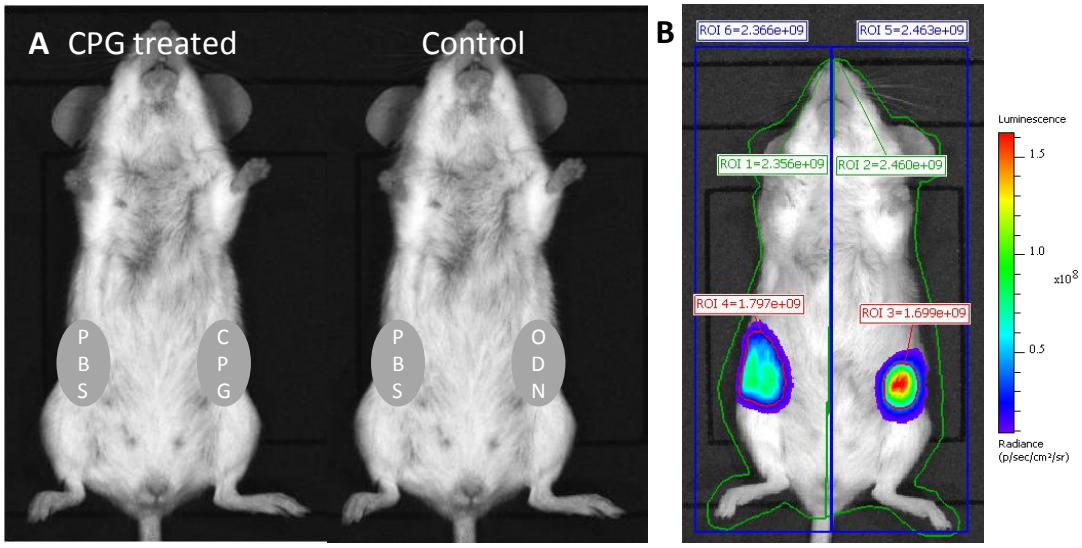

Cosette et al.
Figure 6

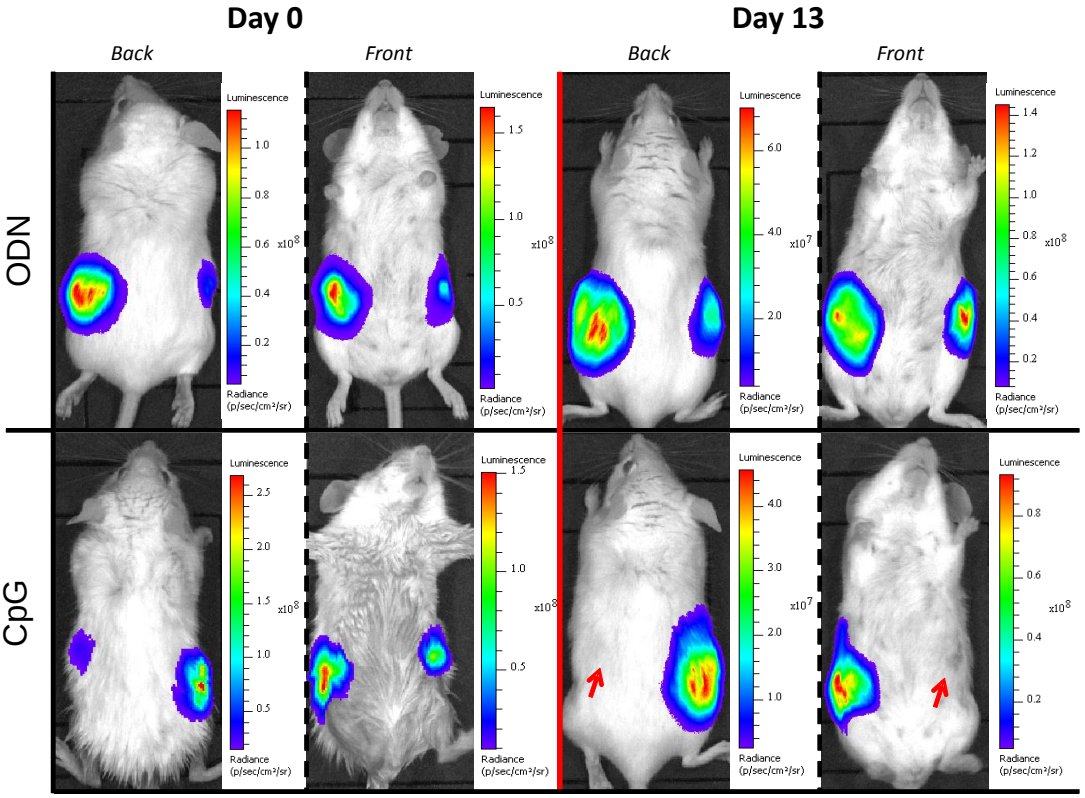

Cosette et al.
Figure 7

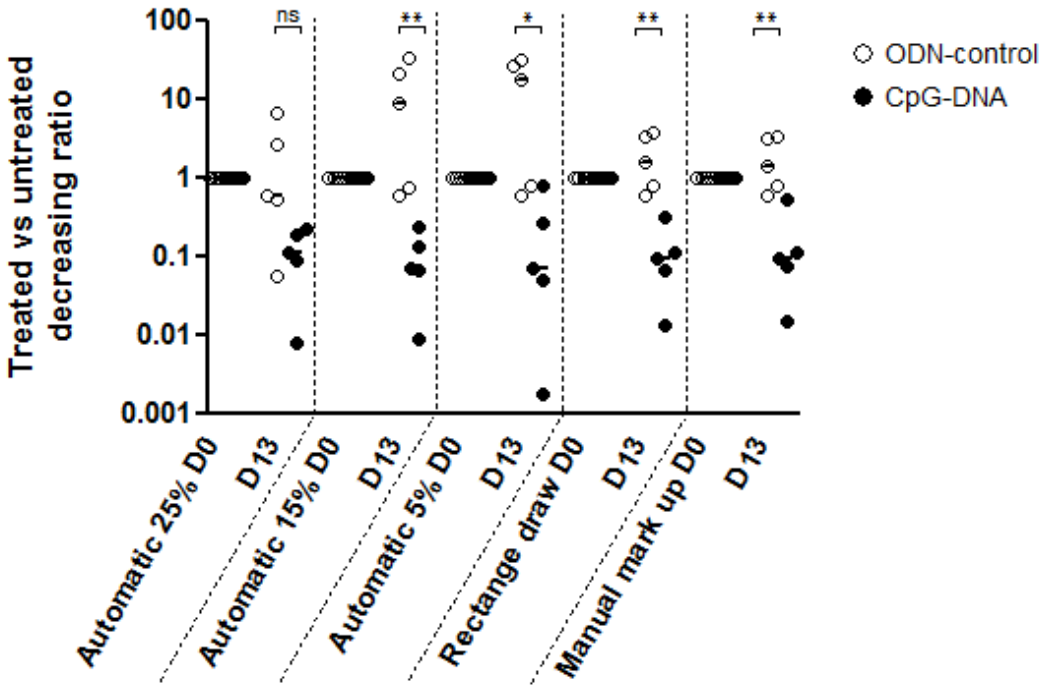

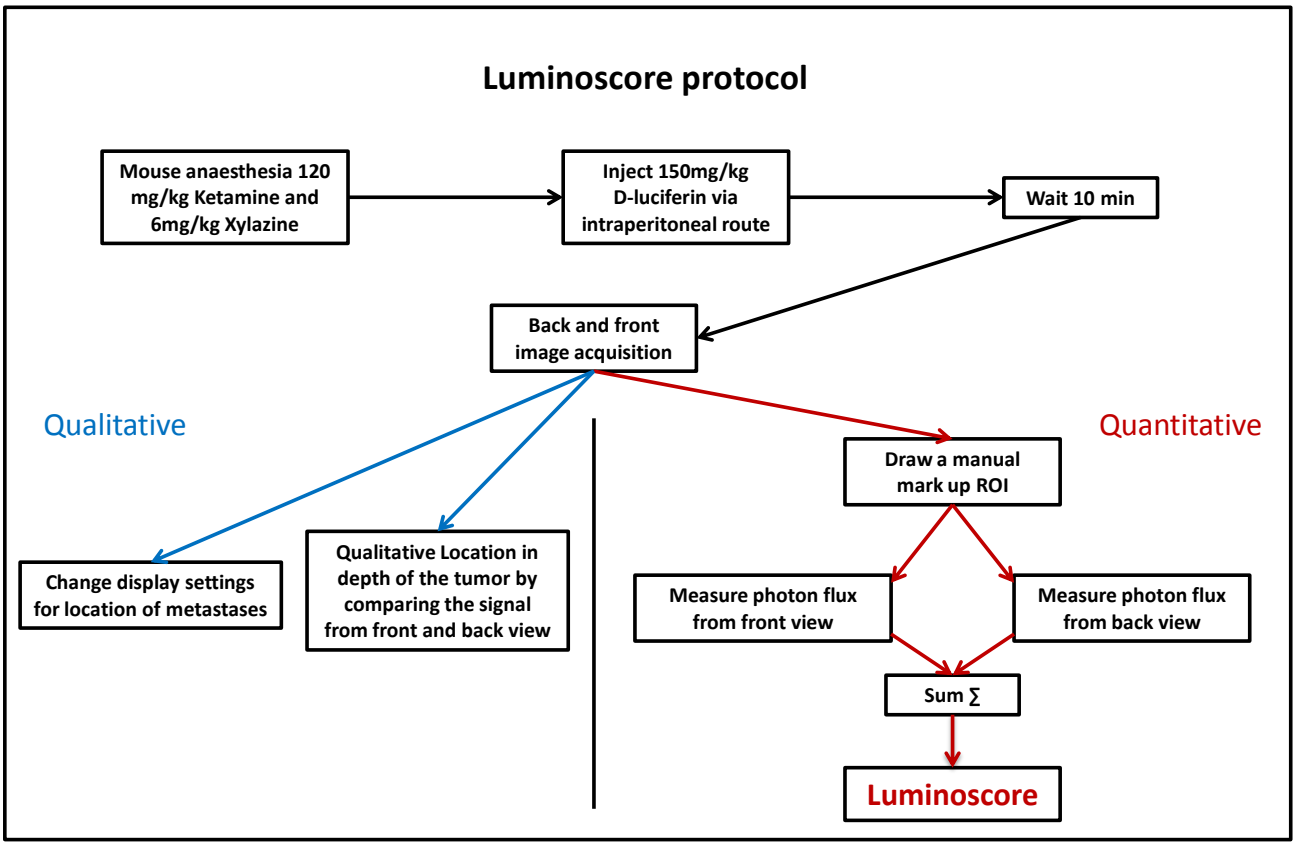
Luminoscore protocol
Mouse anaesthesia 120 mg/kg Ketamine and 6mg/kg Xylazine
Inject 150mg/kg D-luciferin via intraperitoneal route
Wait 10 min
Back and front image acquisition
Qualitative
Quantitative
Change display settings for location of metastases
Qualitative Location in depth of the tumor by comparing the signal from front and back view
Draw a manual mark up ROI
Measure photon flux from front view
Measure photon flux from back view
Sum ∑
Luminoscore

Conclusion on article #3

This article showed that optimizing different parameters to limit user-dependence can lead to reveal statistical significance in the same data set.

The method relies on the calculation of the luminoscore, which is a value corresponding to the tumor burden of the mouse. It is obvious that this quantification method is not absolute. There are many reasons why an absolute quantification is not possible even if we would possess a device that could detect every single photon emitted by tumor cells; one of those reasons is that cells have different levels of expression of luciferase, as any reporter gene among a cell population.

To summarize, we showed that the use of the luminoscore reduces user-dependence by revealing statistical significance on results that were not statistically significant with an automatic analysis.

The main aim of this thesis is to evaluate the effects of different treatments of lymphomas, but also to try to understand the mechanisms of these very effects. Locating the primary tumor site and metastases remains qualitative, and with this paper we provide a tool for quantifying these effects, a first step toward understanding.

The link between metastases and primary tumor is getting clearer and clearer as the CTCs are being investigated. As it was explained in the Introduction, CTCs are a bad prognosis for a patient, but it is not correlated to the number of metastases. However, CTCs are the first step of tumor dissemination.
We wanted to investigate CTCs in our models and understand what would be the effect of these treatments on CTCs. Targeting CTCs could allow to limit metastases and to prevent PIOL patients from lethal metastases. This is why the next parts of the results in the manuscript will deal with non-invasive techniques for in vivo quantification of CTCs: 2-photons microscopy, IVFC, and an improvement of IVFC using excitation laser modulation, which has been validated in vitro.

2-photons microscopy for detecting CTCs

Design of IVFC device for CTCs detection

2-photons microscopy is a very relevant technique for *in vivo* imaging. Its infra-red excitation light limits tissues absorption and provides good penetration depth. As it had been described for *in vivo* imaging and for circulating cells imaging; we wanted to try this approach.

3. 2-photon microscopy for CTCs detection

2-photons microscopy is actually very efficient for imaging living tissues. The infra-red excitation light (960 nm) penetrates deeper in the tissues than conventional excitation for GFP (488 nm).

We collaborated with the Institut Biomedical des Armées (Biomedical Institute of the Army) in Grenoble. The team of Jean-Nicolas Tournier and Daniel Fiole was working on intravital microscopy of immune cells in the lungs of transgenic mice (Fiole *et al.*, 2014). Their knowledge in intravital imaging was really useful to us to perform images of circulating tumor cells.

4.1. Materials and Methods

The cells used were the A20.IIA-GFP, a mouse lymphoma cell line.

The mice are BALB\c, 6 weeks-years old. The mice were injected with either 2.10^6 cells intravenously in the retro-orbital sinus or 5.10^6 cells in the spleen.

The microscope is a ZEISS LSM 710, with a wavelength tunable femtosecond pulsed laser set at 960 nm. The objective is a water immersion ZEISS neofluar 40X 1.1 NA.

Before image acquisition, the mouse is intravenously injected with a rhodamine-dextran (70kDa) solution. The rhodamine allows locating blood vessels as dextran is a macromolecule which prevents rhodamine from diffusing in the tissues through epithelial cells. Collagen is imaged with second harmonic generation.

In summary, the collagen is imaged in blue, the rhodamine (blood vessels) is red, and the cells of interest (tumor cells) are green due to GFP.

The mouse is anaesthetized with a mix of Ketamine and Xylazine as described on paragraph 3.4 and the mouse's ear is covered with aqueous gel and placed between a microscope slide and cover slip. A drop of aqueous gel is laid on the cover slip, and the images are recorded.

4.2. Results

We obtained images of the blood vessel showing that the cells were indeed detectable with this technique.

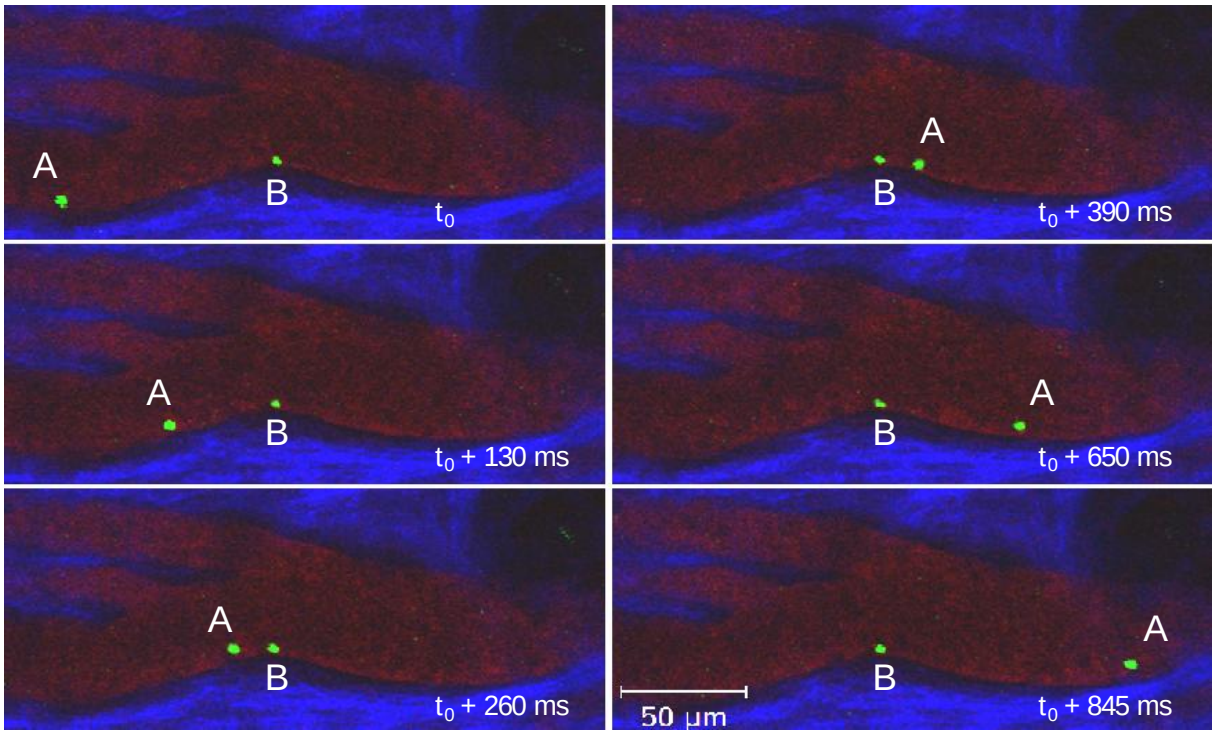

Figure 21: Representative images of ear blood vessesl analyzed by 2-phtons microscopy (ZEISS LSM 710, 960 nm). 5.10^6 A20.IIA-GFP cells (green) and Rhodamine-Dextran (red) were i.v. injected. Collagen was imaged by second harmonic generation (blue). Representative "B" cell is shown to be attached to the inner surface of the blood vessel while "A" cell flows in the vessel, almost rolling on the side of the blood vessel. The "B" cell remained at the same location for 7 minutes whereas the "A" cell made 210µm in about 910ms (velocity of 0.23 mm.s^{-1}).

For each mouse, we counted the number of detected CTCs (Figure 21), and we measured the cell mobilization in tissues (Figure 22). Actually, it has been described that there is an exponential decrease of the number of circulating cells after intravenous cell inoculation (Georgakoudi *et al.*, 2004). This is consistent with what we observed.

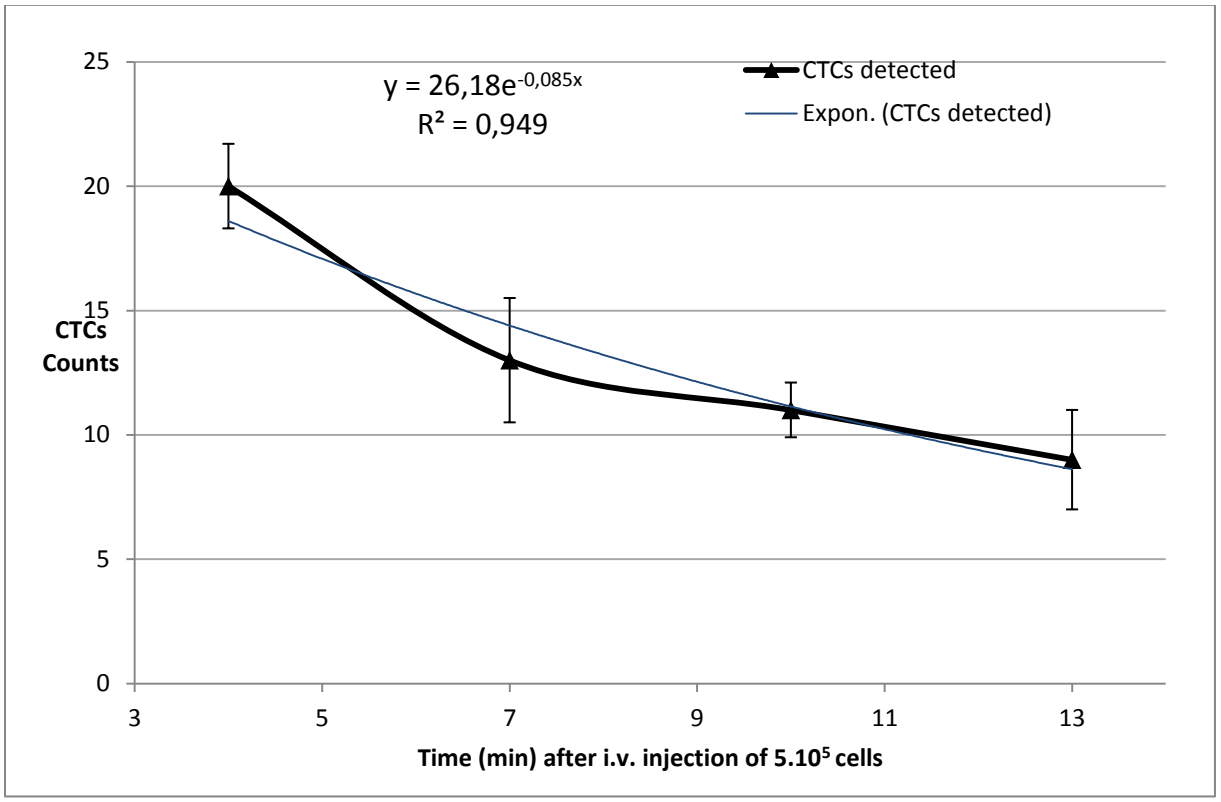

Figure 22: Cell mobilization in the tissues. Data obtained on three mice.

.

After 13 minutes, there are less than half as many CTCs as 4 minutes after injection.

This decrease follow an exponential law

$$N(t)=N_0*e^{-t/\tau}$$

where t is the characteristic time: τ = 11min 45s.

For $t=\tau$, $N(\tau)= N_0*e^{-1} \sim 0.37*N_0$

After 11min 45s, 63% of the injected cells are mobilized in the tissues.

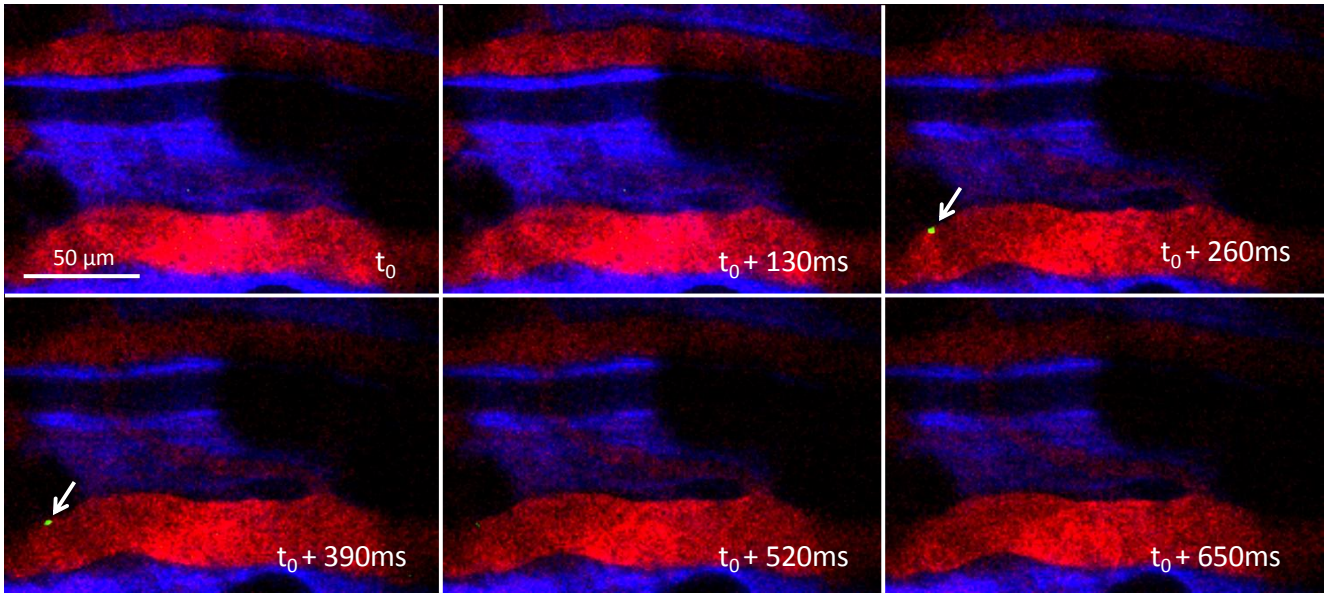

Figure 23: 2-photons microscopy acquisition of mouse ear images. *On this frame, a cell can be seen, flowing from two 50µm-sized microvessel through a smaller vessel. However, the cell cannot be seen on all images. Actually, the cell sometimes goes out of focus, and then come back on the focus plane. This technique is very accurate for detecting cells in the focus plane, but some of them can be missed because the depth of field is very small, around 2µm.*

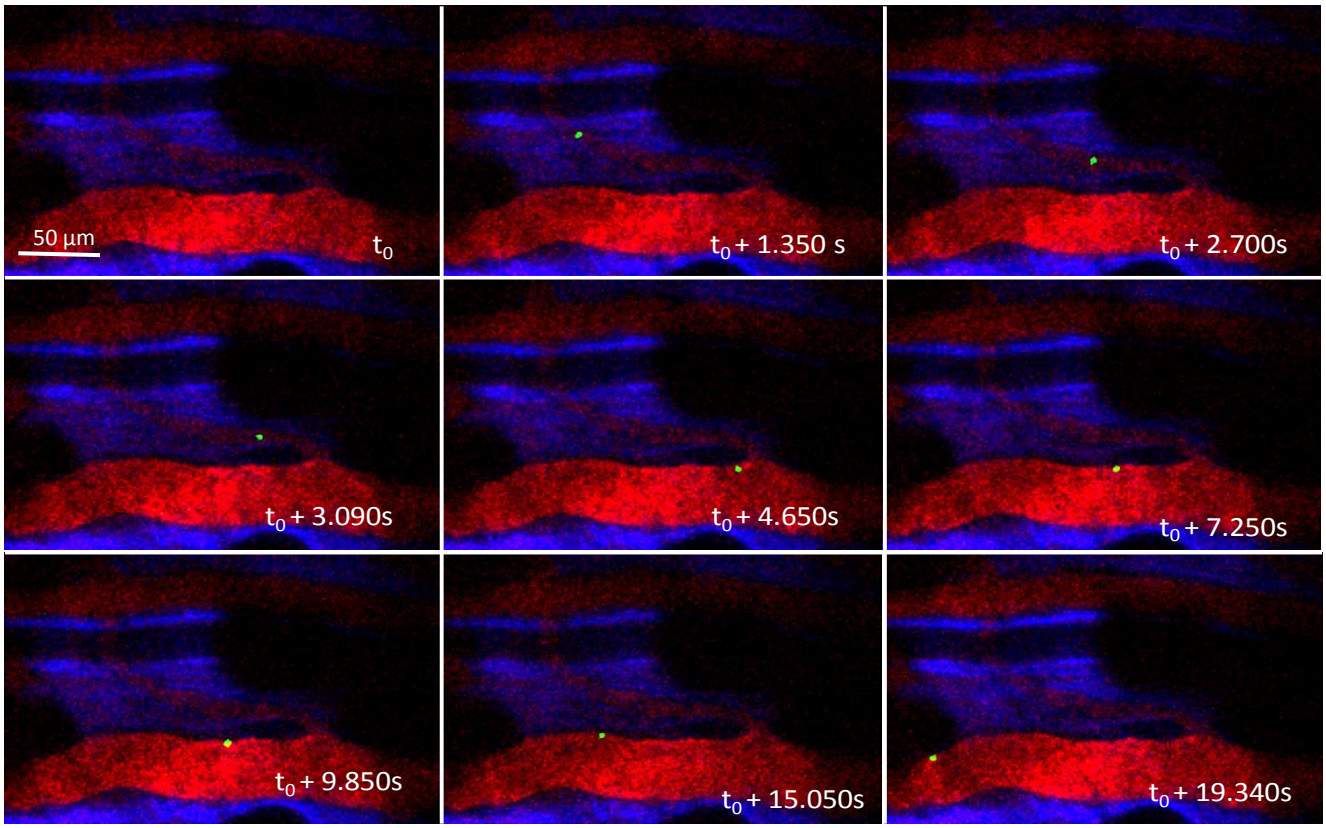

Figure 24: On this frame, another cell at the same location can be observed. On a 20 second follow-up, the cell can be tracked in the blood vessels. It takes about 200ms to acquire an image with the microscope we used. The frequency is thus 5 images per second. We have a 20 seconds acquisition of 100 images; and this cell cannot be detected on more that 50% of the images because of loss of focus.

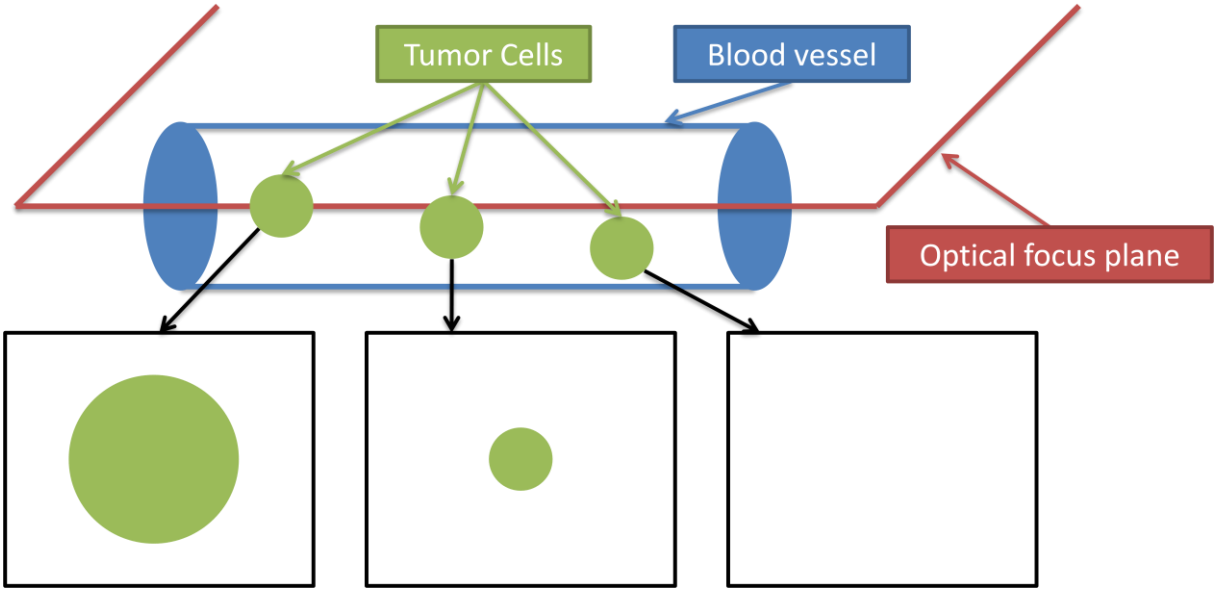

Figure 25: Scheme showing the problem of confocal microscopy (whether it would be single photons or 2-photons) for the detection of CTCs. The focus plane being thin, the explored volume is very low and the probability to miss cells is too high for accurate counting of CTCs.

Optical sectioning allows very good resolution, and is moreover inherent to 2-photons microscopy excitation light. However it remains a problem for us, because cells can be unfocused and thus not detected. The explored volume is, on top that, dramatically reduced (Figure 23,24 and 25).

Conclusion:

2-photons microscopy was tested as a method to quantify CTCs. However it happened that in spite of the very high spatial resolution, the time resolution and the very thin depth of field make 2-photons a technique not optimized for CTCs quantification *in vivo* leading to develop another approach, IVFC.

To solve the problem of optical sectioning, we designed the *in vivo* flow cytometry device by carefully adapting the depth of field in order to minimize the number of missed cells.

4. *In vivo* Flow Cytometry experiments

In vivo flow cytometry was designed to detect circulating cells (tumor or not). We reproduced the *in vivo* flow cytometer and adapted it to our scientific topic: oculo-cerebral migration in a mouse model of PIOL. The aim was to avoid missing cells as we saw it could happen in 2-photons microscopy.

5.1. Material and Methods

Optic:

Our device is close to the initial device described by Georgakoudi *et al.*: one laser, one color, one detector. We shaped the laser into a slit of light with an anamorphic prisms duet and a cylindrical lens. The spherical lens coupled with the cylindrical lens allows widening and adapting the beam in order to lead it in the entrance pupil of the objective. The objective is a ZEISS NEOFLUAR air 40X 0.75 N.A.; and after being filtered by the dichroic beam splitter, the fluorescence photons coming from the objective are gathered by a collection lens, and finally filtered with a BandPass Filter. The photons are detected by a Photomultiplier Tube (PMT) and sent to the measurment electronic.

For this technique, the sample, *i.e.* the blood vessel of the mouse ear should be placed in the focus plane of the objective; the slit is designed to be 100µm * 6µm at the focal plane (Figure 26).

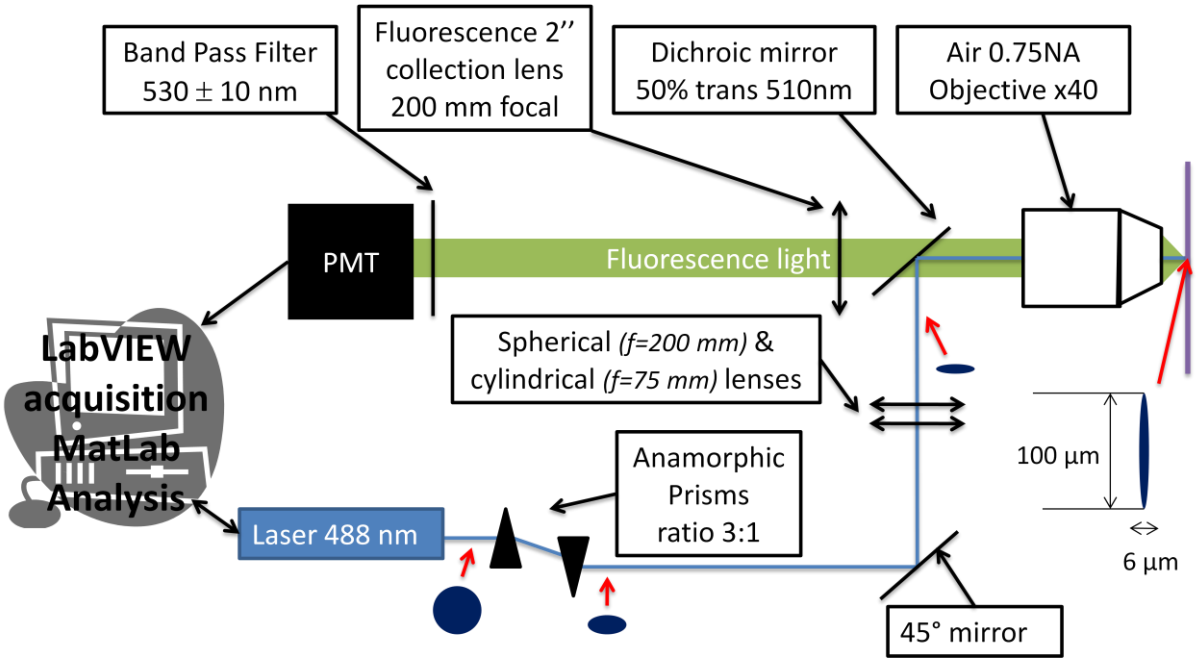

Figure 26: Experimental set up of IVFC. The laser beam is shaped into a slit by an anamorphic prism duet and by a cylindrical lens. Fluorescence is gathered with a dichroic mirror and with a 2" fluorescence collection lense. A bandpass filter select the light propagating to the detector.

The detector is a PMT. It is a light sensor that converts photons into electrons (Figure 27). Photons impact a photocathode, which emits an electron. The dynodes are electrodes put at high potential up to 2000V. When an electron impacts a dynode, new electrons are emitted from the dynode itself. This phenomenon is repeated as long as there are dynodes. The number of electrons is thus amplified and sufficient electrons are collected on the last dynode (called the anode) to create a detectable current. PMT are very sensitive and are still used in microscopy or cytometry.

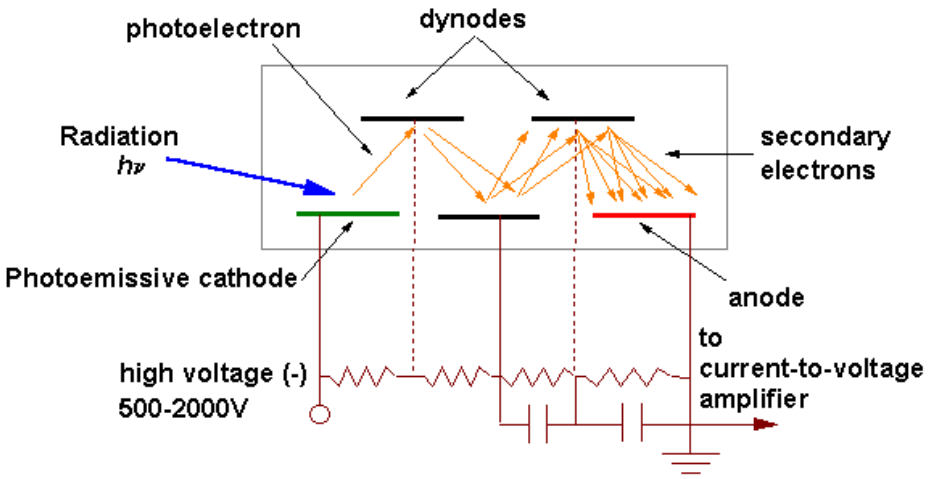

Figure 27: Scheme of a Photomultiplier Tube. A PMT is very sensitive (photon counting) light sensor.

Measuring electronic:

The signal from the PMT is acquired and digitalized on 14 bits with an analog to digital converter (National Instruments DAQ-USB 6009). The frequency of acquisition is 8 000 sample/second. Based on what has been described and our observations, we decided to use acquisition frequency to fulfill the conditions of Shanon-Nyquist theorem: "The acquisition frequency should be at least twice as higher as the frequency of the most frequent periodic event to be detected". If the Shanon-Nyquist theorem is not respected, spectrum overlapping can occurs, inducing errors in signal processing. We are trying to detect cells, whose frequencies are quite low (from 1Hz to 100Hz). By taking 8 000 sample/second, we will have no problem of spectral overlapping.

On the other hand, we also wanted to have enough samples corresponding to a cell to be able to correctly process it. According to the physiological velocities in small blood vessels ($\approx$ 1 mm.s^{-1}), the time taken for a cell to flow under our laser slit ($\approx$ 10µm) is around 10ms. The ideal would be to have around 80-100 samples for one cell, which means an acquisition frequency of 8 000 to 10 000 samples/second. The maximum sampling frequency allowed by the DAS-USB 6009 is 8 000 Hz, and it actually fits our expectations.

The signal is measured and real-time processed by a simple high pass filter to eliminate the continuous component by LabVIEW software (Figure 28). Here is the graphic program that allows the measurement of fluorescence signal.

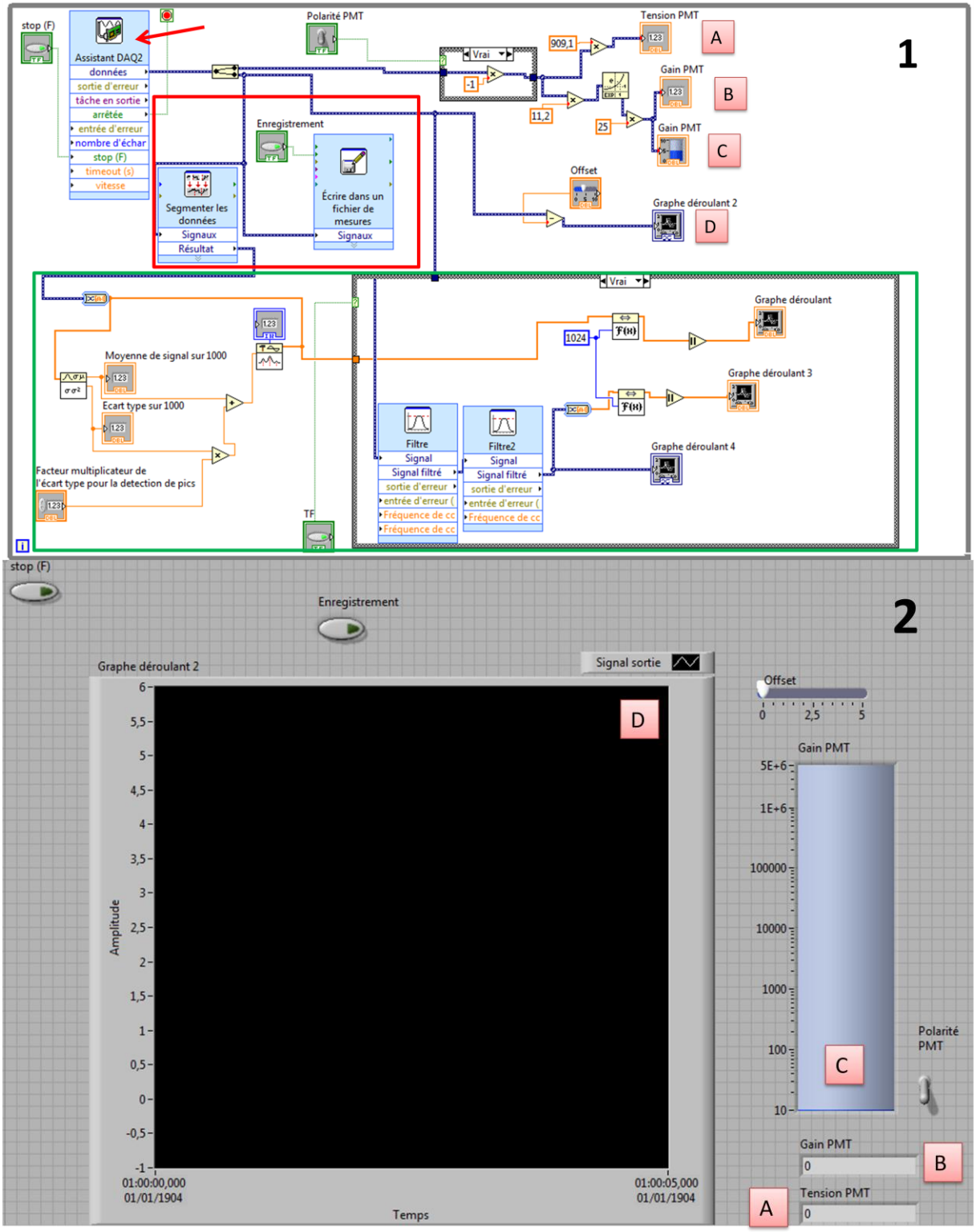

Figure 28: LabVIEW graphic program of measuring electronic and data acquisition. 1- Graphic program. The signal is acquired by a data acquisition function (red arrow) and is recorded in a data file (red box). Other features were developed such as peak detection and Fourier Transform (green box), but they were not used for data recording as signal processing was performed later on another software. A B C D are functions for user monitoring of the device

2- User view of the software. The user can monitor parameters. A is the PMT voltage, from 1 to 1000V. B is the PMT gain, linked to voltage through an exponential relation. C is real time bar chart of PMT gain, and D is the output PMT signal monitored with a running graph.

5.2. Results

In vitro

We validated this device for use *in vitro* before we used it *in vivo*.

We detected cells, and tried to link the number of circulating cells to the number of detected cells.

To do so we realized a silicon phantom of blood vessel. The phantom is a tube embedded in a PDMS matrix. The channel is 120µm diameter.

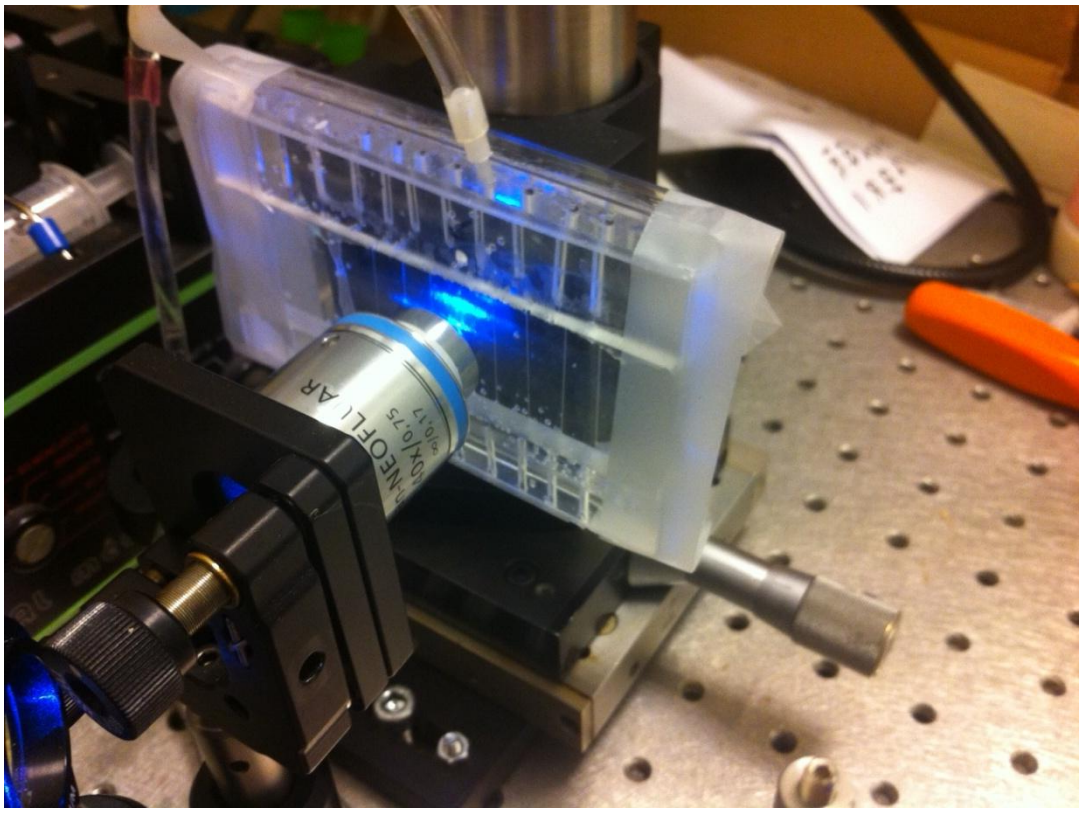

Figure 29: IVFC in vitro validation. Silicon vessel phantom. 120µm diameter tubes are embedded in a silicon matrix. The slit of light intercepts the vessel phantom and fluorescence of circulating cells is analyzed

We introduce in a syringe pump a cell suspension (A20.IIA-GFP) at different concentrations. The number of events per minutes is counted and represented here.

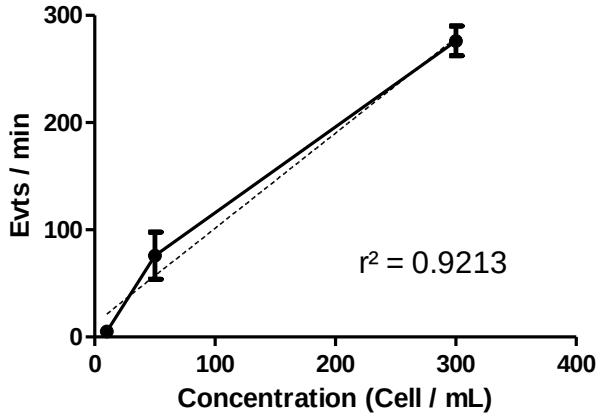

<u>Figure 30:</u> Link between the number of detected fluorescence events and concentration. The expected linear relation is observed. (Repeated 5 times)

There is a linear link between the number of events detected and the concentration of cells, indicating that what we detect are fluorescent cells and no artifacts (Figure 30).

The device allows detection of fluorescent cells, in close conditions to *in vivo*; we could then start *in vivo* experiment.

<u>In vivo</u>:

For *in vivo* experiments, we injected intravenously different amounts of cells A20.IIA-GFP or CFSE labeled A20.IIA-NT, in the tail vein of a BALB/c mouse. The ear of the mouse was put in the between slide and cover slip and positioned in front of the microscope objective (Figure 31).

<u>Figure 31:</u> IVFC laser position monitoring picture. The mouse is anaesthetized with a mix of ketamine / xylazine. Its ear is put between slide and cover slip and the stand his moved until the laser spot is at the correct location. The picture is taken with the monitoring CMOS camera placed

We then analyzed the signal from the fluorescent cells.

We actually were not able to distinguish the cell signal from the native fluorescence signal. The data files recorded are analyzed and displayed with MATLAB software.

This is a representative signal of our *in vivo* experiment. We obtained signals almost identical to this one each time *in vivo* experiments were performed.

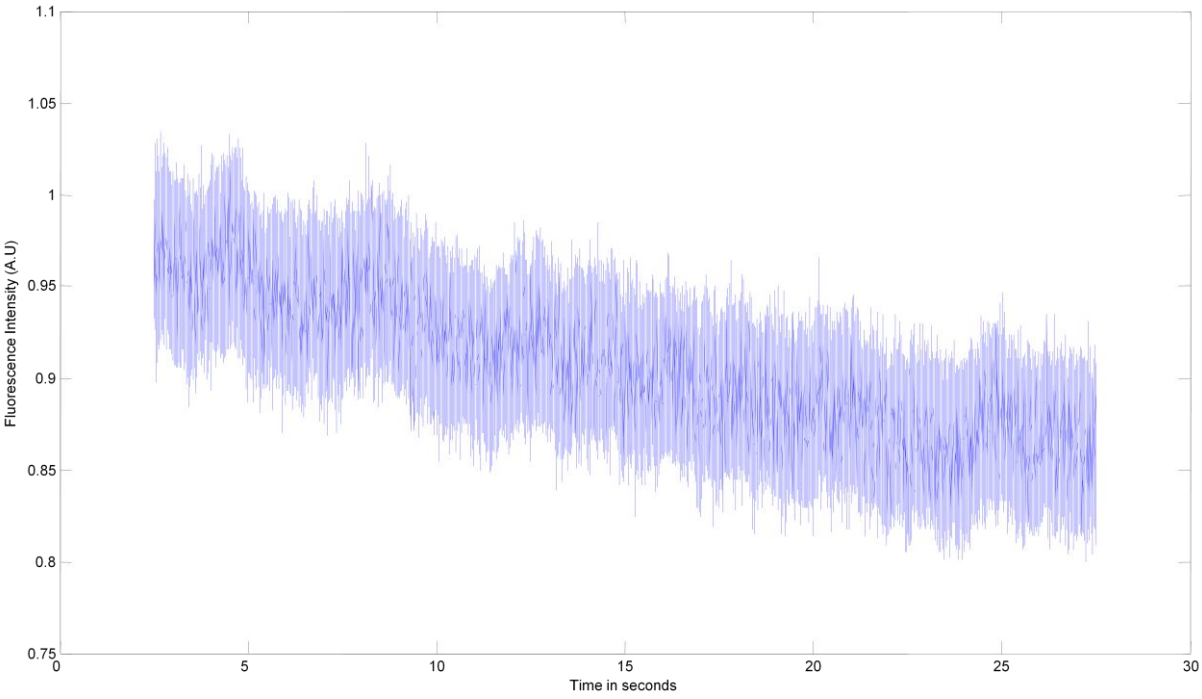

Figure 32: Representative signal of IVFC experiments. The signal is very noisy, and tends to decrease. Signal processing does not eliminate noise in a sufficient way to identify cell signal. Each time we performed this experiment, we observed the same.

We can see that the signal is very noisy. We also observed that the fluorescence signal tends to decrease with time, suggesting the photobleaching of native fluorescence.

It turns out that even using temporal or spatial signal processing methods we were not able to extract the cell signal in this noise. We had to solve the problem of autofluorescence, tissue absorption and cell signal extraction.

Noise reduction:

To get rid of noise we had two parallel approaches. First, we changed the fluorescent protein. A new cell line was engineered expressing mKate protein. mKate is a fluorescent protein whose maximum excitation is around 590 nm and maximum emission is around 635 nm. The fluorescence photons emitted by this red fluorescent protein are less absorbed by tissues. Moreover the 590 nm excitation light penetrates deeper in the tissues (we used a 594 nm orange Laser): less absorption and better penetration. We first validated our new cell line on the vitro dispositive. The results are very promising. The cells are easily detectable as can be seen on the figure, without signal processing (Figure 33 is raw data). There is less autofluorescence of the PDMS phantom.

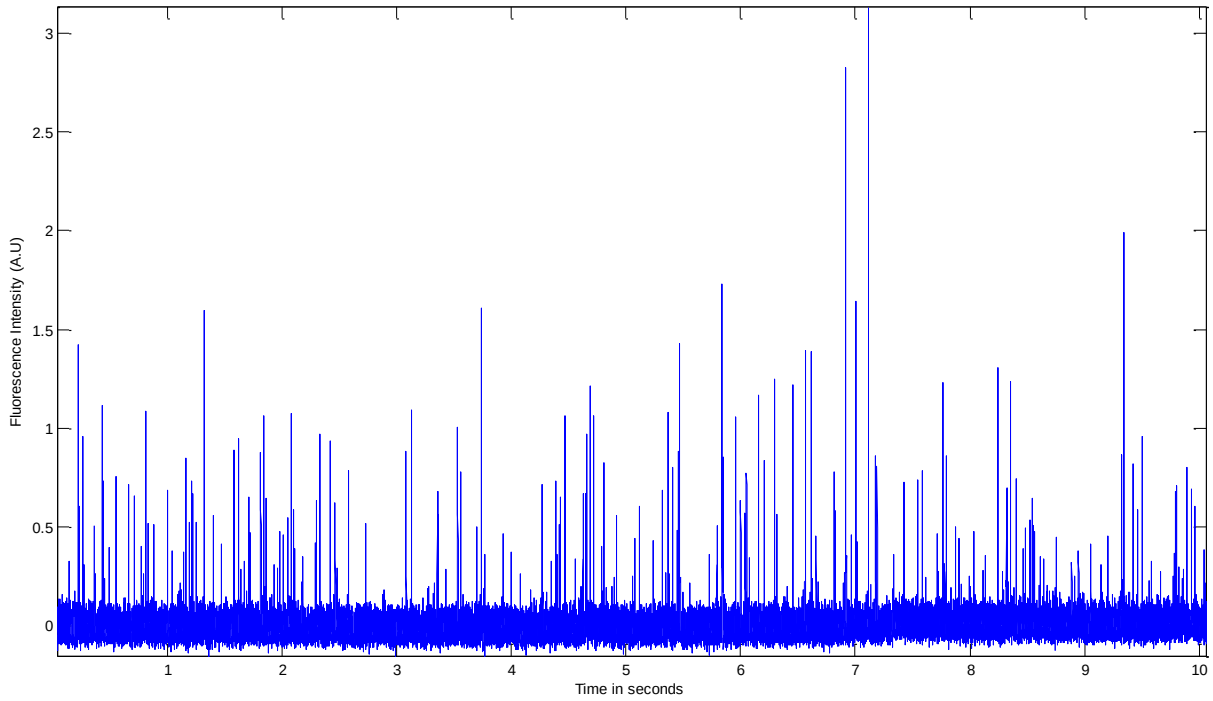

Figure 33: In vitro acquisition of fluorescence signal from A20.IIA-mKate cells. The peaks are easily identifiable without the need of signal processing.

The second approach is based on shaping excitation light accordingly with a signal processing method. It is always difficult to extract from noise a signal that has no signature. There is no way to differentiate it from the noise. However, if we could design the signal from a cell to have a unique shape, we could be able to isolate this cell signature from the noise. To do so, we designed a unique excitation pattern, which will give the circulating cell a unique fluorescence pattern, easily extractible from autofluorescence noise. This is described in the next section.

Conclusion on Results

In the results chapter, we had two different approaches to characterize ("observation" part) tumor sites and to understand metastatic dissemination in the case of PCSNL, with or without treatments.

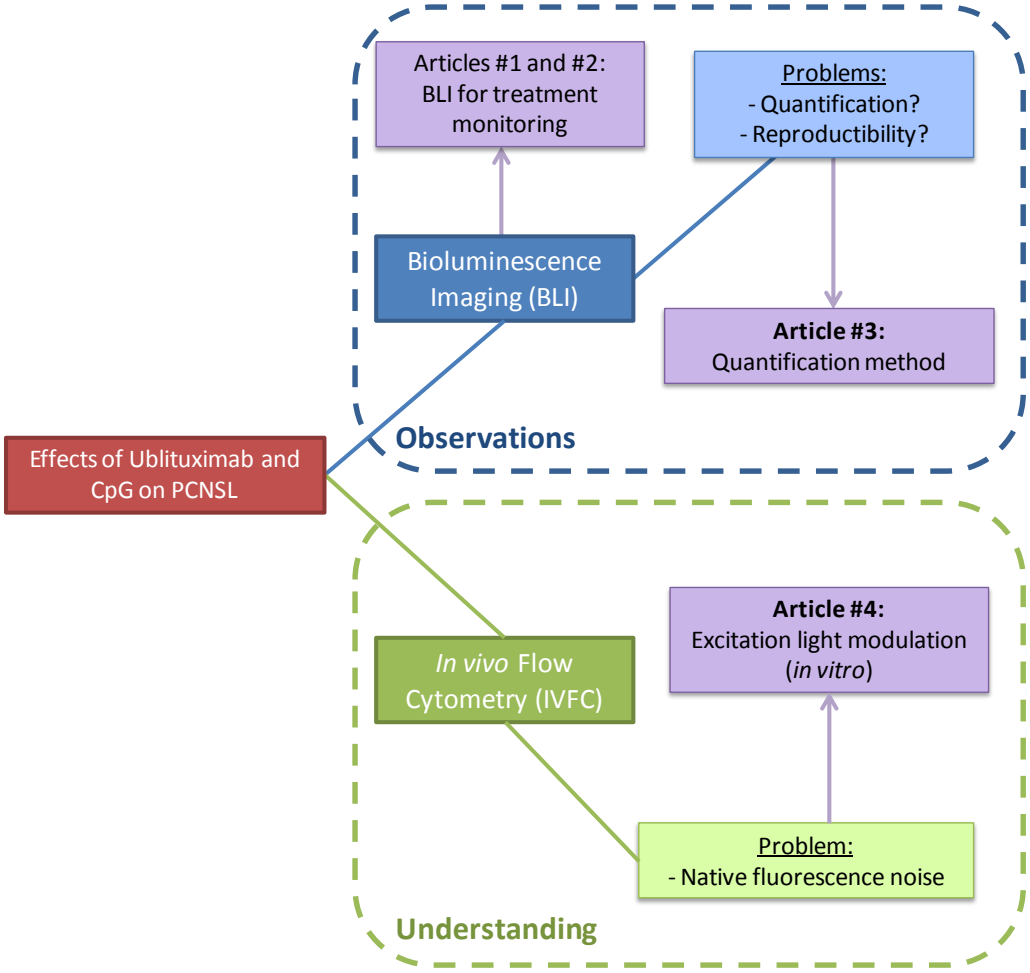

We compared two treatments (Ublituximab and CpG) using BLI. **This technique allowed us to: localize primary tumors, localize metastases, control tumor inoculation and identify responding and non-responding animals.**

Localization remains qualitative and BLI images are not fully used. **We then developed a method to quantify bioluminescence data set with increased statistical significance, reproducibility and decreased user-dependence.**

Finally, we wanted to investigate the effects of treatments on CTCs using IVFC, however, the native fluorescence noise revealed that the initial set up was not optimized. We then developed a laser modulation device, which attributes a unique signature to a cell for accurate detection. **We detected the cells, measured their velocity, and localized the circulating cells inside the vessel phantom (*in vitro*).**

DISCUSSION

PCNSL are aggressive disease with a poor prognosis; so far, there is no efficient targeted therapeutic strategy. We aimed to explore two therapeutic approaches with animal models of lymphomas and innovative imaging or detection modalities.

To investigate the role of circulating cells that are rare events, we used the model of blood lymphomas where cells are injected intravenously. The circulating cells are no more rare events in that case (Georgakoudi *et al.*, 2004) and the study of the detection system is facilitated.

1. Treatments effects on lymphoma cells : CPG and Ublituximab

The brain and the eye are immune sanctuaries. This means that no immune cells are supposed to be in these organs, except for resident antigen presenting cells (APC) such as microglias. Before studying the effects of treatments on tumor cells, the models were developed and characterized. The immune infiltrate was studied and as eye and brain are immune sanctuary, the immune infiltrate is only due to tumor cells. Such analyses provide very precious information about the relationship between the tumor infiltrating immune cells and the microenvironment whether it would be a proinflammatory or a immunosuppressive microenvironment.

1.1. Oligo DeoxyNucleotide - CpG (CpG-ODN) : TLR-9 Agonist

The CpG-ODN activates the immune system through the stimulation of TLR-9. The unmethylated CpG DNA sequences undergo endocytosis, and the motif is recognized inside the cell. TLR-9 is expressed by different innate immune cells such as macrophages (resident in tissues), monocytes (macrophages that entered in the blood circulation) and dendritic cells (belonging to the family of Antigen Presenting Cells). However, it has been shown that TLR-9 was expressed by epithelial cells of different tissues, for instance: gingival epithelial cells (Bahri *et al.*, 2010); intestinal epithelial cells (Gopal *et al.*, 2008), airway epithelial cells (Yong *et al.*, 2012). In the eye, the TLR-9 ligand can be found in the cornea and retina, but is colocalized with $CD68^+$ retinal macrophages and microglia (Chinnery *et al.*, 2012). Another study showed that retina epithelial cells express TLR-9 and secrete IL-8 when stimulated with CpG-ODN. IL-8 is a chemokine that allows recruitment of phagocytic cells.

We showed in the article #2 that CpG-DNA induces *in vitro* apoptosis of lymphoma cells. It turns out that A20.IIA lymphoma cells express TLR-9. This would mean, at first sight, that the engagement of TLR-9 is sufficient to induce apoptosis. This cell death should be observed in epithelial cells and in infiltrating immune cells. This is not the case, suggesting that the intracellular signalization pathway triggered by TLR-9 engagement might be different between lymphoma cells and healthy cells.

Another interesting fact is the efficacy of CpG-ODN. It has been described to induce apoptosis in A20 lymphoma cell lines (Qi *et al.*, 2013). It turns out, as we showed, that there is a difference of efficacy according to the localization of the lymphoma. The treatment not only reduces tumor burden in subcutaneous lymphoma (as previously shown), but reduces tumor burden in primary cerebral lymphoma bearing mice. Surprisingly, CpG-ODN effects are inhibited in the case of Primary Intra Ocular Lymphoma bearing mice. A compound present in the PIOL microenvironment seems to have an effect on CpG-ODN efficacy. This compound has been identified by our team, after proteomic analysis, as a protein, whose molecular weight is between 30kDa and 50kDa. However, this protein has not yet been identified. This protein does not inhibit the CpG-ODN internalization in the cells as it was shown in article #2. There are then several hypothesis that can be done; i) the protein interacts with inner cell signalization proteins in the pathway of apoptosis; ii) the protein triggers a down-regulation of the TLR-9; iii) the protein can bind to TLR-9 and blocks the inner cell signalization; iv) the protein neutralizes the CpG-ODN. Of course those hypotheses are speculative but they are tracks for future investigation.

Efficacy of treatments in PIOL and PCL

These mechanism suggestions are based on the fact that the unidentified compound interacts with the cells or with the CpG molecule. However, in spite of the induction of apoptosis of the lymphoma cells, the strategy of administering CpG-ODN was based on the activation of the immune system in organs where there are no immune cells in physiological conditions. The activation of the immune system means the mobilization of cytotoxic or phagocytic cells in the concerned tissue. These immune cells have to get in contact with the tumor cells to fulfill their tasks.

The position of cells in Intra Ocular Lymphoma has been well described (Touitou *et al.*, 2008): the cells are diffuse in the vitreous and cause vision troubles, and they finally lay on the bottom of the eye because of sedimentation. This means that the tumor cells are not in contact with deeper layers of retina (like in uvea melanoma) in the early disease – of course the metastases observed in the PIOL are evidences that the tumor cells leave the vitreous. The immune cells, mobilized at the tumor site are attracted there by chemokines and come from the periphery. To get in contact with tumor cells, the immune cells have to cross the blood-retinal barrier, and to leave the upper layer of the retina to diffuse in the vitreous and find their target. In this environment (vitreous), their motility might be uncontrolled, reducing the number of efficient contacts with tumor cells.

In the brain, CpG-DNA exhibits good efficacy. Unlike vitreous, which is liquid and diffuse, brain is an organ containing a high density of cells; even though the brain is surrounded by the Cerebro-Spinal

Fluid (CSF). The density of cells makes the brain a location where immune cells can move easier, and where efficient contact with tumor cells might be more frequent than in the vitreous.

According to this suggestion, the number of contact between tumor and immune cells is low because tumor cells lay in the vitreous (in the case of PIOL). The tumor cells then accumulate and are not properly killed by the immune cells. Immune cells induce cell apoptosis, which is a proper death for a cell: vesicles appear and are correctly eliminated by macrophages. When the cell does not enter in apoptosis, it may explodes, and spread the intra cellular medium. The neighbor cells detect the inner molecules of the exploded cell and can either undergo the same cell death or trigger inflammatory molecules secretion. This phenomenon called necrosis can lead to a highly inflammatory context.

In PIOL mice, after several days, necrotic lesions are observed. This is consistent with the hypothesis of low numbers of contacts between tumor cells and immune cells. In the case of PCL, the skull contains the tumor and mice death could be attributed to high intracranial pressure.

1.2. Ublituximab : Engineered (low fucose) anti-humanCD20 monoclonal antibody

Activation of immune system

Antibodies play different roles in the immune response. The target of the antibody can be either living (bacteria, tumor cell, virus etc.) or non-living (toxins, proteins etc.). In the case of non-living targets, a toxin for instance; the antibody recognizes the epitope, neutralizes the toxin and acts like a flag; the toxin is, on one hand, no longer effective because it cannot bind to its receptor anymore, and on the other hand, the complex toxin-antibody is very well recognized by the innate immune cells (phagocytic cells). In the case of a living target, the antibody binds to the target and either kills it by itself or recruits immune cells, which will phagocytize the target (e.g. bacteria); if the target is too large, the effector cell injects cytotoxic proteins inside the target's cytoplasm to trigger apoptosis. The apoptotic vesicles of the target will be then phagocytized.

On top of that let me remind that the complement molecules recognize the Fc part of the antibody and plays an important role in pathogen clearance. Whatever would be what recognizes the antibody (complement molecules, APC or effector cells), the process will lead to an activation of the immune system.

Induce or break tolerance?

The phagocytosis is indeed a key point in activation of the immune system. After digesting the target cell, APC have the ability to present peptides from the target cell at their surface. They then migrate to the lymph node to present those peptides to B-cells and T-cells. Briefly, the presentation of the

antigen will lead to the clonal expansion of B-cells that are specific for this target (Xu *et al.*, 2014). Those ex-B-cells are called plasma cells; they migrate in the periphery and secrete antibodies against the specific antigen. The process lasts for several days.

Usually, the antigen presenting phenomenon does not happen a lot if the reaction has been initiated by an antibody. If an antibody has bound to a target, it means indeed that there are already plasma cells specific for this antigen. Selecting new B-cells is not necessary. This phenomenon is very well-known by obstetricians.

Postpartum administration of anti-Rhesus Immunoglobulin (anti-Rh Ig) is recommended when a Rhesus negative mother delivers a Rhesus positive infant. The rhesus is determined by a protein at red blood cells surface: if the protein is here the rhesus is positive if not, the rhesus is negative. At the delivery, some red blood cells from the baby enter the vascular system of the mother. If the baby is Rh^+ and the mother Rh^-, the mother's immune system will develop anti-Rhesus antibodies. If the mother had a second Rh^+ child, the immune system of the mother could "reject" the baby causing the hemolytic disease of newborn. The aim of administration of anti-Rh Ig is to neutralize the red blood cells of the baby before the mother's adaptive immunity triggers (Sibéryl *et al.*, 2006).

In the case of the hemolytic disease of newborns, the aim is **to induce tolerance** of the antigen. And indeed the risk that a negative mother can be immunized by a positive foetus is reduced from 16% to 0.1% with a proper anti-Rh Ig administration.

This is very close to what is done in immunotherapy. However, in immunotherapy, the administration of the antibody is done to **break tolerance** of the antigen, and precisely to induce adaptive immunity, in the hope that the mouse will create its own anti-humanCD20 antibodies (in our case). That is why inducing memory response after injection of monoclonal antibodies remains a challenge.

Long-lasting response

In spite of the example of hemolytic disease in newborns, it turns out that the administration of anti-hCD20 in PCL bearing mice induced in our model a long-lasting response. Ublituximab has been engineered to activate ADCC, and the number of CD8+ (cytotoxic) T-cells in the brain is indeed increased in PCL bearing mice treated with Ublituximab. Another team in the laboratory is working on a T-cell precursor lymphoma model treated with an anti-hCD20 antibody; they showed (Abès *et al.*, 2010) that not only is there a long-lasting response, but 60% of surviving mice survive a second administration of tumor cells, which would mean that the tolerance has been broken creating then a memory response (Abès *et al.*, 2011).

We also showed that unlike CpG-ODN, Ublituximab keeps its efficacy in PIOL mice. There is indeed an inhibition of tumor cell proliferation, and the mAb treatment prevents metastases from developing in the eye-draining lymph node. The effects on both intra-ocular and cerebral tumor are long-lasting, and Ublituximab has better anti-tumor effects than rituximab (a widely used anti-humanCD20 antibody). Ublituximab has been engineered to enhance ADCC. However, in the eye, Ublituximab may suffer the same problem than CpG. The cells are indeed diffuse in the vitreous, and mobilized effector cells still have to get in contact with opsonized (covered with antibodies) tumor cells. If this hypothesis is validated, it would mean that Ublituximab can induce cell death more efficiently than CpG-ODN by itself; or it would mean that the protein that inhibits CpG-ODN effects does not alter Ublituximab effects or does not interfere with Ublituximab mediated cell death signalization pathway.

We cannot forget either than in our model, the human CD20 is expressed by tumor cells. This antigen is non-murine, and could trigger by itself an immune response. When targeted by an anti-body, human CD20 peptides can be presented by mouse APC to lymphocytes. An adaptive immune response could appear specific for the human CD20. The long lasting response could be due to the humanCD20 immunization of mouse.

Adverse events

The use of monoclonal antibodies in therapeutics has totally changed the approaches to cure cancer disease. As explained before, the aim of immunotherapy is to break tolerance. In the case of CD20, which is a transmembrane receptor expressed in B-cells whether they are cancer cells or healthy cells, breaking the tolerance could lead to serious side effects such as autoimmunity or hypogammaglobulinemia (Marco *et al.*, 2014). The target protein of an immunotherapy must not be expressed by healthy cells. This is one of the big challenges of researchers in immunotherapy, who have to find the good target for antibodies. Actually, CD20 is not expressed on B-cells precursors and on plasma cells (mature B cells secreting antibodies). A DLBCL patient that received anti-CD20 antibodies will have all his B-cells depleted. This depletion only lasts for a while. After both healthy B-cells and lymphoma B-cells are depleted, healthy B-cells can reappear from precursors.

Chimeric antibody: human Fc, murine FcδR

In our mouse model, we did not observe the phenomenon of autoimmunity because the antigen is a humanCD20. As no cell in the mouse naturally expresses humanCD20, there is no chance that autoimmunity occurs in this case. However in spite of being a human Ig, Ublituximab still seems to activate the immune system of the mouse, suggesting cross-reaction between mouse Fcγ receptors and human Ig Fc part.

Immune context

In both cases Ublituximab or CpG, the immune microenvironment was analyzed.

PIOL: In spite of the effector $CD8^+$ T-cells, there are many regulatory T-cells ($CD25^+$ $foxp3^+$) invading the eye. A high proportion of Th17 cells were also detected, but their role in the pro-tumoral / anti-tumoral balance remains unclear (Galand *et al.*, 2011).

PCL: The analysis of the immune microenvironment in the brain revealed the important role of antigen presenting cells. Identified as $CD11b^+$ cells, they are mostly dendritic cells, even though some macrophages and microglia can express $CD11b^+$. The high number of APC in the brain could be one of the reasons why CpG is more efficient in the brain than in the eye.

The regulatory T-cell induction has been widely studied and some studies suggest that intratumoral immunization can occur after mAb treatment (Marabelle *et al.*, 2014), and even immune regulation with TLR agonists (Lu *et al.*, 2014).

1.3. Limits of the models

Like every model, mouse models have their limits.

Using a mouse models means extrapolating results obtained in a mouse to somehow predict what happens in humans. However, even if mouse models are powerful models, it is well known that there are slight differences between mouse's immune system and a human's immune system. In the case of cancer and immunotherapy these differences might be critical. The use of humanized mice (Chargui J et. al, 1995) – mice in which a human immune system is recreated after human hematopoietic stem cells graft – would be very relevant for future studies.

In the model of Ublituximab treatment, the tumor cells express humanCD20. It is fairly conceivable that the mouse can develop antibodies against humanCD20 because humanCD20 is obviously not a mouse protein. This fact could help in breaking the tolerance.

Finally, the way cells are introduced could play a non-negligible role. Cells are introduced in the eye and in the brain through a hole. In these organs it might be different than in subcutaneous injections, where elasticity of tissues fills the hole once the needle is out of the skin. In the case of PIOL or PCL, the hole is not filled instantaneously, the hole is actually used a second time for treatment administration. It is conceivable that some cells go out the primary location by this hole, facilitating the metastasizing process. However, injection is the standard approach. Ublituximab and CpG in certain cases prevent metastases from appearing, and even if the mechanisms of action might remain unclear, the treatments had measurable effects.

In physics, in mathematics, in biology and in any science, a model is a tool that allows understanding mechanisms that are too complicated to be investigated at the same time. These models have limits, and this is an intrinsic property of models. The knowledge of these limits is crucial and is required to draw correct conclusions from any model.

2. Bioluminescence quantification method

We described a standardized method for quantification of tumor burden. A mouse is attributed a luminoscore, which is value calculated according to the protocol we described.

Standardizing the method

Actually, the idea of the luminoscore came from the fact that there is no consensus about both the unit and the way to acquire images in bioluminescence imaging. Everybody has their own method and sometimes, the bioluminescence images are far from being fully exploited. A quick look at Figure1 of the article #3 is generally enough to realize two facts: two different units are widely used to quantify the same thing, and almost everybody uses the same bioluminescence imager (IVIS–Xenogen, Perkin Elmer). We then propose a method, suitable (and developed) with the IVIS software which is standardized, and associated to a protocol that allows comparisons not only between mice, but between experiments.

The method attributes a value to a mouse: the **luminoscore**. This value is calculated from images always acquired the same way, making it a good and comparable indicator for tumor burden. The luminoscore can also be compared between different tumor sites. This can give information about the virulence of the cells in the different tissues where they are localized. Otherwise the luminoscore allows comparisons between different cells in the same location.

Absolute quantification

The signal gathered from the high sensitivity camera is directly linked to the quantity of luciferase. However, the expression of luciferase can change (up to 10 fold) from one cell to another within a cell population. This can be seen for example in conventional cytometry, where a cell population can be a decade wide in terms of fluorescence intensity. The histogram in figure 35 represents the expression of mKate during the clonal selection process to establish the A20.IIA-mKate cell line. The signal is more than one decade wide, yet these are cells all originating from the same single mother cell. This is well known in cytometry, and basically a cell that would correspond to the black arrow on the histogram has 10 times as much fluorescent protein as a cell corresponding to the blue arrow.

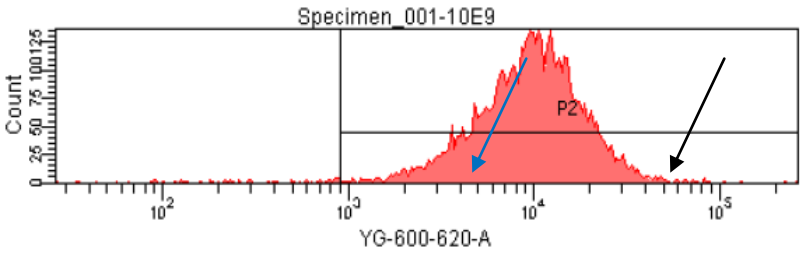

Figure 35: Representative flow cytometry histogram of an A20.IIA-mKate clone. As can be seen, fluorescence intensity covers more than one decade.

For bioluminescence imaging, this effect is quite difficult to measure; however, the phenomenon is the same. For this reason, there is no possibility to achieve an absolute quantification linked to the number of cells.

The luminoscore method is not an absolute quantification method; it gives a standardized estimator of the tumor burden.

User dependance

A key point of the method is to get rid of threshold-dependent effects linked to automatic region of interest (ROI) drawing. The threshold in the automatic ROI drawing is selected manually. A low threshold can make a ROI not significant because some photons that come from noise region might be integrated in the signal. That is why our method is based on a reproducible drawing of the ROI. Two types of ROI give good results: the rectangle draw and the manual mark up. Nevertheless, it is the manual mark up that provides less noise in the signal that has been chosen in the luminoscore method. The analysis using different ROI selection techniques demonstrated that statistical significance can be hidden by user-dependent and setting-dependent factors.

This work considers only 2D imaging. Tomographic 3D-bioluminscence systems are coupled with 3D reconstruction algorithms that provide more precise results. However those devices are very expensive and not widely available. Bioluminescence tomography provides on top of that very accurate information about location of tumor sites. In cancer research, 2D imagers are widely used but provide less specific information concerning precise metastasis and tumor location. However, the position of metastases can be inferred based on a good knowledge of the mouse model. The exact location can only been known by autopsy and histology. Therefore bioluminescence imaging remains a qualitative method for localization of tumor sites, and should be complemented by autopsy whenever autopsy is possible. However, new imaging devices are coupling micro CT-scan and bioluminescence providing very precise information on position of tumor or metastases.

Uncertainty in 2D bioluminescence imaging tecniques

There are different limits of bioluminescence 2D-imaging techniques. Those limits are inherent to all bioluminescence-based imaging techniques.

As a matter of fact, our model and in most of tumor burden following models, luciferase is expressed constitutively after transfection of transduction of the corresponding cDNA. The luciferase gene (*luc2*) is often controlled by a high-expression promoter like SV40 or CMV promoters. Yet, luciferase is not a protein that has a vital function for the cell. Even if a clonal population has been selected with 100% positive cells at the moment when the tumor cells are inoculated, the loss of luciferase

expression is a phenomenon that can occur. In that case, non-expressing luciferase tumor cells are no longer detectable, and can lead to an under-estimation of tumor burden. Unfortunately, this phenomenon is quasi-uncontrollable and this bias is present in every bioluminescence assay.

Another limit to that technique is that the molar absorption coefficient (MAC) is considered as the same in the whole mouse. The MAC corresponds to the amount of photons that a compound can absorb in a given distance. A mouse is composed with 80% water, so very often, the MAC of the mouse's tissues is assimilated with water's. In the described standardization method, only the photon flux is measured, but the assessment of linking the tumor burden with the photon flux implies the acceptance of the hypothesis on the mouse's tissue MAC. It is well known that some organs are more critical than others in terms of absorption; liver and pigmented skin are perfect examples of this. Obviously, a black mouse and an albino mouse won't have the same tissue absorption. The models established in the laboratory were done with albino mice, which was favorable for bioluminescence imaging. Currently, whatever the bioluminescence system is chosen, the problem of "dark tissues" absorption remains. This limit has to be borne in mind when designing animal models for studies including BLI follow-up.

We proposed in our protocol two acquisitions: front and back. Nevertheless, to optimize signal detection, position the mouse according to tumor site location is often suggested. We chose to explore the two natural positions of the mouse that covers the whole eventual metastases sites with the front and back acquisition. These positions should minimize variability due to the placement of the mouse from one day to the next but may not optimize signals originating from all anatomical sites.

Oxygen for light

Finally, the choice of the luciferase protein can be very important in the analysis of images. Firefly luciferase is most commonly used, because it has a good yield and provides a great number of photons in a large spectrum (550 nm max intensity – green). However, to reduce its substrate, luciferin, firefly luciferase needs magnesium, ATP, and oxygen. Therefore, an anoxic or necrotic tumor will not be detected by the imaging system. Again, the knowledge of the model is crucial to make the good choice. If the tumor does not present anoxia or necrosis, firefly luciferase is the best choice. If the tumor present those properties, gaussia luciferase would be better. The gaussia luciferase spectrum has its emission peak at 450nm (blue), and does not require molecular oxygen to reduce its substrate, colenterazine. However, at this wavelength, tissue absorption is higher than around 550nm.

3. *In vivo* flow cytometry and 2-photons microscopy

In vivo flow cytometry has been well-described in the literature; however, very few tumor models have been investigated. Very often, the models that have been considered were human tumor cell lines xenografts in immunodeficient mice. *In vivo* flow cytometry provides an opportunity to gather information on metastasizing processes through the study of circulating tumor cells. Our model is syngeneic and as can be seen in table 1 that sum up the CTCs detection techniques, very few studies have been made on syngeneic model. Actually, the detection of CTCs in mouse is different than in humans where the CellSearch device can be used. As the immunocapture of cells is based on EpCam antigen, which is a human protein, CellSearch is not suitable for mouse models. Some CTC detection and capture devices based on filtration are very efficient; still, they require a blood sample. Even though it is fairly possible to puncture blood in a mouse, this cannot be done very frequently and in a non-invasive way.

Redshift

Thus, *in vivo* flow cytometry is the only device fitting our conditions that could help us answer our questions. Performing longitudinal studies in a syngeneic mouse model requires developments of specific fluorescent protein expressing cell lines. However, the most commonly used fluorescent protein is GFP. GFP requires blue light (488 nm) to be excited, and emits fluorescence in the green part of visible spectrum (530 nm). Blue light does not penetrate living tissues well, yet in our case its use was feasible because we were studying blood vessel located just under the skin (100µm). Blue light excites many endogenous fluorophores creating native-fluorescence noise. On top of that, the emitted fluorescence (530 nm) corresponds to the maximum absorbance of hemoglobin and living tissues.

The problem of autofluorescence and tissue absorption can be addressed by shifting the excitation and emission spectra toward the red and far-red wavelengths. Unfortunately, except for commonly used fluorescent proteins (GFP, YFP, RFP, etc.), proteins are usually fluorescent in the U.V. domain of electromagnetic waves spectrum. In our case, we need a constitutive protein, whose gene can be transfected with the target cell. The fact that we perform longitudinal studies in a syngeneic model does not permit the use of organic fluorophores, whose signal is divided for each cell division. It remains very difficult to design fluorescent proteins in the infra-red domain of electromagnetic waves; however, proteins are available in the far-red domain. This is the case of mKate (or Turbo FP-635), which have its excitation peak at 590 nm and its emission peak at 635nm. This set of wavelengths is more adapted for *in vivo* imaging as the living tissues absorption decreases as the wavelength increases. We developed an mKate expressing cell line but we did not have the time to

test it. We already had a GFP expressing cell line and the double-illumination strategy was the other alternative to address the problem of noise and autofluorescence, without engineering a new cell line.

Depth of field

Currently, 2-photons microscopy gives very good resolution images. The optical sectioning and the explored volume remained nevertheless a significant limitation. We did not want to miss any cell in the blood vessel, and this can occur if the depth of field is too thin. To overcome the problem of autofluorescence, we could have used a high numerical aperture objective to gather more fluorescence photons, and concentrate more excitation photons. But, this would have reduced the depth of field of the device. We designed the device with a 0.75 NA air objective supplemented with several cylindrical and spherical lenses to obtain a beam that was 600µm long, 200µm wide, and set up the detector to obtain a 150µm depth of field. That way, each cell whom GFP is excited is detected, whatever would be its position in the blood vessel. On top of that, the explored volume is optimized allowing a better statistical detection. We chose epifluorescence because the ear of the mouse is placed between microscope slide and slip cover, and there is no place behind the ear to position another objective of lens.

Blood lymphoma

Initially, we had concerns about PIOL and PCL, but we realized that those models were not adapted for developing and testing the new IVFC device. We had no idea whether the cells disseminated in the blood or not, as it was indeed our initial question. We then developed a new model of lymphoma in which we were sure that there were circulating cells, at least for a while after injection. This model is a systemic blood lymphoma model: we injected from 5.10^5 to $2.5.10^6$ cells directly in the blood of the mouse as described initially by I.Georgakoudi. We are however aware that this model is purely artificial and is not adapted to study rare circulating tumor cells.

However, we are conscious that blood is not the only pathway that lymphoma cells use to migrate. Tumor cells can migrate through lymph vessels; this could explain why we saw a lot of lymph node metastases. On the other hand, we identified metastases on the inguinal lymph node. This could suggest that the cells were in the blood at a given time, because if they had migrated only by lymph vessels they would have been stopped in other lymph nodes before the inguinal one. The fact that those cells are initially B-cells also have to be kept in mind: those cells might have a particular homing for lymph node.

4. Double-illumination to pattern excitation light

The double illumination system has been inspired by optical mouse. The optical mouse is based on pattern recognition. The support is photographed several thousands of times per seconds and similar patterns are looked for in the successive images to infer the movement of the mouse. Detection of fluorescent cells is enhanced, and autofluorescence noise is dramatically decreased thanks to the double illumination system. Moreover, spatial modulation of the excitation source allowed us to calculate the time of flight and thus the relative velocity of the cells. This system was used with A20.IIA-GFP^{+} cells.

Poiseuille flow hypothesis

The double illumination device had to be used and calibrated *in vitro* before it is used *in vivo*. That is why we modeled the mouse's blood vessel by a 120µm-wide silicon (PDMS) channel. The PDMS has autofluorescence in the GFP channel, this property that mimics tissue autofluorescence helped us in adapting the signal processing methods to be later applied *in vivo*.

We linked the time-of-flight and the velocity using well-known velocity profiles of Poiseuille flow. This hypothesis is strong, but can be done in the case of sufficiently diluted medium. As for the *in vivo*, this hypothesis is still correct in sufficient-sized vessels. In small vessels the effect of the cell size cannot be neglected, including radial change in cell concentration, and therefore in fluid viscosity. However, these effects are well-known and accurate models have been described linking cell velocity and position in different sized vessel according to the flow rate (Quemada D, 1981).

Diapedesis

Finally, having the velocity and the position of cells on a blood vessel could be crucial to understand the mechanisms of extravasation of tumor cells. A low-flowing cell can indeed be rolling on the inner-surface of the blood vessel; when rolling, the velocity is low until the cell stops, and enters the tissues, especially if they are hematopoietic-derived cells. The number of low-velocity rolling cells could be an interesting parameter for evaluating the metastasizing dynamics.

However, immune cells and lymphoma cells can express integrins (adhesion molecules) at their surface. Those integrins can bind to other adhesion molecules that are expressed by the endothelial cells in the blood vessel. In physiological conditions, those adhesion molecules are expressed by endothelial cells in case of local inflammation to recruit immune effector cells. This system can be used by tumor cells to enter the tissues at an inflammation site. Actually, inflammation and cancer are closely linked.

Excitation modulation and Signal processing method

The fluorescence excitation source modulation, whether it would be spatial (Zharov et al), energetic or temporal (Kiesel *et al.*) is a solution for an enhanced detection of fluorescence and velocity measurement. Coupled with an appropriate signal processing, it could be implemented for real time monitoring of circulating cells velocity. The Gaussian-shaped sliding mean (our method) is low resource consuming. It is actually equivalent to a temporal bandpass filter. Very quick phenomena are smoothen (noise fluctuations) as well as very low phenomenon. Finally only phenomena of the expected duration are retained.

We used in this device a low aperture 10X objective. This dramatically reduces the amount of gathered fluorescence photons. However, this is necessary to obtain two sufficiently spaced excitation slits. A high aperture objective would have a high focusing capacity, and the slits would be very close to each other, increasing the risk of overlapping of the signal coming from the different slits. This would lead to uncertainty in the identification of the peak and thus to an error in the velocity measurements. That would explain why the chosen objective is a 10X low aperture objective. The amount of the fluorescence photons missed by the low aperture objective is, in a way, overcompensated by the brightness of GFP, which is not the case for all fluorescent proteins.

Human after all

To conclude, the double illumination system is very efficient in detection of fluorescent events, and in real time noise elimination. Unfortunately, during my PhD, I did not have sufficient time to go through *in vivo* experiments. *In vivo* flow cytometry is very difficult to adapt for the human being. Indeed, patients positive for CTCs are typically between 0.2 to 10 CTCs per mL, yet some patients can have up to 200 CTCs per mL. The concentration of CTC is a key factor for detection. A mouse model in which tumor cells are injected intravenously is artificial, and moreover mice have only around 1mL of blood. The measures corresponding to humans don't seem to be consistent for mice (this would mean the mouse had only 1 to 10 CTC in whole blood). As we presented earlier, the whole blood volume has to be analyzed 5 times to have a 5% error on the result. For a human being, with a blood volume of 5L, the explored volume should be 25L. If the vessel is 100µm wide, the explored volume is around 0.0004 mL /s (based on a physiological velocity of $10mm.s^{-1}$), and it would take 25000/0.0004 = 62 500 000s = 24 months (!) to be 95% sure there is no CTC in patient blood. The only way to overcome this problem would be to increase the explored volume by increasing the size of the vessel, but the tissue absorption will be increased accordingly.

This device is thus not suitable for the human being; however has been conceived and developed for mice. The study of CTCs on mice models is however relevant for mechanistic investigations.

CONCLUSIONS AND PERSPECTIVES

Since the 2000's immunotherapy is, in certain cases, revolutionizing cancer treatments. We investigated different treatments of immunotherapy in mouse lymphomas models. Those treatments, CpG-ODN and Ublituximab, are based on two fundamental principles: kill the tumor cells by themselves and activate the immune system. CpG-ODN activates better innate immune system whereas Ublitiximab adaptive immunity through ADCC and Antigen Presenting Cells.

We showed that Ublituximab reduces the number of tumor cells in PIOL and in PCL while CpG-DNA exhibited anti-tumor effects in SCL and PCL but not in PIOL. The tumor microenvironment of PIOL indeed inhibits the anti-tumor effects of CPG. Proteomic analyses showed that it was a protein, whose molecular weight is between 30 to 50 kDa. Further investigations on its identification are ongoing.

In the studies of CpG and Ublituximab, cytometry and histology were used. Those techniques require the sacrifice of the animal. However, we wanted to perform longitudinal studies to address different questions on metastatic dissemination mechanisms. We then develop different techniques and methods of non-invasive exploration of tumor cell bearing mice.

We used bioluminescence imaging to localize tumor cells and to see the effects of the treatments on not only the primary, but the metastases than are not detectable with palpation exams or autopsy (infra-clinical). We showed that Ublituximab prevented the apparition of cervical lymph node metastases in both case PIOL and PCL.

The use of bioluminescence allowed us to identify a lack in consensus on the use of bioluminescence imaging data. We then described a quantification method for estimating tumor burden in bioluminescence image. The method is easy to use, easy to adapt in an already settled environment, does not require complex calculation and high resources computers, reduces user-dependence and reveal statistical significance.

Bioluminescence imaging gives us information about localization of primary tumors and metastases but what about the link between those? CTCs are the link. They leave the primary tumor and invade other organs. We wanted to investigate the role of CTC in the PIOL and PCL metastases, but also the effects of treatment on CTCs. To do so we set up an *In Vivo* Flow Cytometry device.

The *in vivo* flow cytometer was set up and was promising. It showed very good results in *in vitro* models, but its limit, autofluorescence noise, did not allowed us to identify fluorescent circulating tumor cells in living mice. The question of autofluorescence noise was addressed in parallel by the engineering of a new cell line A20.IIA-mKate that showed promising results *in vitro*, and by the use of

modulated excitation light. Energy modulation and beam shaping of the excitation light was the solution to several problems. Not only fluorescence detection is enhanced, but the velocity of the cells can be precisely determined. We then linked the velocity of the cell with its position in the channel. Applied *in vivo*, this information could give interesting information about metastasizing dynamics.

The final aim is to gather different types of information: quantify the tumor burden, locate of metastases, measure the number of CTCs, and measure the velocity of CTCs (Figure 36). Put together, such information could help to us understanding metastasis dissemination and effects of innovative treatments on metastasizing mechanisms; effects, that so far remain unclear.

A concrete short term perspective would be the combination of all the methods described in this work (bioluminescence imaging, modulated *in vivo* flow cytometry, conventional cytometry, histology, etc.) to quantify the effects of treatments in regard of their administration route. The *in situ* administration of treatment is very heavy for patients especially for PCL patients (in the brain). The use of intra-venous treatments could be a significant help for patients. This could be done by co administration of the treatment (*e.g.* Ublituximab) with an agent that temporally and reversibly permeabilizes the blood brain barrier. In terms of fundamental research this kind of approach could help understand the link between the metastasis and tumor cells by using double positive A20.IIA-*luc2*-mKate cells.

We started from the topic of lymphomas and the detection of tumor cells and CTCs, nevertheless the use of IVFC could not be restricted to CTCs. Any cell, fluorescently labeled could be detected with this device. This could be applied in cell therapy for the detection of immune cells (autoreactive CD8 T-cells) or hematopoietic stem cells (in the treatment of genetic immune disease).

Recent techniques aiming to kill circulating tumor cells with cold plasma could be coupled to the velocity measurement system to trigger the shot of plasma.

To conclude, this work offers many perspectives. On top of that, we are the only team in France to own an *in vivo* flow cytometry device. The opportunities could be great in different fields of biology such as pharmacokinetics. Finally, this kind of interdisciplinary approach (Fig. 36) using biological and physical tools give increased point of views on a fundamental question, thus leading to have better knowledge on studied mechanisms.

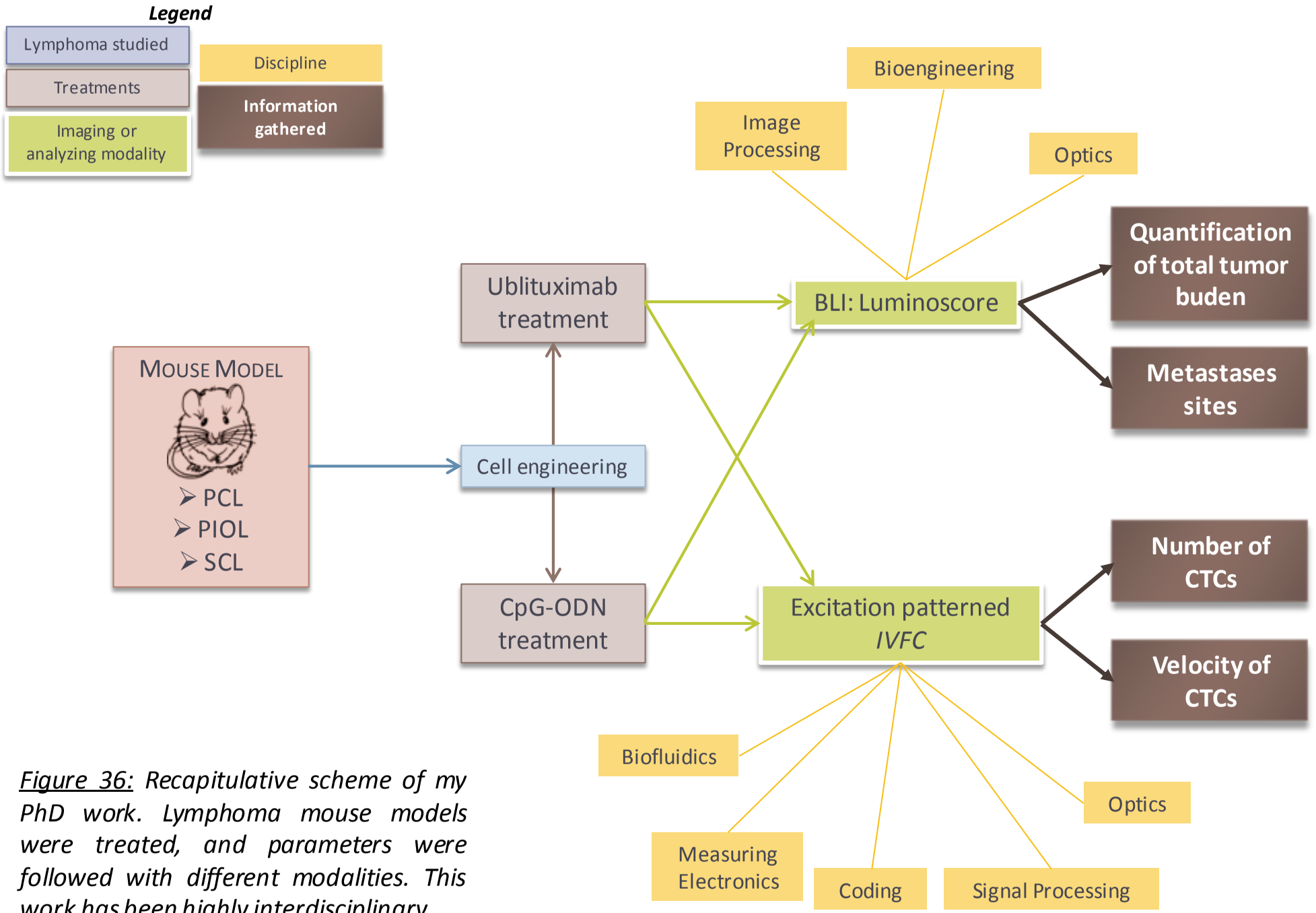

Figure 36: Recapitulative scheme of my PhD work. Lymphoma mouse models were treated, and parameters were followed with different modalities. This work has been highly interdisciplinary

PERSONAL CONCLUSION

This PhD has been very enriching for me. I entered deep in the world of research and I liked it. This interdisciplinary work strengthened my opinion on science. I am now deeply convinced that the bridges created by interdisciplinarity are the foundation of even bigger Science edifications.

This project was really important to me. Actually, this project has a funny historic. I began this project during my Master's degree internship. I came from a discussion I had with Sylvain who had seen the retinal flow cytometer in a congress. He asked me if I wanted to try to do the same. We quickly gave up on the eye but we continued on the ear. I wanted to carry on the project for a PhD but all biology doctoral school I contacted told me it was a Physic subject and vice versa. I finally discovered the Frontiers in Life Science doctoral school; and my project fitted exactly with their scope. They gave me the opportunity to make my projects come true.

At the end of the PhD, I may not have detected circulating tumor cells, yet I participated to a preclinical study, and I developed a quantification method for bioluminescence. But my favorite remains the multi illumination device. I had the idea of measuring cell velocity for a long time; actually during my master's degree internship. It was even, I can remember it, the perspective slide of my master's degree talk. This idea went from the concept to the prototype to a ready to be submitted article. It is very rewarding to realize that my project is well underway while we started from scratch.

Finally, I would like to thank you for reading my manuscript and for sharing 3 years of my scientific life.

REFERENCES – ALPHABETICAL ORDER

Abès, R., Gélizé, E., Fridman, W.H., Teillaud, J.-L., 2010. Long-lasting antitumor protection by anti-CD20 antibody through cellular immune response. Blood 116, 926–934. doi:10.1182/blood-2009-10-248609

Abès, R., Teillaud, J.-L., 2011. Modulation of tumor immunity by therapeutic monoclonal antibodies. Cancer Metastasis Rev. 30, 111–124. doi:10.1007/s10555-011-9282-3

Alt, C., Veilleux, I., Lee, H., Pitsillides, C.M., Cote, D., Lin, C.P., 2007. Retinal flow cytometer. Opt Lett 32, 3450–3452.

Bahri, R., Curt, S., Saidane-Mosbahi, D., Rouabhia Mahmoud, 2010. Normal Human Gingival Epithelial Cells Sense C. parapsilosis by Toll-Like Receptors and Module Its Pathogenesis through Antimicrobial Peptides and Proinflammatory Cytokines. Madiators Inflamm. doi:10.1155/2010/940383

Baji, P., Péntek, M., Czirják, L., Szekanecz, Z., Nagy, G., Gulácsi, L., Brodszky, V., 2014. Efficacy and safety of infliximab-biosimilar compared to other biological drugs in rheumatoid arthritis: a mixed treatment comparison. Eur J Health Econ 15, 53–64. doi:10.1007/s10198-014-0594-4

Baldwin, T.O., Christopher, J.A., Raushel, F.M., Sinclair, J.F., Ziegler, M.M., Fisher, A.J., Rayment, I., 1995. Structure of bacterial luciferase. Curr. Opin. Struct. Biol. 5, 798–809.

Bardenstein, 1998. Intraocular Lymphoma. Cancer Control 5, 317–325.

Bhojwani, D., Sabin, N.D., Pei, D., Yang, J.J., Khan, R.B., Panetta, J.C., Krull, K.R., Inaba, H., Rubnitz, J.E., Metzger, M.L., Howard, S.C., Ribeiro, R.C., Cheng, C., Reddick, W.E., Jeha, S., Sandlund, J.T., Evans, W.E., Pui, C.-H., Relling, M.V., 2014. Methotrexate-induced neurotoxicity and leukoencephalopathy in childhood acute lymphoblastic leukemia. J. Clin. Oncol. 32, 949–959. doi:10.1200/JCO.2013.53.0808

Boutrus, S., Greiner, C., Hwu, D., Chan, M., Kuperwasser, C., Lin, C.P., Georgakoudi, I., 2007. Portable two-color in vivo flow cytometer for real-time detection of fluorescently-labeled circulating cells. J Biomed Opt 12, 020507. doi:10.1117/1.2722733

Brito, A.B.C., Reis, F., de Souza, C.A., Vassallo, J., Lima, C.S.P., 2014. Intracranial primary dural diffuse large B-cell lymphoma successfully treated with chemotherapy. Int J Clin Exp Med 7, 456–

460.

Cassoux, N., Merle-Beral, H., Leblond, V., Bodaghi, B., Miléa, D., Gerber, S., Fardeau, C., Reux, I., Xuan, K.H., Chan, C.C., LeHoang, P., 2000. Ocular and central nervous system lymphoma: clinical features and diagnosis. Ocul. Immunol. Inflamm. 8, 243–250.

Chan, C.-C., Wallace, D.J., 2004. Intraocular lymphoma: update on diagnosis and management. Cancer Control 11, 285–295.

Chargui J, Dye D, Blomberg J, Desgranges C, Touraine JL. The humanized severe combined immunodeficient mouse as a model for primary human humoral response against HIV1 peptides. J Immunol Methods. 1995 Apr 12;181(1):91-100.

Chinnery, H.R., McLenachan, S., Binz, N., Sun, Y., Forrester, J.V., Degli-Esposti, M.A., Pearlman, E., McMenamin, P.G., 2012. TLR9 ligand CpG-ODN applied to the injured mouse cornea elicits retinal inflammation. Am. J. Pathol. 180, 209–220. doi:10.1016/j.ajpath.2011.09.041

Cobo-Ibáñez, T., Loza-Santamaría, E., Pego-Reigosa, J.M., Marqués, A.O., Rúa-Figueroa, I., Fernández-Nebro, A., Cáliz, R.C., López Longo, F.J., Muñoz-Fernández, S., 2014. Efficacy and safety of rituximab in the treatment of non-renal systemic lupus erythematosus: A systematic review. Semin. Arthritis Rheum. doi:10.1016/j.semarthrit.2014.04.002

Cormack, B.P., Valdivia, R.H., Falkow, S., 1996. FACS-optimized mutants of the green fluorescent protein (GFP). Gene 173, 33–38.

Counter, C.M., Avilion, A.A., LeFeuvre, C.E., Stewart, N.G., Greider, C.W., Harley, C.B., Bacchetti, S., 1992. Telomere shortening associated with chromosome instability is arrested in immortal cells which express telomerase activity. EMBO J. 11, 1921–1929.

Crowe, S.E., Ellis-Davies, G.C.R., 2014. Longitudinal in vivo two-photon fluorescence imaging. J. Comp. Neurol. 522, 1708–1727. doi:10.1002/cne.23502

Day, J.C., Tisi, L.C., Bailey, M.J., 2004. Evolution of beetle bioluminescence: the origin of beetle luciferin. Luminescence 19, 8–20. doi:10.1002/bio.749

Ding, Y., Wang, J., Fan, Z., Wei, D., Shi, R., Luo, Q., Zhu, D., Wei, X., 2013. Signal and depth enhancement for in vivo flow cytometer measurement of ear skin by optical clearing agents. Biomed Opt Express 4, 2518–2526. doi:10.1364/BOE.4.002518

Donnou, S., Galand, C., Touitou, V., Sautès-Fridman, C., Fabry, Z., Fisson, S., 2012. Murine models of

B-cell lymphomas: promising tools for designing cancer therapies. Adv Hematol 2012, 701704. doi:10.1155/2012/701704

Ducharme, D., Tessier, A., Leblanc, R.M., 1979. Design and characteristics of a cell for photoacoustic spectroscopy of condensed matter. Rev Sci Instrum 50, 1461. doi:10.1063/1.1135740

Einstein, A., 1906. Eine neue Bestimmung der Moleküldimensionen. Ann. Phys. 324, 289–306. doi:10.1002/andp.19063240204

Ferreri, A.J.M., Ciceri, F., Brandes, A.A., Montanari, M., Balzarotti, M., Spina, M., Ilariucci, F., Zaja, F., Stelitano, C., Bobbio, F., Corazzelli, G., Baldini, L., Reni, M., 2014. MATILDE chemotherapy regimen for primary CNS lymphoma: results at a median follow-up of 12 years. Neurology 82, 1370–1373. doi:10.1212/WNL.0000000000000314

Fields, K., Milikowski, C., Jewell, T., Fields, J., 2014. Localized diffuse melanosis associated with melanoma successfully treated with imiquimod cream 5%: a case report and review of the literature. Cutis 93, 145–150.

Fine, H.A., Mayer, R.J., 1993. Primary central nervous system lymphoma. Ann. Intern. Med. 119, 1093–1104.

Fiole, D., Deman, P., Trescos, Y., Mayol, J.-F., Mathieu, J., Vial, J.-C., Douady, J., Tournier, J.-N., 2014. Two-photon intravital imaging of lungs during anthrax infection reveals long-lasting macrophage-dendritic cell contacts. Infect. Immun. 82, 864–872. doi:10.1128/IAI.01184-13

Fisson, S., Ouakrim, H., Touitou, V., Baudet, S., Ben Abdelwahed, R., Donnou, S., Miloudi, A., Galand, C., Bodaghi, B., Lehoang, P., Brissard, M., Le Garff-Tavernier, M., Fridman, W.H., Sautès-Fridman, C., Cassoux, N., Merle-Béral, H., 2013. Cytokine profile in human eyes: contribution of a new cytokine combination for differential diagnosis between intraocular lymphoma or uveitis. PLoS ONE 8, e52385. doi:10.1371/journal.pone.0052385

Galand, C., Donnou, S., Crozet, L., Brunet, S., Touitou, V., Ouakrim, H., Fridman, W.H., Sautès-Fridman, C., Fisson, S., 2011. Th17 cells are involved in the local control of tumor progression in primary intraocular lymphoma. PLoS ONE 6, e24622. doi:10.1371/journal.pone.0024622

Galanzha, E.I., Kim, J.-W., Zharov, V.P., 2009a. Nanotechnology-based molecular photoacoustic and photothermal flow cytometry platform for in-vivo detection and killing of circulating cancer stem cells. J Biophotonics 2, 725–735. doi:10.1002/jbio.200910078

Galanzha, E.I., Shashkov, E.V., Spring, P.M., Suen, J.Y., Zharov, V.P., 2009b. In vivo, noninvasive, label-free detection and eradication of circulating metastatic melanoma cells using two-color photoacoustic flow cytometry with a diode laser. Cancer Res. 69, 7926–7934. doi:10.1158/0008-5472.CAN-08-4900

Galanzha, E.I., Zharov, V.P., 2011. In vivo photoacoustic and photothermal cytometry for monitoring multiple blood rheology parameters. Cytometry A 79, 746–757. doi:10.1002/cyto.a.21133

Georgakoudi, I., Solban, N., Novak, J., Rice, W.L., Wei, X., Hasan, T., Lin, C.P., 2004. In vivo flow cytometry: a new method for enumerating circulating cancer cells. Cancer Res. 64, 5044–5047. doi:10.1158/0008-5472.CAN-04-1058

Gopal, R., Birdsell, D., Monroy, F.P., 2008. Regulation of toll like receptors in intestinal epithelial cells by stress and Toxoplasma gondii infection. Parasite Immunol 30, 563–576. doi:10.1111/j.1365-3024.2008.01055.x

Göppert-Mayer, M., 1931. Über Elementarakte mit zwei Quantensprüngen. Annalen der Physik 401, 273–294. doi:10.1002/andp.19314010303

Gould, S.J., Subramani, S., 1988. Firefly luciferase as a tool in molecular and cell biology. Anal. Biochem. 175, 5–13.

Grimm, S.A., McCannel, C.A., Omuro, A.M.P., Ferreri, A.J.M., Blay, J.-Y., Neuwelt, E.A., Siegal, T., Batchelor, T., Jahnke, K., Shenkier, T.N., Hall, A.J., Graus, F., Herrlinger, U., Schiff, D., Raizer, J., Rubenstein, J., Laperriere, N., Thiel, E., Doolittle, N., Iwamoto, F.M., Abrey, L.E., 2008. Primary CNS lymphoma with intraocular involvement: International PCNSL Collaborative Group Report. Neurology 71, 1355–1360. doi:10.1212/01.wnl.0000327672.04729.8c

Happel, J., Brenner, H., 1983. Low Reynolds Number Hydrodynamics: With Special Applications to Particulate Media. Springer.

Hauser, S.L., Waubant, E., Arnold, D.L., Vollmer, T., Antel, J., Fox, R.J., Bar-Or, A., Panzara, M., Sarkar, N., Agarwal, S., Langer-Gould, A., Smith, C.H., HERMES Trial Group, 2008. B-cell depletion with rituximab in relapsing-remitting multiple sclerosis. N. Engl. J. Med. 358, 676–688. doi:10.1056/NEJMoa0706383

Hoang-Xuan, K., Chinot, O.L., Taillandier, L., 2003. Treatment of primary central nervous system lymphoma in the elderly. Semin. Oncol. 30, 53–57.

Hoang-Xuan, K., Taillandier, L., Chinot, O., Soubeyran, P., Bogdhan, U., Hildebrand, J., Frenay, M., De Beule, N., Delattre, J.Y., Baron, B., European Organization for Research and Treatment of Cancer Brain Tumor Group, 2003. Chemotherapy alone as initial treatment for primary CNS lymphoma in patients older than 60 years: a multicenter phase II study (26952) of the European Organization for Research and Treatment of Cancer Brain Tumor Group. J. Clin. Oncol. 21, 2726–2731. doi:10.1200/JCO.2003.11.036

Hooper, C.E., Ansorge, R.E., Browne, H.M., Tomkins, P., 1990. CCD imaging of luciferase gene expression in single mammalian cells. J. Biolumin. Chemilumin. 5, 123–130. doi:10.1002/bio.1170050208

Houot, R., Levy, R., 2009. T-cell modulation combined with intratumoral CpG cures lymphoma in a mouse model without the need for chemotherapy. Blood 113, 3546–3552. doi:10.1182/blood-2008-07-170274

Huen, A.O., Rook, A.H., 2014. Toll receptor agonist therapy of skin cancer and cutaneous T-cell lymphoma. Curr Opin Oncol 26, 237–244. doi:10.1097/CCO.0000000000000048

Inoue, Y., Kiryu, S., Watanabe, M., Tojo, A., Ohtomo, K., 2010. Timing of imaging after d-luciferin injection affects the longitudinal assessment of tumor growth using in vivo bioluminescence imaging. Int J Biomed Imaging 2010, 471408. doi:10.1155/2010/471408

Inouye, S., Shimomura, O., 1997. The use of Renilla luciferase, Oplophorus luciferase, and apoaequorin as bioluminescent reporter protein in the presence of coelenterazine analogues as substrate. Biochem. Biophys. Res. Commun. 233, 349–353. doi:10.1006/bbrc.1997.6452

Irthum, B., Lemaire, J., 1999. Encyclopédie Medico Chirurgicale.

Kamio, T., Yokohama, A., Hayashi, T., Toyama, K., Koya, H., Hoshino, T., Saitoh, T., Hanyuda, N., Mukai, R., Handa, H., Murakami, H., Tsukamoto, N., Nojima, Y., 2014. [Relapsed primary intraocular lymphoma treated with intravitreal methotrexate and high-dose chemotherapy followed by autologous stem cell rescue]. Rinsho Ketsueki 55, 244–248.

Kiesel, P., Beck, M., Johnson, N., 2011. Monitoring CD4 in whole blood with an opto-fluidic detector based on spatially modulated fluorescence emission. Cytometry A 79, 317–324. doi:10.1002/cyto.a.21042

Krieg, A.M., 2002. CpG motifs in bacterial DNA and their immune effects. Annu. Rev. Immunol. 20, 709–760. doi:10.1146/annurev.immunol.20.100301.064842

Lapotko, D., Romanovskaya, T., Zharov, V., 2002. Photothermal images of live cells in presence of drug. J Biomed Opt 7, 425–434. doi:10.1117/1.1481902

Lapotko, D.O., Romanovskaya, T.R., Shnip, A., Zharov, V.P., 2002. Photothermal time-resolved imaging of living cells. Lasers Surg Med 31, 53–63. doi:10.1002/lsm.10068

Le Garff-Tavernier, M., Herbi, L., de Romeuf, C., Nguyen-Khac, F., Davi, F., Grelier, A., Boudjoghra, M., Maloum, K., Choquet, S., Urbain, R., Vieillard, V., Merle-Béral, H., 2014. Antibody-dependent cellular cytotoxicity of the optimized anti-CD20 monoclonal antibody ublituximab on chronic lymphocytic leukemia cells with the 17p deletion. Leukemia 28, 230–233. doi:10.1038/leu.2013.240

Lee, H., Alt, C., Pitsillides, C.M., Puoris'haag, M., Lin, C.P., 2006. In vivo imaging flow cytometer. Opt Express 14, 7789–7800.

Li, Y., Wang, Y., Liu, X., 2012. The Role of Airway Epithelial Cells in Response to Mycobacteria Infection. Clin Dev Immunol 2012. doi:10.1155/2012/791392

London, A.L. joint author, Shah, R.K., 1978. Laminar flow forced convection in ducts a source book for compact heat exchanger analytical data. Academic Press, New York.

Lu, H., 2014. TLR Agonists for Cancer Immunotherapy: Tipping the Balance between the Immune Stimulatory and Inhibitory Effects. Front Immunol 5. doi:10.3389/fimmu.2014.00083

Marabelle, A., Kohrt, H., Caux, C., Levy, R., 2014. Intratumoral immunization: a new paradigm for cancer therapy. Clin. Cancer Res. 20, 1747–1756. doi:10.1158/1078-0432.CCR-13-2116

Marco, H., Smith, R.M., Jones, R.B., Guerry, M.-J., Catapano, F., Burns, S., Chaudhry, A.N., Smith, K.G., Jayne, D.R., 2014. The effect of rituximab therapy on immunoglobulin levels in patients with multisystem autoimmune disease. BMC Musculoskelet Disord 15, 178. doi:10.1186/1471-2474-15-178

Martini, J., Recht, M.I., Huck, M., Bern, M., Johnson, N., Kiesel, P., 2012. Time Encoded Multicolor Fluorescence Detection in a Microfluidic Flow Cytometer+. Lab Chip 12. doi:10.1039/c2lc40515f

Mauri, C., Bosma, A., 2012. Immune regulatory function of B cells. Annu. Rev. Immunol. 30, 221–241. doi:10.1146/annurev-immunol-020711-074934

Murad, Y.M., Clay, T.M., Lyerly, H.K., Morse, M.A., 2007. CPG-7909 (PF-3512676, ProMune): toll-like

receptor-9 agonist in cancer therapy. Expert Opin Biol Ther 7, 1257–1266. doi:10.1517/14712598.7.8.1257

Nedosekin, D.A., Juratli, M.A., Sarimollaoglu, M., Moore, C.L., Rusch, N.J., Smeltzer, M.S., Zharov, V.P., Galanzha, E.I., 2013. Photoacoustic and photothermal detection of circulating tumor cells, bacteria and nanoparticles in cerebrospinal fluid in vivo and ex vivo. J Biophotonics 6, 523–533. doi:10.1002/jbio.201200242

Nedosekin, D.A., Khodakovskaya, M.V., Biris, A.S., Wang, D., Xu, Y., Villagarcia, H., Galanzha, E.I., Zharov, V.P., 2011. In vivo plant flow cytometry: a first proof-of-concept. Cytometry A 79, 855–865. doi:10.1002/cyto.a.21128

Novak, J., Georgakoudi, I., Wei, X., Prossin, A., Lin, C.P., 2004. In vivo flow cytometer for real-time detection and quantification of circulating cells. Opt Lett 29, 77–79.

Novak, J., Puoris'haag, M., 2007. Two-color, double-slit in vivo flow cytometer. Opt Lett 32, 2993–2995.

Padmanabhan, K., Andrews, S.E., Fitzpatrick, J.A.J., 2001. Multi-Photon Imaging, in: Current Protocols in Cytometry. John Wiley & Sons, Inc.

Pitsillides, C.M., Runnels, J.M., Spencer, J.A., Zhi, L., Wu, M.X., Lin, C.P., 2011. Cell labeling approaches for fluorescence-based in vivo flow cytometry. Cytometry A 79, 758–765. doi:10.1002/cyto.a.21125

Prendergast, F.G., Mann, K.G., 1978. Chemical and physical properties of aequorin and the green fluorescent protein isolated from Aequorea forskålea. Biochemistry 17, 3448–3453.

Qi, X.-F., Zheng, L., Kim, C.-S., Lee, K.-J., Kim, D.-H., Cai, D.-Q., Qin, J.-W., Yu, Y.-H., Wu, Z., Kim, S.-K., 2013. CpG oligodeoxynucleotide induces apoptosis and cell cycle arrest in A20 lymphoma cells via TLR9-mediated pathways. Mol. Immunol. 54, 327–337. doi:10.1016/j.molimm.2013.01.001

Quemada, D., 1981. A rheological model for studying the hematocrit dependence of red cell-red cell and red cell-protein interactions in blood. Biorheology 18, 501–516.

Quemada, D., 1983. Blood Rheology and Its Implication in Flow of Blood, in: Rodkiewicz, C.M. (Ed.), Arteries and Arterial Blood Flow, International Centre for Mechanical Sciences. Springer Vienna, pp. 1–127.

Richardson, S.M., 1989. Fluid Mechanics. CRC Press.

Sarimollaoglu, M., Nedosekin, D.A., Simanovsky, Y., Galanzha, E.I., Zharov, V.P., 2011. In vivo photoacoustic time-of-flight velocity measurement of single cells and nanoparticles. Opt Lett 36, 4086–4088.

SCHERER, W.F., SYVERTON, J.T., GEY, G.O., 1953. Studies on the propagation in vitro of poliomyelitis viruses. IV. Viral multiplication in a stable strain of human malignant epithelial cells (strain HeLa) derived from an epidermoid carcinoma of the cervix. J. Exp. Med. 97, 695–710.

Schneider, C.K., 2008. Monoclonal antibodies--regulatory challenges. Curr Pharm Biotechnol 9, 431–438.

Shaner, N.C., Steinbach, P.A., Tsien, R.Y., 2005. A guide to choosing fluorescent proteins. Nat. Methods 2, 905–909. doi:10.1038/nmeth819

Shcherbo, D., Merzlyak, E.M., Chepurnykh, T.V., Fradkov, A.F., Ermakova, G.V., Solovieva, E.A., Lukyanov, K.A., Bogdanova, E.A., Zaraisky, A.G., Lukyanov, S., Chudakov, D.M., 2007. Bright far-red fluorescent protein for whole-body imaging. Nat. Methods 4, 741–746. doi:10.1038/nmeth1083

Shcherbo, D., Murphy, C.S., Ermakova, G.V., Solovieva, E.A., Chepurnykh, T.V., Shcheglov, A.S., Verkhusha, V.V., Pletnev, V.Z., Hazelwood, K.L., Roche, P.M., Lukyanov, S., Zaraisky, A.G., Davidson, M.W., Chudakov, D.M., 2009. Far-red fluorescent tags for protein imaging in living tissues. Biochem. J. 418, 567–574. doi:10.1042/BJ20081949

Shimomura, O., 1985. Bioluminescence in the sea: photoprotein systems. Symp. Soc. Exp. Biol. 39, 351–372.

SHIMOMURA, O., JOHNSON, F.H., SAIGA, Y., 1962. Extraction, purification and properties of aequorin, a bioluminescent protein from the luminous hydromedusan, Aequorea. J Cell Comp Physiol 59, 223–239.

Sibéril, S., de Romeuf, C., Bihoreau, N., Fernandez, N., Meterreau, J.-L., Regenman, A., Nony, E., Gaucher, C., Glacet, A., Jorieux, S., Klein, P., Hogarth, M.P., Fridman, W.-H., Bourel, D., Béliard, R., Teillaud, J.-L., 2006. Selection of a human anti-RhD monoclonal antibody for therapeutic use: impact of IgG glycosylation on activating and inhibitory Fc gamma R functions. Clin. Immunol. 118, 170–179. doi:10.1016/j.clim.2005.10.008

Stanley, P.E., 1997. Commercially available luminometers and imaging devices for low-light level measurements and kits and reagents utilizing bioluminescence or chemiluminescence: survey update 5. J. Biolumin. Chemilumin. 12, 61–78. doi:10.1002/(SICI)1099-1271(199703/04)12:2<61::AID-BIO452>3.0.CO;2-7

Taillia, H., Bompaire, F., Jacob, J., Noël, G., 2013. [Cognitive evaluation during brain radiotherapy in adults: a simple assessment is possible]. Cancer Radiother 17, 413–418. doi:10.1016/j.canrad.2013.07.139

Teillaud, J.-L., 2012. [Mix-up of Fc receptors in the response to monoclonal antibodies]. Med Sci (Paris) 28, 11–13. doi:10.1051/medsci/2012281003

Thastrup, O., Tullin, S., Poulsen, L.K., Bjoern, S.P., 2001. Fluorescent proteins. US6172188 (B1).

The Immune System par Peter Parham: Garland Science 9780815340935 2nd - Better World Books [WWW Document], n.d. URL http://www.abebooks.fr/servlet/BookDetailsPL?bi=12582945817&searchurl=isbn%3D0815340931%26amp%3Bx%3D108%26amp%3By%3D9 (accessed 6.5.14).

Touitou, V., Bodaghi, B., de Kozak, Y., Lehoang, P., Sautès-Fridman, C., Fisson, S., 2008. Animal models of intraocular lymphomas. Ophthalmic Res. 40, 208–211. doi:10.1159/000119878

Tseng, S.-H., Grant, A., Durkin, A.J., 2008. In vivo determination of skin near-infrared optical properties using diffuse optical spectroscopy. J Biomed Opt 13, 014016. doi:10.1117/1.2829772

Tsien, R.Y., 1998. The green fluorescent protein. Annu. Rev. Biochem. 67, 509–544. doi:10.1146/annurev.biochem.67.1.509

Wang, C.-C., Carnevale, J., Rubenstein, J.L., 2014. Progress in central nervous system lymphomas. Br. J. Haematol. doi:10.1111/bjh.12938

Wei, X., Sipkins, D.A., Pitsillides, C.M., Novak, J., Georgakoudi, I., Lin, C.P., 2005. Real-time detection of circulating apoptotic cells by in vivo flow cytometry. Mol Imaging 4, 415–416.

Weiner, G.J., 2010. Rituximab: mechanism of action. Semin Hematol 47, 115–123. doi:10.1053/j.seminhematol.2010.01.011

Xu, W., Banchereau, J., 2014. The Antigen Presenting Cells Instruct Plasma Cell Differentiation. Front Immunol 4, 504. doi:10.3389/fimmu.2013.00504

Zackrisson, S., van de Ven, S.M.W.Y., Gambhir, S.S., 2014. Light in and sound out: emerging translational strategies for photoacoustic imaging. Cancer Res. 74, 979–1004. doi:10.1158/0008-5472.CAN-13-2387

Zharov, V.P., Galanzha, E.I., Shashkov, E.V., Khlebtsov, N.G., Tuchin, V.V., 2006a. In vivo photoacoustic flow cytometry for monitoring of circulating single cancer cells and contrast agents. Opt Lett 31, 3623–3625.

Zharov, V.P., Galanzha, E.I., Tuchin, V.V., 2006b. In vivo photothermal flow cytometry: imaging and detection of individual cells in blood and lymph flow. J. Cell. Biochem. 97, 916–932. doi:10.1002/jcb.20766

Zharov, V.P., Galanzha, E.I., Tuchin, V.V., 2007. Photothermal flow cytometry in vitro for detection and imaging of individual moving cells. Cytometry A 71, 191–206. doi:10.1002/cyto.a.20384